FUNCTIONALISATION OF DNA BINDING METALLOSUPRAMOLECULAR HELICATE CYLINDERS

by

CALLUM DONALD JAMES CAMPBELL

UNIVERSITY OF BIRMINGHAM

A thesis submitted to the University of Birmingham for the degree of

DOCTOR OF PHILOSOPHY

School of Chemistry,

College of Engineering and Physical Sciences,

University of Birmingham.

September 2019.

Abstract

Previous work in the Hannon group has shown that metallosupramolecular helicate "cylinders" can bind at the heart of DNA three-way junctions. As pseudo three-way junctions are formed during DNA replication within cells, these cylinders could potentially hinder the uncontrolled cell replication that is associated with cancers, offering them potential as a cancer therapeutic. However, a number of factors have prevented the cylinders from reaching the clinic, including uncertainty around the fate of the compound within cells and the stability of these compounds in solution. These cylinders do not have any feature that would make them target cancerous cells over healthy cells, a common hurdle in the design of anti-cancer drugs. The work described in this thesis aims to structurally modify triple stranded cylinders to incorporate useful functionalities that could address these hurdles, such as a fluorescent tag to allow tracking of the cylinder *in vivo* or a receptor targeting moiety that would favour uptake by cancer cells. The work presented is focussed on two main aims. The first was to develop a synthetic route to modify the cylinder structure in such a way that the ligands are connected through a covalent "cap", with the goal of improving upon the physiochemical properties exhibited by previous functionalised cylinders. Various strategies were trialled that used different covalent linkages to connect the cylinder ligands to a capping moiety. A reliable route to a novel tripyridyl-aldehyde cap was developed, yet conditions to synthesise a discrete capped cylinder were not identified. A substantial grounding for further work towards the synthesis of a capped cylinder is set, with recommendations made on what steps should be taken next. The second aim was to synthesis azide functionalised cylinders which could undergo post-assembly modifications with alkynes. Two novel cylinders, $Fe_2L^A{}_3Cl_4$ and $Fe_2L^B{}_3Cl_4$, were synthesised. Circular and linear dichroism experiments were performed to investigate the binding behaviour of these cylinders to double stranded DNA, and polyacrylamide gel electrophoresis experiments were performed to investigate their binding to a DNA three-way junction. These investigations show that the additional azide functionalities do not dramatically detract from the desirable DNA binding properties exhibited by the original cylinder. An initial study suggests that one of the novel cylinders undergoes a post assembly modification with a strained cyclooctyne without losing the ability to bind to a DNA three-way junction. This tantalising result justifies further investigation into the potential for these novel azide cylinders to undergo post-assembly modifications.

Acknowledgements

I would like to thank my supervisor Professor Mike Hannon for the opportunity to work in his research group. I am very grateful for the guidance and insight he offered on my research, and for his willingness to discuss the wider developments and challenges in our field. Thanks also to Professor Zoe Pikramenou for her input and guidance during my progress reviews, and thanks to the School of Chemistry for the scholarship.

Various Hannon group members past and present have played a big part over the last four years, and my thanks go out to everyone who I have had the pleasure to work alongside. Thanks are due to James Craig for his help in getting the DNA binding experiments up and running, as well as his constant reminders to not take life too seriously. Thanks to my predecessors for setting the foundations that my work has built upon, particularly Jenifer White whose thesis has served as a consistently helpful presence on my desk over the last four years. Thanks to all the Analytical Facilities staff who have run experiments for me and showed tremendous patience when I needed help, particularly Chi Tsang, Cecile Le Duff and Allen Bowden. Thanks also to Dr Doug Browning of the Institute of Microbiology and Infection, School of Biosciences, for his training and support in running the PAGE experiments.

Thank you to all those who contributed to my wider development at the University of Birmingham, particularly Dr John Wilkie and Professor Jon Preece for their support during my term as Chair of the Research School Liaison Committee as well as all the committee members who supported me. Thanks also to Dr Holly Prescott from the Careers Network for her guidance in helping me work out what my next challenge should be. Thank you to all my friends outside of the University who have made such a positive impact on my life in the West Midlands, particularly members of the Birmingham Central St John Ambulance Unit who have offered camaraderie and a fantastic leadership opportunity.

Finally, immeasurable thanks are due to my family for being beside me no matter what. Specifically, I would like to thank my mum for inspiring me to pursue my interest in science, and to my wonderful wife Kate for being amazing. Without your faith, support and advice, none of this would have been possible. For these reasons, this thesis is dedicated to you both.

Abbreviations

Abbreviation/symbol	Definition
3WJ	three-way junction
4WJ	four-way junction
Abs	absorbance
Ac_2O	acetic anhydride
AcOH	acetic acid
AP	atmospheric pressure
aq	aqueous
ATP	adenosine triphosphate
B-DNA	B-form of deoxyribonucleic acid
Boc	tert-butoxycarbonyl
^oC	degrees Celcius
Cbz	benzyloxycarbonyl
CD	circular dichroism
CDI	carbonyldiimidazole
Ci	curies
d	doublet
DCM	dichloromethane
DEAD	diethyl azodicarboxylate
DMAP	4-dimethylaminopyridine
DME	dimethoxyethane
DMF	dimethylformamide
DMSO	dimethyl sulfoxide
DNA	deoxyribonucleic acid
dsDNA	double stranded DNA
EDC·HCl	N-(3-Dimethylaminopropyl)-N’-ethylcarbodiimide hydrochloride
ESI	electrospray ionisation

Et_2O	diethyl ether
Et_3N	triethylamine
EtOAc	ethyl acetate
EtOH	ethanol
FT	Fourier transform
h	hour(s)
HBTU	N,N,N',N'-Tetramethyl-O-(1H-benzotriazol-1-yl)uronium hexafluorophosphate
HPLC	high performance liquid chromatography
ICD	induced circular dichroism
ILD	induced linear dichroism
iPrOH	isopropanol
IR	Infrared
J	coupling constant (NMR)
LD	linear dichroism
M	moles dm^{-3}
m	multiplet
max	maximum
mCPBA	meta-chloroperoxybenzoic acid
Me	methyl group, CH_3
MeCN	acetonitrile
MeOH	methanol
mg	milligrams
min	minute
mL	millilitre
mol	moles
MS	mass spectrometry
n-BuLi	*n*-butyllithium
NIR	near-infrared
nm	nanometre
NMR	nuclear magnetic resonance

Nu	nucleophile
PAGE	polyacrylamide gel electrophoresis
Pd/C	palladium on carbon
PPh_3	triphenylphosphine
*p*TsOH	*para*-toluene sulfonic acid
R_f	retention factor
RT	room temperature
R_t	retention time
s	singlet
sat.	saturated
SPAAC	strain promoted alkyne-azide cycloaddition
ssDNA	single stranded DNA
t	triplet
TBAF	*tert*-butylammonium fluoride
TBDMSCl	*tert*-butyldimethylsilyl chloride
t-BuOH	*tert*-butanol
THF	tetrahydrofuran
THF	tetrahydrofuran
TLC	thin layer chromatography
TOF	time of flight
UV	ultraviolet
w/v	weight/volume
wt	weight
ε	molar extinction coefficient
λ	wavelength
µL	microlitre
µm	micrometre
µM	micromolar

Contents

Chapter 1:
Introduction

Deoxyribose nucleic acid (DNA) underpins the majority of known life. Most of cellular DNA is found in cell nuclei, containing the genetic information required to regulate and maintain cellular functions. Abnormal behaviour of DNA, whether arising from abnormalities in the code itself or in its processing, forms the root of many diseases. As such, DNA makes for an attractive therapeutic target. Yet there are a number of challenges associated with this, including targeting specific sections of DNA and targeting DNA in specific tissues. Finding new tools to selectively recognise DNA regions or motifs and alter their processing is key to forming successful therapeutic strategies.

The work described in this thesis concerns the development of novel DNA binding metallosupramolecular compounds, in the context of their DNA binding properties offering them potential as a future anticancer therapeutic. In order to provide the reader with a firm grounding in this work's background, this chapter will introduce structures of DNA and the structural features of synthetic agents that have been shown to bind to them. There will be particular emphasis on binders that have demonstrated an antiproliferative effect on cancer cell lines (that is, an ability to inhibit their growth). DNA-binding supramolecular agents will then be introduced, with particular focus on the helicates that have underpinned much of the Hannon group's research over the last two decades. How this knowledge contributes to the aims of the work contained in this thesis will then be described.

1.1 DNA structure

DNA is a polymeric molecule consisting of monomers called nucleotides. Each nucleotide consists of three components: a deoxyribose sugar, a phosphate anion, and an aromatic nitrogen containing base (either a purine or pyrimidine). When describing the bases that form DNA in the context of synthetic chemistry, the term "nucleobase" is often used to distinguish them from the broader Lewis or Brønsted definition of a base. The phosphate anion is linked to the deoxyribose ring via the 5' carbon, while the base is attached via the 1' carbon (Figure 1.1). These nucleotide units condense to form links between the phosphate anion of one

nucleotide and the 3' carbon of the deoxyribose of the next. This alternating sequence of deoxyribose sugars and phosphates forms the "backbone" of the DNA strand.[1,2]

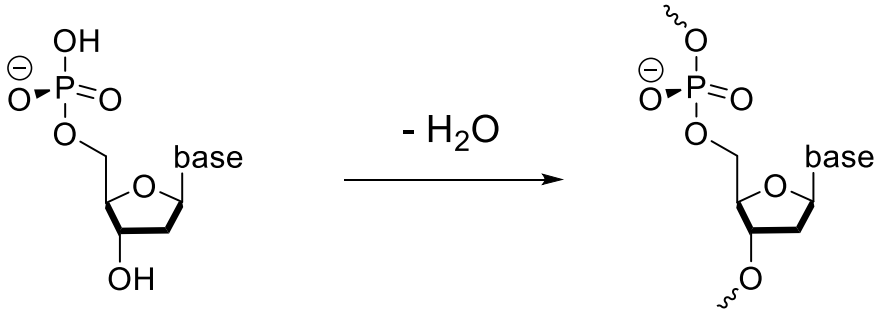

Figure 1.1 Structure of a nucleotide (left) and condensation to the DNA polymer (right).

DNA predominantly exists as a double helix (Figure 1.2).[3] Two antiparallel DNA strands are orientated together, with their bases forming the inside of the helix and their backbones running along the outside. This structure is often compared to that of a ladder, with the backbone acting as the vertical rails and the bases acting as the rungs. There are four bases: adenine (A), thymine (T), cytosine (C) and guanine (G). Figure 1.2 illustrates the complimentary hydrogen bonding patterns that form between A and T, and C and G (known as Watson-Crick base pairing).[3] Base pairing usually occurs in the A-T and C-G pairs shown. The aromaticity of the bases results in stabilising π-stacking interactions between consecutive nucleobase pairs, arising from the electrostatic attraction between the δ- delocalised electron density of one base and the δ+ carbon framework of its neighbours. This attraction holds the two strands of DNA together in combination with the hydrogen bonding, despite the electrostatic repulsion between the negatively charged backbones.

As the bonds between the nucleobase and the sugar are not orientated directly opposite each other, an alternating pattern of short and long twists form along the helix. These twists are known as the major and minor grooves, and are labelled in Figure 1.2. There are various forms that duplex DNA can take, which vary in the number of base pairs per helical turn and in the handedness (right or left) of the turn. By far the most abundant form is B-DNA, which is a right handed helix with 10 base pairs per helical turn.

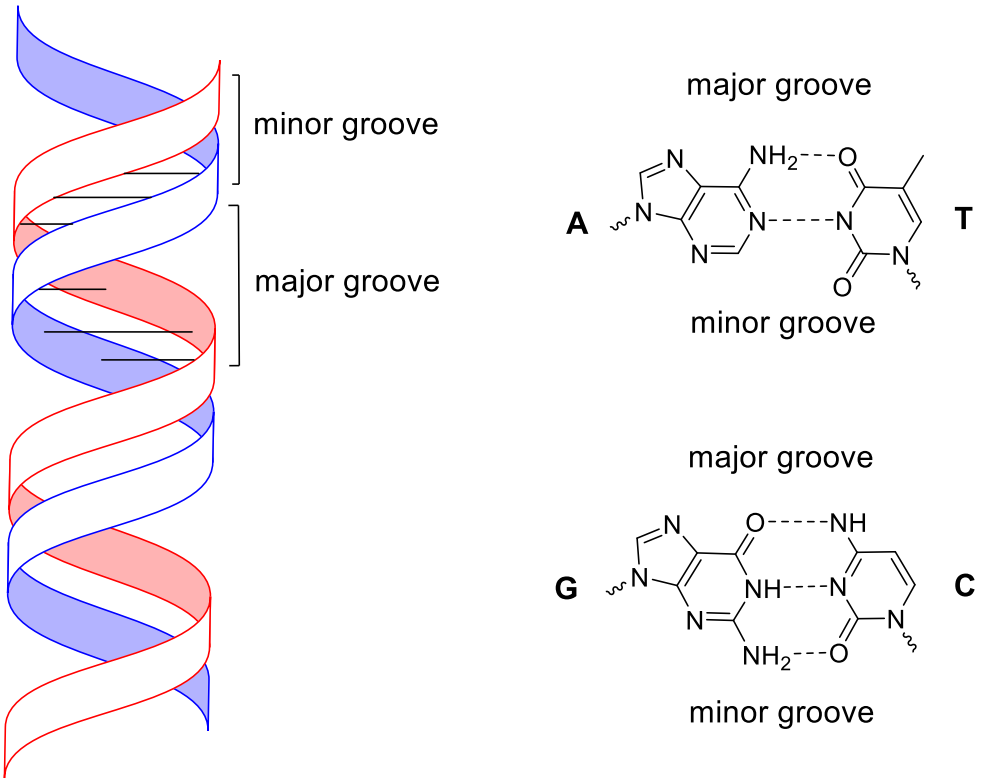

Figure 1.2 Double helix structure, with each DNA strand represented as a ribbon. The bases are situated within the helix, perpendicular to the helical axis, as represented by the black lines. The major and minor grooves are highlighted on the left. Hydrogen bonding between complimentary Watson-Crick base pairs are shown on the right.

1.2 B-DNA recognition

DNA can be recognised by both natural and synthetic agents in a variety of ways, including formation of covalent bonds with the DNA nucleobases; intercalating between the π-stacked nucleobase pairs; and through interactions with the helical grooves.

1.2.1 Covalent binding to DNA nucleobases

Covalent binding largely occurs with the purine bases (A and G) which have multiple sites susceptible to nucleophilic attack, as highlighted in Figure 1.3. The most well-known DNA binders are the Pt(II) therapeutics cisplatin, carboplatin and oxaliplatin (Figure 1.4), which are prescribed globally for the treatment of cancer.[4] Cisplatin has seen global use since the late

1970s, and is the common benchmark against which new anticancer candidates are compared. The mechanism of action involves one of the chlorides being substituted for a H_2O ligand, which is driven by the low intracellular saline concentration.[4] This new water ligand is then displaced by coordination of N in the 7-position of a purine base, usually guanine. Once bound, the second chloride is then displaced, often by an adjacent purine.[5,6] This displacement causes a dramatic conformational change in the B-DNA, effectively forming a 45° kink to the normal helical axis. This change in secondary structure is recognised by the cell's DNA repair mechanisms. The coordination bond formed is very strong so the cell's repair efforts are often unsuccessful, resulting in cellular apoptosis: controlled cell death.[6]

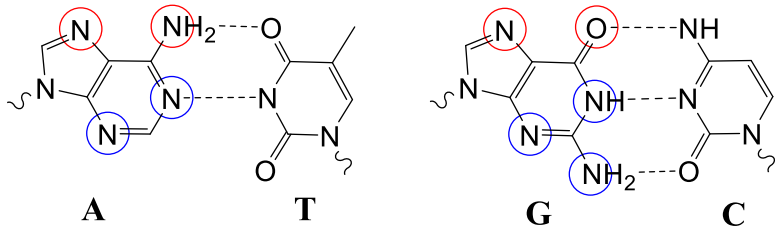

Figure 1.3 Common sites of bond formation with synthetic agents in the major groove (red) and in the minor groove (blue).

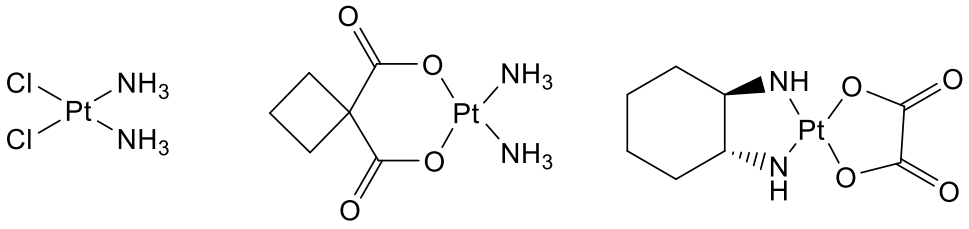

Figure 1.4 Structures of cisplatin and related analogues carboplatin and oxaliplatin, which are used globally in the treatment of cancer.

While the strong affinity of cisplatin for purine bases makes it highly cytotoxic, the hurdles resulting from its lack of selectivity for cancer cells over healthy cells has yet to be overcome. Wide ranging adverse side effects are associated with cisplatin use, including nephrotoxicity, neurotoxicity and severe nausea.[7] With the aim of minimising these effects, extensive

research has resulted in over 30 derivatives of cisplatin entering clinical trials since the early 1980s. Carboplatin (Figure 1.4), introduced in the clinic nearly two decades after cisplatin, was developed on the hypothesis that a more stable leaving group than chloride might reduce adverse side effects while maintaining efficacy against tumour growth. This hypothesis proved correct, with carboplatin dosing programmes demonstrating an equivalent efficacy to cisplatin but with off-target toxicities greatly reduced.[7] However, tumour resistance to cisplatin and carboplatin is frequently observed, either as an inherent characteristic of a tumour or one that develops during dosing treatments.[8] Oxaliplatin was developed to overcome cisplatin resistance mechanisms, and is now most often utilised in the treatment of advanced colorectal cancers.[6]

More recent work on platinum binders has focussed on improving their pharmacokinetic properties and cisplatin resistance by developing Pt(IV) prodrugs. These prodrugs generally retain the equatorial coordination sphere of cisplatin (or one of its derivatives), adding an additional two ligands in the axial positions. Pt(IV) prodrugs are designed to be reduced to their active Pt(II) form *in vivo* by cellular reducatses.[9] As they are octahedral d^6 complexes, they are more kinetically inert, granting them potential to be orally administrable,[10] a desirable property as it would allow patients to self-administer their own medication, without the need to be in a hospital environment. A prominent example is Satraplatin (Figure 1.6), which reached a phase III clinical trial as an orally administered drug.[11] Significant efforts have focussed on adding useful moieties in the axial positions to grant multiple modes of action to the Pt(IV) complexes,[12] with recent reports describing multiple action prodrugs whose axial ligands cause further cytotoxic effects in cancerous cells when released from the complex. A illustrative example is cis,trans,cis-$[Pt(NH_3)_2(OA)(PhB)Cl_2]$ (Figure 1.6) developed by Brabec and coworkers,[13] which releases phenyl butyrate (PhB) and octanoic acid (OA) when the platinum is reduced. PhB inhibits the histone deacetylase enzyme, which results in DNA unwinding from chromatin (an adduct of DNA wrapped around a histone protein), exposing it to the Pt(II) agent. OA interferes with DNA methyltransferase, resulting in hypermethylation of DNA. The combination of these three modes of action resulted in a higher potency than cisplatin in MDF-7 breast cancer cell cultures.

Complexes of other metals have been shown to covalently bind to DNA, including some half-sandwich metal-arene “piano stool” complexes. Examples of such complexes with Ru(II),

Ir(III) and Rh(III) binding to DNA have been recently reported,[14–17] although their mechanism of action can vary. Espino, García and co-workers have reported a series of Ru(II)-arene complexes, the generic structure of which is shown in Figure 1.7, which bind readily to the N7 of guanine in a manner similar to cisplatin. The aryl ring is thought to form hydrophobic interactions with adjacent bases, and the heterocycles can hydrogen bond to them.[18] Interestingly, these complexes demonstrated a comparable antiproliferative effect in cisplatin resistant A2780 lung cancer cells as the non-resistant line.[19] More recently, it has been reported that di-Ru(II) piano stool systems can cross-link across different DNA strands.[20]

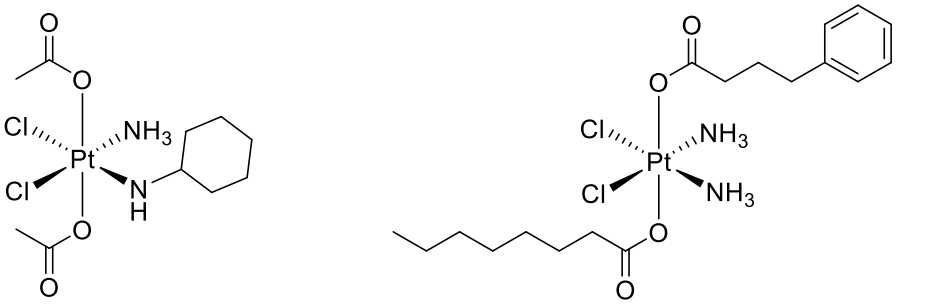

Figure 1.6 Examples of Pt (IV) prodrugs which have demonstrated anticancer properties. Covalently binding Pt(II) species are generated when the prodrugs are reduced by cellular reductases.

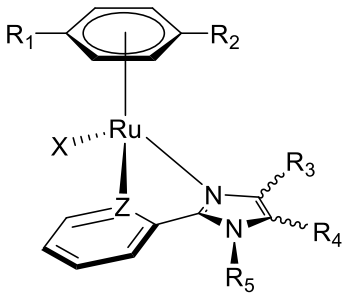

Figure 1.7 General structure of the Ru(II) piano stool complexes investigated by Espino, García and co-workers.[19]

1.2.2 Intercalation

Intercalation, first proposed by Lerman in 1961,[21] involves the insertion of a planar moiety in between stacked base pairs. The gap between stacked base pairs increases by approximately 3.4 Å to accommodate the intercalating species, causing a slight unwinding of the double helix, but overall the helical structure is maintained.[1] Intercalation is the most common binding mode amongst DNA-targeting agents and is promoted by planar, heteroaromatic structures. The heteroatom grants polarity to the structure, and favourable π-stacking interactions form between the intercalated moiety and the structurally similar DNA bases on either side.[1] Electrostatics play an important role, with many intercalators bearing a positive charge. Intercalators proflavine and ethidium (Figure 1.8) are both used as dyes for visualising DNA.[22,23] Adriamycin and daunorubcin (also in Figure 1.8) are naturally occurring products used extensively in cancer chemotherapy that are known to intercalate.[24]

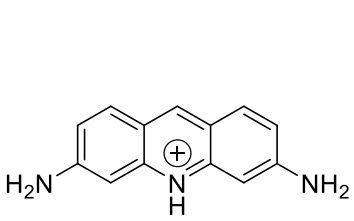

Proflavine

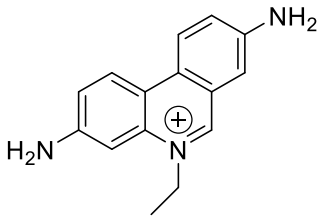

Ethidium

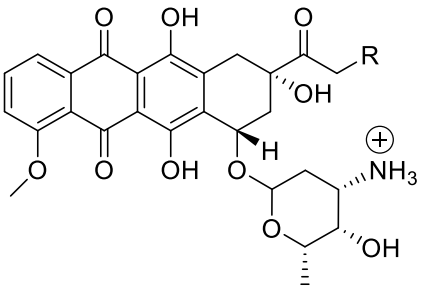

Daunorubicin (R=H);
Adriamycin (R=OH)

Figure 1.8 Examples of intercalating agents.

Incorporating metal centres into the design of intercalating agents can offer a number of advantages. Metal ions at the centre of complexes bear positive charges which increases the electrostatic contribution to binding. They can also introduce useful properties such as luminescence, as exemplified by $Ru(phen)_2(dppz)^{2+}$ (Figure 1.9), developed by Barton and co-workers. They discovered that $Ru(phen)_2(dppz)^{2+}$ luminesces strongly when intercalating with helical DNA but is inactive in free solution, which has resulted in these compounds being referred to as DNA "light switches".[25] Metallointercalators tend to be coordinatively saturated, so that the metal does not coordinate to the nucleobases. With $Ru(phen)_2(dppz)^{2+}$, the larger dppz ligand is responsible for the intercalation, while the ancillary phen ligands position in the grooves of helical DNA. Major groove selectivity can be achieved using larger ancillary ligands.[26] Recent reports of metallointercalators have utilised the redox activity of Co(III), Rh(III) and Ir(III) complexes to photocleave DNA strands,[14,27] and next generation anticancer platinum compounds have been designed to incorporate intercalating moieties.[28]

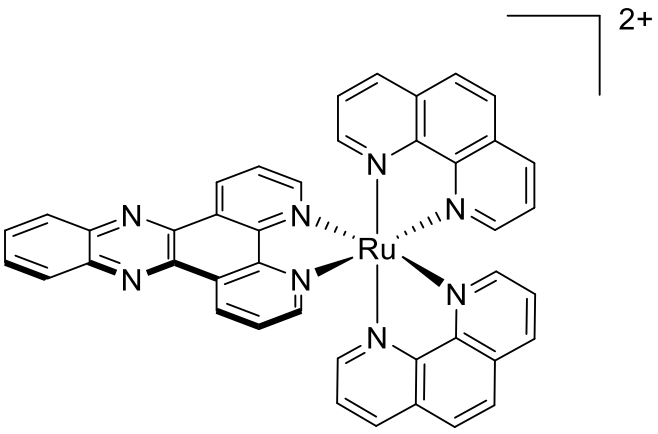

Figure 1.9 $Ru(phen)_2(dppz)^{2+}$, first reported by Barton and coworkers.[25] The large planar dppz ligand intercalates between DNA bases pairs.

1.2.3 Interaction in the major and minor grooves

Recognition of DNA through interactions with the major and minor grooves allows access to the nucleobase sequence of helical DNA, which offers up the potential of targeting specific sequences. Major groove binding is dominated by large macromolecules such as proteins and other polymeric nucleic acids. The exact size of the major groove varies depending on the

base sequence but is usually around 12 Å wide.[2] Various proteins recognise the major groove of duplex DNA through hydrogen bond donor/acceptor functionalities of amino acid side chains, examples of which can be seen in Figure 1.10. Generally, proteins recognise the major groove through the binding of α-helix domains, which can fit snuggly into the major groove but are too large to fit into the minor groove. Such α-helices, termed "zinc fingers", are found in various transcription factor proteins.[1,29,30] There is no correlation between specific amino acid residues binding specific nucleobases in the DNA sequence, which has stopped the design of sequence specific peptide therapeutics.

The minor groove is much narrower and deeper than the major groove, and as such minor groove binding is dominated by smaller synthetic agents. Different structural classes of minor groove binders include heterocyclic dications, bisbenzimidazoles and polyamides, examples of which can be seen in Figure 1.11. Several structural features contribute towards their affinity for the minor groove. Firstly, the cationic charge grants an electrostatic contribution to their binding. Secondly, the linked aromatic rings (rather than the fused rings found in many intercalators) offer sufficient conformational flexibility to slot into the minor groove and achieve an orientation that maximises hydrogen bonding and van der waals' contacts.[1] DAPI and Hoecht 33258 fluoresce when bound to DNA, leading to their wide use as nucleic acid stains in fluorescence microscopy applications. Distamycin and Netropsin are natural antibiotic agents which have influenced the development of analogues that demonstrate cytotoxic activity in cancer cell lines.[31,32]

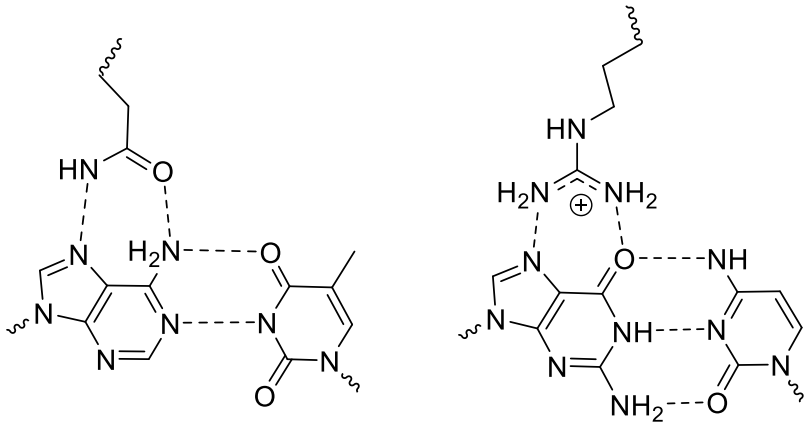

Figure 1.10 Examples of amino acid residues hydrogen bonding to DNA base pairs from the major groove side. A glutamine residue is shown bonding to an A-T pair (left) and an arginine residue bonding to a C-G pair (right).

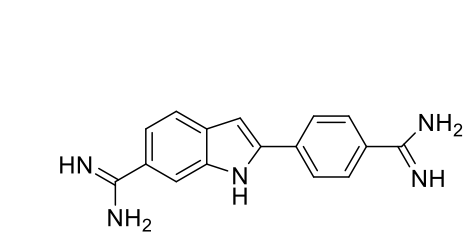

DAPI

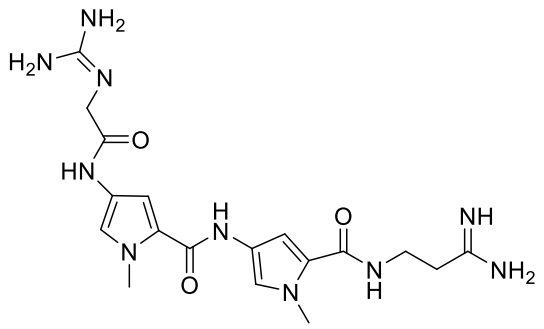

Netropsin

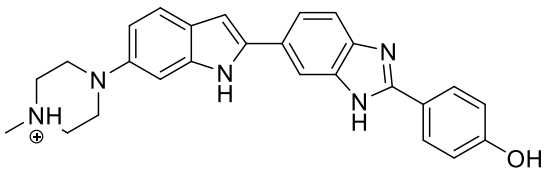

Hoechst 33258

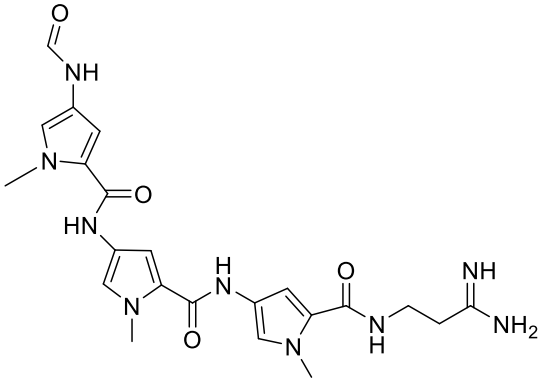

Distamycin

Figure 1.11 Examples of minor groove binding agents.

1.3 Recognition of non-canonical DNA structures

Helical B-DNA is essentially dormant. While it is useful for storage of genetic information, DNA must adopt a different structure for that genetic information to be used in cellular processes such transcription and replication. The binding agents discussed thus far do not show any selectivity between healthy and diseased DNA. As cancer is characterised by uncontrolled cell replication, one tactic to introduce some degree of selectivity may be to target different DNA structures that are more prevalently found in cells that are constantly replicating. Accumulation of a non-canonical DNA structure in the cell, by stabilising it with a synthetic binder, may lead to the cell recognising the DNA as damaged which would induce apoptosis. G-quadruplexes, i-motifs, and junction structures will be described in this section, and published examples of agents that bind to each will be discussed.

1.3.1 *G-quadruplex binders*

G-quadruplexes (GQ) can form in guanine-rich regions of DNA. They consist of at least two coplanar orientations of four G nucleobases (G-quartets) which are held together through Hoogsteen hydrogen bonding (an alternative arrangement to that proposed by Watson and Crick) and connected by loops of single stranded DNA (Figure 1.12a). Each plane has four-fold symmetry and the planes stack atop each other, stabilised through π-stacking interactions. GQs can be intra- or intermolecular, with the latter giving rise to parallel or antiparallel structures depending on the relative orientations of the connecting DNA backbones (Figure 1.12b).[33] The centre of the GQ bears an overall negative charge due to the orientation of the O6 of each guanine, and it is believed that these are stabilised by Na^+ and K^+ cations in nature.[34] GQs are prominently found in gene promoter regions and telomeres.[33] Telomeres are none gene coding stretches of DNA, found at the end of chromosomes (complexes of DNA coiled around proteins called histones) in the cell nucleus. Telomeres are not completely reproduced during DNA replication and become shorter with each cell cycle, leading to aging. In 85-90% of human cancer cells, these regions are elongated by hyperaction of telomerase enzymes, making them immortal.[35] Binding agents that stabilise quadruplex structures and disrupt the normal action of telomerase therefore offer an alternative approach to cancer therapy.

The first report of a small molecule that preferentially bound GQs over duplex DNA was from Hurley, Neidle and coworkers.[36] Their active 2,6-diamidoanthraquinone derivative (Figure 1.13) is believed to bind to the top of the GQ, stabilising it through π-stacking interactions between the anthraquinone moiety and the topmost G-quartet. The positively charged side chains provide an electrostatic contribution to the binding, as well as improving aqueous solubility. Large planar aromatic structures and positive charges have been a consistent structural features of hundreds of organic GQ binders that have since been reported.[37]

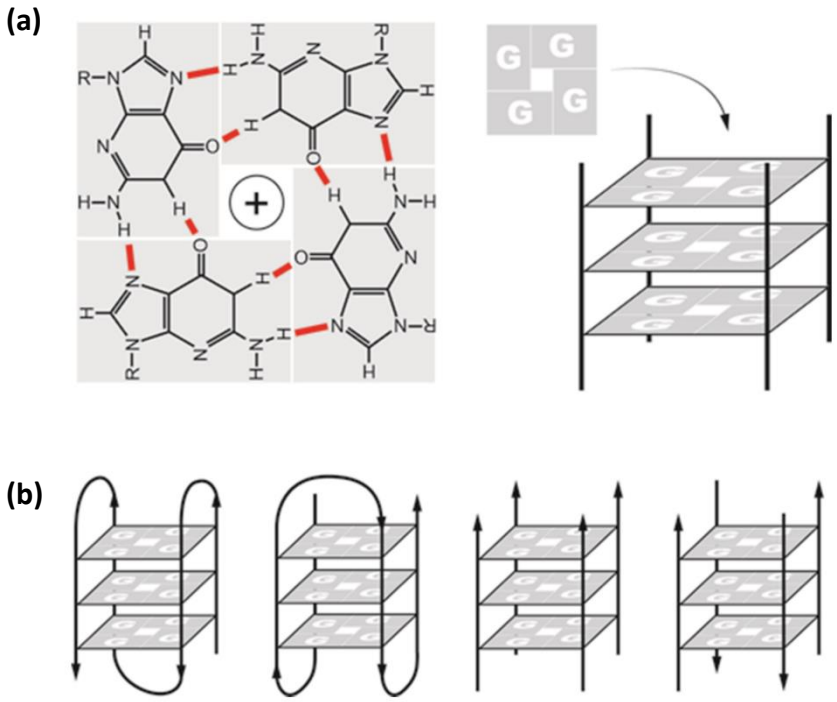

Figure 1.12 (a) Planar arrangements of four guanidine bases (stabilised by Hoogsteen hydrogen bonding) can form stacked structures called G-quadruplexes. (b) Examples of different intramolecular G-quadruplexes, and intermolecular parallel and antiparallel structures. The black arrows represent the DNA sugar phosphate backbones. Taken from reference 33 with permission.

Using organometallic complexes to target GQs offers a number of advantages. Firstly, it situates a positively charged metal centre near the centre of the binder, which occupies the space where Na^+ or K^+ would be *in vivo*. Secondly, it draws electron density away from the

organic framework, which improves the binder's ability to π-stack with the topmost G-quartet.[38] Two classes of metal containing GQ binders that have received significant attention are the metal-porphyrins, exemplified by $ZnTMPyP_4$ (Figure 1.13),[39] and metal-salphens, exemplified by the Ni(II) complex pioneered by Neidle, Vilar, and coworkers (also shown in Figure 1.13).[40] Both consist of large aromatic structures with a central metal cation. $ZnTMPyP_4$ has been known to bind to nucleic acids for decades,[41] and Hurley and coworkers first explored its ability to bind to GQs. The Zn(II) centre of $ZnTMPyP_4$ adopts a square-pyramidal geometry, with the porphyrin occupying the square plane and a water ligand in an axial position. It is this geometry that grants its preference to bind atop GQs rather than intercalating between the G-quartets.[42,43] The Ni(II)-salphen complex in Figure 1.13 incorporates piperidine functionalised side chains, which are protonated at physiological pH and provide an additional electrostatic contribution to the negatively charged backbone loops of GQs. A couple of more recent examples of metal-salphen GQ binders include one that has incorporated a fluorescein moiety into the ligand structure,[44] and another that features a Pt(IV) metal centre which is reduced to the active Pt(II) form by intracellular reductases.[45] The structures of these are shown in Figure 1.14.

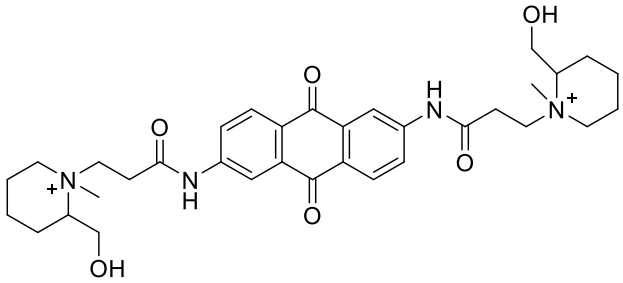

Hurley's 2,6-diamidoanthraquinone

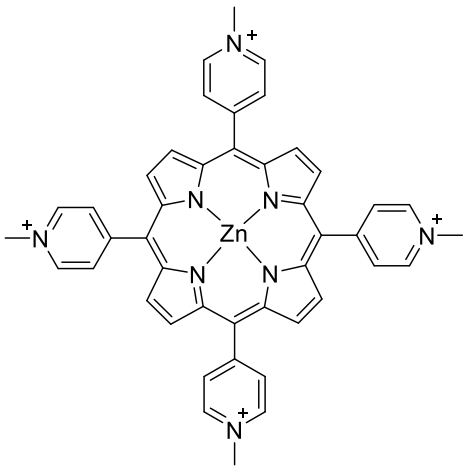

$ZnTMPyP_4$

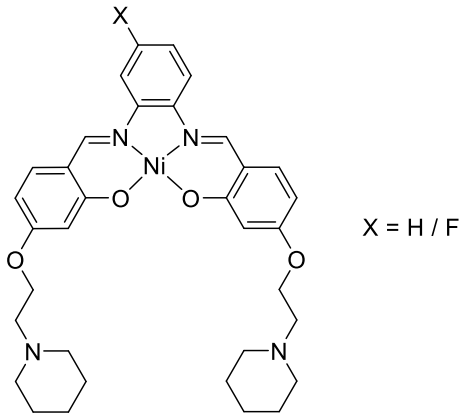

Vilar's Ni(II)-salphens

Figure 1.13 Examples of G-quadruplex binders. Common features include large, planar aromatic moieties and cationic charge.

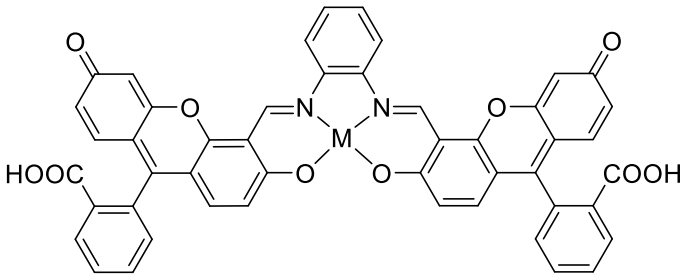

Fluorescein-salphen complex

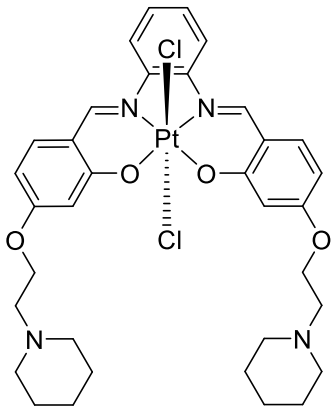

Pt(IV)-salphen complex

Figure 1.14 Examples of recently reported metal-salphen G-quadruplex binders.

1.3.2 *I-motif binders*

Intercalated motifs, commonly referred to as "i-motifs", rely on base pairing between cytosines. I-motifs were first characterised in 1993 by Gehring and coworkers.[46] They observed that one of the cytosines was protonated, allowing three hydrogen bonds to form between CC^+ base pairs (Figure 1.15a). I-motifs consists of four intramolecular DNA strands, with stacked CC^+ pairs forming between parallel strands. These pairs form an alternating ladder-rung type structure, effectively intercalating one duplex with the other. Illustrations of this structure (taken from refs 47 and 48) are given in sections b and c of Figure 1.15**.** Analysis of the human genome has identified i-motif compatible sequences in gene promoter regions, including *C-Myc* [49] and *Bcl-2.*[50] I-motifs are believed to be much more dynamic than GQs,[48] and insight into their biological role is much more limited. The requirement for acidic conditions to protonate one of the C bases has caused debate as to whether i-motifs play a physiological role, although the recent detection of i-motifs in human cells by an i-motif binding antibody suggests that they do.[47]

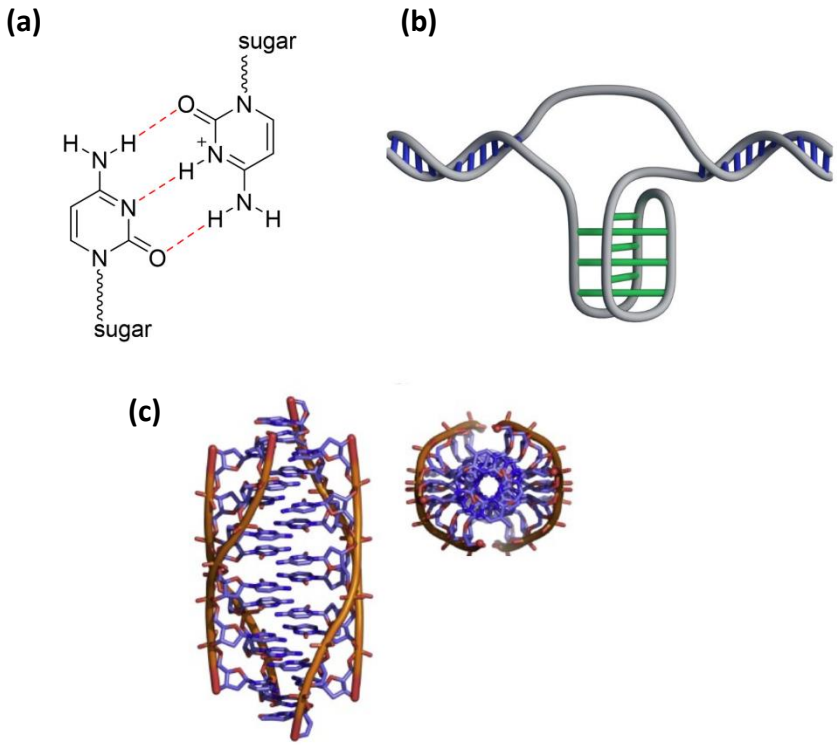

Figure 1.15 Structure of an i-motif. (a) CC^+ base pairing; (b) illustration of the interlocking intramolecular bonding between four strands, taken from reference 47 with permission; (c) representations of the crystal structure of an i-motif, side on and end on, taken from reference 48 with permission.

While there has been notably less effort directed at finding synthetic binding agents for i-motifs than for GQs, several interesting examples have been reported. The first study into an i-motif binder came from Hurley and coworkers, who investigated the binding properties of porphyrin $TMPyP_4$ (Figure 1.16).[51] While a dissociation constant of 45 µM was measured with an i-motif, this complex showed a preference for binding to both GQs and double stranded DNA. 2D 1H NMR NOESY experiments suggested that the porphyrin was binding to the i-motif externally via a non-intercalative mechanism. The bis-acridine binder BisA (Figure 1.16), reported by Alberti and coworkers,[52] similarly showed a lack of selectivity for the i-motif over GQs. A mono-acridine control showed that the two acridine units are necessary to see any stabilisation of either structure. A later study from Hurley and coworkers investigated the effect of two steroidal molecules, IMC-48 and IMC-76 (Figure 1.16), on the stability of the i-motif sequence found in the *Bcl-2* promoter region.[50] This i-motif is in equilibrium with a DNA hairpin structure, and IMC-48 was found to stabilise the i-motif structure while IMC-76 was

found to destabilise it (thus favouring the hairpin). IMC-48 was found to be selective for the i-motif, showing no evidence of binding with the GQ sequence that is also present in the *Bcl-2* promoter region. A more recent example comes from Dash and coworkers, who reported the binding properties of structurally similar peptidomimetic molecules PBP1 and PBP2 (Figure 1.16).[53] PBP1 and PBP2 differ in the relative positions of their triazole and prolinamide moieties on the phenyl rings. PBP1 was found to preferentially bind to the i-motif from the *Bcl-2* promoter region over numerous GQ structures, while PBP2 selectively bound to GQs. To observe such a dramatic change in behaviour for such similar structures is intriguing, yet no structural studies of the binding modes have yet been reported. There have not yet been any reports of metal containing binders designed to target i-motifs, likely due to the need for acidic pH to study i-motifs *in vitro* which would destabilise metal complexes.

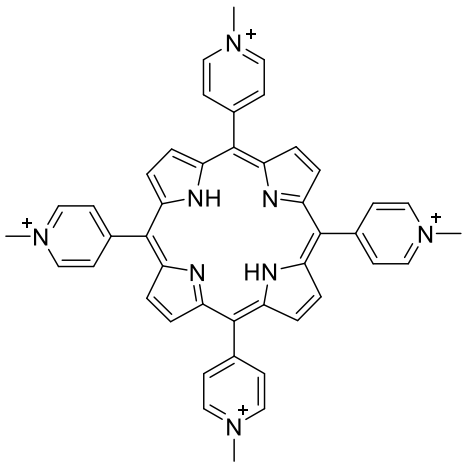

$TMPyP_4$

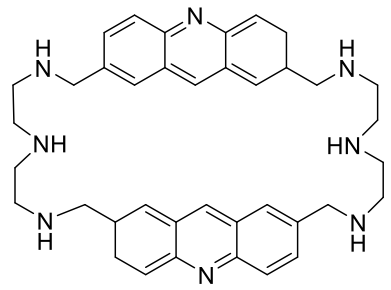

BisA

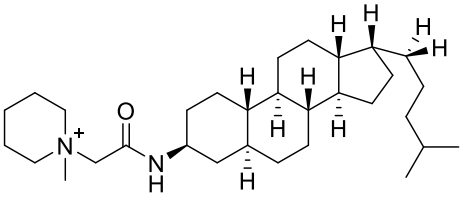

IMC-48

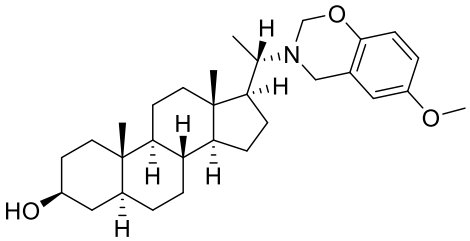

IMC-76

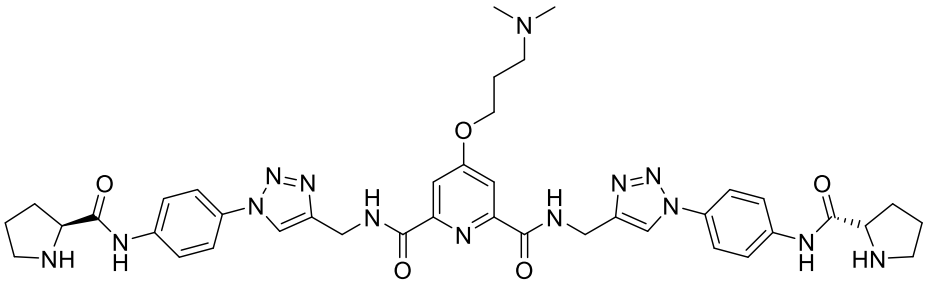

PBP1

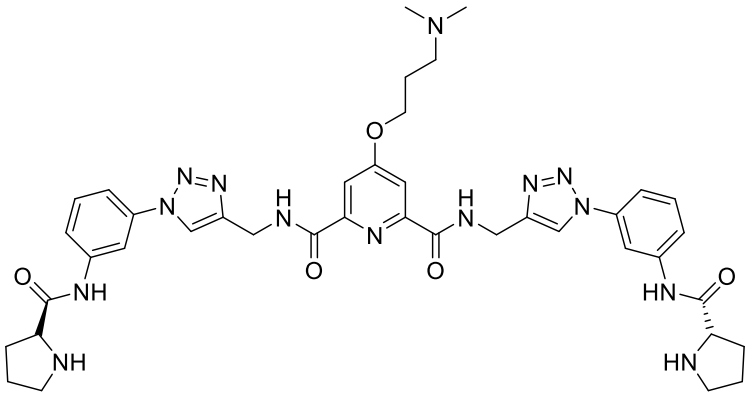

PBP2

Figure 1.16 Structures of i-motif binding agents.

1.3.3 *DNA junction binders*

DNA can form various multi-helix junction structures, where multiple branches of double stranded DNA converge and exchange strands. Three-way junctions (3WJ) and four-way junctions (4WJ) are known to occur in nature.[54] The structure and stability of five-way and six-way junctions have also been investigated,[55] but no biological role has yet been found. There have been numerous reports of synthetic binders that stabilise 3WJs and 4WJs, and these will looked at more closely in this section.

1.3.3.1 *Four-way junction binders*

4WJs (also known as "Holliday junctions" [56]) occur when two DNA duplexes come together and exchange strands. Such structures are formed transiently during homologous genetic recombination, a process that underpins cellular DNA repair mechanisms.[57] They are X-shaped, with DNA helices forming the arms and a crossover region in the centre where DNA strands are exchanged (Figure 1.17).[58] Cardin, Searcey and co-workers have developed a series of compounds that bind to a pseudo Holliday junction.[59] These bis-acridine binders (Figure 1.18) connect two intercalating moieties via alkyl chains of varying length. The hydrophobic alkyl chain sits in the minor groove side of the junction, and the cationic charge partially stabilises the electrostatic repulsion arising from the close proximity of the DNA backbones. Figure 1.18**,** taken from reference 59, illustrates such a compound binding to the pseudo 4WJ. More recently, Bonnet and coworkers have reported a distorted square planar Pt(II) complex that induces a Holliday-type structure from palindromic hexanucleotides (DNA strands with six nucleobases in a sequence that can complement another copy of itself, in this case 5'-CGTACG-3').[60] A crystal structure of the complex in the heart of the 4WJ suggests that the complex is sandwiched between two nucleobase quartets at the branch point, with the whole structure stabilised through resultant π-π stacking interactions. While an antiproliferative effect was observed in a number of cancerous cell lines, there is no evidence as yet whether 4WJ stabilisation is the predominant mechanism of action.

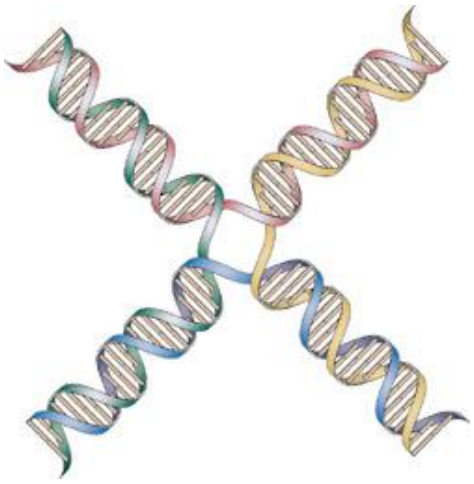

Figure 1.17 Illustration of a Holliday junction, where two duplex B-DNA molecules meet and exchange strands. Taken from reference 58 with permission.

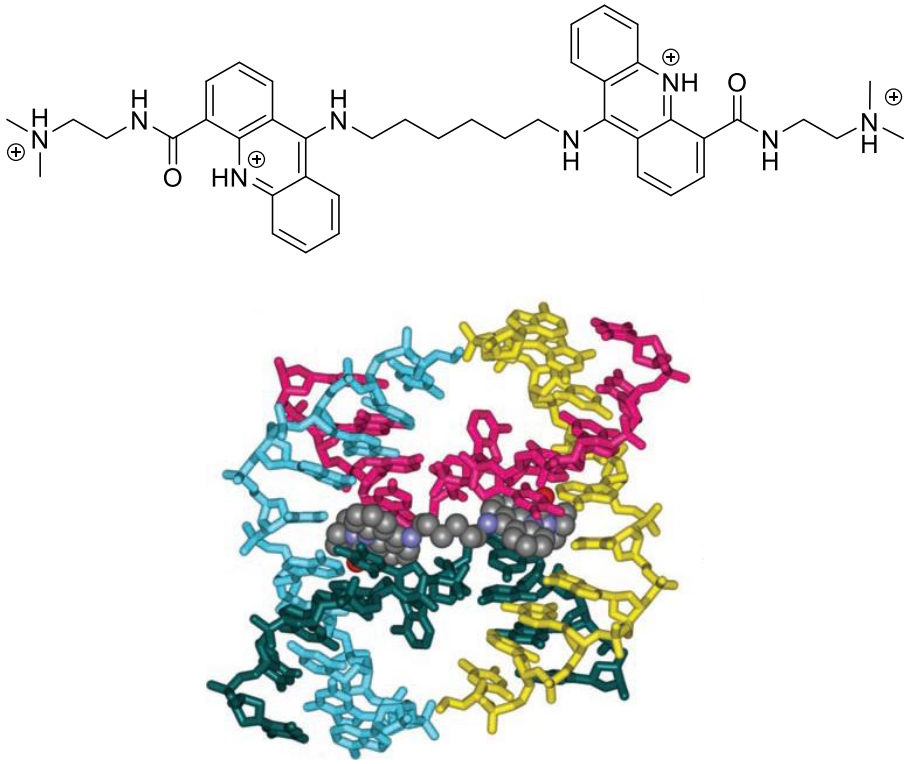

Figure 1.18 Structure of Cardin and Searcey's bisacridine 4WJ binder (upper); representation of the cocrystal structure of the binder (spheres) in a 4WJ (lower, adapted from reference 59 with permission).

1.3.3.2 *Three-way junction binders*

3WJs are formed when three strands of DNA converge at a single branch point. They can be found in ribosomal RNA [61] and are transiently formed during DNA replication.[62] Fast, unregulated replication is associated with tumour cells, making the 3WJ an interesting anticancer target. Studies into the structure of 3WJs from Lilley [63] and Kallenbach [64] from 1990 suggest that a fully matched 3WJ adopts a Y shaped structure. Figure 1.19 gives a schematic representation of how three DNA helices can come together and form a 3WJ.[65] 3WJs can also form with some nucleobases remaining unpaired, forming a bulge. These junctions tend to be T-shaped, as illustrated in Figure 1.20.[66] Molecular modelling techniques suggesting that the six bases at the branch point are unpaired.[67] The branch point offers a unique binding site for synthetic agents.

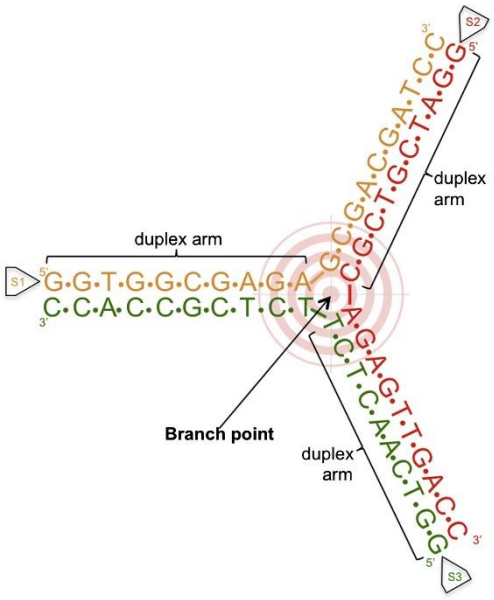

Figure 1.19 Schematic showing how three DNA duplexes can converge at a branch point and exchange partner strands while still maintaining complimentary base pairing. Adapted from reference 65 with permission.

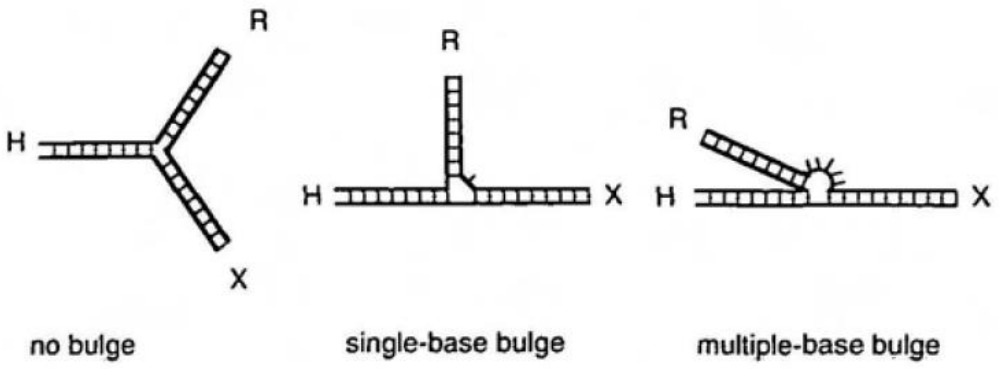

Figure 1.20 Representation of Y-shaped 3WJ without unpaired bases (no bulge) and representations of 3WJ with bulges arising from single and multiple unpaired nucleobases. Adapted from reference 66 with permission.

Recognition of a 3WJ by a synthetic agent was first reported by Hannon and coworkers, [68] which will be discussed in detail in section 1.4.1.1. Briefly, Hannon's triple stranded metallohelicate cylinder binds at the heart of the 3WJ (Figure 1.21), stabilised by the π-π interactions between the phenyl rings of the ligands and the six nucleobases situated at the branch point. Since then, a small selection of synthetic agents has been designed to target the 3WJ. These have all incorporated three aromatic moieties in a 3-fold symmetrical arrangement to adopt a similar binding interaction at the 3WJ's branch point.

Monchaud and coworkers have reported a 1,4,7-triazocyclononane ligand (TACN-Q) that demonstrates 3WJ binding.[65] Fluorescence Resonance Energy Transfer (FRET) techniques were used to show that TACN-Q bound readily to a 3WJ while showing little binding interaction with dsDNA. The presence of relatively high concentrations of Li^+ ions were required to see this binding, suggesting that it is the Li complex of TACN-Q (shown in Figure 1.22) that is active. Upon complexation, TACN-Q can adopt a helicoidal conformation where the planar quinoline groups are arranged with three fold symmetry, which presumably allows π-π interactions to form with the nucleobases at the branching point similar to Hannon's cylinders. The same experiments performed on TACN-Q analogues (which replaced the quinolones with acridine and naphthalene) showed weaker 3WJ affinity. This supports the idea that 3WJ binding is dependent on this helicoid geometry, which occurs when the quinoline arms coordinate to the metal centre.

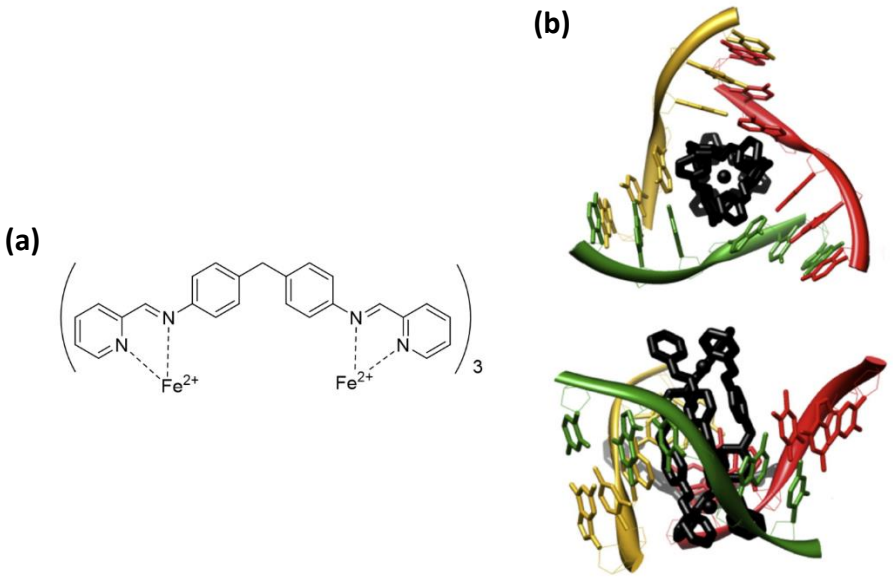

Figure 1.21 Hannon's triple stranded iron metallohelicate cylinder. (a) Representation of the cylinder structure, highlighting the two metal binding sites of the ligand. (b) Views of the crystal structure showing the iron cylinder bound in the central cavity of a 3WJ: view with the cylinder end on (upper) and side on (lower). Adapted from reference 65 with permission.

Monchaud has also reported preliminary work investigating the ability of a series of azocryptands to induce and stabilise 3WJs.[69] Figure 1.23 shows the structures of the compounds studied. 3,3'-TrisBP and 2,7-TrisNP were both shown to stabilise 3WJs, although again the presence of high concentrations of Li^+ and K^+ in the buffer solutions used suggest that the metal complexes may be the active forms. These cryptands are structurally similar to Hannon's cylinder, with planar aromatic moieties situated on the outer face. Monchaud concluded that the flexible nature of the ligands allows them to adopt conformations that optimise the π-π interactions with the nucleobases at the central cavity of the 3WJ. Both azocryptands showed promising antiproliferative activity in melanoma cell models.

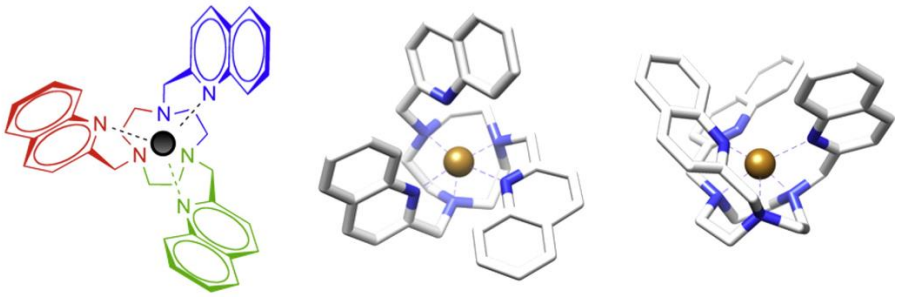

Figure 1.22 Monchaud's TACN-Q ligand coordinated to a metal centre. The quinoline moieties can adopt a helicoid arrangement which is believed to mimic the positioning of Hannon's cylinder in the 3WJ branch point. Adapted from reference 65 with permission.

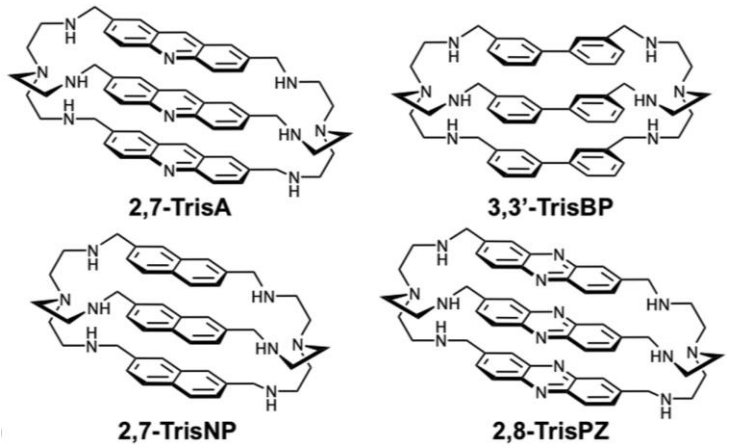

Figure 1.23 The azocryptands investigated for 3WJ binding by Monchaud and coworkers. Adapted from reference 69 with permission.

Chemoweth and co-workers have developed a series of triptycene based binders which, similarly to TACN-Q, preferentially bind to DNA 3WJs over dsDNA.[70] This selectivity arises from the three-fold symmetrical planar phenyl ring system (illustrated in Figure 1.24), which can form π stacking interactions with the bases located in the heart of the junction yet are not large enough to intercalate between nucleobase pairs of dsDNA. These early triptycene derivatives showed promising activity inhibiting the proliferation of cisplatin resistant A2780 human ovarian carcinoma cells. Chenoweth's group went on to incorporate positively charged amino acid residues on to the triptycene scaffold, in an effort to strengthen the electrostatic attraction to DNA.[71] Studies of these derivatives showed that junction binding

was maintained, although no comment was made on whether the derivatives demonstrated a notable increase in binding affinity. Chenoweth has also reported solid phase synthetic methods to produce triptycenes functionalised with larger peptide sequences.[72] Presumably, investigations into the 3WJ binding properties of these peptide functionalised triptycenes are ongoing.

A team led by Yang has recently developed a calix[3]carbazole (Figure 1.25) that demonstrates increasing fluorescence in the presence of increasing concentrations of 3WJ.[73] In a similar manner to the other 3WJ binders already described, the calix[3]carbozole features three planar aromatic moieties that presumably form π-π stacking interactions at the branch point of the 3WJ. This calix[3]carbozole also features cationic side chains, which improve aqueous solubility as well as introducing a further electrostatic contribution to DNA binding. The prospect of a binder's fluorescence increasing upon binding to a 3WJ offers up interesting applications as a 3WJ probe, as it could behave in a similar fashion to Barton's Ru DNA "light switch" compounds described in section 1.2.2. However, investigations into the behaviour of calix[3]carbazole in the presence of other DNA structures are limited, and further investigations into its selectivity need to be performed before it's potential as a 3WJ probe can be considered.

While efforts to find 3WJ binders remain much narrower than those directed towards the development of GQ binders, the recent development of a fluorescence based screening method by Monchaud and coworkers to identify 3WJ binders offers a promising tool which could aid development of this field in the near future. [74,75]

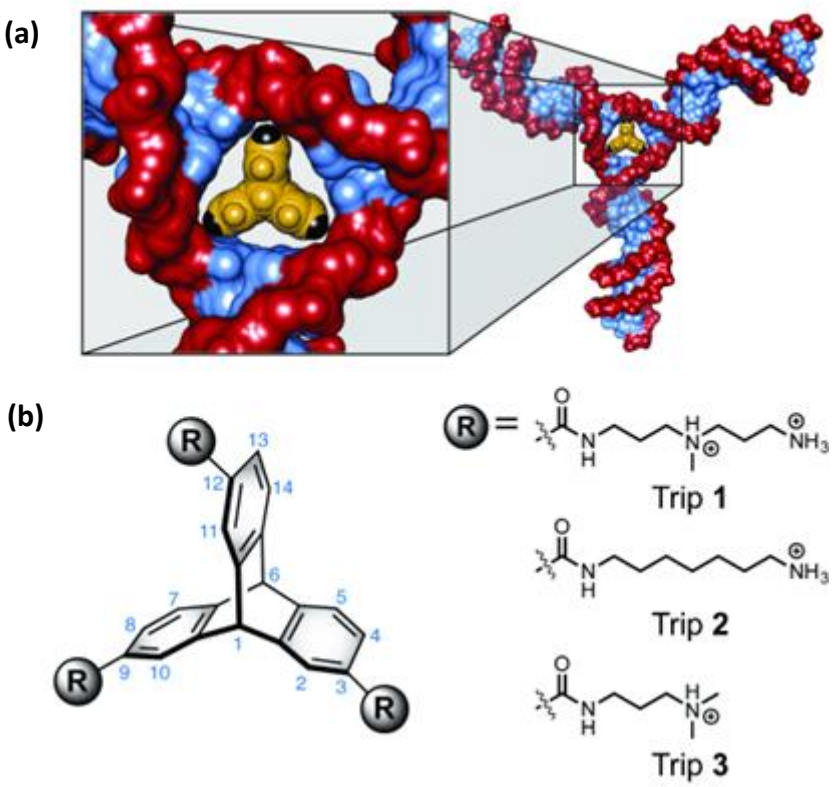

Figure 1.24 Illustrations of Chenoweth's triptycene-based 3WJ binders. (a) Computational model of triptycene binding in the central cavity of a 3WJ. (b) Structures of triptycene derivatives initially investigated. Taken from reference 70 with permission.

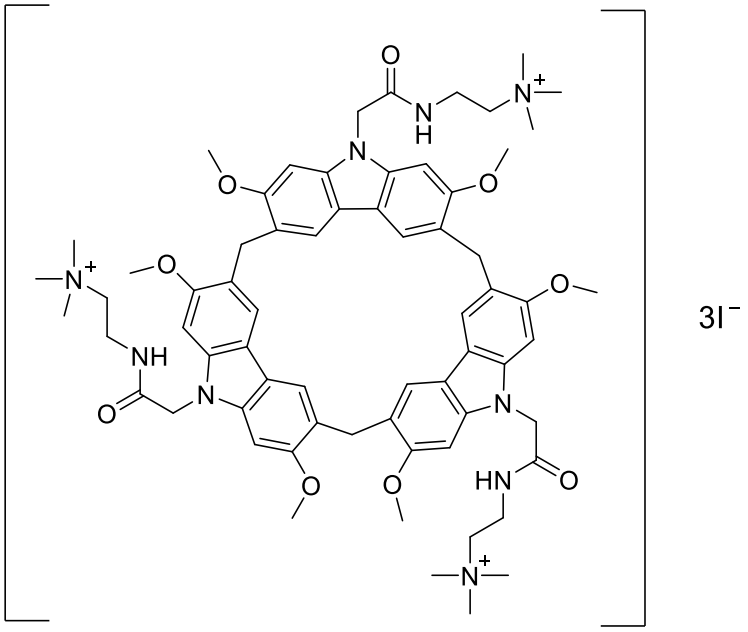

Figure 1.25 Structure of Yang's calix[3]carbazole 3WJ binder.

1.4 Recognition of DNA by metallosupramolecular species

Supramolecular chemistry involves molecular assemblies held together by non-covalent, intermolecular interactions such as electrostatic interactions, hydrogen bonding, van der waals' dispersion forces and hydrophobic effects.[76] While individually weaker than covalent bonds, these effects can cumulatively have tremendous influence, resulting in a variety of diverse and interesting structures.[77] Metallosupramolecular structures are of particular interest in the context of DNA binding. As stated earlier, the inclusion of positive metal ions brings a strong electrostatic attraction to the negatively charged sugar-phosphate backbone of the DNA. The choice of metals can also confer interesting photochemical and electrochemical properties, such as fluorescence (e.g. Ru(II)) and redox properties which can result in DNA cleavage through generation of reactive oxygen species (e.g. Cu(II)). Alongside mononuclear complexes (many examples of which have already been mentioned) multi-nuclear supramolecular complexes including helicates, flexicates and cages have demonstrated DNA binding and antiproliferative properties in cancer cell lines. Examples from these structural classes of metallosupramolecular compounds will be further discussed in this section.

1.4.1 Metallosupramolecular helicates

Metallosupramolecular helicates can form when organic ligands have multiple binding sites that coordinate to different metal ions. The ligands wrap around the metal centres forming a helical structure, with the metals located along the helical axis (Figure 1.26). For this structure to form, the ligands must be sufficiently flexible yet have a rigid enough linker between the binding sites to prevent their coordination to a single metal ion. For triple stranded helicates, optical isomerism at the metal centres (Δ or Λ) gives rise to helical chirality, with helical enantiomers classed as either right handed *P* (Δ, Δ) or left handed *M* (Λ, Λ). This classification essentially refers to the direction of ligand twist along the metal-metal axis. A wide range of multi-stranded helicate structures have been reported, utilising a variety of different metal centres and ligands.[78] While early applications were based around anion capture, therapeutic applications of metallohelicates have been receiving increasing attention over the last decade.

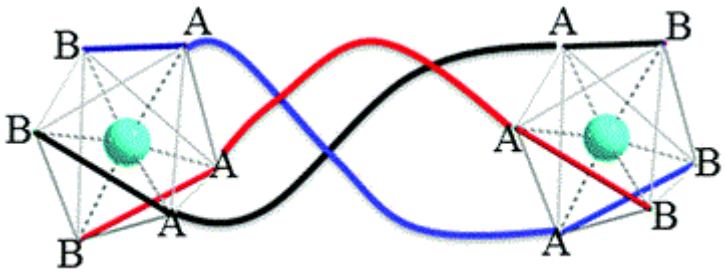

Figure 1.26 Schematic of a dinuclear, triple stranded metallosupramolecular helicate. Each ligand strand (represented in different colours) has two coordinating atoms at each end, marked A and B. The blue spheres represent the metal centres. Adapted from reference 79 with permission.

The first report of a helicate binding to DNA came from Lehn and Schoentjes in 1995.[80] They reported a series of double stranded Cu(I) helicates, which varied in the number of copper centres and in the number of repeated bipyridine binding units incorporated into the ligand structure (Figure 1.27). The structure of the trinuclear helicate was confirmed by x-ray crystallography, the dimensions of which (17 Å in length, 6 Å in diameter) where similar to that of the major groove of B-DNA, leading to the hypothesis that this is where the helicate would bind. UV-Vis investigations showed the characteristic MLCT band was shifted 5 nm lower in frequency when titrated with calf thymus DNA, while the bipyridine π-π* transition band remained unchanged. The fact that the MLCT band was still present suggests that the helicate remained intact while binding to the DNA. The helicate slowed down the mobility of calf thymus DNA through a porous gel, further suggesting that a binding interaction was occurring. Lehn and Schoentjes went on to discover that the helicate inhibited the activity of restriction enzymes which are known to bind to the major groove of B-DNA. This observation supported their hypothesis that the helicates were binding in the major groove.

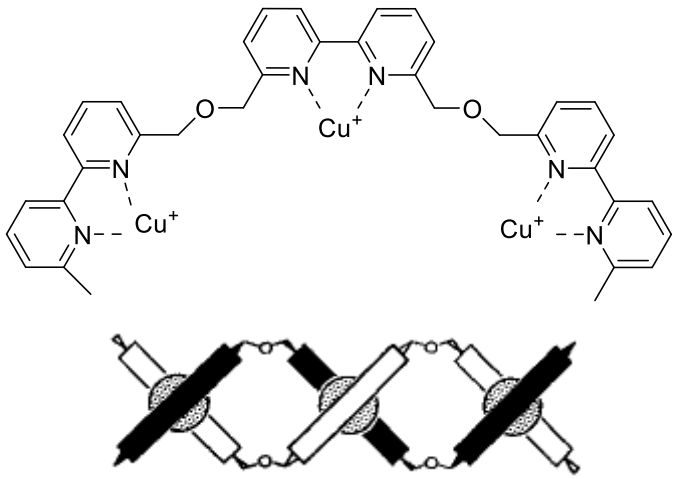

Figure 1.27 Lehn's trinuclear, double stranded Cu(I) helicate, with ligand structure (above) and schematic showing how the ligand wraps around the metal centres (below). Adapted from reference 80 with permission.

1.4.1.1 Metallohelicate cylinders

Investigations into DNA binding metallohelicates was revisited with the work of Hannon and coworkers, who have developed numerous helicate "cylinders". These triple stranded helicates have the general formula $[M_2L_3]X_4$, where M is a metal dication, L is a diimine ligand, and X is a counterion. The first report of a cylinder demonstrating DNA binding properties was published in 2001.[81] One of the attractive features of these cylinders is their straightforward synthesis. Scheme 1.1 shows the steps involved in the synthesis of $Fe_2L_3X_4$ (as reported in reference 82) where X is PF_6 or BF_4. Ligand L was formed through spontaneous condensation of two equivalents of 2-pyridinecarboxaldehyde with 1 equivalent of 4,4'-methylenedianiline in ethanol. After isolation by filtration, three equivalents of L were heated with two equivalents of $FeCl_2$ in methanol. A dramatic colour change was observed due to a MLCT, indicating self-assembly of the complex. This was isolated through a counterion exchange step where excess NH_4X was added to the reaction mixture, causing the complex to precipitate out of solution. $[Fe_2L_3]Cl_4$ is the most studied of Hannon's cylinders due to its high aqueous solubility, which makes it suitable for biological studies.[83] As the work contained in this thesis is largely concerned with developing analogues of $Fe_2L_3Cl_4$, a modified procedure was used to generate gram quantities of $Fe_2L_3Cl_4$ and this is discussed in more detail in section 3.2. A representation of the crystal structure of $Fe_2L_3Cl_4$ as published by Hannon is shown in

Figure 1.28. [84] Each Fe(II) centre has an octahedral geometry with three bidentate pyridine-imine moieties surrounding it, coordinated through the nitrogens. The central methylenediphenyl moiety of each ligand acts as a rigid linker. The aromatic rings of the linker are arranged such that face-edge π-interactions can occur between different strands, granting a rigidity to the cylinder not seen with Lehn's earlier helicates.[82] NOESY NMR experiments suggest that $Fe_2L_3Cl_4$ binds in the major groove of B-DNA, and AFM studies showed an unprecedented supercoiling effect upon binding.[81] Further investigation indicated that the dimensions of the cylinder (approximately 2 nm by 1 nm) played an important role, as increasing the chain length between the diphenyl core and the pyridine rings resulted in a much smaller coiling effect.[85] Cellulose column chromatography has been used to separate the M and P enantiomers of $Fe_2L_3Cl_4$.[86] The importance of this helicity was highlighted by a series of optical DNA binding investigations which suggested that the M enantiomer binds to the major groove of B-DNA, while the P isomer binds randomly along the backbone.[87] $Fe_2L_3Cl_4$ demonstrates antiproliferative activity in a range of cancer cell lines, including those derived from human breast and ovarian cancers, as well as leukaemia.[83] The antiproliferative activity of $Fe_2L_3Cl_4$ was also tested against a non-cancerous cell line, and was found to show comparable activity. This observation indicates that $Fe_2L_3Cl_4$ has no inherent selectivity to target cancer cells over healthy cells, which is an ongoing challenge with chemotherapy. This study did show that the activity of $Fe_2L_3Cl_4$ is comparable to that of carboplatin. Yet unlike the platinum agents discussed in section 1.2.1, the cylinder did not show any evidence of DNA cleavage which suggests that metal coordination to nucleobases does not feature in its mechanism of action.

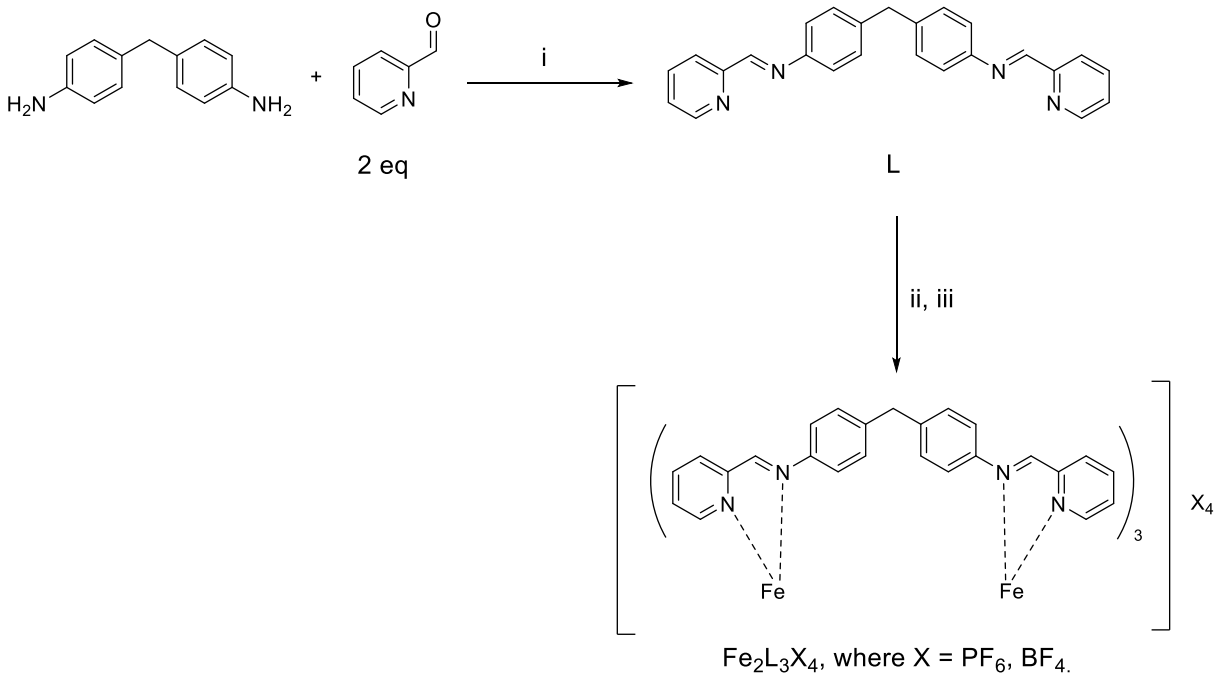

Scheme 1.1 Reported synthesis of Hannon's $Fe_2L_3X_4$ cylinder as reported in reference 82. (i) EtOH, RT, 8 h; (ii) $FeCl_2$, MeOH, reflux, 4 h; (iii) NH_4X.

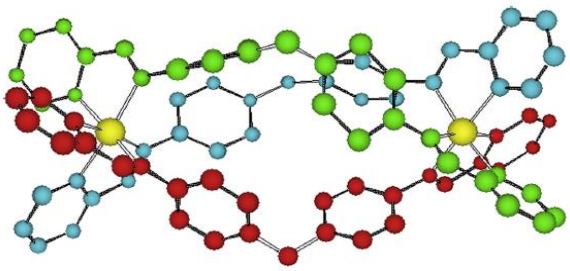

Figure 1.28 A representation of the crystal structure of the $[Fe_2L_3]^{4+}$ cation. The metal ions are represented by yellow spheres, and the framework of each ligand is shown in a different colour. Taken from reference 83 with permission.

Further insight into the cylinder's antiproliferative activity may be given by its ability to induce the formation of DNA 3WJs. This behaviour was discovered through co-crystallisation of the racemic cylinder with palindromic hexanucleotides.[68] The crystal structure obtained showed 3WJ-cylinder adducts with the cylinder nestled in the branch point (Figure 1.29). By comparing crystal structures of the free cylinder to that found in the 3WJ adduct, it was

observed that the cylinder had not undergone any notable structural change upon binding. Similarly, the crystal structure of the 3WJ almost perfectly overlays that of a 3WJ bound to a *Cre* recombinase protein. This indicates that the geometry of the cylinder is perfectly suited to stabilising a DNA 3WJ at the branch point. A comprehensive NMR study of $Fe_2L_3Cl_4$ and this 3WJ suggested that the adduct remains intact in solution, with observed shifts of the phenyl proton signals suggesting that there is substantial π-π interactions with the six nucleobases at the branch point.[88]

.

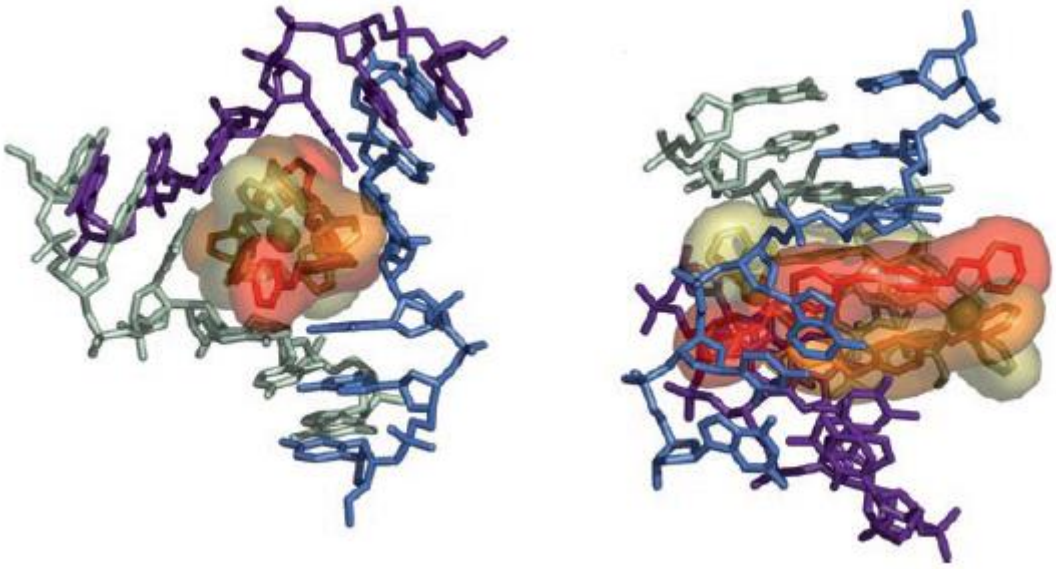

Figure 1.29 Representations of $[Fe_2L_3]^{4+}$ at the heart of a DNA 3WJ, viewing the cylinder head on (left) and when viewed from the side (right). Adapted from reference 68 with permission.

The unprecedented binding of the cylinder to a 3WJ led Hannon and coworkers to develop analogues of $Fe_2L_3Cl_4$, varying both the metal centres and the structure of the ligands. The properties of both the $Ru_2L_3Cl_4$ and $Ni_2L_3Cl_4$ are of particular interest. The inherent photoluminescent properties of $Ru_2L_3Cl_4$ were shown to be enhanced upon binding to B-DNA.[89] This enhanced photoluminescence, in combination with the kinetic inertness of the Ru centres, gives it exciting potential to be used in microscopy investigations in cellular models. The cellular accumulation of $Ru_2L_3Cl_4$ could be tracked, with its stability granting confidence that any antiproliferative effect observed would be due to the intact complex rather than its constituent parts. However, due to the inert nature of Ru(II), the purification steps required to isolate the discrete helicate (the thermodynamic product) from the

polymeric by-products (the kinetic products) are laborious, giving analytically pure yields of less than 1%. This labour intensive procedure has been a hurdle to further investigations. Fortunately, $Ni_2L_3Cl_4$ is as straight forward to synthesise as $Fe_2L_3Cl_4$. Qu and coworkers have shown that the P enantiomer of $Ni_2L_3Cl_4$ selectively induces formation of GQ in the human telomeric sequence.[90] Such a stabilising effect is not observed with other GQ sequences, and the M enantiomer is inactive. More recently, Hannon and McKeating have reported that both $Ru_2L_3Cl_4$ and $Ni_2L_3Cl_4$ bind to Trans Activation Response (TAR) RNA, a looped structure found in the genome of HIV.[91] Both cylinders are believed to bind to a three nucleobase bulge region of TAR RNA, with the binding sufficiently strong to outcompete the binding of ADP-1, a synthetic peptide that mimics the binding site of the transactivator (TAT) protein. When the virus invades a host cell, TAT recognises the TAR bulge and initiates viral transcription. This RNA binding presents an interesting new application for these cylinders as antiviral agents.

Swapping the metal centre for Cu(I) produces double stranded dicationic cylinders with the general formula $Cu_2L_2X_2$, which can from the meso (box shaped) isomer or the rac (helical) isomer (Figure 1.30). Incorporating ethyl substituents on the phenyl rings, ligand L' (Figure 1.30) favours the helicate form as this avoids the steric clash that would result between the ethyl groups if the rings occupied the same plane. $Cu_2L'_2Cl_2$ has shown DNA cleaving properties when irradiated with light.[92] The presence of peroxide is required, suggesting that DNA cleavage occurs due to the generation of reactive oxygen species. As part of this study, the Cu(I) cylinder did not demonstrate the supercoiling effect observed with $Fe_2L_3Cl_4$, indicating that the high 4+ charge of the latter is an important contributor to this behaviour.

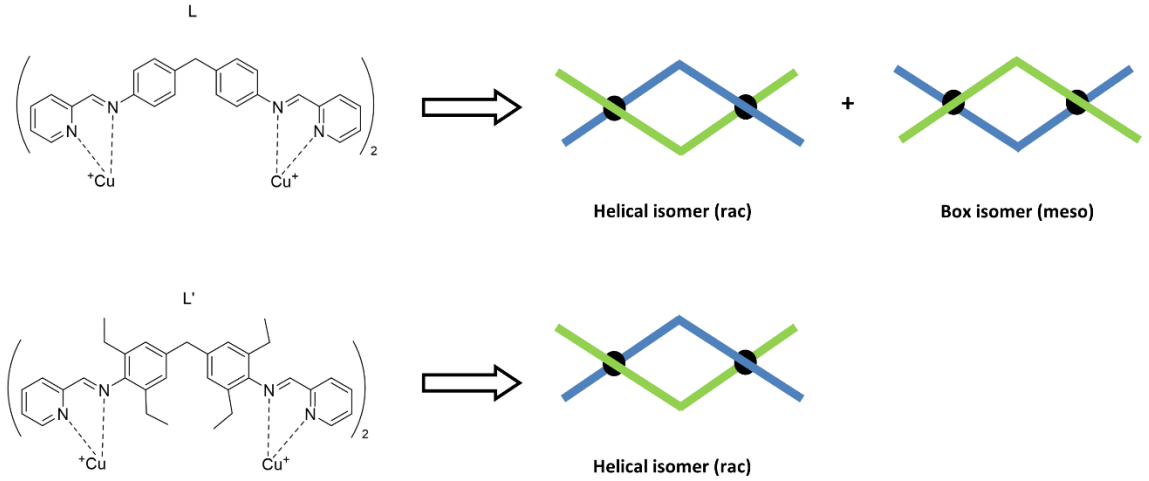

Figure 1.30 Illustration of *meso* (box shaped) and *rac* (helical) isomers of double stranded cylinders. The black spheres represent the metal centres, with the green and blue strands representing the two ligands. A double stranded helicate using ligand L gives a mixture of the two isomers, while using ligand L' results in just the helical isomer being formed.

1.4.1.2 Other helicates

As already discussed, one of the hurdles with using Hannon's cylinders is that the synthesis generates two helical isomers (right-handed *P* and left-handed *M*) which have different binding modes. While these can be separated on cellulose, this separation can be time consuming. Scott and coworkers synthesised a similar diamine ligand that incorporates chirality by using 2- phenylglycinol units in the structure (L^{1a}, Figure 1.31a).[93] Using the (*R*)-phenylglycinol unit in the ligand structure generated the Δ,Δ Fe complex exclusively, while using the (*S*)-isomer generated the Λ,Λ orientation. Due to the flexible nature of the linker used, the crystal structure reveals that the ligands do not wrap around the metal-metal axis as they do with Hannon's cylinders. To distinguish this class of compounds, Scott termed them "flexicates". Scott investigated the DNA binding properties of Fe(II) and Zn(II) flexicates with L^{1a}, as well as analogues using a aliphatic chain in the linker (L^2, Figure 1.31b). Flexicates with L^{1a} demonstrated a specific binding mode with dsDNA, assumed to be major groove binding based on the flexicate's dimensions. The other flexicates showed a non-specific binding interaction. Scott has gone on to demonstrate that both the Λ- and the Δ-Fe flexicates with L^{1a} stabilise 3WJ structures,[94] although to a lesser extent than Hannon's helicates, likely due to having less aromatic surface in the linker. An interesting finding from this study was

the observation that the Λ-flexicate stabilised a T-shaped 3WJ, whereas the Δ-flexicate did not. This was the first report of a synthetic binding agent distinguishing between different shapes of 3WJ structure. Related flexicates have demonstrated antiproliferative activity on some cancerous cell lines, comparable to cisplatin, [95] which led to further efforts to develop new flexicate analogues. Scott's latest work has shown that the flexicates are stable to post-assembly modifications (that is, performing reactions on a pre-assembled complex).[96] Cu(I) catalysed alkyne-azide cyloaddition (CuAAC) "click" chemistry was performed on alkyne functionalised flexicates. Scott has shown that that flexicates clicked with aryl groups show increased cytotoxic selectivity for HCT116 (colorectal) cancer cells over ARPE-19 (retinal) non-cancerous cells.

Crowley and coworkers have also reported the use of CuAAC reactions in the design of helicate ligands. They reported a dinuclear Ru(II) triple stranded helicate, with ligands formed of two pyridine rings connected to a central phenyl ring by 1,2,3-triazoles (Figure 1.32a).[97] Yields as high as 58% were reported using a microwave synthetic procedure, dramatically different to the <1% yields reported by Hannon and coworkers with the synthesis of their Ru(II) cylinder.[89] Crowley's Ru(II) helicate showed antimicrobial activity and presumably further biological testing is ongoing. More recently, Crowley and coworkers have reported a related Co(III) helicate, with the two triazole units of the ligand linked together by a methylene group (Figure 1.32b). This helicate showed no antimicrobial activity, leading the authors to conclude that the 6+ charge was too high to cross the bacterial cell membranes.[98]

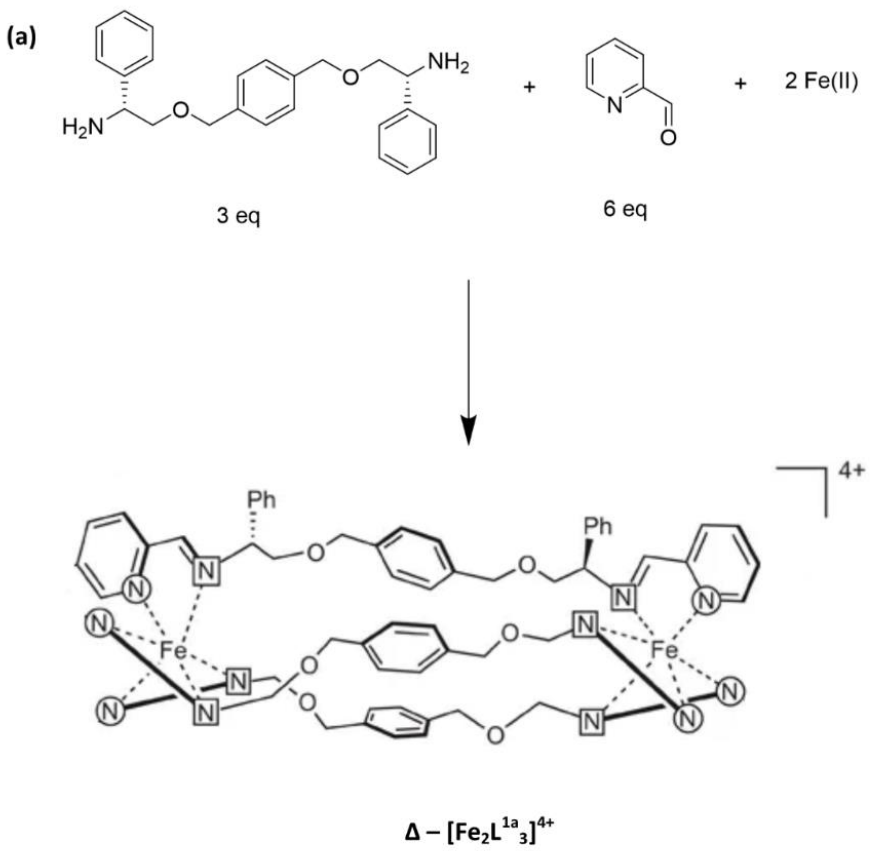

Figure 1.31 (a) Schematic showing the structure of Scott's ΔFe-L^{1a} flexicate, and the constituent reagents used to synthesise this. (b) Ligand L^2, which has a flexible linker between the two binding sites. Adapted from reference 93 with permission.

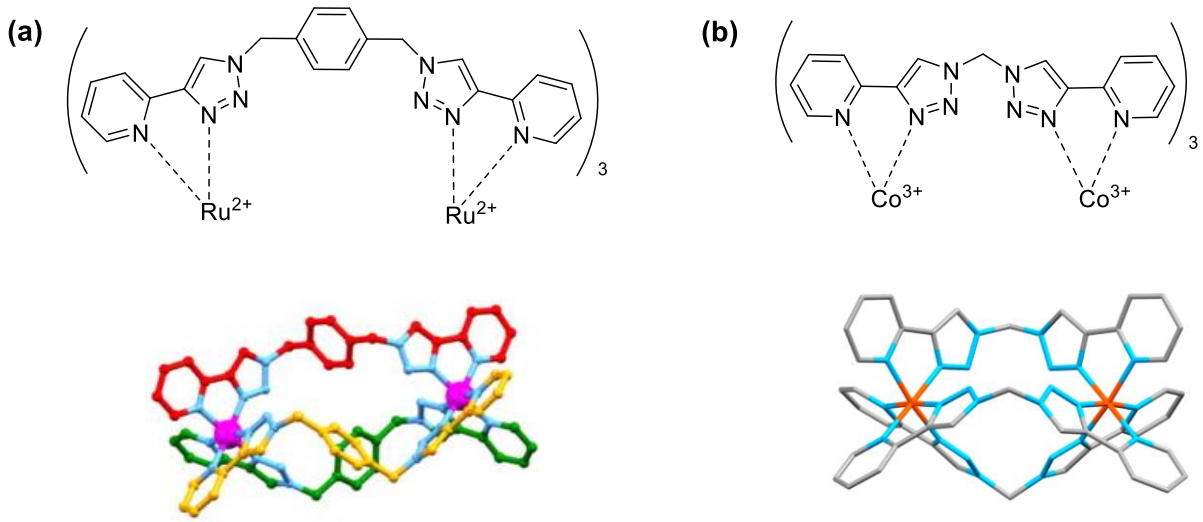

Figure 1.32 Structure of Crowley's helicates. (a) Ru(II) helicate with aromatic linker; (b) Co(III) helicate with methylene linker. Crystal structure representations adapted from references 97 and 98 respectively, with permission.

Patroniak and coworkers have synthesised dinuclear double-stranded helicate complexes of Cu(I) and Ag(I) using the dimethylquaterpyridine ligand shown in Figure 1.33.[99] The rigidity of the ligand and the tetrahedral geometry of the coordinated metals result in the formation of the helicate isomer rather than the box shaped isomer. Interactions with B-DNA were observed, and computational modelling studies suggested that these helicates could bind to either the major or minor grooves of B-DNA. This binding is stabilised through π-π stacking and face-edge π interactions between the nucleobases and the exposed aromatic surfaces at the ends of the helicate, rather than those in the core of the helicate structure as is the case with Hannon's cylinders.

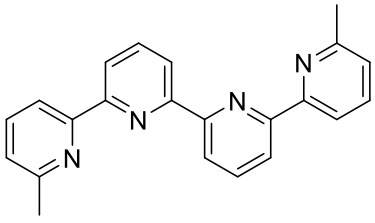

quaterpyridine ligand

Figure 1.33 The quaterpyridine ligand used to make Patroniak's dinuclear double stranded Ag(I) and Cu(I) helicates.

1.4.2 Supramolecular metallocages

Supramolecular metallocages are another class of supramolecular architecture that has demonstrated interesting DNA binding properties. Specifically, there are relatively recent reports of tetrahedral cages demonstrating binding to GQs and 3WJs. Tetrahedral cages feature four octahedral metal centres, coordinated with three bidentate moieties from different ligands. These ligands are similar to those of the helicates, in that they have two bidentate coordination sites but the ligands are straighter in shape which gives a tetrahedral topology as shown in Figure 1.34.[79] Gu and coworkers have reported on two $[Ni_4L_6]^{8+}$ cages (one incorporating flexible aliphatic linkers in the ligand structure and the other with rigid linkers) that stabilise GQ structures *in vitro*. [79,100] The large dimensions of the cage prevent any specific binding to the structure of dsDNA, giving the cages impressive selectivity for GQ structures.

Recent efforts by Nitschke and co-workers have also investigated biological applications of metallocages. Nitschke has demonstrated that the central cavity of a fluorescent 4 Zn(II) tetrahedral cage can host biologically relevant species such as adenosine mono- and tri-phopshate.[101] Binding of such species resulted in quenching of the fluorescence, which gives this cage potential use as a biosensor. Nitschke has also published on a $[Fe_4L_4]^{8+}$ tetrahedal cage, which has trigonal shaped ligands with three imine-pyridine binding moieties (Figure 1.35).[102] This cage was found to quench the fluorescence of 6-carboxyfluorescein (FAM), and so the effect of the cage on various DNA structures labelled with FAM was investigated. Based on the measured fluorescence, Nitschke concluded that this cage stabilised a 3WJ to a higher degree than dsDNA or 4WJ. Further investigations showed that increasing the distance between the FAM label and the branching point resulted in less of a quenching effect, indicating that the branch point was the likely site of binding for the metallocage.

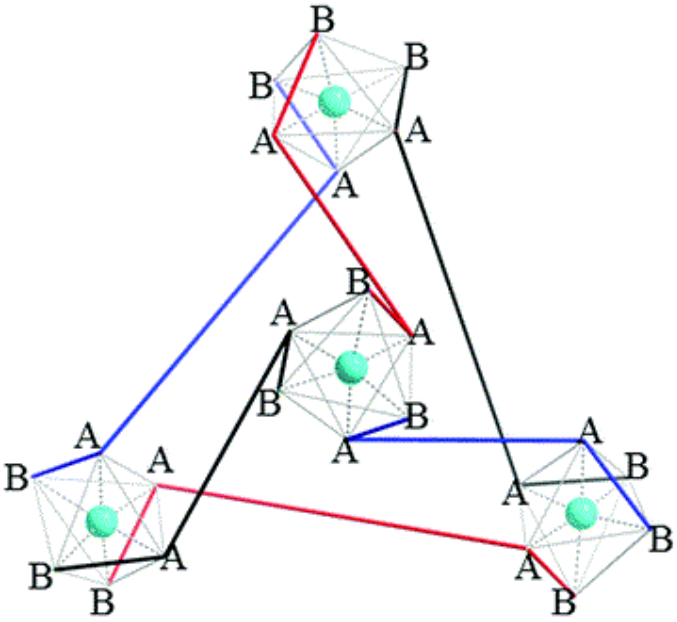

Figure 1.34 Schematic representation of the structure of a M_4L_6 supramolecular cage. The octahedral metal centres are represented by blue spheres, with the coloured lines representing the ligands. Adapted from reference 79 with permission.

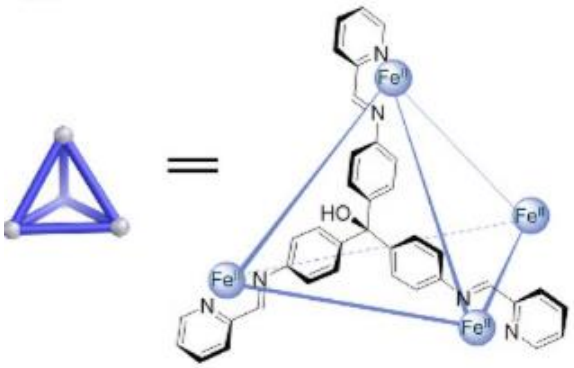

Figure 1.35 Schematic of the structure of Nitschke's DNA binding $[Fe_4L_4]^{8+}$ metallocage. Adapted from reference 102 with permission.

1.5 Functionalisation of metallosupramolecular cylinders

While the 3WJ binding properties of $Fe_2L_3Cl_4$ offers exciting potential as an alternative cancer therapeutic, the cylinder does not show any selectivity in targeting cancer cells over healthy cells. Previous work in the Hannon group has produced functionalised analogues of $Fe_2L_3Cl_4$ in an attempt to overcome this challenge. Biological receptor targeting moieties have been incorporated in the ligand structure which have an affinity for receptors that are commonly over-expressed by cancerous cells. Other conjugation has aimed to control which helical enantiomer is formed upon coordination of the ligands to the metal centres, or to introduce anchors that attach to nanoparticle surfaces. Examples of relevant functionalised cylinders will be discussed in this section. In these examples, functionalisation has occurred at the 5-position of the pyridine ring (Figure 1.36) as this should minimise any interference with the binding interactions between the cylinder's core phenyl rings and the nucleobases at the branch point of the 3WJ.

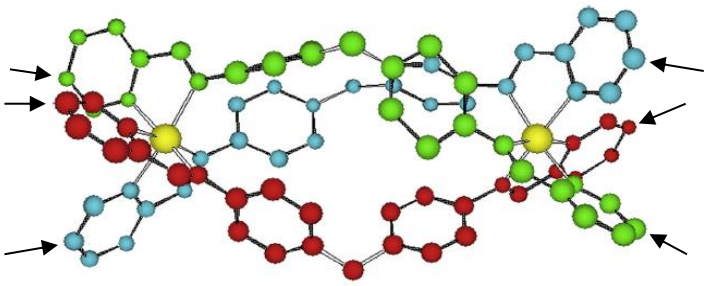

Figure 1.36 Schematic of $[Fe_2L_3]^{4+}$, with arrows indicating the 5-position of each pyridyl ring. Functionalisation at these points should offer minimal interference with the interactions between the cylinder's core and the 3WJ. Adapted from reference 83 with permission.

1.5.1 Conjugation with amino acids

Cardo and Hannon have reported conjugating the cylinder with arginine amino acids using the ligands shown in Figure 1.37.[103] Arginine is an attractive conjugate, as it is the amino acid residue that features most prominently in nucleic acid protein binding domains, largely due

to its stable positive charge at physiological pH.[1] There is a precedent for arginine moieties improving both the cellular uptake and localisation of organometallic agents at the nucleus.[104] By incorporating both L- and D-arginine onto the ligand, it was discovered that the chirality at the α-carbon of the amino acid influenced the helicity of the formed helicate. The ligand incorporating L-arginine formed the *P* enantiomer, and that with the D-arginine formed the *M* enantiomer. In addition, gel electrophoresis studies of both the L-Arg and D-Arg conjugated cylinders showed that 3WJ binding activity was maintained. Both cylinders were shown to have a higher antiproliferative activity than $Fe_2L_3Cl_4$ in an ovarian cancer cell line (A2780). This work showed that it is possible to positively affect both the chemical and biological features of cylinders using smart functionalisation. However, the conjugated complexes are less stable in solution than $Fe_2L_3Cl_4$, which is likely due to having three positive charges in close proximity to each other at each cylinder end.[105]

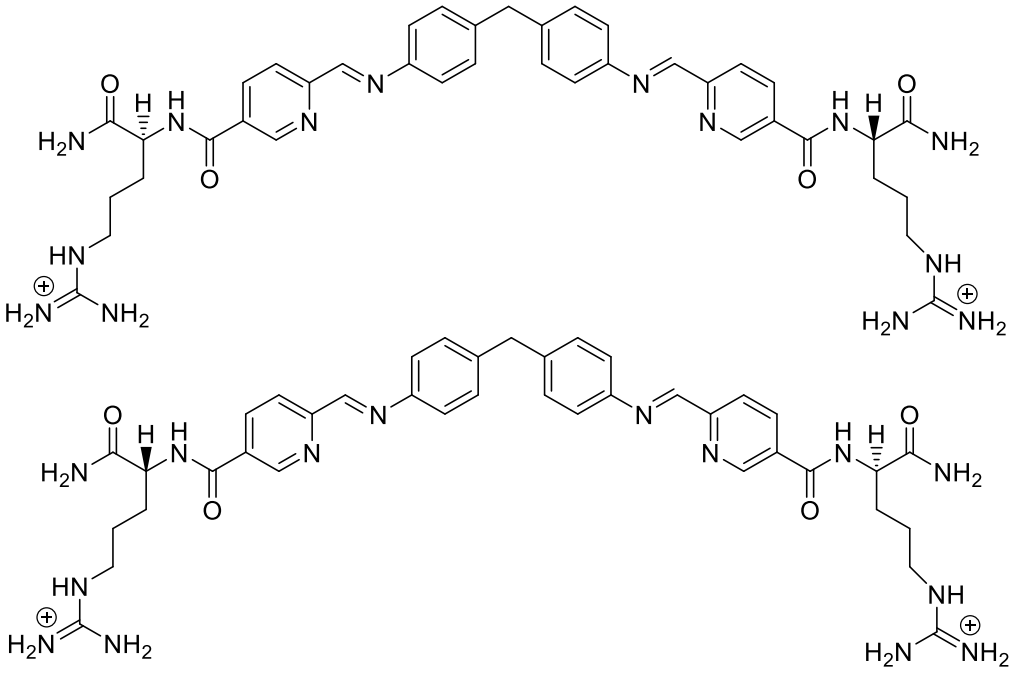

Figure 1.37 Cylinder ligands incorporating L-Arg (upper) and D-Arg (lower) connected through the 5-position of the pyridyl ring.

1.5.2 Conjugation with receptor targeting moieties

Various cancers are associated with overexpression of cell surface receptors, such as estrogen and folate receptors.[106] This overexpression has driven efforts to conjugate moieties with a high affinity for these receptors to known anti-cancer therapeutics, especially platinum based agents.[107] While direct coordination of estradiol to a platinum centre did not result in an observed affinity for estrogen receptors,[108] hope in this targeting strategy remained after Lippard and coworkers reported some success. They coordinated estrogen moieties in the axial positions of a Pt(IV) prodrug, which released cisplatin when reduced by intracellular reductases. Lippard quoted a 2-fold increase in activity in an estrogen receptor positive (ER+) cell line, compared to a line that did not express the receptor (ER-). Very recently, Griffith and coworkers conjugated estrogens onto Pt(II) through CuAAC click chemistry, and have demonstrated a 30-fold selectivity for ER+ cancer cells over an ER- line.[106] The conjugation of testosterone and estrogen onto cylinders using the ligands shown in Figure 1.38 has been achieved through use of Sonagashira coupling.[109] Disappointingly, these cylinders proved to have low solubility in water, preventing assessment of their cellular cytotoxicity. However they were soluble upon addition of methanol, which allowed DNA binding studies to be performed. While binding to B-DNA was observed, the steroid functionalised cylinders did not appear to bind to 3WJs, presumably as there is too much steric bulk at the ends of the cylinder which clashes with the helices of the 3WJ arms.

Sonagashira coupling has also been used to conjugate carbohydrates onto the cylinder.[109] Glucose transporter membrane proteins are overexpressed by many types of tumour cells, in efforts to take up as much sugars as possible to generate the ATP required for their survival.[110] Using sugars as pilot molecules for the delivery of anti-cancer agents has been an active area of research for the last two decades.[111] It was thought that the conjugated sugar moiety would also maintain this cylinder's aqueous solubility, which was a key problem with the hormone-functionalised cylinders. Cylinders were synthesised with ligands incorporating acetyl β-D-glucosaminide and hydroxyl β-D-glucosaminide (Figure 1.39). While the analogue with the free hydroxyl groups proved to be water soluble, it's stability in aqueous solution was very low. This instability is likely due to steric clash at each end of the cylinder, where three bulky sugars are brought close together when coordinated to the metal centres.

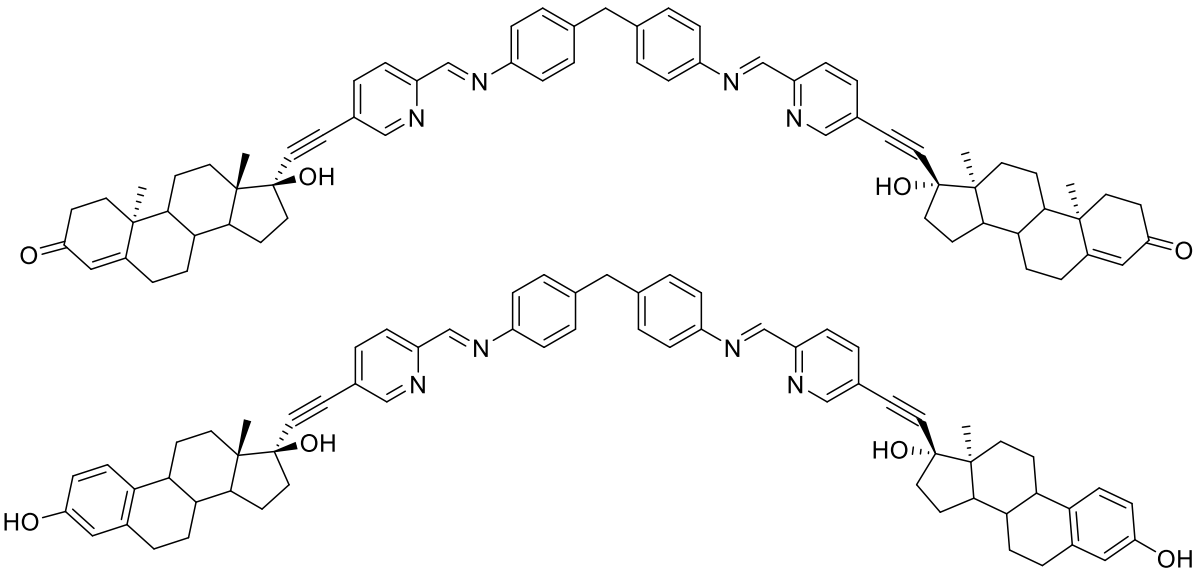

Figure 1.38 Cylinder ligands functionalised with testosterone (upper) and estrogen (lower) moieties in the 5-position of the pyridine rings.

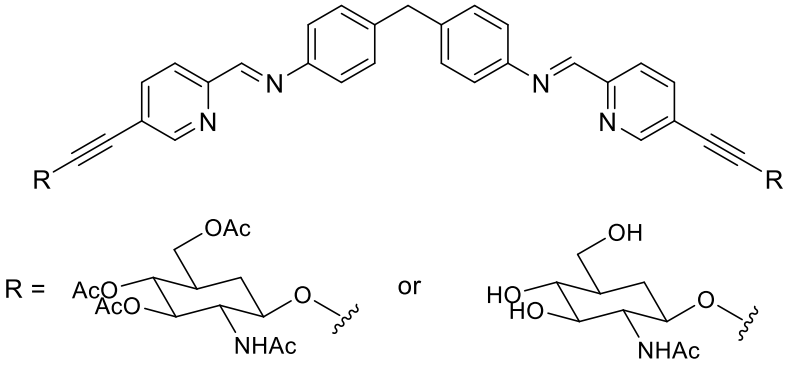

Figure 1.39 Structure of cylinder ligands functionalised with sugar moieties. Acetyl β-D-glucosaminide (left) and hydroxyl β-D-glucosaminide (right).

1.5.3 Functionalised cylinders for nanoparticle attachment

Cylinder analogues have been synthesised that incorporate sulfide linkers (Figure 1.40) for attachment to the surface of gold nanoparticles (AuNPs).[112] The rationale behind this was that by attaching cylinders to a surface, high local concentrations of cylinder could be achieved in solution. A high local concentration of cylinder could result in multiple DNA interactions occurring simultaneously, which may demonstrate a cooperative binding effect similar to that of a protein with multiple zinc fingers binding to major grooves of B-DNA.[30] CuAAC click chemistry was used to attach thioacetate chains to the cylinder ligand. The ligand with the long alkyl chain had poor aqueous solubility, which led to the substitution of the alkyl chain with a poly-ethylene glycol chain. This cylinder was soluble in acetonitrile when the $(BF_4)^-$ counterion was used. This thioacetate functionalised cylinder was shown to induce formation of 3WJs and proved even more potent in a breast cancer cell line than $Fe_2L_3Cl_4$, with an IC_{50} value comparable to that of cisplatin. While successful attachment to AuNPs was achieved, ellipsometry indicated that the cylinders were lying flat along the gold surface. This structural feature arose as both ends of the cylinder were binding to the gold surface, resulting in an observed decrease in DNA affinity and increased aggregation of the AuNPs.

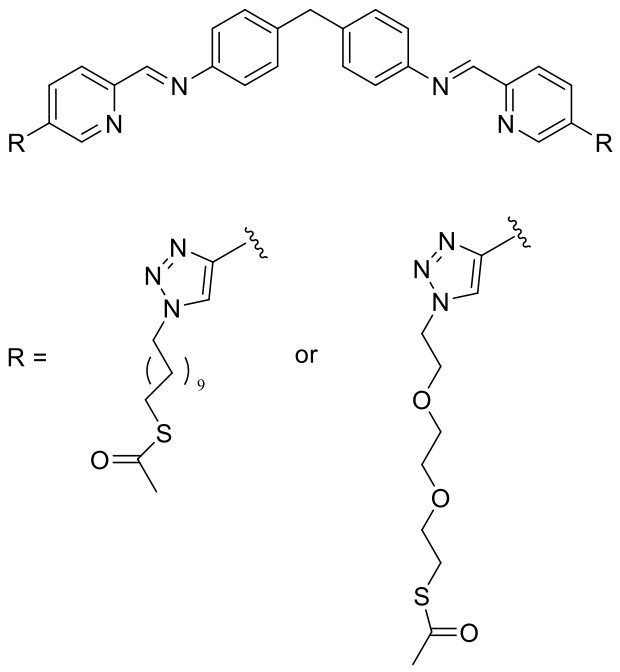

Figure 1.40 Structures of cylinder ligands functionalised with thioacetate chains for binding to gold nanoparticles. The chains are attached to the pyridyl rings using 1,2,3-triazoles.

1.6 Overview and Project Aims

Nucleic DNA contains genetic information that dictates cellular function. Abnormal behaviour of DNA underpins many diseases including cancers, and designing therapeutics to directly target affected DNA is an attractive prospect. Traditional agents that recognise B-DNA do so by forming covalent adducts with the nucleobases, intercalating between base pairs, or by binding to the grooves of the helical structure. The discovery of non-canonical DNA structures has led to efforts in developing new synthetic agents that specifically bind to these structures. Supramolecular metallohelicates are receiving considerable attention for their DNA binding properties. Hannon's dinuclear triple stranded helicates have demonstrated an unprecedented binding to DNA three-way junctions, which resemble DNA replication forks and thus offer potential as a cancer therapeutic that binds to an active form of DNA.

However, there is nothing inherent about the design of these cylinders that could make them selectively target cancerous cells over healthy ones. As such, if it were to reach a clinical setting, it is expected that they would show similar adverse side effects to the widely used platinum chemotherapeutics used globally in cancer treatment regimens today. While functionalisation of the original cylinder structure may offer a solution, efforts to produce functionalised analogues of $Fe_2L_3Cl_4$ (Hannon's most studied cylinder) have thus far faced two sizeable hurdles. Firstly, all functionalisation efforts have produced cylinder analogues with diminished stability in solution, which is likely a consequence of bringing together too much steric bulk at the ends of the cylinder or by bringing together repellent charges. Secondly, aqueous solubility has decreased due to increasing the size of the lipophilic ligands.

The work described in this thesis aims to address these hurdles by adopting strategies that could minimise the unfavourable effects that produce them. Chapter 2 details work undertaken towards synthetically "capping" the cylinder, such that the three sites of functionalisation at each end of the cylinder are replaced by just one. The rationale behind this is that any unfavourable steric or electrostatic effects between the ligands would be removed, and that through anchoring the ligands together the cylinder's stability would increase. A key requirement was that the synthetic cap would have a functional head group, to which a useful functionality (for example, a receptor targeting molecule or a fluorescent group) could be attached. Chapter 3 describes the development of a cylinder functionalised

with azide groups. The goal here is to use these cylinders in post-assembly cycloaddition reactions with alkynes. Such reactions are considered biorthogonal: as alkynes and azides are not naturally present in cells, no cellular machinery should prevent these reactions from occurring *in vivo*. Both areas of work are new to the Hannon group, and the work presented represents a solid stepping stone towards achieving both goals.

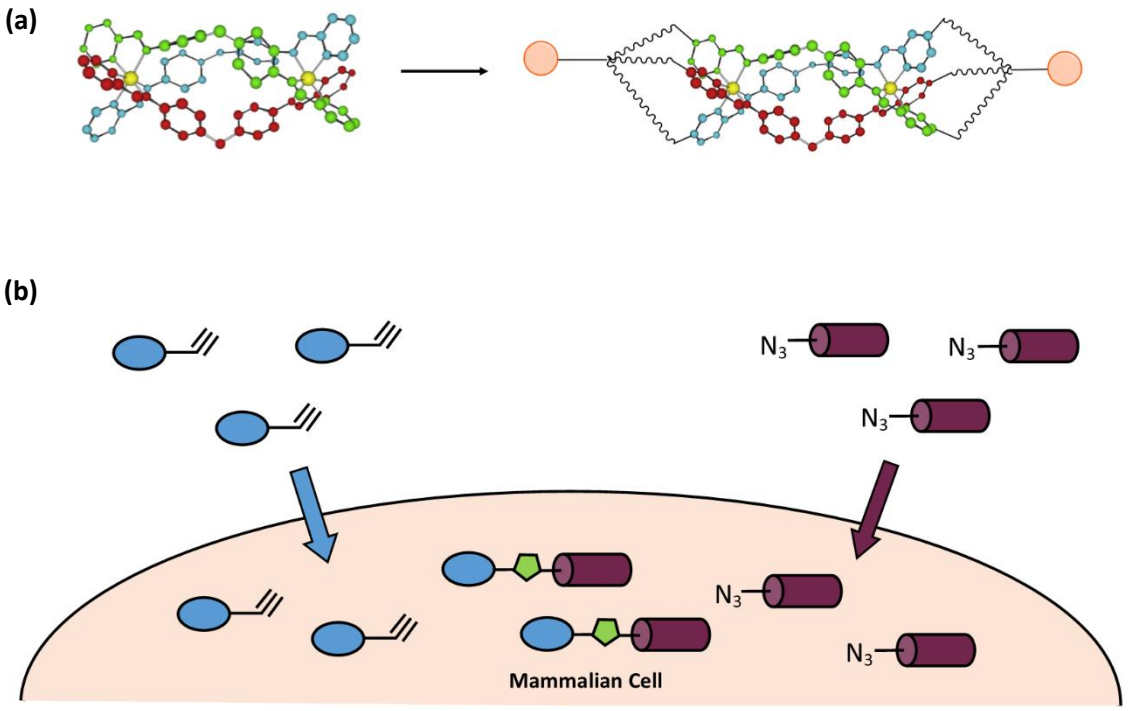

Figure 1.41 Illustration highlighting the two main aims of the thesis. (a) Capping each end of a $[M_2L_3]^{4+}$ cylinder, replacing three sites of functionalisation with just one. Functional head groups are represented by orange spheres; (b) Illustration of a biorthogonal reaction between a functional alkyne (blue) and a cylinder functionalised with azide groups (purple). If each compound is incubated with cells one after the other, the two compounds can react within the cell, connecting the cylinder to the alkyne's functionality.

1.7 References

1 S. Neidle, *Nucleic Acid Structure and Recognition*, Oxford University Press, Oxford, 2002.

2 L. Stryer, *Biochemistry*, W. H. Freeman and Company, New York, Third., 1988.

3 J. D. Watson and F. H. C. Crick, *Nature*, 1953, **171**, 737–738.

4 R. Oun, Y. E. Moussa and N. J. Wheate, *Dalt. Trans.*, 2018, **47**, 6645–6653.

5 M. El-Khateeb, T. G. Appleton, L. R. Gahan, B. G. Charles, S. J. Berners-Price and A.-M. Bolton, *J. Inorg. Biochem.*, 1999, **77**, 13–21.

6 L. Kelland, *Nat Rev Cancer*, 2007, **7**, 573–584.

7 E. Wong and C. M. Giandomenico, *Chem. Rev.*, 1999, **99**, 2451–2466.

8 L. Galluzzi, L. Senovilla, I. Vitale, J. Michels, I. Martins, O. Kepp, M. Castedo and G. Kroemer, *Oncogene*, 2012, **31**, 1869–1883.

9 A. Nemirovski, Y. Kasherman, Y. Tzaraf and D. Gibson, *J. Med. Chem.*, 2007, **50**, 5554–5556.

10 D. Gibson, *J. Inorg. Biochem.*, 2019, **191**, 77–84.

11 A. Bhargava and U. N. Vaishampayan, *Expert Opin. Investig. Drugs*, 2009, **18**, 1787–1797.

12 M. Ravera, E. Gabano, M. J. McGlinchey and D. Osella, *Inorganica Chim. Acta*, 2019, **492**, 32–47.

13 H. Kostrhunova, E. Petruzzella, D. Gibson, J. Kasparkova and V. Brabec, *Chem. – A Eur. J.*, 2019, **25**, 5235–5245.

14 P. A. Vekariya, P. S. Karia, B. S. Bhatt and M. N. Patel, *Appl. Biochem. Biotechnol.*, 2019, **187**, 556–569.

15 A. Gilewska, B. Barszcz, J. Masternak, K. Kazimierczuk, J. Sitkowski, J. Wietrzyk and E. Turlej, *JBIC J. Biol. Inorg. Chem.*, 2019, **24**, 591–606.

16 N. K.S., J. Eswaran, T. M., B. Nattamai S.P, N. M.A. and K. M. Velusamy, *Appl. Organomet. Chem.*, 2019, **33**, e4751.

17 R. Gandhaveeti, R. Konakanchi, P. Jyothi, N. S. P. Bhuvanesh and S. Anandaram, *Appl. Organomet. Chem.*, 2019, **33**, e4899.

18 H. Chen, J. A. Parkinson, S. Parsons, R. A. Coxall, R. O. Gould and P. J. Sadler, *J. Am. Chem. Soc.*, 2002, **124**, 3064–3082.

19 M. Martínez-Alonso, N. Busto, F. A. Jalón, B. R. Manzano, J. M. Leal, A. M. Rodríguez, B. García and G. Espino, *Inorg. Chem.*, 2014, **53**, 11274–11288.

20 H. J. Lozano, N. Busto, G. Espino, A. Carbayo, J. M. Leal, J. A. Platts and B. García, *Dalt. Trans.*, 2017, **46**, 3611–3622.

21 L. S. Lerman, *J. Mol. Biol.*, 1961, **3**, 18–30.

22 J. C. Thomes, G. Weill and M. Daune, *Biopolymers*, 1969, **8**, 647–659.

23 J. L. Bresloff and D. M. Crothers, *J. Mol. Biol.*, 1975, **95**, 103–123.

24 A. H. J. Wang, G. Ughetto, G. J. Quigley and A. Rich, *Biochemistry*, 1987, **26**, 1152–1163.

25 A. E. Friedman, J. C. Chambron, J. P. Sauvage, N. J. Turro and J. K. Barton, *J. Am. Chem. Soc.*, 1990, **112**, 4960–4962.

26 B. M. Zeglis, V. C. Pierre and J. K. Barton, *Chem. Commun.*, 2007, 4565–4579.

27 N. Nambagari, S. Perka, R. K. Vuradi and S. Satyanarayana, *Nucleosides, Nucleotides and Nucleic Acids*, 2019, **38**, 400–417.

28 B. J. Pages, K. B. Garbutcheon-Singh and J. R. Aldrich-Wright, *Eur. J. Inorg. Chem.*, 2017, 1613–1624.

29 N. P. Pavletich and C. O. Pabo, *Science (80-.).*, 1991, **252**, 809–817.

30 N. P. Pavletich and C. O. Pabo, *Science (80-.).*, 1993, **261**, 1701–1707.

31 F. J. Scott, M. Puig-Sellart, A. I. Khalaf, C. J. Henderson, G. Westrop, D. G. Watson, K.

Carter, M. H. Grant and C. J. Suckling, *Bioorg. Med. Chem. Lett.*, 2016, **26**, 3478–3486.

32 A. A. Kurmis, F. Yang, T. R. Welch, N. G. Nickols and P. B. Dervan, *Cancer Res.*, 2017, **77**, 2207–2212.

33 D. Rhodes and H. J. Lipps, *Nucleic Acids Res.*, 2015, **43**, 8627–8637.

Figure 1.12 reprinted from D. Rhodes, H.J. Lipps, G-quadruplexes and their regulatory roles in biology, *Nucleic Acids Research,* 2015, **43**, 18, 8627-8637, by permission of Oxford University Press.

34 N. V Hud, F. W. Smith, F. A. L. Anet and J. Feigon, *Biochemistry*, 1996, **35**, 15383–15390.

35 N. W. Kim, M. A. Piatyszek, K. R. Prowse, C. B. Harley, M. D. West, P. L. Ho, G. M. Coviello, W. E. Wright, S. L. Weinrich and J. W. Shay, *Science (80-.).*, 1994, **266**, 2011–2015.

36 D. Sun, B. Thompson, B. E. Cathers, M. Salazar, S. M. Kerwin, J. O. Trent, T. C. Jenkins, S. Neidle and L. H. Hurley, *J. Med. Chem.*, 1997, **40**, 2113–2116.

37 S. Neidle, *J. Med. Chem.*, 2016, **59**, 5987–6011.

38 R. Vilar, *Metallo-Drugs: Development and Action of Anticancer Agents*, De Gruyter, Berlin, Boston, 2018.

39 D. F. Shi, R. T. Wheelhouse, D. Sun and L. H. Hurley, *J. Med. Chem.*, 2001, **44**, 4509–4523.

40 J. E. Reed, A. A. Arnal, S. Neidle and R. Vilar, *J. Am. Chem. Soc.*, 2006, **128**, 5992–5993.

41 R. F. Pasternack, E. J. Gibbs and J. J. Villafranca, *Biochemistry*, 1983, **22**, 2406–2414.

42 E. Boschi, S. Davis, S. Taylor, A. Butterworth, L. A. Chirayath, V. Purohit, L. K. Siegel, J. Buenaventura, A. H. Sheriff, R. Jin, R. Sheardy, L. A. Yatsunyk and M. Azam, *J. Phys. Chem. B*, 2016, **120**, 12807–12819.

43 X. Yao, D. Song, T. Qin, C. Yang, Z. Yu, X. Li, K. Liu and H. Su, *Sci. Rep.*, 2017, **7**, 10951.

44 A. Ali, M. Kamra, S. Roy, K. Muniyappa and S. Bhattacharya, *Bioconjug. Chem.*, 2017, **28**, 341–352.

45 S. Bandeira, J. Gonzalez-Garcia, E. Pensa, T. Albrecht and R. Vilar, *Angew. Chemie - Int. Ed.*, 2018, **57**, 310–313.

46 K. Gehring, J.-L. Leroy and M. Guéron, *Nature*, 1993, **363**, 561–565.

47 M. Zeraati, D. B. Langley, P. Schofield, A. L. Moye, R. Rouet, W. E. Hughes, T. M. Bryan, M. E. Dinger and D. Christ, *Nat. Chem.*, 2018, **10**, 631–637.

Figure 1.15b reprinted by permission from Springer Nature Customer Service Centre GmbH: *Nature Chemistry*, I-motif DNA structures are formed in the nuclei of human cells, M. Zeraati, D. B. Langley, P. Schofield, A. L. Moye, R. Rouet, W. E. Hughes; T. M. Bryan; M. E. Dinger & D. Christ, **10**, pages 631-637, Copyright (2018).

48 H. A. Day, P. Pavlou and Z. A. E. Waller, *Bioorg. Med. Chem.*, 2014, **22**, 4407–4418.

Figure 1.15c reprinted from *Bioorganic & Medicinal Chemistry*, **22**, H. A. Day, P. Pavlou, Z. A. E. Waller, i-Motif DNA: Structure, stability and targeting with ligands, page 4407-4418, Copyright (2014), with permission from Elsevier.

49 T. Simonsson, M. Pribylova and M. Vorlickova, *Biochem. Biophys. Res. Commun.*, 2000, **278**, 158–166.

50 S. Kendrick, H.-J. Kang, M. P. Alam, M. M. Madathil, P. Agrawal, V. Gokhale, D. Yang, S. M. Hecht and L. H. Hurley, *J. Am. Chem. Soc.*, 2014, **136**, 4161–4171.

51 O. Y. Fedoroff, A. Rangan, V. V Chemeris and L. H. Hurley, *Biochemistry*, 2000, **39**, 15083–15090.

52 P. Alberti, J. Ren, M. P. Teulade-Fichou, L. Guittat, J.-F. Riou, J. B. Chaires, C. Hélène, J.-P. Vigneron, J.-M. Lehn and J.-L. Mergny, *J. Biomol. Struct. Dyn.*, 2001, **19**, 505–513.

53 M. Debnath, S. Ghosh, A. Chauhan, R. Paul, K. Bhattacharyya and J. Dash, *Chem. Sci.*, 2017, **8**, 7448–7456.

54 J. L. Kadrmas, A. J. Ravin and N. B. Leontis, *Nucleic Acids Res.*, 1995, **23**, 2212–2222.

55 Y. Wang, J. E. Mueller, B. Kemper and N. C. Seeman, *Biochemistry*, 1991, **30**, 5667–5674.

56 R. Holliday, *Genet. Res.*, 1964, **5**, 282–304.

57 Y. Aylon and M. Kupiec, *DNA Repair (Amst).*, 2004, **3**, 797–815.

58 J. Reynolds, *Nat. Cell Biol.*, 2004, **6**, 184.

59 A. L. Brogden, N. H. Hopcroft, M. Searcey and C. J. Cardin, *Angew. Chemie Int. Ed.*, 2007, **46**, 3850–3854.

60 V. H. S. van Rixel, A. Busemann, M. F. Wissingh, S. L. Hopkins, B. Siewert, C. van de Griend, M. A. Siegler, T. Marzo, F. Papi, M. Ferraroni, P. Gratteri, C. Bazzicalupi, L. Messori and S. Bonnet, *Angew. Chemie Int. Ed.*, 2019, **58**, 9378–9382.

61 J. Christiansen, R. S. Brown, B. S. Sproat and R. A. Garrett, *EMBO J.*, 1987, **6**, 453–460.

62 M. R. Singleton, S. Scaife and D. B. Wigley, *Cell*, 2001, **107**, 79–89.

63 D. R. Duckett and D. M. Lilley, *EMBO J.*, 1990, **9**, 1659–1664.

64 Q. Guo, M. Lu, M. E. A. Churchill, T. D. Tullius and N. R. Kallenbach, *Biochemistry*, 1990, **29**, 10927–10934.

65 S. Vuong, L. Stefan, P. Lejault, Y. Rousselin, F. Denat and D. Monchaud, *Biochimie*, 2012, **94**, 442–450.

66 J. B. Welch, D. R. Duckett and D. M. J. Lilley, *Nucleic Acids Res.*, 1993, **21**, 4548–4555.

Figure 1.20 was reproduced from J. Welch, D. Duckett, Structures of bulged three-way DNA junctions, *Nucleic Acids Research,* 1993, **21**, 19, pages 4548-4555, by permission of Oxford University Press.

67 T. Sabir, A. Toulmin, L. Ma, A. C. Jones, P. McGlynn, G. F. Schröder and S. W. Magennis, *J. Am. Chem. Soc.*, 2012, **134**, 6280–6285.

68 A. Oleksi, A. G. Blanco, R. Boer, I. Usón, J. Aymamí, A. Rodger, M. J. Hannon and M. Coll, *Angew. Chemie Int. Ed.*, 2006, **45**, 1227–1231.

Figure 1.29 reproduced with permission, Copyright 2006 Wiley-VCH Verlag GmbH & Co. KGaA, Weinheim.

69 J. Novotna, A. Laguerre, A. Granzhan, M. Pirrotta, M.-P. Teulade-Fichou and D. Monchaud, *Org. Biomol. Chem.*, 2015, **13**, 215–222.

Figure 1.23 used with permission of Royal Society of Chemistry from Cationic azacryptands as selective three-way DNA junction binding agents, J. Novotna, A. Laguerre, A. Granzhan, M. Pirrotta, M-P. Teulade-Fichouc, D. Monchaud, **13**, 2015; permission conveyed through Copyright Clearance Center, Inc.

70 S. A. Barros and D. M. Chenoweth, *Angew. Chemie Int. Ed.*, 2014, **53**, 13746–13750.

Figure 1.24 reproduced with permission, Copyright 2014 Wiley-VCH Verlag GmbH & Co. KGaA, Weinheim.

71 S. A. Barros and D. M. Chenoweth, *Chem. Sci.*, 2015, **6**, 4752–4755.

72 S. A. Barros, I. Yoon, S.-E. Suh and D. M. Chenoweth, *Org. Lett.*, 2016, **18**, 2423–2426.

73 Z. Yang, Y. Chen, G. Li, Z. Tian, L. Zhao, X. Wu, Q. Ma, M. Liu and P. Yang, *Chem. – A Eur. J.*, 2018, **24**, 6087–6093.

74 L. Guyon, M. Pirrotta, K. Duskova, A. Granzhan, M.-P. Teulade-Fichou and D. Monchaud, *Nucleic Acids Res.*, 2017, **46**, e16–e16.

75 K. Duskova, J. Lamarche, S. Amor, C. Caron, N. Queyriaux, M. Gaschard, M.-J.

Penouilh, G. de Robillard, D. Delmas, C. H. Devillers, A. Granzhan, M.-P. Teulade-Fichou, M. Chavarot-Kerlidou, B. Therrien, S. Britton and D. Monchaud, *J. Med. Chem.*, 2019, **62**, 4456–4466.

76 J. M. Lehn, *Pure Appl. Chem.*, 1978, **50**, 871–892.

77 P. D. Beer Gale, P. A., Smith, D. K., *Supramolecular Chemistry*, Oxford University Press, Oxford, 1999.

78 M. J. Hannon and L. J. Childs, *Supramol. Chem.*, 2004, **16**, 7–22.

79 S.-F. Xi, L.-Y. Bao, J.-G. Lin, Q.-Z. Liu, L. Qiu, F.-L. Zhang, Y.-X. Wang, Z.-D. Ding, K. Li and Z.-G. Gu, *Chem. Commun.*, 2016, **52**, 10261–10264.

Figures 1.26 and 1.34 reproduced with permission of Royal Society of Chemistry from Enantiomers of tetrahedral metal–organic cages: a new class of highly efficient G-quadruplex ligands with potential anticancer activities, S-F. Xi, L-Y. Bao, J-G. Lin, Q-Z. Liu, L. Qiu, F-L. Zhang, Y-X. Wang, Z-D. D, K. Lib and Z-G. Gu, **52**, 2016; permission conveyed through Copyright Clearance Center, Inc.

80 B. Schoentjes and J.-M. Lehn, *Helv. Chim. Acta*, 1995, **78**, 1–12.

Figure 1.27 reproduced with permission, Copyright 1995 Verlag GmbH & Co. KGaA, Weinheim.

81 M. Hannon, I. Meistermann, C. J. Isaac, A. Rodger, V. Moreno, M. J. Prieto, E. Sletten and E. Moldrheim, *Angew. Chemie - Int. Ed.*, 2001, **86**, 879–884.

82 M. J. Hannon, C. L. Painting, A. Jackson, J. Hamblin and W. Errington, *Chem. Commun.*, 1997, 1807–1808.

83 A. C. Hotze, N. J. Hodges, R. E. Hayden, C. Sanchez-Cano, C. Paines, N. Male, M. K. Tse, C. M. Bunce, J. K. Chipman and M. J. Hannon, *Chem Biol*, 2008, **15**, 1258–1267.

Figure 1.28 reprinted from *Chemistry & Biology*, **15**, A.C. Hotze, N. J. Hodges, R. E. Hayden, C. Sanchez-Cano, C. Paines, N. Male, M.K. Tse, C. M. Bunce, J. K. Chipman, M. J. Hannon, Supramolecular iron cylinder with unprecedented DNA binding is a potent

cytostatic and apoptotic agent without exhibiting genotoxicity, pages 1258-1267, Copyright (2008), with permission from Elsevier.

84 J. M. C. A. Kerckhoffs, J. C. Peberdy, I. Meistermann, L. J. Childs, C. J. Isaac, C. R. Pearmund, V. Reudegger, S. Khalid, N. W. Alcock, M. J. Hannon and A. Rodger, *Dalt. Trans.*, 2007, 734–742.

85 C. Uerpmann, J. Malina, M. Pascu, G. J. Clarkson, V. Moreno, A. Rodger, A. Grandas and M. J. Hannon, *Chem. Eur. J.*, 2005, **11**, 1750–1756.

86 M. J. Hannon, I. Meistermann, C. J. Isaac, C. Blomme, J. R. Aldrich-Wright and A. Rodger, *Chem. Commun.*, 2001, 1078–1079.

87 I. Meistermann, V. Moreno, M. J. Prieto, E. Moldrheim, E. Sletten, S. Khalid, P. M. Rodger, J. C. Peberdy, C. J. Isaac, A. Rodger and M. J. Hannon, *Proc. Natl. Acad. Sci. U. S. A.*, 2002, **99**, 5069–5074.

88 L. Cerasino, M. J. Hannon and E. Sletten, *Inorg. Chem.*, 2007, **46**, 6245–6251.

89 G. I. Pascu, A. C. G. Hotze, C. Sanchez-Cano, B. M. Kariuki and M. J. Hannon, *Angew. Chemie-International Ed.*, 2007, **46**, 4374–4378.

90 C. Zhao, J. Geng, L. Feng, J. Ren and X. Qu, *Chem. – A Eur. J.*, 2011, **17**, 8209–8215.

91 L. Cardo, I. Nawroth, P. J. Cail, J. A. McKeating and M. J. Hannon, *Sci. Rep.*, 2018, **8**, 13342.

92 L. J. Childs, J. Malina, B. E. Rolfsnes, M. Pascu, M. L. Prieto, M. L. Broome, P. M. Rodger, E. Sletten, V. Moreno, A. Rodger and M. J. Hannon, *Chem. Eur. J.*, 2006, **12**, 4919–4927.

93 S. E. Howson, A. Bolhuis, V. Brabec, G. J. Clarkson, J. Malina, A. Rodger and P. Scott, *Nat. Chem.*, 2012, **4**, 31–36.

Figure 1.31 reprinted by permission from Springer Nature Customer Service Centre GmbH: *Nature Chemistry*, Optically pure, water-stable metallo-helical 'flexicate' assemblies with antibiotic activity, S. E. Howson, A. Bolhuis, V. Brabec, G. J. Clarkson, J. Malina, A. Rodger, P. Scott, **4**, pages 31-36, Copyright (2012).

94 V. Brabec, S. E. Howson, R. A. Kaner, R. M. Lord, J. Malina, R. M. Phillips, Q. M. A. Abdallah, P. C. McGowan, A. Rodger and P. Scott, *Chem. Sci.*, 2013, **4**, 4407–4416.

95 A. D. Faulkner, R. A. Kaner, Q. M. A. Abdallah, G. Clarkson, D. J. Fox, P. Gurnani, S. E. Howson, R. M. Phillips, D. I. Roper, D. H. Simpson and P. Scott, *Nat. Chem.*, 2014, **6**, 797–803.

96 H. Song, N. J. Rogers, S. J. Allison, V. Brabec, H. Bridgewater, H. Kostrhunova, L. Markova, R. M. Phillips, E. C. Pinder, S. L. Shepherd, L. S. Young, J. Zajac and P. Scott, *Chem. Sci.*, , DOI:10.1039/C9SC02651G.

97 S. V Kumar, W. K. C. Lo, H. J. L. Brooks and J. D. Crowley, *Inorganica Chim. Acta*, 2015, **425**, 1–6.

Figure 1.32a reprinted from *Inorganica Chimica Acta*, **425**, S. V. Kumar, W. K. C. Lo, H. J. L. Brooks, J. D. Crowley, Synthesis, structure, stability and antimicrobial activity of a ruthenium(II) helicate derived from a bis-bidentate “click” pyridyl-1,2,3-triazole ligand, pages 1-6, Copyright (2015), with permission from Elsevier.

98 R. A. S. Vasdev, D. Preston, S. Ø. Scottwell, H. J. L. Brooks, J. D. Crowley and M. P. Schramm, *Molecules*, 2016, **21**, 1548.

99 A. Adamski, M. A. Fik, M. Kubicki, Z. Hnatejko, D. Gurda, A. Fedoruk-Wyszomirska, E. Wyszko, D. Kruszka, Z. Dutkiewicz and V. Patroniak, *New J. Chem.*, 2016, **40**, 7943–7957.

100 S.-F. Xi, L.-Y. Bao, Z.-L. Xu, Y.-X. Wang, Z.-D. Ding and Z.-G. Gu, *Eur. J. Inorg. Chem.*, 2017, **2017**, 3533–3541.

101 A. J. Plajer, E. G. Percástegui, M. Santella, F. J. Rizzuto, Q. Gan, B. W. Laursen and J. R. Nitschke, *Angew. Chemie*, 2019, **131**, 4244–4248.

102 J. Zhu, C. J. E. Haynes, M. Kieffer, J. L. Greenfield, R. D. Greenhalgh, J. R. Nitschke and U. F. Keyser, *J. Am. Chem. Soc.*, 2019, **141**, 11358–11362.

103 L. Cardo, V. Sadovnikova, S. Phongtongpasuk, N. J. Hodges and M. J. Hannon, *Chem. Commun.*, 2011, **47**, 6575–6577.

104 C. A. Puckett and J. K. Barton, *Bioorg. Med. Chem.*, 2010, **18**, 3564–3569.

105 L. Cardo, PhD Thesis, University of Birmingham, 2008.

106 E. Kitteringham, E. Andriollo, V. Gandin, D. Montagner and D. M. Griffith, *Inorganica Chim. Acta*, 2019, **495**, 118944.

107 S. van Zutphen and J. Reedijk, *Coord. Chem. Rev.*, 2005, **249**, 2845–2853.

108 C. Cassino, E. Gabano, M. Ravera, G. Cravotto, G. Palmisano, A. Vessières, G. Jaouen, S. Mundwiler, R. Alberto and D. Osella, *Inorganica Chim. Acta*, 2004, **357**, 2157–2166.

109 J. Norman, PhD Thesis, University of Birmingham, 2012.

110 R. G. Kenny and C. J. Marmion, *Chem. Rev.*, 2019, **119**, 1058–1137.

111 E. C. Calvaresi and P. J. Hergenrother, *Chem. Sci.*, 2013, **4**, 2319–2333.

112 J. White, PhD Thesis, University of Birmingham, 2016.

Chapter 2:

Capping the triple stranded metallohelicate cylinder

2.1 Introduction and Aims

As discussed in section 1.4, Hannon's helicate cylinders have potential for use as a cancer therapeutic. However, there are several challenges that would stand in the way of these compounds reaching the clinic. These include selectivity, solubility, and stability. The $[M_2L_3]^{4+}$ cylinders have no feature to make them target cancer cells over healthy cells. Traditional cancer therapies used today, including cisplatin, demonstrate various side effects in the clinic due to the drugs affecting healthy cells as well as the tumour cells.[1,2] As such, a degree of selectivity would be required in order to provide a therapeutic benefit over anticancer agents already in use. In the anticancer drug field, the controversial Enhanced Permeability and Retention (EPR) effect is often used to rationalise the higher degree of accumulation of macromolecular drugs in cancerous tissue over healthy tissue. This effect arises from a higher permeability of tumour blood vessels compared to those in healthy tissue.[3–5] However, cylinders are too small for this effect to be a factor, so ideally a targeting moiety would be incorporated into the structure of the cylinder complex to direct the cylinder towards cancerous cells. Examples already discussed in section 1.5 include attachment of a steroid to increase uptake by steroidal receptors that are over-expressed by some cancer cells, as well as carbohydrate moieties to increase uptake through sugar receptors. Yet such attachment can drastically decrease the aqueous solubility of the complex, and increasing the steric bulk of the ligands can greatly reduce the stability of the complex in solution. Unless the metal fluoresces (as is the case with Hannon's Ru cylinder, discussed in section 1.4), nothing in the cylinder structure offers any means of monitoring the journey taken by the cylinder once it has entered a cell. As such, when we consider cylinders with iron, nickel or any other non-fluorescent metal centre, it cannot be stated with certainty whether any observed effect is caused by the intact complex or whether it is converting to some other active species.

To overcome some of these challenges, work was undertaken to synthetically "cap" the cylinder. The aim was to incorporate a synthetic moiety that links the three ligands of the helicate together, replacing three sites of functionalisation at each end of the cylinder with just one. Ideally, a strategy would be found that allows capping at just one end of the cylinder,

further contributing to desirable physiochemical properties by keeping the overall molecular weight of the complex as low as possible. A graphical representation of this aim is shown in Figure 2.1. A further goal is to use this site of functionalisation to attach a biological targeting molecule such as a steroid or sugar, or for the attachment of a fluorescent dye that would allow the cylinder to be tracked within cells using fluorescence microscopy. Having only one of these functional groups at the end of the cylinder should also increase the cylinder's stability as, by linking the three ligands covalently, they will effectively be held in place. This would make the complex much less likely to dissociate.

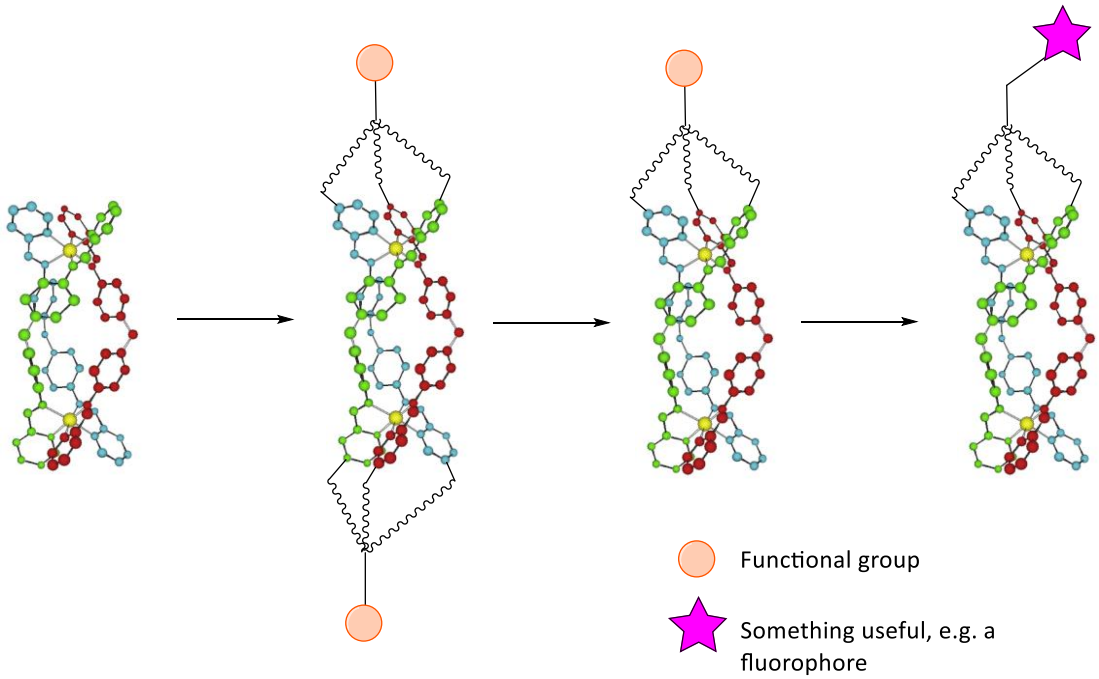

Figure 2.1 Illustration of the aim to synthetically cap the ends of the cylinder, and where this could then lead to once achieved. Representation of the crystal structure was taken from reference 6.

There are several factors to consider when designing a capping moiety. Firstly, the cap should be attached to the ligands through a linkage that is sterically non-bulky, so as to minimise any clash that might make the capped cylinder unfavourable to form. Secondly, the linkage used should be chemically stable to confer stability to the whole complex. Thirdly, the synthesis of the cap itself should be relatively simple to perform and the chemistry should be reproducible, as synthetic simplicity is one of the key attractions of the original iron and nickel $[M_2L_3]^{4+}$ cylinders. With these factors in mind, it was decided to focus efforts on synthesising a tripod shaped capping moiety that is based around a quaternary carbon, with the ligands

attached to the three "arms" of the tripod and a functional group on the "head" (as illustrated in Fig 2.1). The head group could be used to attach desired functionality to the cylinder. Influence for such a design was found in literature from the field of dendrimer synthesis, [7–11] where such monomers are described as being "AB_3", "1→3" or "C-branched" due to having a head group and three identical arms connected to a quaternary carbon. The work described in this chapter focused on finding suitable synthetic linkages to attach such a quaternary carbon-based capping moiety to the cylinder structure, through the 5-position of the pyridine rings of the cylinder ligand. Various synthetic linkages were tried, and each of these will be discussed in distinct sections.

2.2 Using amide bonds to form a capping moiety

Initial efforts were focused on using amide linkages to connect the pyridine rings of the ligand to the tripodal capping moiety. The retrosynthetic approach adopted is shown in Figure 2.2. Using amide bonds to link the cap to the complex provides several benefits which help address the challenges around complex stability and solubility. Amide bonds are highly stable due to the resonance effects of the lone electron pairs of the nitrogen and carbonyl oxygen. The resultant double bond nature between the N and carbonyl C make the bond planar. As the arms of the cap will be forced close together when the cylinder forms, having planar bonds should minimise any steric influences that could have a destabilising effect on the complex. The polar nature of amide bonds should also increase the aqueous solubility of the complex, due to the ability of amide bonds to act as both a hydrogen bond donor (N-H) and acceptor (C=O). As described in section 1.5, previous work in the group has also successfully incorporated amino acids into the cylinder structure, through functionalisation at the 5-position of the pyridine ring.[12,13]

Amide coupling is used extensively in organic synthesis, and the drive to develop efficient methods of peptide synthesis has led to the development of an expansive toolkit of different coupling reagents.[14] In general, these reagents activate the carbonyl group of the acid towards nucleophilic attack from the nitrogen lone pair on the amine. Figure 2.3 demonstrates a coupling between an amine and carboxylic acid using a carbodiimide, a traditional class of coupling reagent.[15] The first step involves transfer of the labile proton of the carboxylic acid to one of nitrogens of the carbodiimide. The electrophilic carbon of the

protonated carbodiimide is attacked by the carboxylate to form the *O*-acylisourea, a reactive intermediate that is attacked by the primary amine. The final step involves a proton transfer from the amine to form the urea by-product and generate the amide.

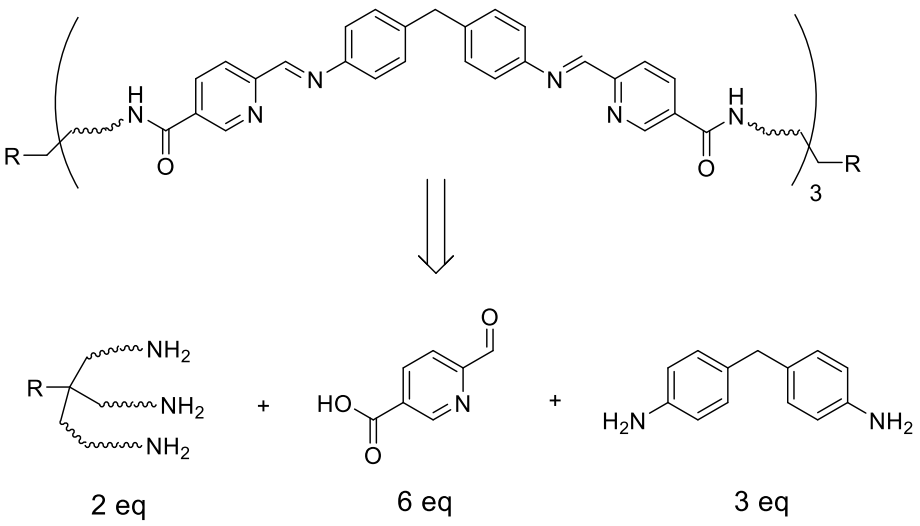

Figure 2.2 The retrosynthetic approach taken towards the design of a capped cylinder ligand, using amide bonds to link the cap molecule to the metal binding ligand.

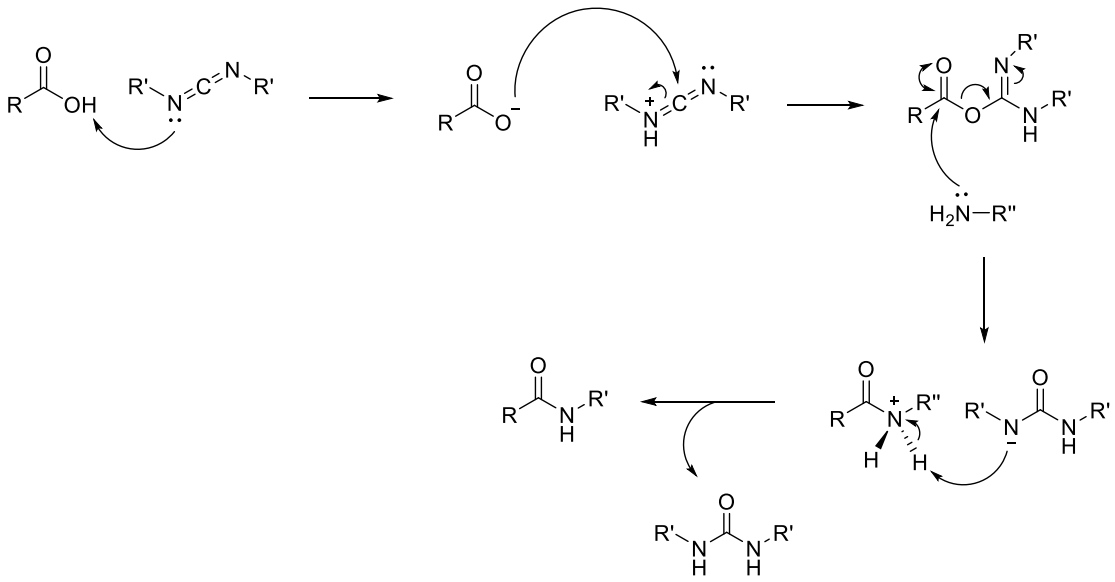

Figure 2.3 Mechanism showing amide bond formation between a carboxylic acid and a primary amine using a carbodiimide as a coupling agent.

The initial synthetic strategy that was followed is outlined in Schemes 2.1 – 2.2. Scheme 2.1 outlines the synthesis of nicotinic acid **3**, with a dimethyl acetyl protected aldehyde in the 2-position and a carboxyl group in the 5-position. Scheme 2.1 has been used by the Hannon group previously, and the procedures reported in reference 12 were followed. Scheme 2.2 is based on a published procedure for converting the carboxylic acid functionalities of nitromethanetrispropionic acid to primary amines.[16] Scheme 2.3 illustrates the intention to couple triamine **6** with three equivalents of **3**, followed by regeneration of the aldehydes in the 2-position of the pyridine rings. Two equivalents of this trialdehyde would then be condensed with three equivalents of 4,4'-methylenedianiline to produce the dicapped ligand. Ideally, this ligand would wrap around two iron centres to form the helicate upon addition of $FeCl_2$. It was expected that the condensation step of Scheme 2.3 would have to be performed as a one pot synthesis in the presence of $FeCl_2$, where the metal centres could act as a template for ligand assembly. This design features a nitro group at the "head" of the cap. While the nitro group itself does not lend itself to attachment of a useful moiety, it was rationalised that the synthesis could be modified to include a hydrogenation step to convert the nitro group to a primary amine, once a route to a capped cylinder had been established. The primary amine could then be coupled to any useful moiety containing a carboxylic acid functionality.

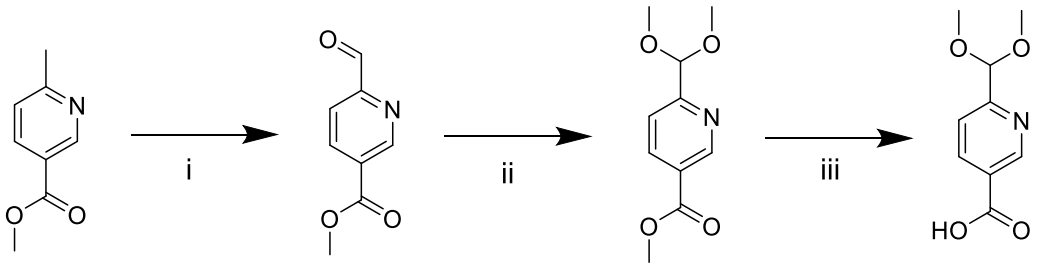

1 **2** **3**

Scheme 2.1 Synthesis of the 5-carboxylic acid functionalised pyridine **3**, following procedures from reference 12. (i) I_2, DMSO, 160 °C; 2.5 h; (ii) $CH(OMe)_3$, HCOOH, H_2SO_4, 50 °C; 10 min, then RT for 17 h; (iii) 1M NaOH (aq), MeOH, 17 h.

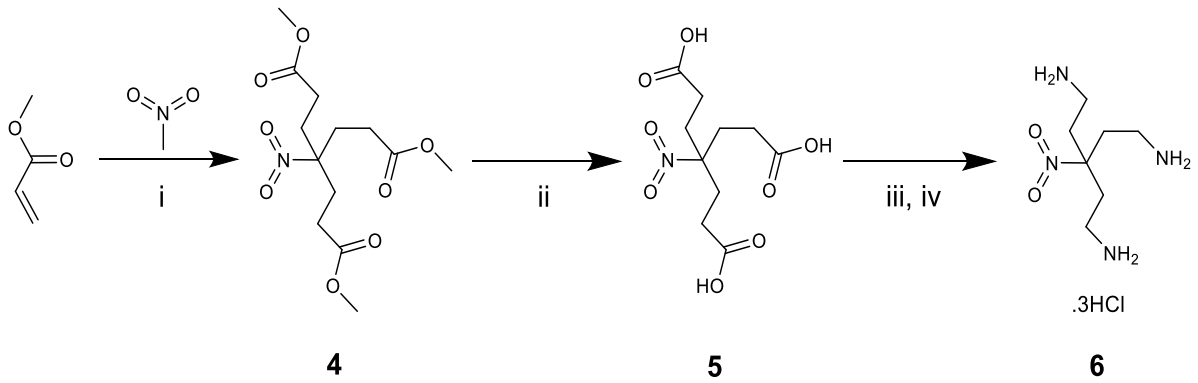

Scheme 2.2 Proposed synthesis of triamine cap. (i) benzyltrimethylammonium hydroxide, DME, 70 °C; 17 h; (ii) 1M NaOH (aq), MeOH; RT, 18 h; (iii) $SOCl_2$, reflux; 3 h; (iv) Trimethylsilyl azide, 80 °C, 30 min followed by aqueous acid work up.

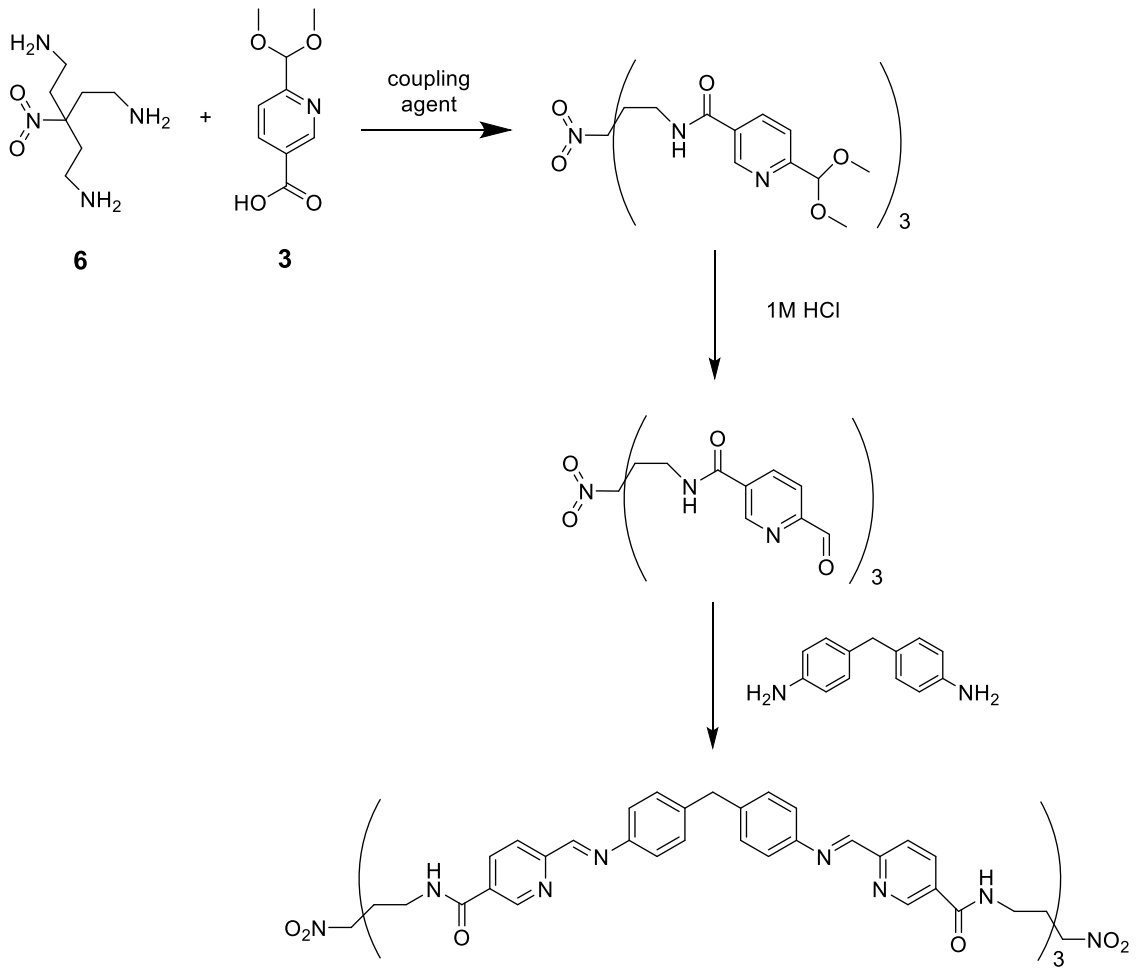

Scheme 2.3 Proposed synthetic route to the capped cylinder ligand, involving the coupling of functionalised nicotinic acid **3** with triamine **6**, followed by deprotection of the aldehyde and subsequent condensation with the dianiline linker.

In Scheme 2.1, commercially available methyl 6-methylnicotinate is oxidised using iodine C-H activation and DMSO as the oxidant, producing **1** with an isolated yield of 28%. The resultant aldehyde must then be protected to prevent it from immediately forming an imine with the amino groups of triamine **6** in the first step of Scheme 2.3. This protection is achieved by heating with trimethylorthoformate in acidic conditions, converting the aldehyde into the dimethyl acetyl, producing **2** with a yield of 77%. The third step hydrolyses the methyl ester to the desired nicotinic acid, giving **3** with an isolated yield of 62%. All steps were completed with similar yields to those previously reported from the group.[12]

Attempts to synthesise triamine **6** (outlined in Scheme 2.2) proved challenging. Scheme 2.2 starts with a Michael addition of nitromethane to three equivalents of methyl acrylate in the presence of benzyltrimethylammonium hydroxide, which acts as a phase transfer catalyst.[17] While Michael additions are typically cooled due to their exothermicity, it was found that heating the reaction to 70 ^{o}C resulted in a higher conversion to the triester compared to the same reaction at room temperature, where traces of the monoester and diester were observed by ^{1}H NMR spectroscopy. **4** was isolated with a yield of 32%. After base catalysed hydrolysis of **4** to the corresponding triacid **5** (88%), conversion to the acyl chloride was achieved by refluxing in excess $SOCl_2$. Despite being reported in the literature,[16] the final step proved difficult to reproduce. Treatment with trimethylsilyl azide should convert the acyl chloride to the acyl azide, which upon heating should undergo a Curtius rearrangement to the isocyanate. This should then hydrolyse to the amine when mixed with aqueous hydrochloric acid (Figure 2.4), forming the HCl salt.[18] A small amount of light brown precipitate was isolated, which showed shifts similar to those quoted by ^{1}H NMR spectroscopy [16] and the expected *m/z* of 191 (arising from $[M+H]^{+}$) by ESI mass spectrometry. However, the yield was less than 1% so a more reliable alternative was sought.

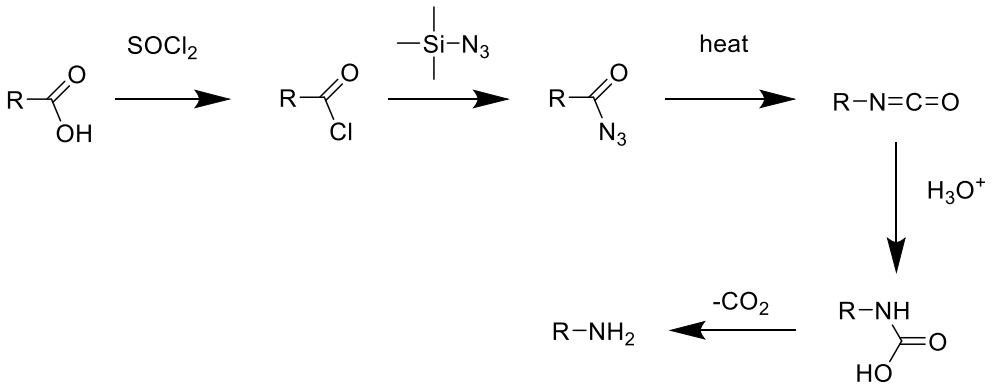

Figure 2.4 Illustration of the conversion of carboxylic acid functionalities to primary amines, used in step iv of Scheme 2.2. A Curtius rearrangment occurs upon heating the acyl azide, which is hydrolysed to the unstable carbamic acid. This decomposes to release CO_2 and generate the amine.[18]

Following the difficulties faced with the first strategy, a new route was devised to synthesise amino-pyridine **10** (Scheme 2.4). This swaps the carboxylic acid functionality in the 5-position with an amine. This amine could be coupled to triacid **5**, which would sidestep the low yeilding conversion of triacid **5** to triamine **6.** This strategy effectively swaps the positions of the NH and CO in the resultant amide, which would not be expected to alter the solubility or stability of the resultant complex. Scheme 2.4 uses procedures from two literature sources.[19,20] The first two steps (performed as a one-pot synthesis) feature the conversion of the 2-chloride substituent to 2-methyl, via the malonic ester and subsequent decarboxylations. The combined yield over these steps was 40%. **7** is then oxidised with selenium dioxide in 1,4-dioxane (52%) before protection of the resultant aldehyde by conversion to the 1,3-dioxolane (producing **9** with a yield of 83%). Achieving good yields for this reaction requires the use of Dean-Stark apparatus, which allows easy removal of H_2O generated from the condensation reaction. Based on Le Chatelier's principle, this drives the equilibrium towards the product. The yield achieved is higher than that of the dimethyl acetyl formation step (producing **2**) in Scheme 2.1. The final step is the catalytic hydrogenation of the nitro group using a palladium catalyst. This hydrogenation was expected to proceed in near quantitative yield, yet the crude product appeared to contain residual starting material, even after two days of stirring under a hydrogen atmosphere. Amine **10** was isolated by silica column chromatography with a lower than expected yield of 22%.

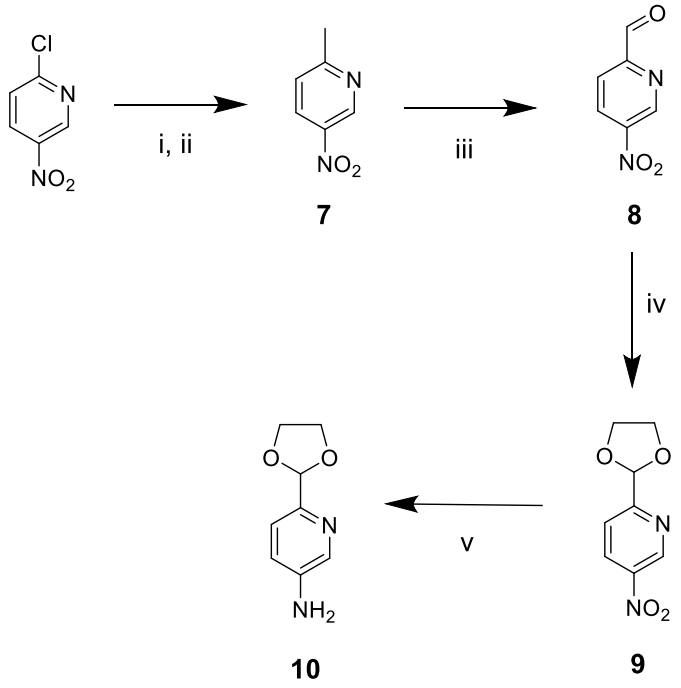

Scheme 2.4 Synthetic route to a pyridyl ring with protected aldehyde in the 2-position and amino group in the 5-position. (i) Na, diethyl malonate, toluene, reflux, 3.5 h; (ii) 6M HCl (aq), reflux, 4 h; (iii) SeO_2, 1,4-dioxane, reflux, 18 h; (iv) ethylene glycol, *p*TsOH·H_2O, toluene, reflux, 18 h; (v) H_2 (g), 5% Pd/C, EtOH, RT, 20 h.

Coupling of amine **10** with triacid **5** was attempted using HBTU as the coupling agent. After several days of stirring at 45 ^oC, followed by an aqueous work-up and silica column chromatography, 2 mg of a brown oil was obtained (yield <3%). The ^1H NMR spectrum measured showed aromatic shifts similar to that of the pyridine unit and the broad singlet of the amino group has disappeared. While the disappearance of the amino shift suggests that the coupling did proceed, the spectrum showed other species were still present and that further purification would be required. Given the already very low yield, purification was not attempted and efforts were focused on an alternative strategy.

A procedure to synthesise a Boc protected analogue of triamine **6**, with extra carbon atoms in the tripod arms, was found amongst the dendrimer literature from Bradley and co-workers.[9] Synthesis of **11** (Scheme 2.5) is achieved in a one-pot process from commercially available tris(2-cyanoethyl)nitromethane. A solution of borane in THF is used to reduce the nitrile groups to primary amines, and this is immediately followed by Boc protection of these. Boc protection of the amines makes the molecule much more lipophilic, making it easier to extract and purify. The Boc groups of **11** are then removed by stirring in 4M HCl in dioxane

to give **12**. Once complete, removal of the solvent under vacuum yields the triamine as the tris-HCl salt. As coupling to the pyridine unit is completed under basic conditions, it was reasoned that this hydrochloride salt could be used directly in a coupling reaction, provided extra equivalents of base are added. Synthesis of **11** was achieved with an isolated yield of 25%. Deprotection to **12** proceeded with a yield of 92%. Coupling of **12** with **3** was then trialled on a 0.15 mmol scale (Scheme 2.6). Carbonyl diimidazole (CDI) was selected as the coupling agent as, upon reacting with a carboxylic acid, one equivalent of imidazole is produced. This makes CDI coupling compatible with HCl salts of amine starting materials.[14]

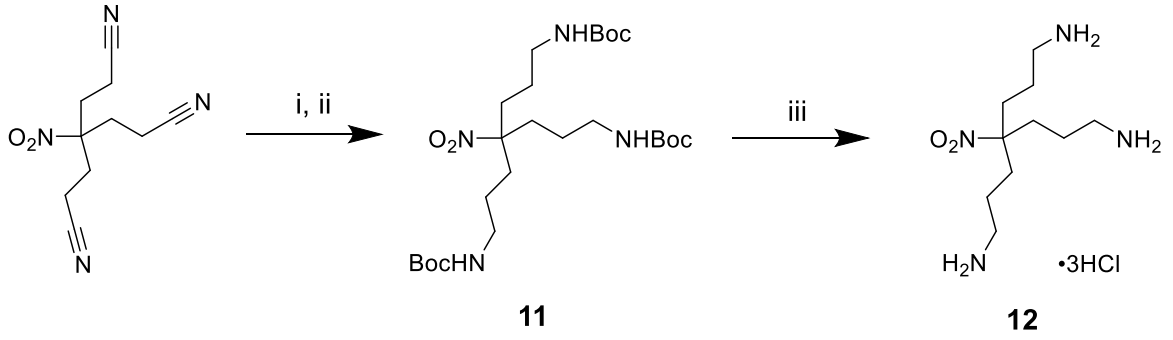

11 **12**

Scheme 2.5 Synthesis of triamine **12**. (i) BH_3·THF, THF, reflux,17 h; (ii) Boc_2O, Et_3N, MeOH, reflux, 20 h; (iii) 4M HCl in 1,4-dioxane, RT, 2 h.

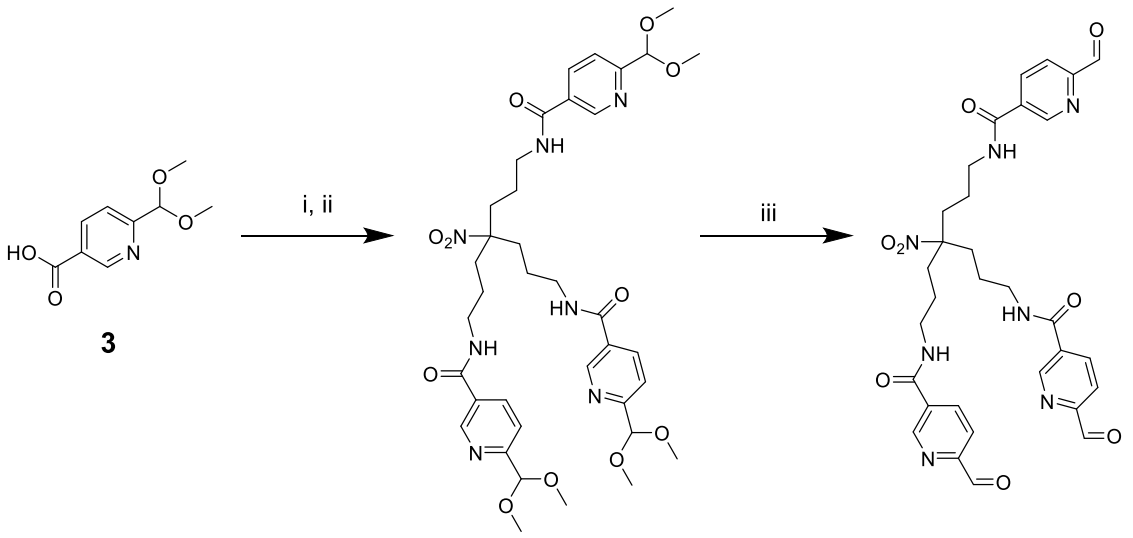

13

Scheme 2.6 Proposed synthesis of a trialdehyde cap. (i) CDI, DMF, Ar, RT, 1.5 h; (ii) **12**, Et_3N, DMF, RT, 18 h; (iii) 1M HCl (aq) : THF (1:1 v:v), RT.

6.75 equivalents of CDI were stirred under argon with 4.5 equivalents of **3** for 1.5 hours, before the addition of 1 equivalent of **12** premixed with 1.5 equivalents of triethylamine. On first attempt, the reaction was left stirring at room temperature for over 72 hours. After a basic aqueous workup and SiO_2 column chromatography, a light brown oil was obtained in 17% yield. Initial NMR and MS data looked promising, so the reaction was repeated and monitored by reverse phase analytical HPLC, using a solvent gradient of 0-100% MeCN in H_2O over 40 min. Through monitoring a series of repeat experiments, product degradation was observed after 17 hours of stirring at room temperature. Purification by prep-HPLC produced **13** as an off-white, oily solid with yields as high as 61%. Having successfully isolated the triamide with sufficient purity, deprotection of **13** was then trialled by stirring in a 1M HCl (aq)/THF mixture. From previous deprotections of this type performed in the group, it was known that this deprotection requires long reaction times of up to several days, and the reaction progress can be monitored by analytical reverse phase HPLC.[12] Due to the low pH of the reaction mixture, samples were diluted with THF before being injected in order to bring the pH of the sample within the tolerated limits of the column. Figure 2.5 shows chromatograms obtained during the monitoring of this reaction. Figure 2.5a shows a peak corresponding to **13** at 19.3 min at the start of the reaction. Figure 2.5b shows the reaction progress after 29 hours of stirring at room temperature. Starting material is still present, and a complex mixture of product peaks can be observed. It was thought that some of these peaks corresponded to stable intermediates formed during the reaction, and that over time these would progress to one product peak. Successive additions of 1 mL of 1M HCl (aq) were added after each day in an effort to drive the deprotection forward, however the mixture remained complex, and after 3 days no further change was observed by HPLC. The gradient was altered in an attempt to achieve better separation of these peaks to allow identification of the product peak by mass spectrometry (method: 0 -20% MeCN in H_2O over 8 min, 20 – 50% over 60 min, 50 – 60% over 4 min, 100%). The resultant chromatogram is shown in Figure 2.5c. Sufficient separation of the peaks was not achieved. Due to the difficulties faced in getting this deprotection to run to completion, efforts were focussed on investigating the use of an alternative protection/deprotection strategy of the aldehydes in the 2-position of the pyridine rings.

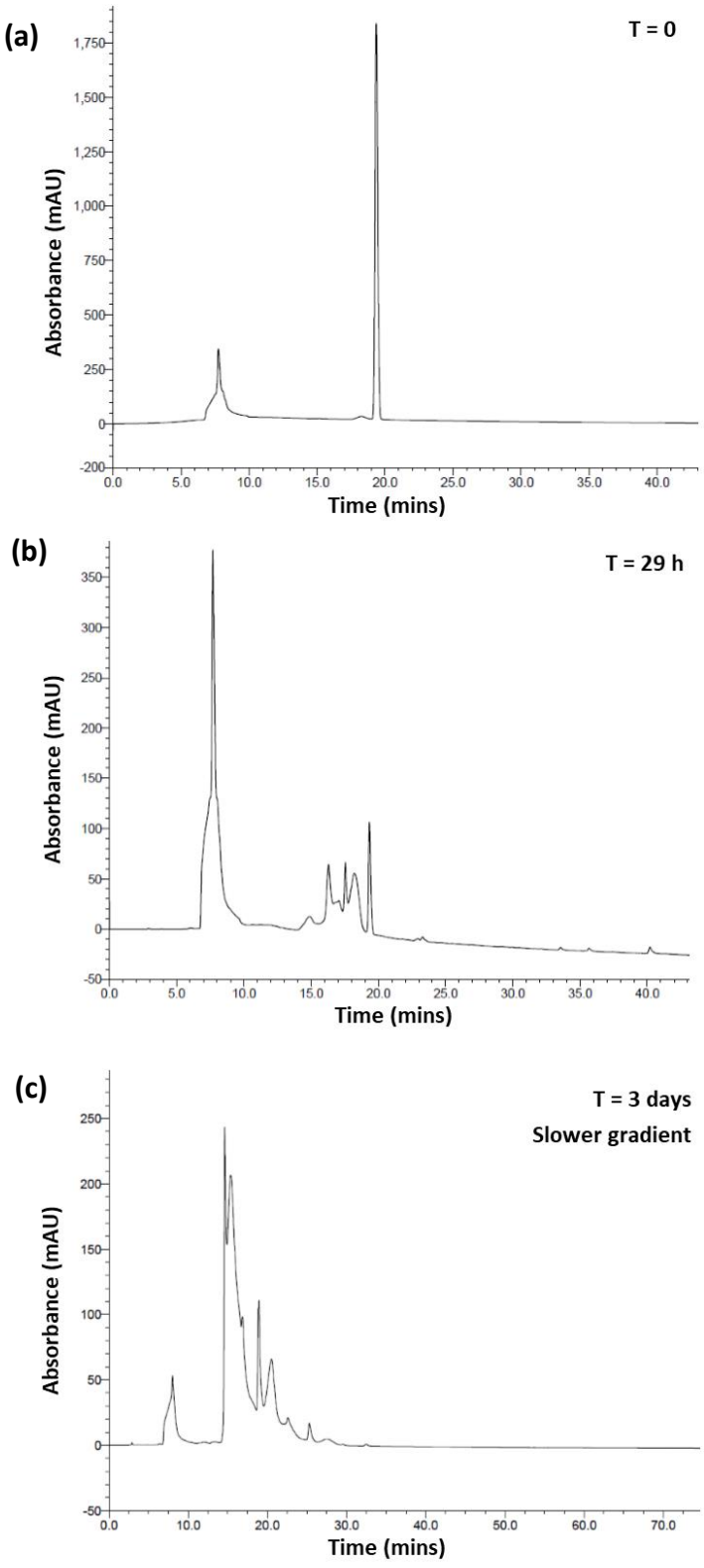

Figure 2.5 HPLC chromatograms monitoring deprotection of **13**. (a) at the start of the reaction; (b) after 29 h; (c) after 3 days, using a slower gradient to increase resolution: 0 to 20% MeCN in H_2O over 8 min, 20 – 50% over 60 min, 50 – 60% over 4 min, 100% for 4 min. The prominent peak observed around 8 min is attributed to the solvent.

The dioxolane protecting group can be deprotected by refluxing in acetone, using a weak acid as a catalyst.[21] In order to generate sufficient quantities of material to investigate these deprotection conditions further, **16** (a triester analogue of **13**) was synthesised which was isolable without the time consuming HPLC purification required for **13**. **16** uses dioxolane protection at the 2-position of the pyridine ring instead of the dimethyl acetyl, as shown in Scheme 2.7.

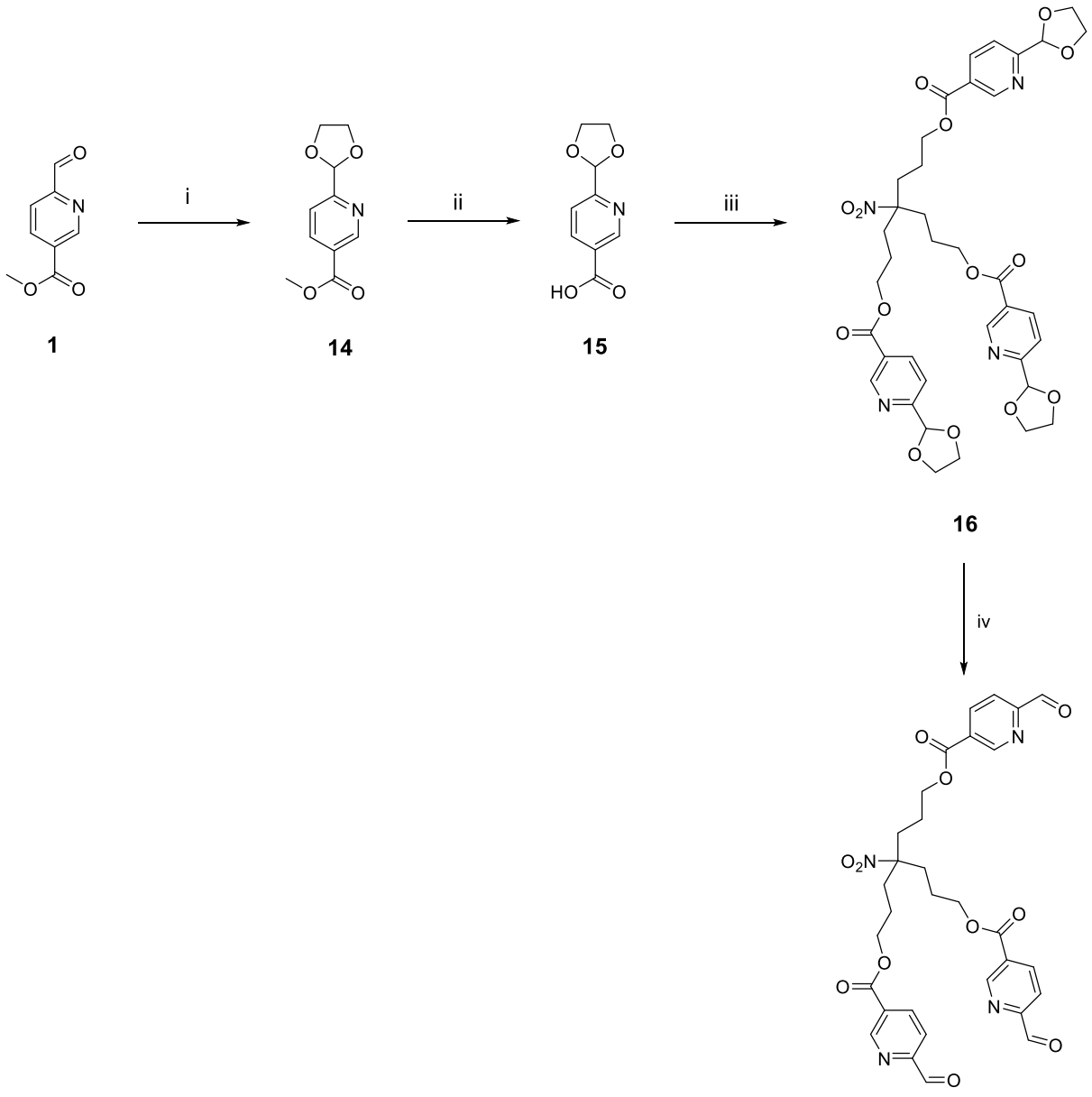

Scheme 2.7 Synthesis adopted towards a ester-linked trialdehyde. (i) ethylene glycol, *p*TsOH·H_2O, toluene, 6h, reflux; (ii) 1M NaOH (aq), MeOH, 29 h, RT; (iii) Nitromethanetrispropanol, EDC·HCl, DMAP, 18 h, N_2, RT; (iv) *p*TsOH·$5H_2O$, acetone, H_2O, reflux, 40 h.

The aldehyde of compound **1** was protected by conversion to a 1,3-dioxolane group to form **14**. As with the synthesis of compound **9**, the aldehyde was refluxed in toluene using Dean-Stark apparatus which allowed easy separation of the generated H_2O from the reaction mixture. **14** was isolated with a yield of 87%. The methyl ester was then hydrolysed in aqueous base to give **15** with a yield of 44%. Acid **15** was then coupled to nitromethanetrispropanol using EDC·HCl, a carbodiimide that follows the same mechanism as that shown in Figure 2.3. A catalytic quantity of DMAP was included, which activates the acid to nucleophilic attack from the lone pairs of one of EDC's nitrogens. The role of DMAP is highlighted in Figure 2.6. After stirring overnight, triester **16** was isolated with a yield of 81%. As triester **16** was synthesised using commercially available nitromethentrispropanol, this procedure generated sufficient material to trial the dioxolane deprotection while avoiding the time consuming synthesis that would have been required to make the triamine analogue. Synthesis of the triamine analogue would have required a similar procedure to that used to generate **13**, as shown in Scheme 2.5. Deprotection of **16** (the final step of Scheme 2.7) did not run as cleanly as hoped. The reaction progress was monitored using ^{1}H NMR spectroscopy after stirring overnight. A small scale work up was performed by taking an aliquot of the reaction mixture, removing the solvent, and then partitioning the residue between sat. $NaHCO_3$ (aq) and DCM. The DCM layer was then washed with water and dried over $MgSO_4$ before being concentrated under reduced pressure. The residue was then dissolved in $CDCl_3$ and analysed by ^{1}H NMR spectroscopy. Figure 2.7 shows some of the key findings from the ^{1}H NMR spectra. The spectrum shown in Figure 2.7b shows an aldehyde proton peak around 10.1 ppm which suggests that conversion of the dioxolane group to the aldehyde was proceeding. However, both the aromatic region between 9.5 and 7.0 ppm show that multiple pyridine species are present. The aliphatic region (4.5 – 1.0 ppm) also appears complex, suggesting that the tripod arms are not identical. The reaction was stirred for a further 17 h with heating under reflux. As the reaction had not visibly progressed (Figure 2.7c), the remaining reaction mixture was worked up in a similar fashion to the prior aliquots. Purification was attempted by silica column chromatography but the ^{1}H NMR spectrum of the isolated material appeared just as impure as Figure 2.7c. This suggests that multiple species run very closely on silica, which makes purification difficult. While HPLC could have proved more successful, at the time these experiments were carried out the HPLC equipment was unavailable.

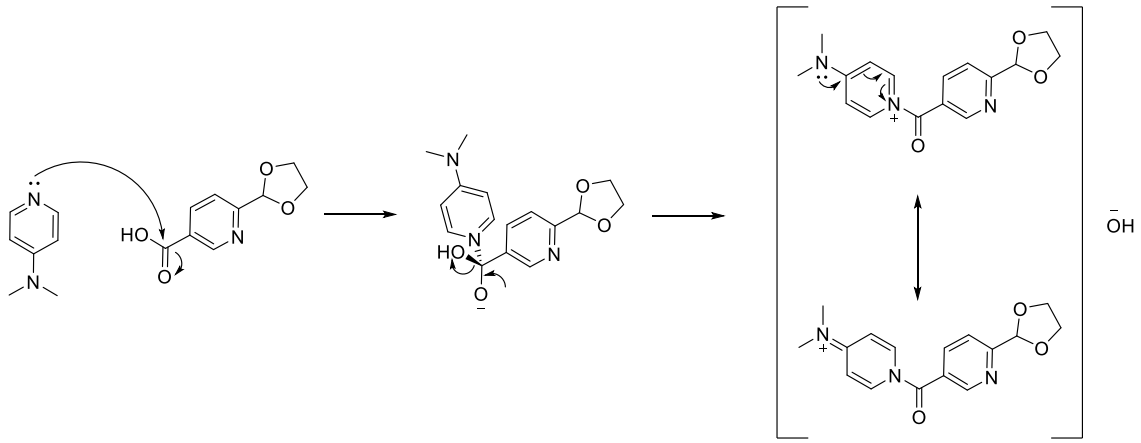

Figure 2.6 Mechanism for the activation of carboxylic acid **15** by DMAP, increasing the carbonyl's susceptibility to nucleophilic attack from EDC. The structure of DMAP offers stabilisation of the positive charge through resonance.

Given the challenges faced with the aldehyde protection and deprotection strategies required when coupling these nicotinic acids with primary amines, it was decided to focus efforts on investigating whether different linking groups could be used. If this work were to be revisited in future, monitoring this deprotection using analytical HPLC may offer some insight into whether the trialdehyde is generated as the main product, and whether purification by prep-HPLC is feasible.

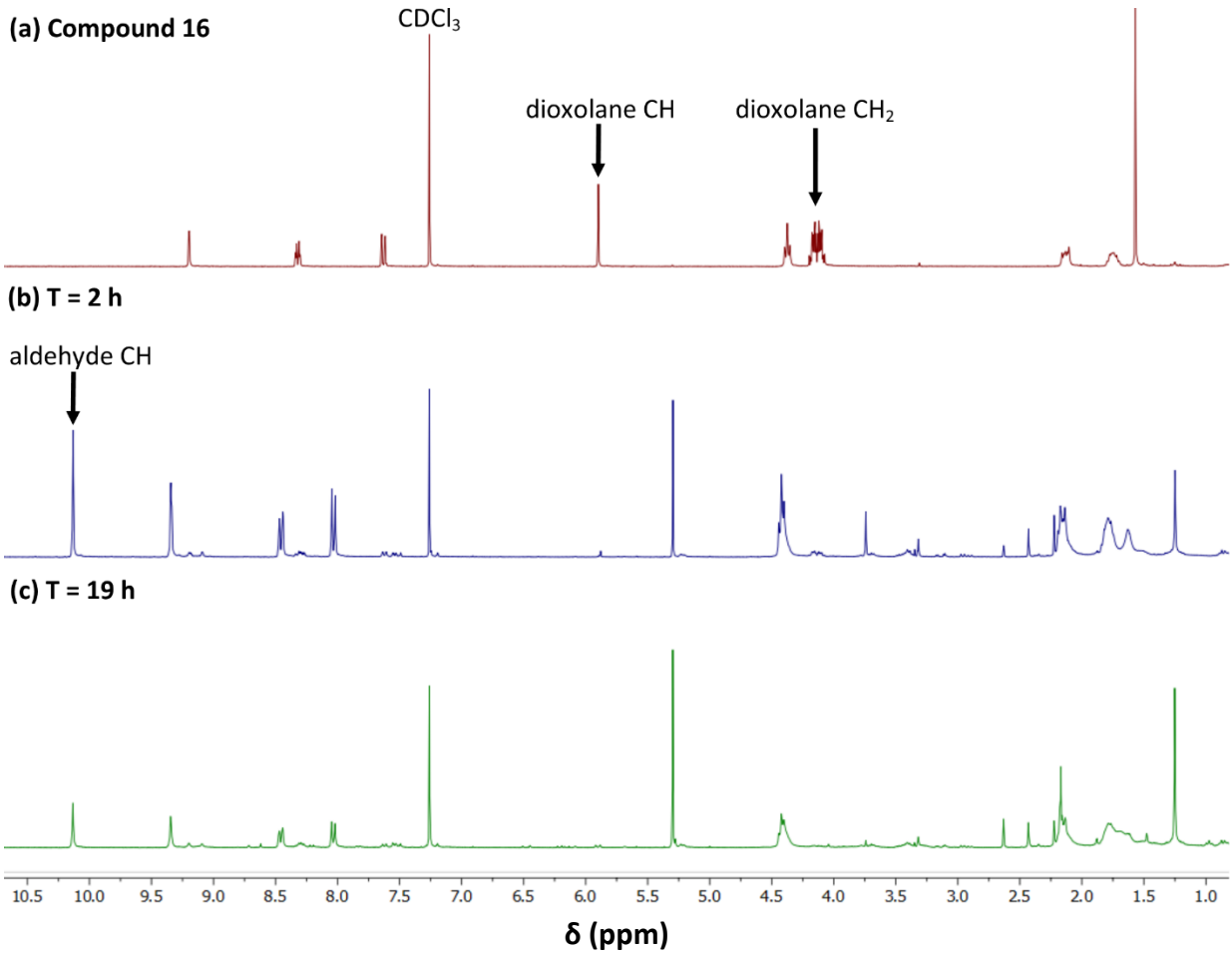

Figure 2.7 1H NMR spectra monitoring the progress of the deprotection of triester **16.**

2.3 Using copper catalysed alkyne-azide cycloadditions to form a capping moiety

An alternative linkage through which to attach the pyridine rings of the ligand to a capping moiety is the formation of 1,2,3-triazoles. These triazoles are formed through the cycloaddition reaction of a terminal alkyne and an azide functional group. Such cycloadditions have been known to occur when sufficient thermal energy is provided since the late nineteenth century,[22] but it was the publication of the use of copper(I) as a catalyst for the reaction in the early 2000s [23,24] that marked the beginning of their wide spread use in organic synthesis.[25] A general mechanism for the reaction is shown in Figure 2.8. The inclusion of a copper(I) catalyst increases the reaction rate dramatically, from scales of hours (or even days) to minutes. The Cu cayalsed reaction selectively forms the 1,4-disubstituted triazole rather

than yielding a mixture of the two possible regioisomers. Depending on the substrates, the reaction can often be run at room temperature or with gentle heating, making the reaction compatible with reagents that may otherwise be unstable to the excessive heating previously required.[26] Perhaps the largest benefit of this chemistry is that the reaction can be used to connect two molecules together, often in high yield, while tolerating other functional groups. This last benefit makes using these triazoles as a linker particularly applicable to this work, as the aldehyde functionality should be tolerated and therefore not require protection. The need for a deprotection step would also be avoided if CuAAC could be used, overcoming the main hurdle for the amide bond strategy.

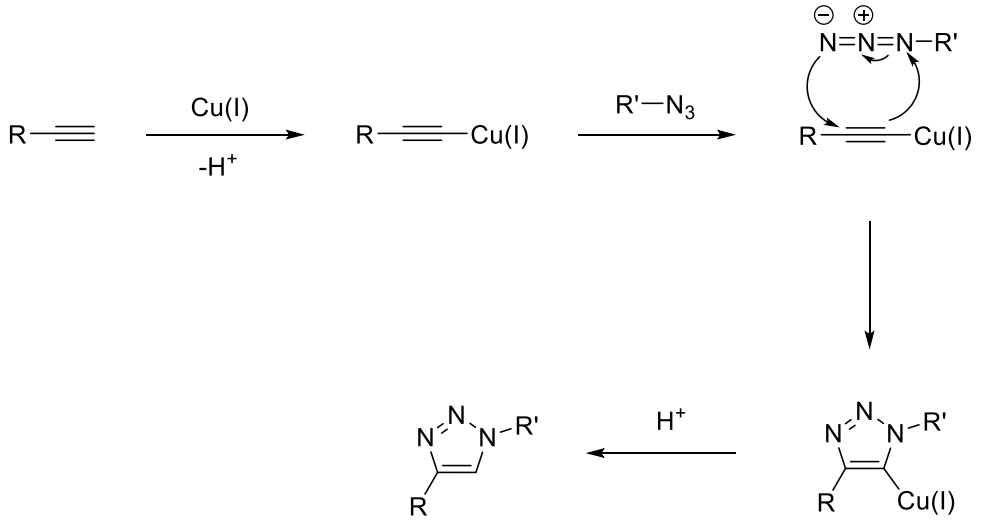

Figure 2.8 General mechanism representing the the Cu(I) catalysed cylocaddition of a terminal alkyne and azide.

An initial strategy was planned that followed synthetic work that had previously been completed in the group. Jenifer White used a two-step procedure to synthesise 5-ethynyl-2-pyridinecarboxaldehyde,[27] using procedures from reference 28 (Scheme 2.8). The first step involves a Sonogashira coupling between 5-bromo-2-pyridinecarboxaldehyde and ethynyltrimethylsilane to generate **17**, which is followed by basic cleavage of the silyl group to generate the terminal alkyne of **18**. **17** was synthesised with a yield of 60% and the cleavage of the silyl group to generate **18** ran with a yield of 54%.

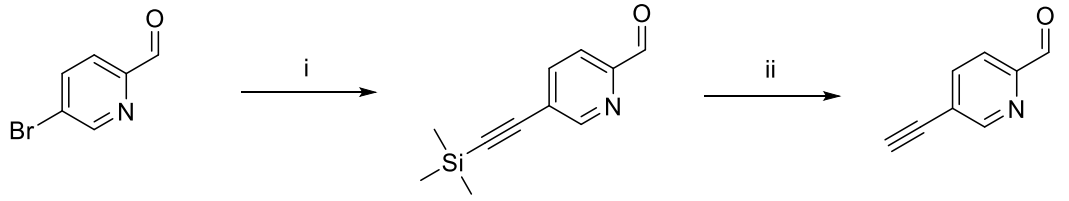

17 **18**

Scheme 2.8 Synthesis of alkyne functionalised pyridinecarboxaldehyde **18.** (i) ethynyltrimethylsilane, $Pd(PPh_3)_2Cl_2$, CuI, PPh_3, Et_3N, THF, Ar, reflux, 4.5 h; (ii) K_2CO_3, MeOH, RT, 2 h.

Having obtained an alkyne functionalised pyridinecarboxaldehyde, a two-step strategy to synthesise a triazide capping moiety was planned (Scheme 2.9). The first step involved conversion of the three hydroxyl groups of nitromethanetrispropanol to the corresponding mesylates using $MeSO_2Cl$ (following a procedure reported in reference 8) with an isolated yield of 83%. The trimesylate was then stirred with sodium azide in DMF, giving triazide **20** with a yield of 55%. Characterising this triazide proved difficult. The ^1H NMR spectrum of the isolated material shows that the peak corresponding to the methyl protons of the mesylate group has disappeared and a prominent band at 2090 cm^{-1} was observed on the IR spectrum, arising from an azide stretch. However, the product peak could not be observed by ESI +ve mass spectrometry, which was dominated by an unidentified high intensity peak with *m/z* = 236.2. Mass spectrometry was repeated using atmospheric pressure ionisation and a low intensity peak with *m/z* = 311.3 (corresponding to the expected $[M+H]^+$) was observed. Tandem mass spectrometry techniques were used to observe any fragmentation products when this peak was subjected to higher fragmentation energy. This did not reveal a peak with *m/z* = 236, suggesting that the base peak observed in the original MS experiment was not a fragmentation product of the desired triazide. Despite the uncertainty around this, the triazide product was carried through to the copper(I) catalysed cycloaddition with **18** (Scheme 2.10). These cycloaddition conditions use copper(II) sulfate as the copper source. Sodium ascorbate is added to reduce the Cu(II) to the catalytically active Cu(I). Initial trials of this experiment did not appear to progress by TLC at room temperature, and so the reaction was heated to 50 °C and monitored by analytical HPLC using a gradient eluent of 0-100% MeCN in H_2O over 40 minutes. The pyridine starting material is clearly observed when monitoring at

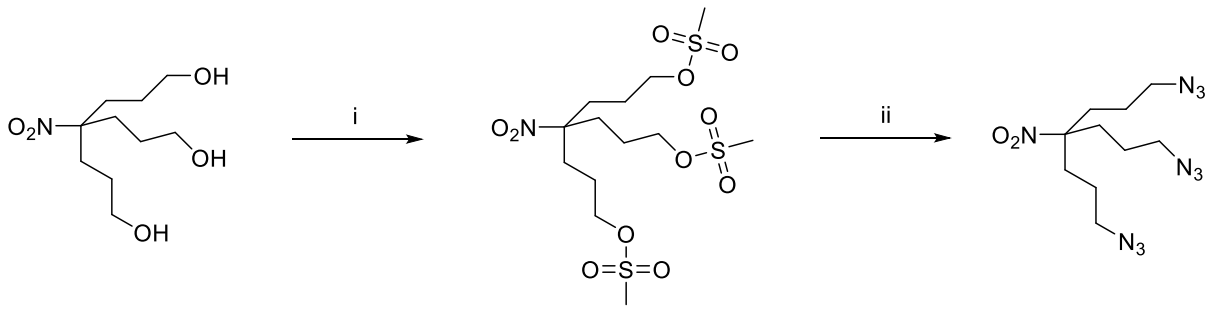

19 **20**

Scheme 2.9 Two step synthesis from nitromethanetrispropanol to triazide **20**. (i) $MeSO_2Cl$, Et_3N, THF, 0 °C – RT, 24 h. (ii) NaN_3, DMF, Ar, RT, 17 h.

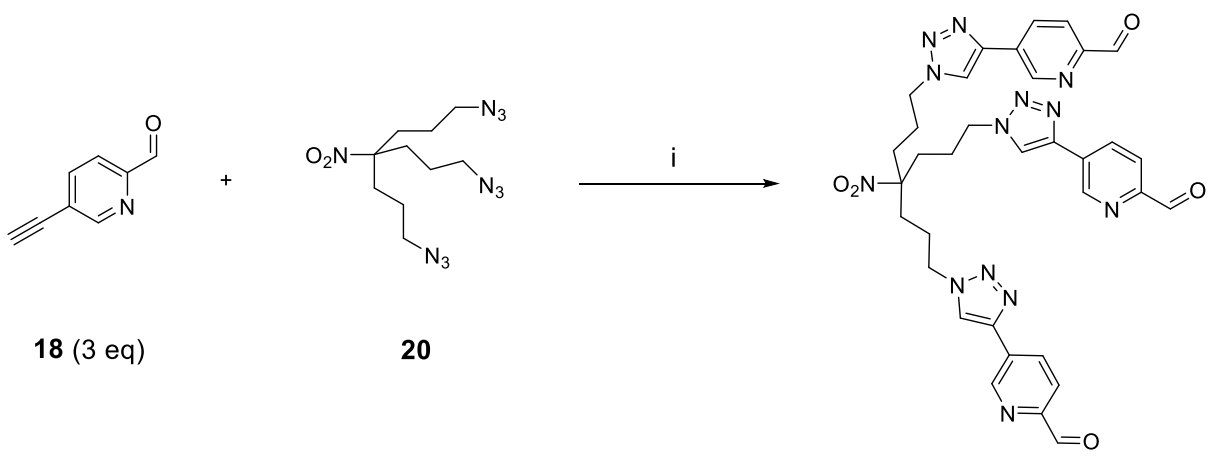

18 (3 eq) **20**

Scheme 2.10 Copper(I) catalysed cycloaddition of alkyne **18** and triazide **20**. (i) $CuSO_4.5H_2O$, Na ascorbate, 1:1 H_2O:*t*-BuOH, 40 °C.

265 nm and after 1.5 h three new peaks can be seen on the chromatogram with retention times of 22.4, 25.4, and 28.9 minutes (Figure 2.9). The reaction did not appear to progress between T= 3.0 h and T = 4.5 h, and so the three product peaks were collected and analysed by ESI-MS. The first peak (R_T = 22.4 min) showed a MS base peak at *m/z* = 726.3, corresponding to $[M+Na]^+$ of the desired tri-clicked product, while the second (R_T = 25.4 min) had a base peak corresponding to the di-clicked product (*m/z* = 595.2, $[M+Na]^+$). The third peak (R_T = 28.9 min) showed a MS peak corresponding to the mono-clicked product (*m/z* = 467.1, $[M+Na]^+$). Given that **18** is in excess and the reaction was run at 50 °C there should be enough drive for this reaction to reach completion, so this mixture may arise due to the instability of triazide **20**. The difficulties in obtaining MS characterisation data for triazide **20**

supports this rationale. The reaction mixture appeared as a series of very close running spots by TLC, and so purification of the reaction by silica chromatography was not attempted. Purification would be possible by prep-HPLC but the relative areas underneath each peak indicate that the yield of the desired tri-clicked product would be relatively low. There were also concerns around whether compound **20** might be explosive, due to the high number of nitrogens present on a relatively small molecule. Efforts were instead focussed on swapping the positions of the click functionalities, such that an azide functionalised pyridine was reacting with a trialkyne capping moiety.

A literature procedure from the dendrimer work of Roy and co-workers [11] influenced the strategy adopted to synthesise the trialkyne capping moiety shown in Scheme 2.11. Roy's procedure involves deprotonating Boc-protected tris(hydroxymethyl)aminomethane with potassium hydroxide and reacting the resultant oxides with propargyl bromide to generate the corresponding trialkyne. In Scheme 2.11, a similar procedure is applied to Cbz-protected tris(hydroxymethyl)aminomethane. The Cbz protecting group was chosen as it is traditionally cleaved by catalytic hydrogenation [21] and so was expected to be stable under these conditions. The presence of the benzyl ring should also make the product easier to monitor, as it should be visible on a TLC plate under short wave UV light.

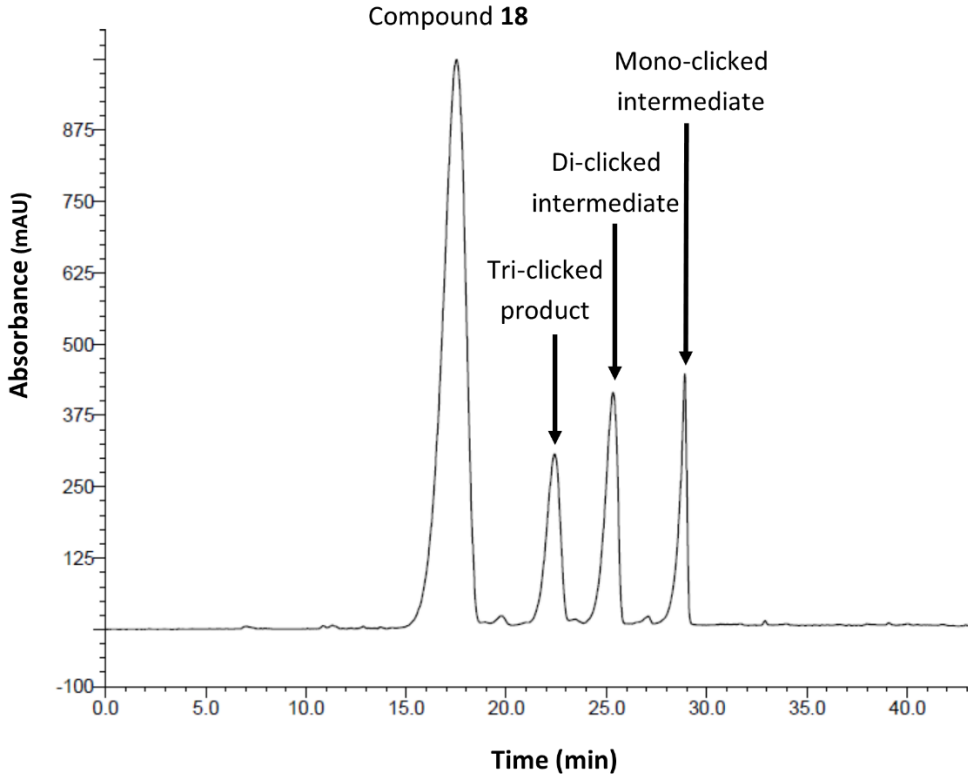

Figure 2.9 HPLC chromatogram of an aliquot taken from the reaction shown in Scheme 2.10 after 4.5 h. Three distinct product peaks can be observed corresponding to the tri-clicked, di-clicked and mono-clicked compounds. Conditions used: 0 – 100% MeCN in H_2O over 40 min, monitoring at 265nm.

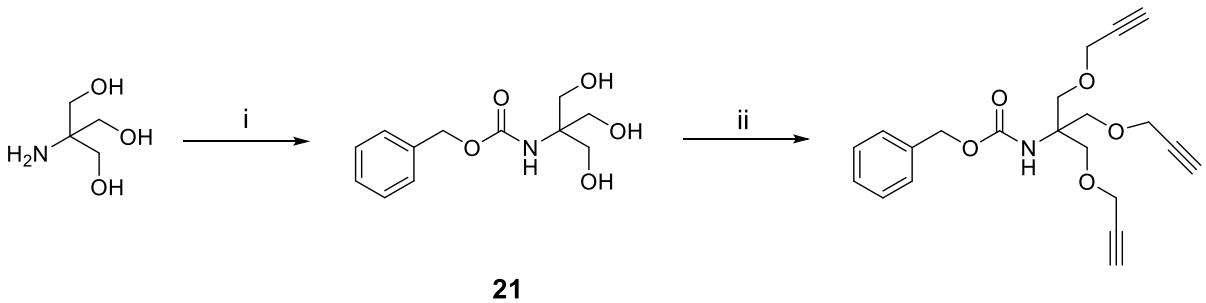

21

Scheme 2.11 Attempted synthesis performed to generate a trialkyne capping moiety. (i) $NaHCO_3$, CbzCl, EtOAc, RT, 6 h; (ii) propargyl bromide, KOH, DMF, Ar, 0 - 35 °C, 23 h.

The Cbz protection step proceeded cleanly to produce **21** with an isolated yield of 72%. However, the Cbz protecting group appears to be unstable under the conditions used in the second step. Monitoring by analytical HPLC showed chromatograms with numerous species present (Figure 2.10). When no change was observed between T = 20 h and T = 23 h, the reaction was quenched and the product extracted into EtOAc. Purification by silica column chromatography was performed to isolate what appeared to be the predominant product observable by TLC. This yielded a yellow oil, which did not appear to have any aromatic protons by ^{1}H NMR spectroscopy (Figure 2.11), suggesting that the protecting group was cleaved during the reaction. This is surprising, as the CBz group is reported to be resistant to a pH of up to 12, unless high temperatures are applied.[21] The number of alkyne proton environments visible on the ^{1}H NMR spectrum suggest that the exposed nitrogen may have reacted with the electrophilic carbon of propargyl bromide, giving the tetra-alkyne (Figure 2.11). Given this complication, it was decided to repeat the experiment using nitromethanetrispropanol as the starting material. Even though the nitro group is not itself suited to coupling with a desirable moiety, it's conversion to the amino group would be considered in future if the chemistry proved useful for forming a capping moiety. Scheme 2.12 shows the reaction performed, using the same conditions as those used with the attempted conversion of **21**. Trialkyne **22** was isolated with a yield of 50%.

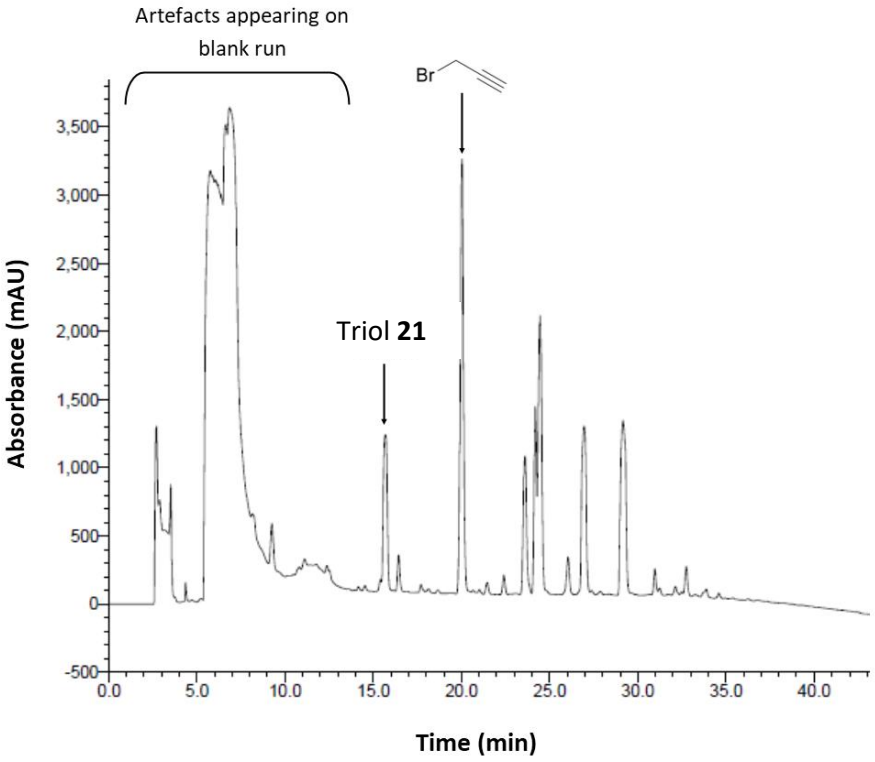

Figure 2.10 HPLC chromatogram of an aliquot taken at T = 23 h during the attempted conversion of **21** to a trialkyne capping moiety. Conditions used: 0 – 100% MeCN in H_2O over 40 min. Monitoring at 210 nm.

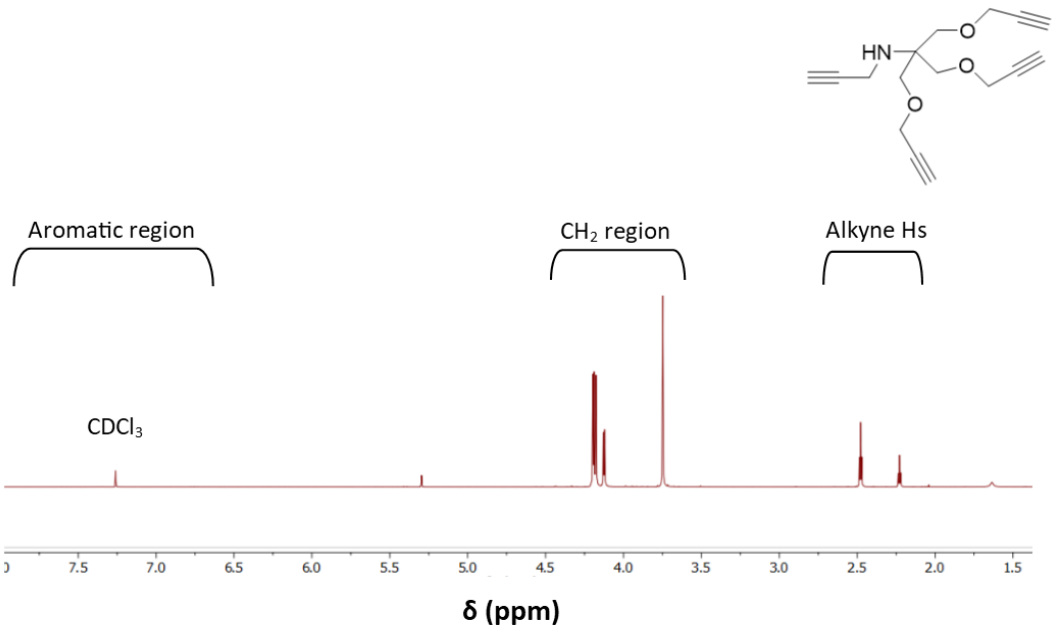

Figure 2.11 ^{1}H NMR spectrum of the isolated product from the reaction attempting to convert **21** to a trialkyne, and the proposed structure of the actual product isolated.

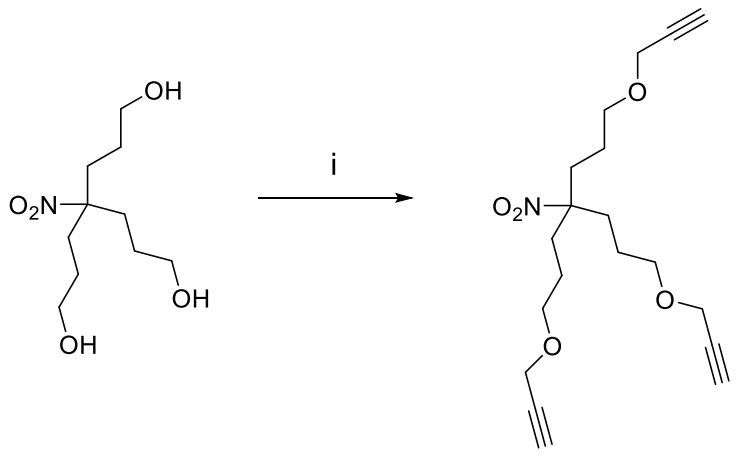

22

Scheme 2.12 Conversion of nitromethanetrispropanol to trialkyne **22**. (i) propargyl bromide, KOH, DMF, Ar, 0 - 35 °C, 17 h.

With a trialkyne in place, efforts were focussed on synthesising an azide functionalised pyridine. Scheme 2.13 shows the strategy used to synthesise model azidopyridine **26**, which was then used in the trial click reaction shown in Scheme 2.14. The first step in Scheme 2.13 involves a lithium-halogen exchange in the 5-position, followed by a DMF quench to give pyridinecarboxaldehyde **23**. The choice of solvent influences the site of lithiation in this reaction. Diethyl ether is used as it is a coordinating solvent, which has been reported to favour lithiation in the 5-position.[29] 2-bromo-5-lithiopyridine is believed to be the kinetic product, as the diethyl ether coordinates between the nitrogen of the ring and the polar C-Br bond adjacent to this. This makes it more favourable to substitute the bromo substituent in the 5-position rather than the one in the 2-position. **23** was isolated with a yield of 63%. Sodium borohydride was then used to reduce **23** to primary alcohol **24**, which was isolated with a yield of 86%. The alcohol was then covered into mesylate **25** to increase the reactivity of the adjacent carbon towards nucleophilic attack. Methanesulfonic anhydride proved a more reliable agent for this step than methanesulfonyl chloride, which was used when running this reaction for the first time. When methanesulfonyl chloride was used, the free Cl^- reacted with the generated mesylate, converting it the corresponding chloride (2-bromo-5-(chloromethyl)pyridine). While this chloride would still have been suitable for conversion to the azide, its apparent instability in solution made purification difficult. When methanesulfonic anhydride is used, there is no free chloride in the reaction mixture and therefore only the desired mesylate is produced. The final step involves conversion of the

mesylate group to the corresponding azide, achieved by mixing **25** with sodium azide in DMF. **26** was isolated with a yield of 61%. Azide **26** then reacted with trialkyne **22**, as shown in Scheme 2.14. **27** was isolated in sufficient purity with a yield of 59%. This moderate yield suggests that using cycloaddition click chemistry to form trialdehyde capping moieties with azide functionalised pyridines is a viable option to synthesise a capped cylinder.

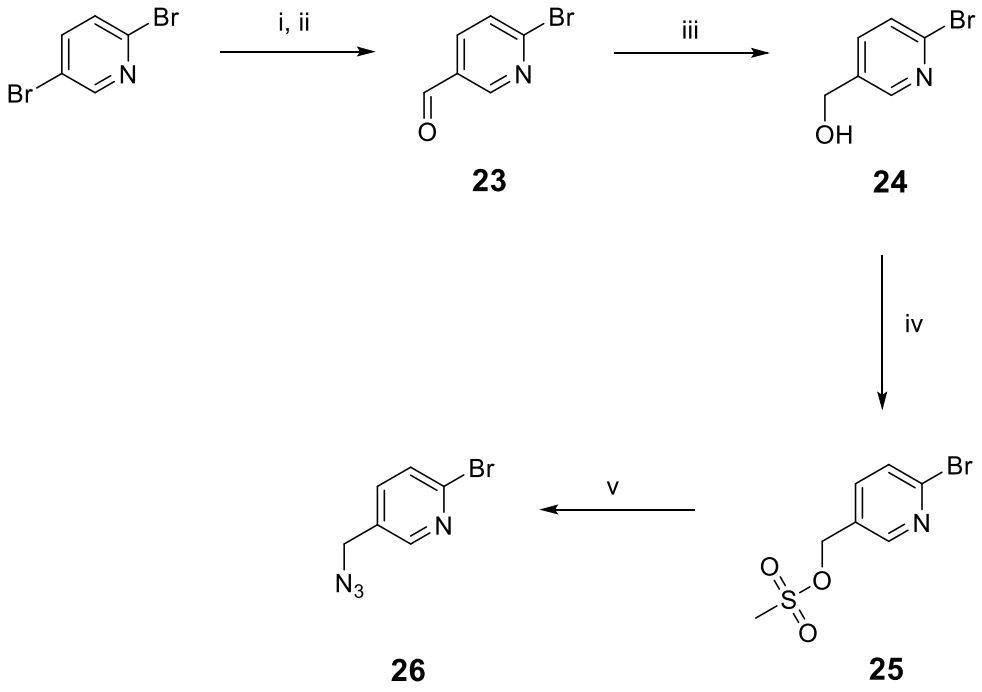

Scheme 2.13 Synthesis of azide functionalised pyridine **31.** (i) *n*-BuLi, Et_2O, -78 °C, 1 h; (ii) DMF, -78 °C, 1 h; (iii) $NaBH_4$, MeOH, 0 °C – RT, 1 h; (iv) $(MeSO_2)_2O$, DCM, 0 °C, 1 h; (v) NaN_3, DMF, 0 °C – RT, 17.5 h.

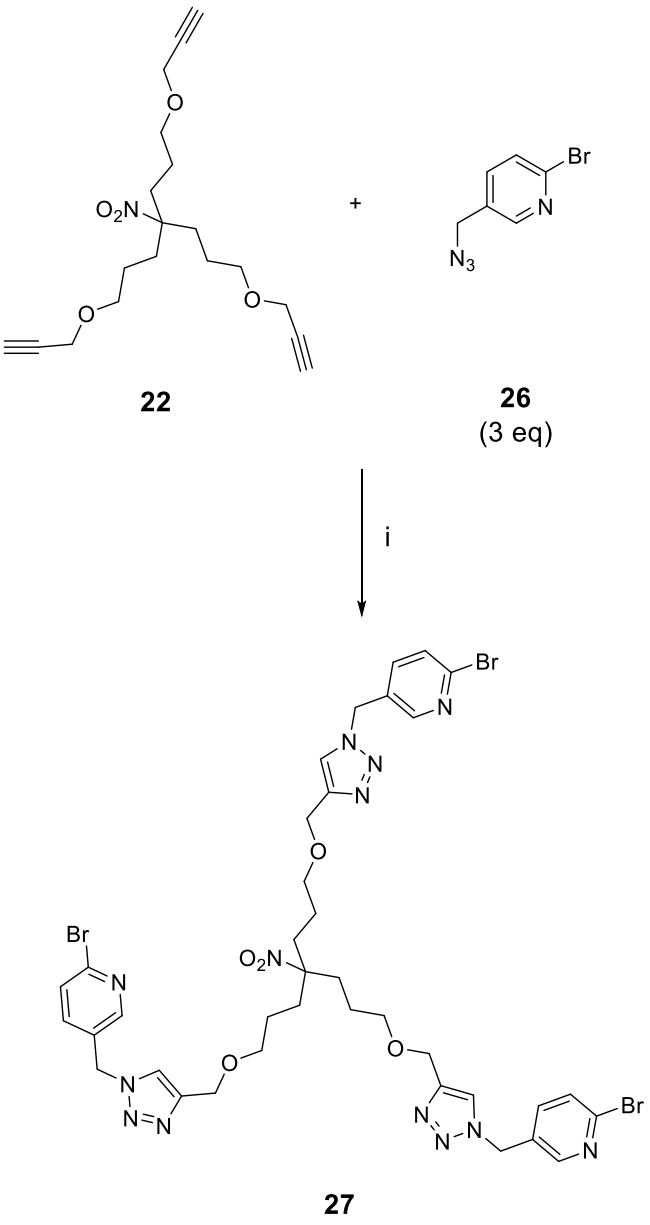

Scheme 2.14 Copper(I) catalysed cycloaddition of trialdehyde **22** and azide functionalised pyridine **26.** (i) $CuSO_4 \cdot 5H_2O$, Na ascorbate, THF:H_2O, 60 °C, 35 h.

Tribromide **27** was then subject to lithium-halogen exchange with *n*-BuLi followed by a DMF quench, using the same procedure used to generate pyridinecarboxaldehyde **23.** The aim was to convert tribromide **27** to the corresponding trialdehyde, as shown in Scheme 2.15. However, the ^{1}H NMR spectrum of the crude material showed a complex mixture and no product peak was observed by ESI +ve mass spectrometry, suggesting that tribromide **27** cannot withstand the harsh *n*-BuLi conditions. A solution could be to modify Scheme 2.13 to include a step to convert 2-bromopyridine **24** into the 2-carboxaldehyde analogue using *n*-BuLi followed by DMF. The hydroxyl group of **24** would first needed to be protected,

otherwise the hydroxyl group will be deprotonated by *n*-BuLi. After conversion of the bromide to the carboxaldehyde, the hydroxyl group would need to be deprotected before its conversion to the mesylate. With the addition of these three steps, a pyridine ring with an aldehyde in the 2-position and methylazide in the 5-position could be synthesised, which could then be reacted with trialkyne **22**. However, this chemistry wasn't explored any further in this context, although it is used in Chapter 3. Efforts were instead focussed on parallel work that looked more promising at the time, using alternate linkages between the tripod molecule and the pyridinecarboxaldehydes.

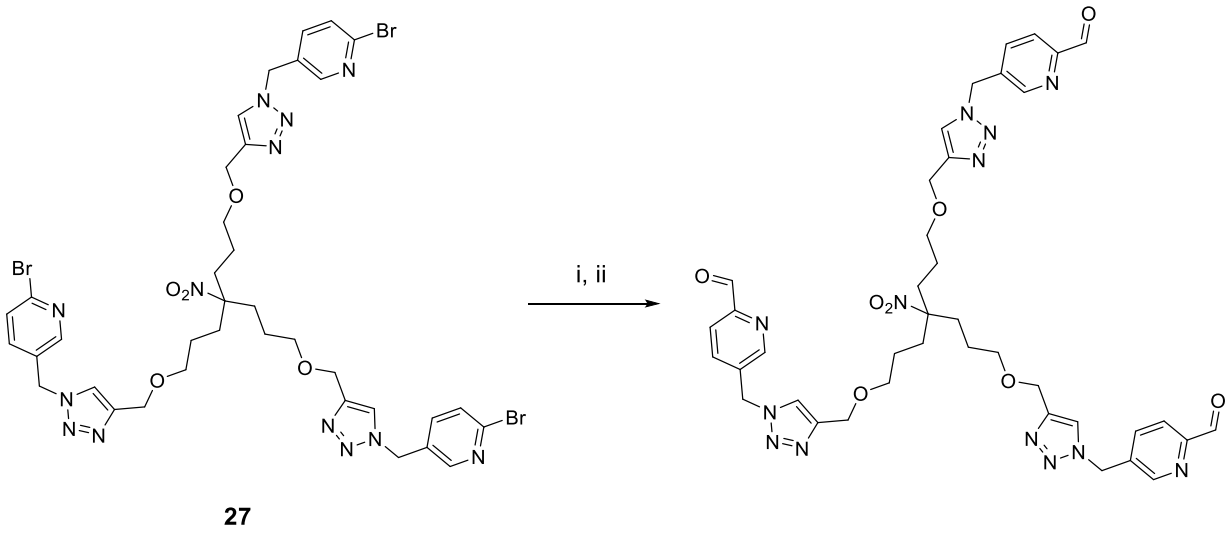

27

Scheme 2.15 Attempted synthesis of trialdehyde 32. (i) *n*-BuLi, THF, -78 ^{o}C, 2 h; (ii) DMF, -78 ^{o}C, 1 h.

2.4 Using Mitsunobu chemistry to form a capping moiety

Using Mitsunobu chemistry to link functionalised pyridines to tripod capping moieties was also explored as part of this work. The Mitsunobu reaction offers a means of converting an alcohol to a variety of functional groups through nucleophilic attack of an oxy-nucleophile at the α-carbon of the alcohol. This reaction relies on the action of triphenylphosphine and an azodicarboxylate, commonly diethyl azodicarboxylate (DEAD). Despite this reaction being widely used since its publication by Oyo Mitsunobu in the 1960s [30] the exact mechanism is still open to debate. One likely mechanism is illustrated in Figure 2.12. This mechanism consists of four key stages. The first involves the formation of a betaine by addition of triphenylphosphine to the weak N=N bond of the azodicarboxylate. This betaine is stabilised by the adjacent ester group, and has been observed through ^{31}P NMR and ESI-MS. [31,32] In the next step, the negatively charged N of the betaine deprotonates the nucleophile, which is followed by the lone pair on the alcohol oxygen attacking the cationic phosphrous to generate the alkoxyphosphonium salt. The exposed nucleophile then reacts with the α-carbon, generating the desired product and triphenylphosphine oxide. The reaction is driven by the generation of the strong P=O and N-H bonds of the two by-products: triphenylphosphine oxide and the reduced urea form of whichever azodicarboxylate is used. Generation of ethers using the Mitunobu reaction has been extensively used on hydroxyl containing substrates such as sugars [33] and has previously been used in the Hannon group to functionalise cylinders with large aromatic groups.[34] This previous work influenced a strategy to synthesise 5-hydroxypyridine-2-carboxaldehyde (**31**, Scheme 2.16) which would serve as a nucleophile in the planned Mitunobu reaction outlined in Scheme 2.17. The aim of this work was to investigate whether three equivalents of **31** could react with nitromethanetrispropanol under Mitsunobu conditions to generate the trialdehyde capping moiety shown in Scheme 2.17.

The first step of Scheme 2.16 involves oxidation of 2-methyl-5-hydroxypyridine to corresponding *N*-oxide **28.** Initially, this step was performed using *m*CPBA, following a literature procedure from Gütlich and co-workers.[35] This procedure involved recrystallizing the product by adding diisopropyl ether as a co-solvent to a solution of the crude product in hot EtOH, which provided the N-oxide as white crystals with a yield of 71%. However, traces of the *m*- chlorobenzoic acid byproduct were visible by ^{1}H NMR spectroscopy and as such an alternate procedure was adopted. Hydrogen peroxide was used as an alternative oxidant to

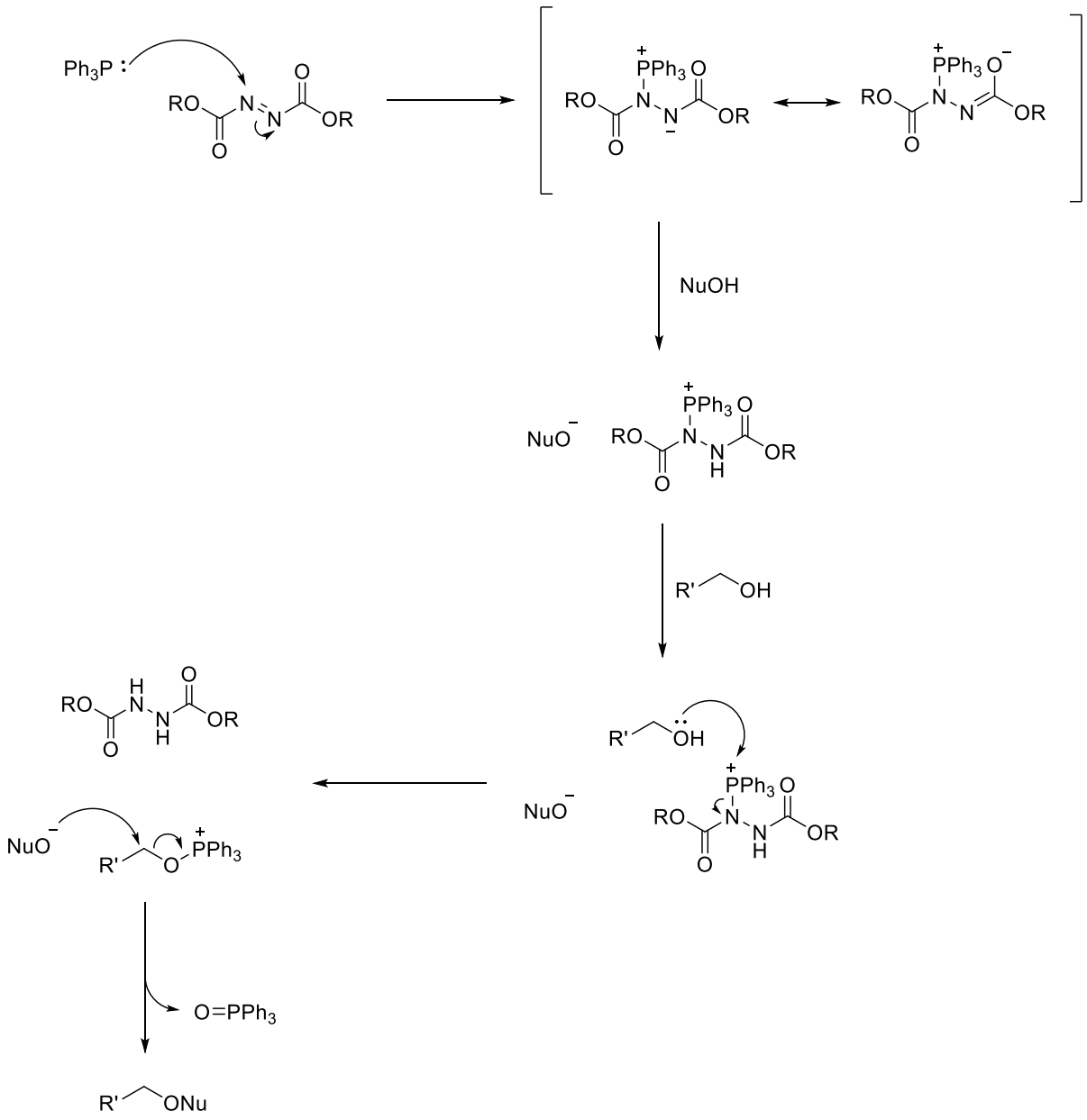

Figure 2.12 Postulated mechanism for the Mitunobu reaction between a primary alcohol and an oxy-nucleophile (NuOH).

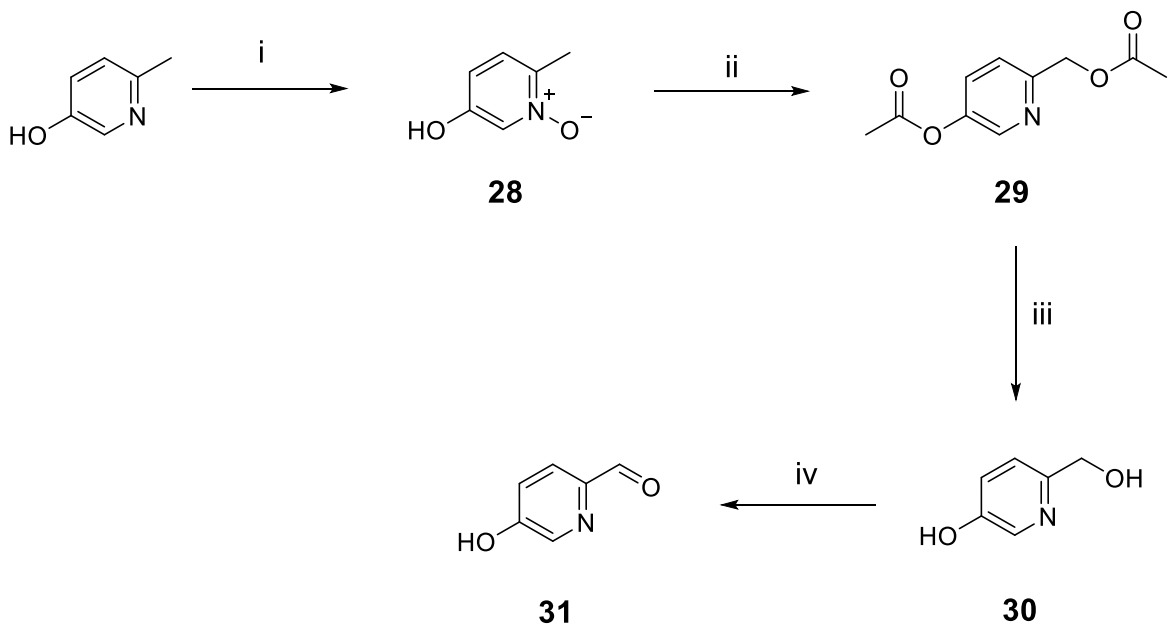

Scheme 2.16 Synthesis of 5-hydroxypyridine-2-carboxaldehyde **31**. (i) H_2O_2, AcOH, reflux, 3.5 h; (ii) Ac_2O, reflux, 2 h; (iii) HCl (aq), reflux, 1 h; (iv) activated MnO_2, iPrOH, reflux, 2.5 h.

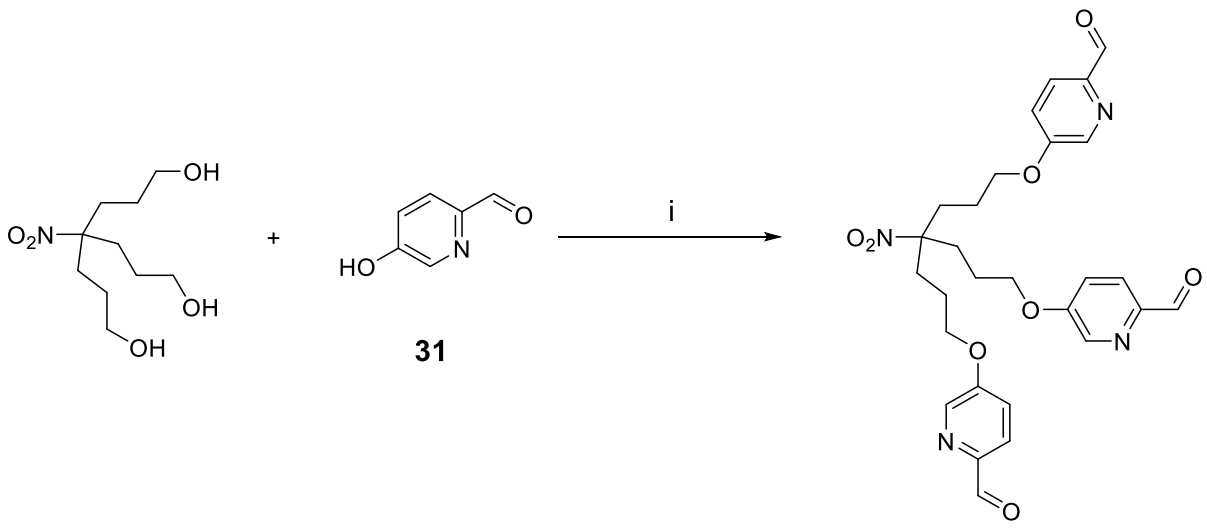

Scheme 2.17 Proposed synthesis of a trialdehyde capping moiety using Mitsunobu reaction conditions. (i) PPh_3, DEAD, THF, 0 °C – RT, 40 h.

generate **28** with a comparable yield of 74%. Refluxing in acetic anhydride converts **28** to diacetyl **29**, with a near quantitative yield of 98%. This conversion occurs via the mechanism shown in Figure 2.13, which involves nucleophilic attack of the oxide on acetic anhydride, followed by a [3,3]-sigmatropic shift of the resultant acetate. Another nucleophilic attack on

acetic anhydride from the hydroxyl oxygen generates **29**.[36] The resultant acetate groups are then cleaved by refluxing in concentrated HCl (aq) to yield diol **30** with an isolated yield of 33%. This low yield is not representative of the conversion, but rather the difficulty of isolating the product. After the reaction has reached completion, the reaction is neutralised by slow addition of Na_2CO_3 (aq) and this must be followed by concentration under reduced pressure as **30** is very aqueous soluble. A sticky residue results which must be triturated with hot solvent so that the organic material is dissolved, leaving behind any inorganic salts. Trituration was achieved using boiling acetonitrile. The Büchner funnel used to separate the solution from the salts was continuously heated with a heat gun to minimise the amount of product precipitating back out of solution. The material obtained was then further purified by silica chromatography to isolate **30** in adequate purity. This difficult purification protocol leads to loss of product, as reflected in the low yield. The final step involves oxidation of the primary alcohol of **30** to aldehyde **31** using activated manganese dioxide. The yield for this step is also low (36%) which again reflects more on the isolation method than the conversion. Aldehyde **31** was isolated by centrifuging the reaction mixture and separating the supernatant from the manganese residue. Despite multiple resuspensions of the residue, it is likely that some product remained trapped in the solids.

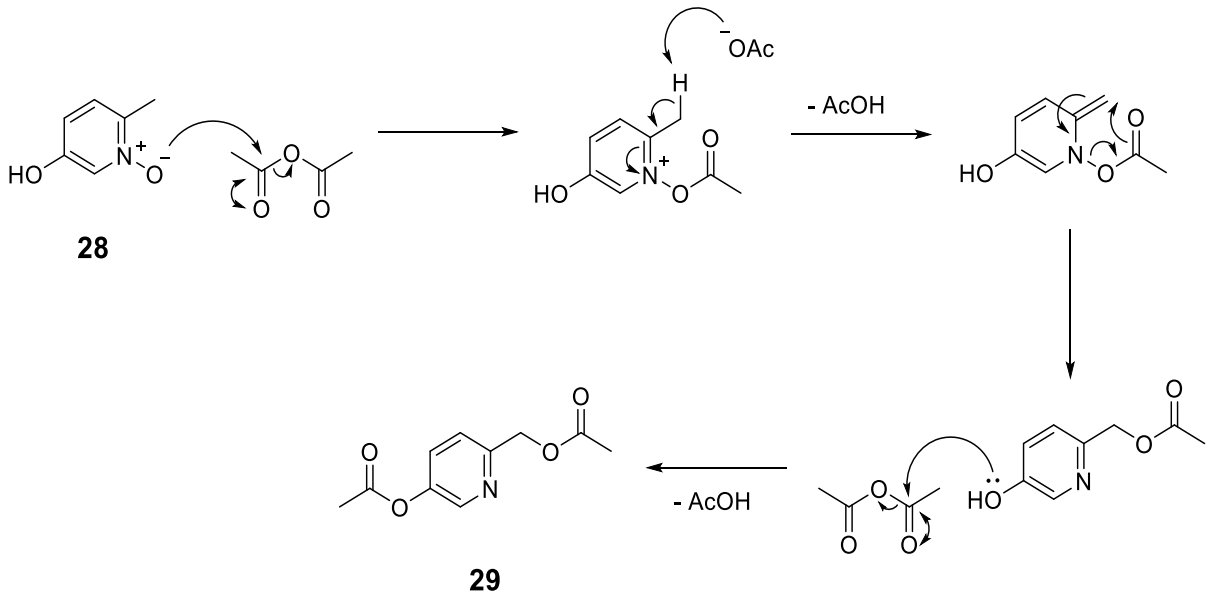

Figure 2.13 Mechanism showing the conversion of *N*-oxide **28** to diacetyl **29.**

With a route to 5-hydroxypyridine-2-carboxaldehyde established, **31** and nitromethanetrispropanol were mixed under Mitsunobu conditions to see whether the tri-aldehyde would form (Scheme 2.17). Six equivalents of triphenylphosphine were dissolved in THF under N_2, and this mixture was cooled in an ice bath. Six equivalents of DEAD were then added dropwise. The mixture was left stirring for 15 minutes to allow the betaine intermediate to form before one equivalent of nitromethanetrispropanol was added. After stirring for 30 minutes, a solution of six equivalents of **31** in THF was added. The reaction was then allowed to warm to room temperature and monitored by analytical HPLC, with an eluent gradient of 0 - 100% B in A (where A = H_2O + 0.05% TFA; B= MeCN + 0.05% TFA) over 40 min. Figure 2.14 shows the measured chromatogram after 40 h. The two most prominent new peaks at 19 min and 26 min were collected and analysed by ESI-MS, however both peaks appeared complex and neither showed the mass peak of the desired product. This apparent lack of product may indicate that the betaine intermediate is not basic enough to deprotonate nitromethanetrispropanol, although the TLC of the reaction mixture (using 10% MeOH in DCM as eluent) did show that the nitromethanetrispropanol starting material had been consumed. The reaction was repeated using 1,1'-(Azodicarbonyl)dipiperidine instead of DEAD and used PMe_3 in place of the PPh_3, as this combination is reported to form a more basic betaine which deprotonates weak acids with a pKa of up to 11.[37] Disappointingly, no evidence of the product was found by ESI-MS of the crude material. Given the apparent complexity of the mixture, further efforts to generate a trialdehyde cap using Mitsunobu chemistry were halted in favour of performing the same chemistry via a simpler ether synthesis.

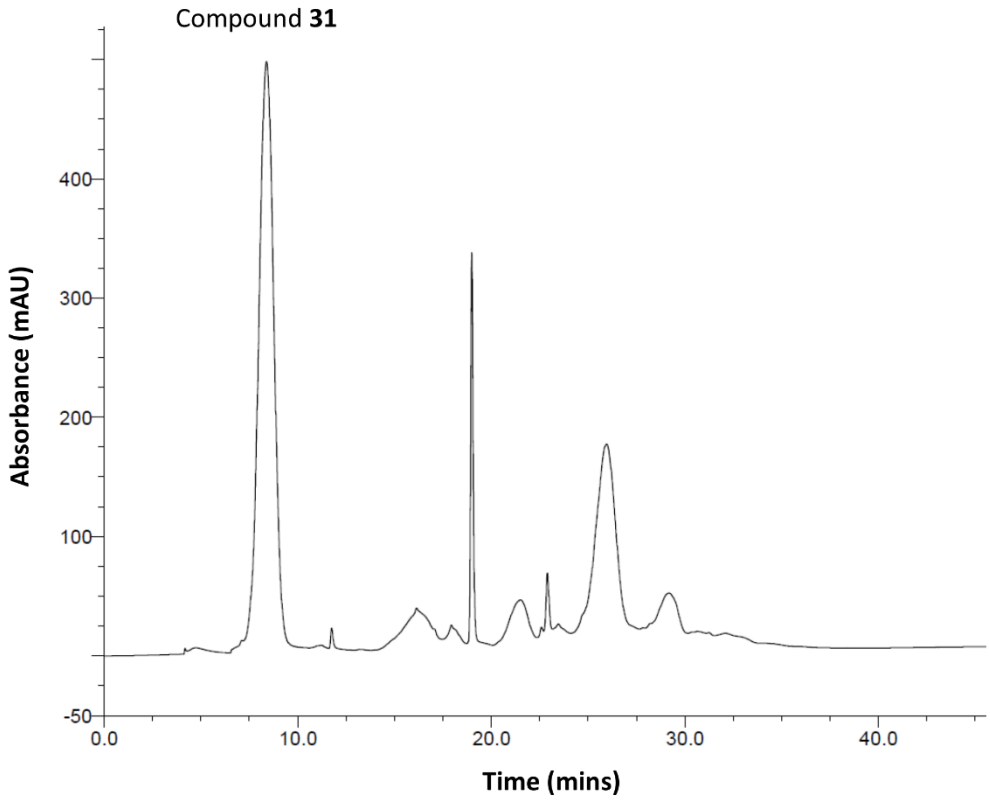

Figure 2.14 HPLC chromatogram of an aliquot taken from the Mitsunobu reaction shown in Scheme 2.17 at T = 40 h.

2.5 Using S_N2 ether synthesis to form a capping moiety

Given the hurdles faced when trying to synthesise a trialdehyde cap using Mitsunobu chemistry, an alternative method to generate a triether from nitromethanetrispropanol and hydroxylpyridine **31** was investigated. One of the most common methods used to make ethers is the Williamson ether synthesis, which reacts an alkoxide with an organohalide as illustrated in Figure 2.15. There are two requirements that must be met for the ether synthesis to be successful. Firstly, a base must be used that is strong enough to deprotonate the alcohol starting material. Secondly, X must be a good leaving group. A literature search identified a procedure that reacts a phenol analogue of **31** with 1,2-dibromoethane.[38] This procedure uses potassium carbonate as a base and proceeds with a near quantitative yield of 95%. This was used as the basis for a trial reaction, outlined in Scheme 2.18, to check that hydroxypyridine **31** is stable under these conditions.

Figure 2.15 General mechanism of the Williamson Ether Synthesis.

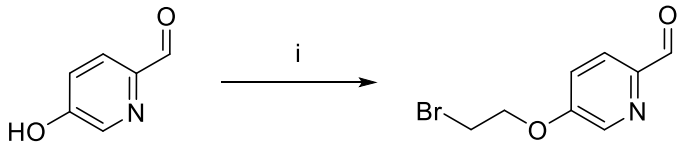

31 **32**

Scheme 2.18 Trial reaction to check the stability of **31** in ether synthesis conditions. (i) 1,2-dibromoethane, K_2CO_3, DMF, Ar, 100 °C, 1 h.

Under an argon atmosphere, anhydrous potassium carbonate was used to deprotonate **31** and then 1 equivalent of 1,2-dibromoethane was then added. Only 1 equivalent of the dibromide was added to minimise formation of the disubstituted by-product. The reaction was heated at 100 °C and monitored by TLC. After 1 hour of heating, conversion of the starting material was complete and the product was isolated with a yield of 52%. Characterisation using NMR and MS indicated that the reaction had been successful.

With the knowledge that **31** is stable under these basic conditions, a strategy to use the same chemistry to react **31** with a derivative of nitromethanetrispropanol was adopted. Previous work in this chapter has already detailed the conversion of nitromethanetrispropanol to the corresponding trimesylate (**19** in Scheme 2.9) and this was used in place of a trihalide analogue. Scheme 2.19 outlines the conditions used. Five equivalents of potassium carbonate were mixed with four equivalents of **31** in DMF under Ar. After stirring at 100 °C for 1 h, one equivalent of **19** was added and the reaction was monitored by TLC. After heating for a further 1 h, **19** appeared to be consumed. After extraction into EtOAc, trialdehyde **33** was isolated by silica column chromatography as a light brown solid in 82% yield.

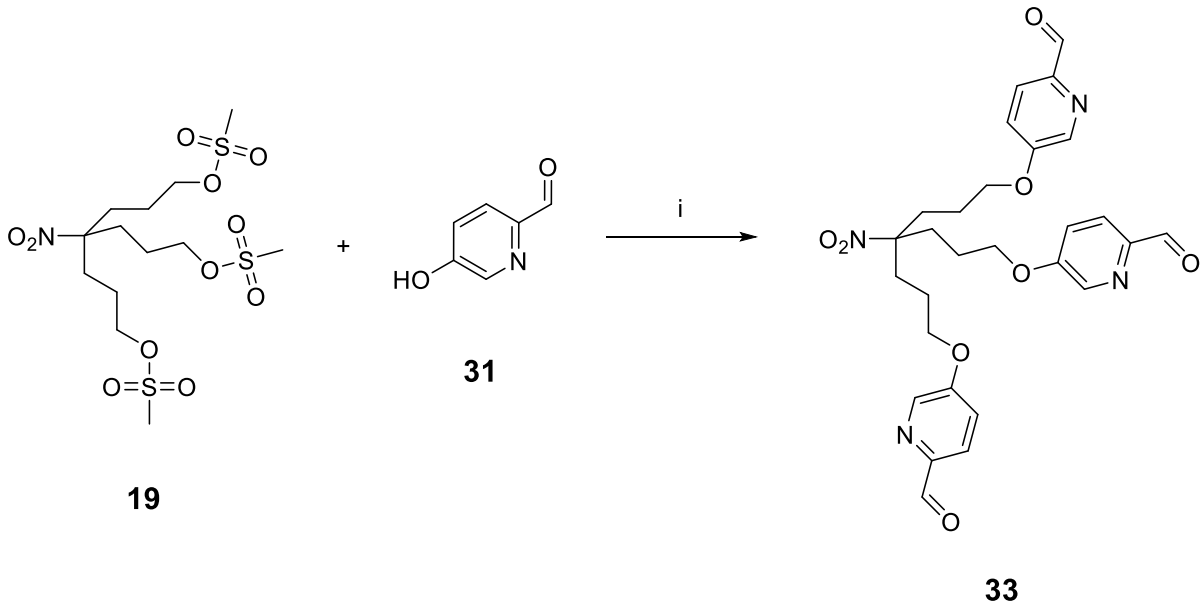

19 31 33

Scheme 2.19 Synthesis of trialdehyde **33** using Williamson ether synthesis conditions. (i) K_2CO_3, DMF, Ar, 100 °C, 1 h.

Figure 2.16 shows the ^{1}H NMR spectrum recorded for trialdehyde **33**. Only one set of pyridine aromatic resonances is visible between 7.6 and 8.6 ppm, suggesting that all of the arms of the capping moiety have reacted. A single aldehyde proton peak is also present at 10.0 ppm, indicating that the aldehyde functionality has been retained and is stable in these conditions. A CH_2 triplet is clearly resolved at 4.16 ppm, arising from to the aliphatic carbon α to the ether link. Again, the clear definition of a single triplet indicates that all three arms of the capping moiety are structurally identical. Two complex multiplets are present between 1.8 and 2.3 ppm, arising due to the other two aliphatic carbons that form the arms of the cap. It was expected that these peaks would also appear as resolved triplets. The fact that they do not may indicate that there is a degree of conformational lock during the NMR timescale, resulting in these protons being in slightly different environments. It may be that there is a degree of non-covalent interaction between the three pyridine rings that contributes to this, possibly edge to face π interactions. Alternatively, the *J* values arising from NOE coupling between protons on different arms may be sufficiently large to influence the observed multiplicity of these peaks. Twelve resonances are observed by ^{13}C NMR spectroscopy as expected, and the *m/z* corresponding to $[M+H]^+$ and $[M+Na]^+$ are observed by ESI-MS. This suggests that the desired trialdehyde has been isolated. The NMR data was recorded again after storing

trialdehyde **33** as a solid at room temperature for several months. No changes to the spectra were observed, indicating that the trialdehyde cap is stable at room temperature.

A synthetic route to a trialdehyde cap has been found through linking a pyridinecarboxaldehyde through ether formation to an AB_3 tripod molecule. This route is relatively simple, reliable, and proceeds in good yield.

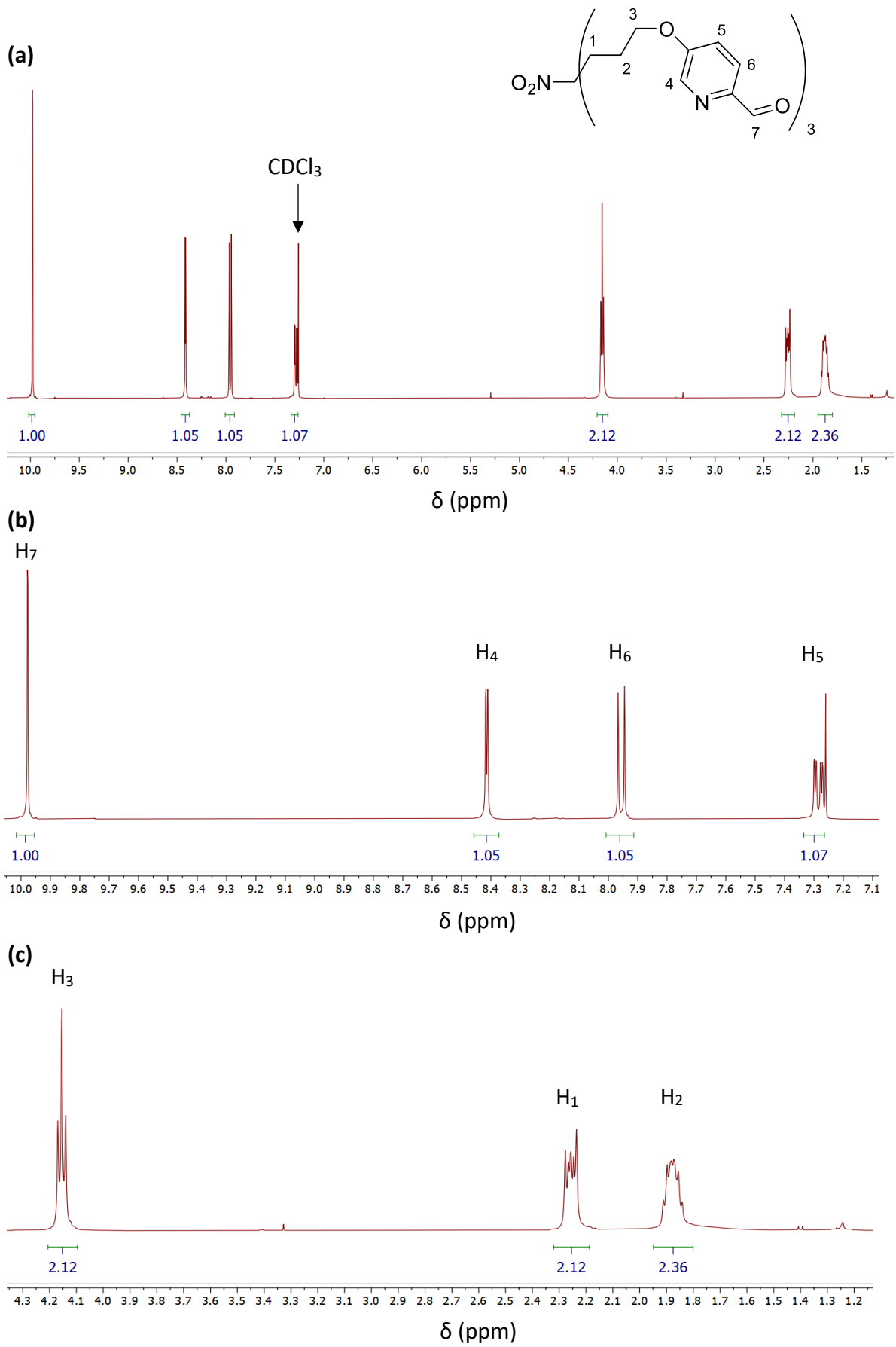

Figure 2.16 (a) The 1H NMR spectrum of trialdehyde **33**; (b) an closer view of the aromatic region; (c) a closer view of the aliphatic region.

2.6 Using a trialdehyde capping moiety to make a capped metallohelicate cylinder

With a route to a trialdehyde cap established, the next step was to investigate whether this will form a capped cylinder when mixed with the other required components: 4,4'-methylenedianiline and a source of M^{2+} ions. As $Fe_2L_3Cl_4$ is the most extensively studied in the group, $FeCl_2$ was chosen as the metal source. The planned reaction is illustrated in Scheme 2.20, using the same principle as Scheme 2.3.

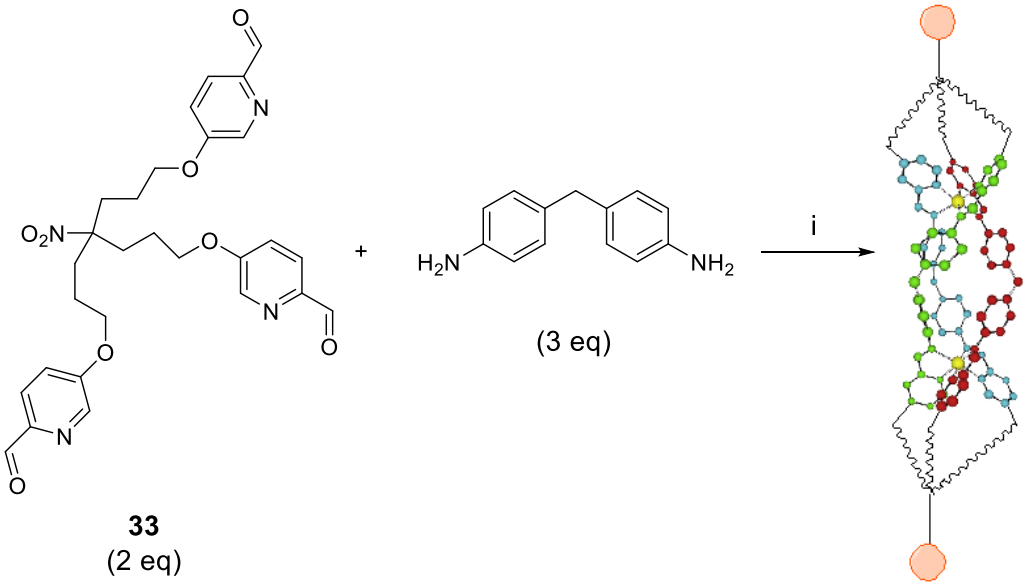

33
(2 eq)

Scheme 2.20 Proposed synthetic route to a dicapped metallosupramolecular cylinder. (i) $FeCl_2.4H_2O$, MeOH, reflux, 2 h.

Two approaches were considered when planning this experiment, which differ in the order that reagents are added. The first approach would form the dicapped cryptand-like ligand structure before the metal ions are introduced, by pre-mixing two equivalents of **33** with three equivalents of 4,4'-methylenedianiline. The second approach involves mixing **33** with the metal first, and then adding the dianiline linker. This second approach was selected, as it was hoped that the iron cations would act as a template, bringing the three arms of the cap together by coordinating to the nitrogens of each pyridine ring and the adjacent carbonyl oxygens. Upon addition of 4,4-methylenedianiline, it was hoped that imine formations would occur and effectively link two of these complexes together, forming the cylinder.

Two equivalents of trialdehyde **38** were mixed with two equivalents of iron(II) chloride in methanol. After five minutes of stirring, three equivalents of 4,4'-methylenedianline were

added. Unfortunately, a purple precipitate immediately formed, which did not redissolve with a further two hours of heating under reflux. The purple colour suggests that coordination to the metal did occur, so this precipitate may be a polymeric species created when the arms of the cap coordinate to different metal centres. As with the synthesis of the $Ru_2L_3Cl_4$ described in section 1.4, this polymer is likely the kinetic product. When synthesising cylinders, the reaction can usually be driven to the thermodynamic product (that is, the discrete triple stranded cylinder) by providing sufficient thermal energy through heating under reflux. However, if the polymeric species precipitates out of solution, it is difficult to get enough energy into the system. The precipitate was isolated and dissolution attempted in a variety of deuterated solvents with the aim of investigating the structure using NMR spectroscopy. Chloroform-d, methanol-d4, acetonitrile-d3, dimethyl sulfoxide-d6, and dimethylformamide-d7 were all tested, but the precipitate did not dissolve in any of these solvents. Over several days, samples of the solid in DMSO and DMF did gradually turn blue, indicating that the metal ions were slowly dissociating from the ligands and coordinating to the solvent molecules. The experiment was repeated, but this time the mixture of **33** and iron(II) chloride was heated under reflux before the 4,4'-methyldianiline was added. It was hoped that by already having the reaction mixture at reflux temperature, there would be enough energy to break up any polymeric species before they got large enough to precipitate out of solution. However, this strategy proved ineffective and again a precipitate formed immediately upon addition of the dianiline linker.

2.7 Summary and further work

The work in this chapter has outlined the efforts taken towards developing a synthetic route to a "capped" triple stranded metallosupramolecular cylinder. It was decided to focus efforts on using a quanternary carbon based "tripod" to maintain synthetic simplicity and to keep the structure of this capped cylinder as close to that of the original cylinder as possible. This would incorporate a functional group located at the "head" and three identical "arms" that would connect to the pyridine rings making up each end of the cylinder ligand. The first strategy that was explored aimed to use amide bonds to link the pyridine ring of the ligand to the tripodal cap, however this approach necessitated the protection of the aldehyde group in the 2-position of the pyridine ring and it proved difficult to drive the subsequent deprotection

step to completion. As such, strategies that avoided the need to protect the aldehyde functionality were then explored. Using copper(I) catalysed alkyne-azide cycloadditions gave mixtures of mono-, di-, and tri-clicked products and using Mitsunobu chemistry to form triethers proved unsuccessful. A tripyridylaldehyde cap was successfully synthesised and isolated using ether forming conditions. First, a hydroxyl group was introduced in the 5-position of the pyridinecarboxaldehyde. This was then deprotonated, with the resultant alkoxides reacting with a trimesylate capping moiety. The desired trialdehyde **33** was isolated with a promising yield of 82%. Unfortunately, preliminary efforts to use this trialdehyde cap in a one-pot synthesis to make the a capped cylinder proved unsuccessful, due to the propensity of the reagents to form polymeric species which precipitate out of solution before the discrete cylinder could be formed.

Looking ahead, there are two paths that warrant further investigation. Firstly, attempts should be made to optimise the conditions used when attempting to synthesise the capped cylinder. High dilution conditions should favour the formation of discrete cylinders rather than the polymeric species. Other solvents could also be investigated, particularly those with higher boiling points. These would offer a higher reflux temperature, allowing a larger energy input into the system to drive the reaction to the thermodynamic product. Secondly, the strategy could be modified to target synthesis of a cylinder capped at only one end. This could be feasible by initially reacting one equivalent of trialdehyde **33** with one equivalent of an iron(II) salt and then subsequently adding three equivalents of 4,4-methylenedianiline followed by three equivalents of 2-nitrosopyridine. This approach essentially builds up the cylinder sequentially from the capped end to the open end (Figure 2.17). The reaction between 2-nitrosopyridine and the amino functionalities of 4,4'-methylenedianiline is well known in the group, as it has been used to make analogues of the original cylinder structure which use azo groups to connect the pyridine rings to the dianiline spacer rather than imines.[39] 2-nitrosopyridine can be synthesised via the two step procedure shown in Scheme 2.21.[40] The first step is a one-pot conversion of 2-aminopyridine to the dimethylsulfinimine using N-chlorosuccinimide and dimethylsulfide, which behave in a similar manner as when used in Corey-Kim oxidation.[41] The sulfinimine is then oxidised to the corresponding nitroso group using *m*CPBA.

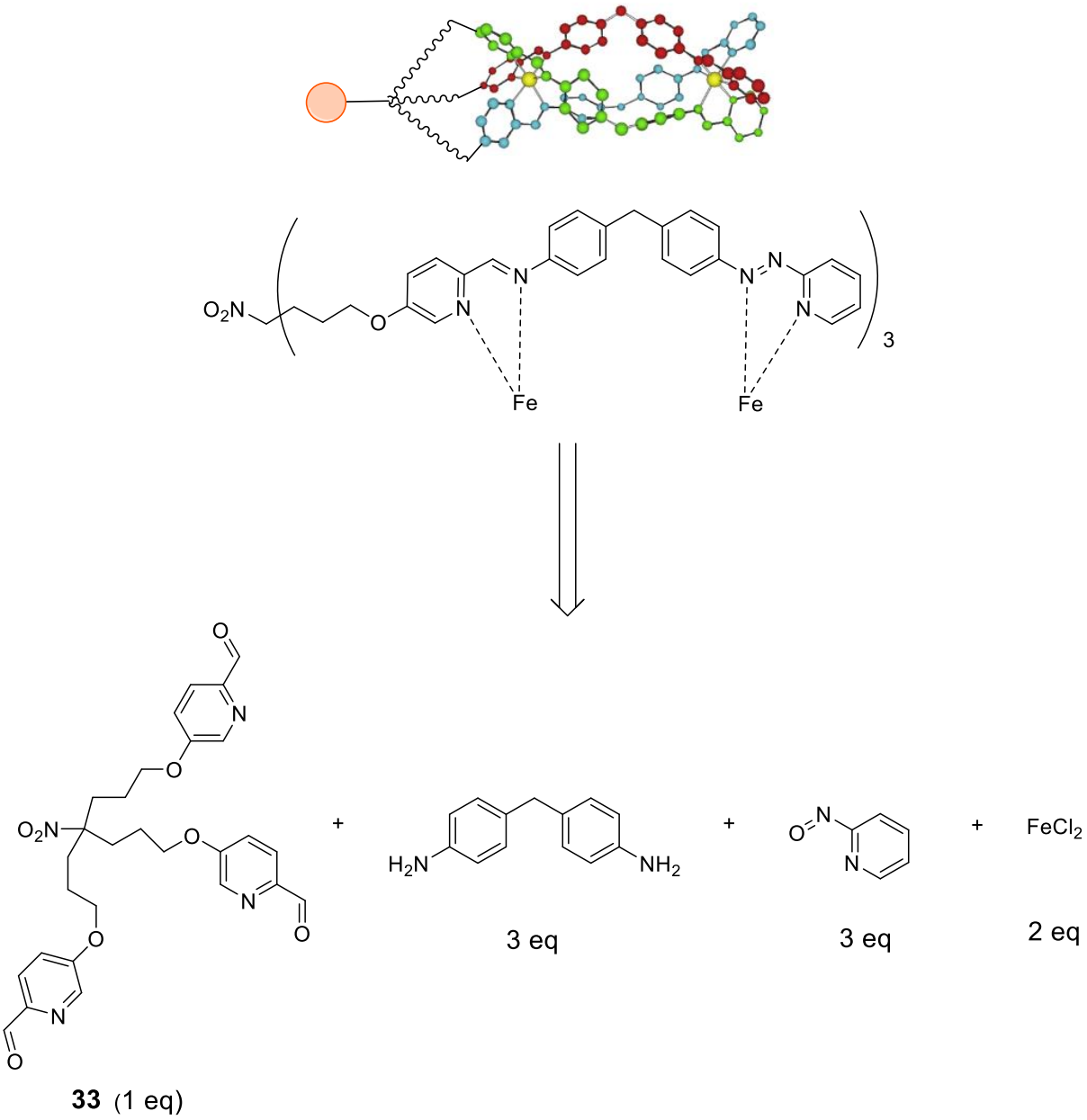

Figure 2.17 Retrosynthesic approach to a metallohelicate cylinder capped at only one end.

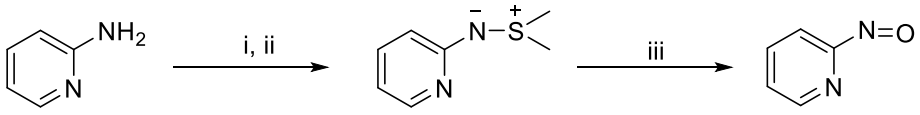

Scheme 2.21 Literature procedure to 2-nitrosopyridine from 2-aminopyridine.[40] (i) SMe_2, N-chlorosuccinimide, DCM, -20 °C – RT, 3 h; (ii) NaOMe, MeOH, H_2O, RT, 4 h; (iii) *m*CPBA, DCM, 0 °C, 1.5 h.

To further reduce the likelihood of polymers forming, the azo "half ligand" could be synthesised prior to cylinder formation, as shown in Scheme 2.22. If an excess of 4,4-

methylenedianiline is used in this reaction, the "half-ligand" product will be the major product and could be isolated by reverse phase prep-HPLC. This could be mixed with trialdehyde **33** with a ratio of three half ligands for every trialdehyde to generate the capped ligand, and the metal source could then be added. This proposed reaction is summarised in Scheme 2.23.

Using a more labile metal centre may offer another solution. For example, Zn^{2+} could be used as the metal source. It's d^{10} configuration would mean that the strength of the coordination bonds would be weaker than those formed with Fe^{2+}, which has a d^6 configuration. As such, less energy would be required to break apart the kinetic polymers and drive the reaction forward to form the discrete cylinder. While the Zn(II) cylinder would be likely to have lower stability in aqueous solutions, it may offer valuable insight as to whether the synthesis actually works.

Overall, the work detailed in this chapter represents notable progress towards developing a synthetic route to a capped metallohelicate cylinder. Despite the challenges faced with polymeric species precipitating out of solution during the initial attempts to synthesise a dicapped cylinder, reacting trialdehyde **33** with the azo-half ligand to form a monocapped cylinder looks feasible if the right conditions are found.

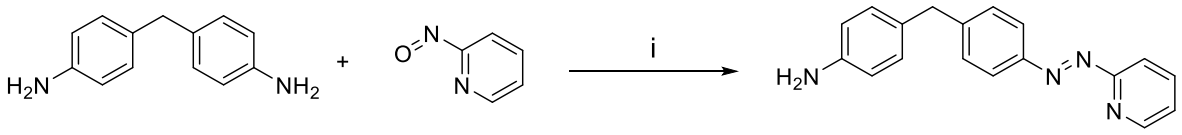

Scheme 2.22 Synthesis of azo "half-ligand". (i) DCM, AcOH, RT, 18 h.

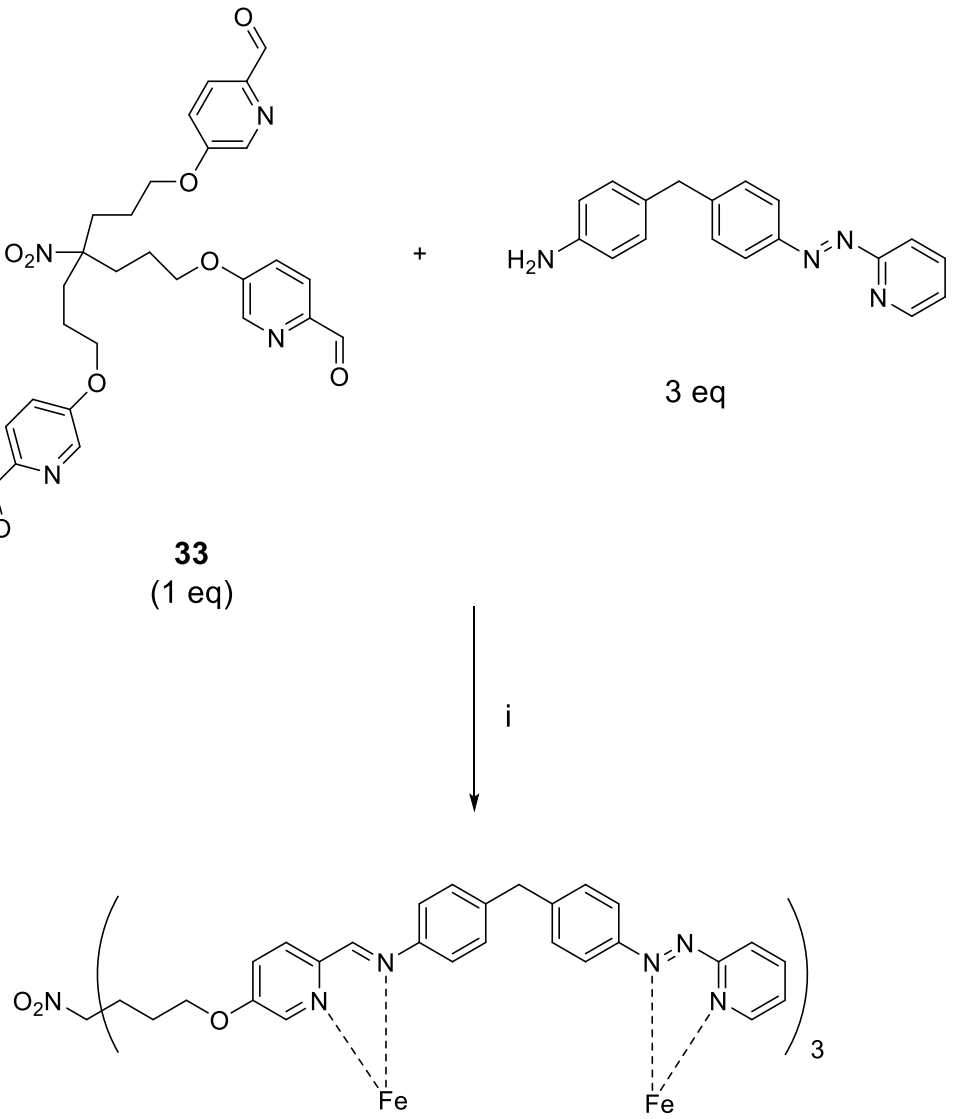

Scheme 2.23 Proposed route to a monocapped cylinder through a one-pot synthesis of trialdehyde **33**, half-ligand, and iron(II) chloride. (i) $FeCl_2 \cdot H_2O$, MeOH, reflux.

2.8 References

1 C. Kosmas, N. B. Tsavaris, N. A. Malamos, M. Vadiaka and C. Koufos, *J. Clin. Oncol.*, 2001, **19**, 119–126.

2 Y. Iwasaki, K. Nagata, M. Nakanishi, A. Natuhara, Y. Kubota, M. Ueda, T. Arimoto and H. Hara, *Chest*, 2005, **128**, 2268–2273.

3 H. Maeda, J. Wu, T. Sawa, Y. Matsumura and K. Hori, *J. Control. Release*, 2000, **65**, 271–284.

4 H. Maeda, K. Tsukigawa and J. Fang, *Microcirculation*, 2016, **23**, 173–182.

5 V. Mannancherril and B. Therrien, *Inorg. Chem.*, 2018, **57**, 3626–3633.

6 A. C. Hotze, N. J. Hodges, R. E. Hayden, C. Sanchez-Cano, C. Paines, N. Male, M. K. Tse, C. M. Bunce, J. K. Chipman and M. J. Hannon, *Chem Biol*, 2008, **15**, 1258–1267.

7 G. R. Newkome, Z. Yao, G. R. Baker and V. K. Gupta, *J. Org. Chem.*, 1985, **50**, 2003–2004.

8 D. K. Smith, A. Zingg and F. Diederich, *Helv. Chim. Acta*, 1999, **82**, 1225–1241.

9 S. Lebreton, N. Newcombe and M. Bradley, *Tetrahedron Lett.*, 2002, **43**, 2475–2478.

10 S. Lebreton, S. E. How, M. Buchholz, B. E. Yingyongnarongkul and M. Bradley, *Tetrahedron*, 2003, **59**, 3945–3953.

11 Y. M. Chabre, C. Contino-Pépin, V. Placide, T. C. Shiao and R. Roy, *J. Org. Chem.*, 2008, **73**, 5602–5605.

12 L. Cardo and M. J. Hannon, *Inorganica Chim. Acta*, 2009, **362**, 784–792.

13 L. Cardo, V. Sadovnikova, S. Phongtongpasuk, N. J. Hodges and M. J. Hannon, *Chem. Commun.*, 2011, **47**, 6575–6577.

14 C. A. G. N. Montalbetti and V. Falque, *Tetrahedron*, 2005, **61**, 10827–10852.

15 M. Mikolajczyk and P. Kiezlbasiński, *Tetrahedron*, 1981, **37**, 233–284.

16 X. Zhao and K. S. Schanze, *Chem. Commun.*, 2010, **46**, 6075–6077.

17 C. D. Weis and G. R. Newkome, *J. Org. Chem.*, 1990, **55**, 5801–5802.

18 J. March, *Advanced Organic Chemistry*, McGraw-Hill International Book Company, 2nd edn., 1977.

19 J. Regan, A. Capolino, P. F. Cirillo, T. Gilmore, A. G. Graham, E. Hickey, R. R. Kroe, J. R. Madwed, M. Moriak, R. Nelson, C. A. Pargellis, A. Swinamer, C. Torcellini, M. Tsang and N. Moss, *J. Med. Chem.*, 2003, **46**, 4676–4686.

20 M. C. Liu, T. S. Lin and A. C. Sartorelli, *J. Med. Chem.*, 1992, **35**, 3672–3677.

21 T. W. . W. Greene P. G. M., *Protective Groups in Organic Synthesis*, John Wiley &

Sons, Inc. , 3rd edn., 1999.

22 R. Huisgen, *Angew. Chemie Int. Ed. English*, 1963, **2**, 565–598.

23 V. V. Rostovtsev, L. G. Green, V. V. Fokin and K. B. Sharpless, *Angew. Chemie - Int. Ed.*, 2002, **41**, 2596–2599.

24 C. W. Tornøe, C. Christensen and M. Meldal, *J. Org. Chem.*, 2002, **67**, 3057–3064.

25 J. E. Hein and V. V Fokin, *Chem. Soc. Rev.*, 2010, **39**, 1302–1315.

26 L. Liang and D. Astruc, *Coord. Chem. Rev.*, 2011, **255**, 2933–2945.

27 J. White, PhD Thesis, University of Birmingham, 2016.

28 C. Schouwey, M. Papmeyer, R. Scopelliti and K. Severin, *Dalt. Trans.*, 2015, **44**, 2252–2258.

29 X. Wang, P. Rabbat, P. O'Shea, R. Tillyer, E. J. J. Grabowski and P. J. Reider, *Tetrahedron Lett.*, 2000, **41**, 4335–4338.

30 O. Mitsunobu and M. Yamada, *Bull. Chem. Soc. Jpn.*, 1967, **40**, 2380–2382.

31 D. Camp and I. D. Jenkins, *J. Org. Chem.*, 1989, **54**, 3045–3049.

32 S. R. Wilson, J. Perez and A. Pasternak, *J. Am. Chem. Soc.*, 1993, **115**, 1994–1997.

33 P. Rollin, W. Klaffke, T. K. Lindhorst, J. Hain and T. K. Lindhorst, *Beilstein J. Org. Chem.*, 14, 1619–1636.

34 G. I. Pascu, University of Birmingham, 2007.

35 M. Seredyuk, A. B. Gaspar, V. Ksenofontov, Y. Galyametdinov, J. Kusz and P. Gütlich, *J. Am. Chem. Soc.*, 2008, **130**, 1431–1439.

36 J. Clayden, N. Greeves and S. Warren, *Organic Chemistry*, Oxford University Press, Oxford, 2nd edn., 2012.

37 T. Tsunoda, Y. Yamamiya and S. Itô, *Tetrahedron Lett.*, 1993, **34**, 1639–1642.

38 C. P. Ortmeyer, G. Haufe, K. Schwegmann, S. Hermann, M. Schäfers, F. Börgel, B. Wünsch, S. Wagner and V. Hugenberg, *Bioorg. Med. Chem.*, 2017, **25**, 2167–2176.

39 L. J. Childs, PhD Thesis, University of Warwick, 2002.

40 E. C. Taylor, C. P. Tseng and J. B. Rampal, *J. Org. Chem.*, 1982, **47**, 552–555.

41 E. J. Corey and C. U. Kim, *J. Am. Chem. Soc.*, 1972, **94**, 7586–7587.

Chapter 3:

Synthesis and DNA binding properties of azide functionalised metallohelicate cylinders

3.1 Introduction and aims

To date, whenever any functionalisation has been introduced to the original $[M_2L_3]^{4+}$ cylinders, the ligand has been functionalised prior to the formation of the complex. The reason for this is that the conditions required for the functionalisation (or subsequent purification) result in destruction of the metal complex or affect the oxidation state of the metal ions. Any reaction requiring a metal catalyst is potentially problematic, as the catalyst used could displace the desired metal ions from the cylinder. This displacement could halt reactivity and lead to a complex mixture of different metal species. In addition to this, contamination from metal residues has the potential to skew any findings from subsequent biological investigations. Previous work in the group (adding Sonagashira coupling [1] and CuAAC click chemistry [2] to the group's functionalisation toolkit) functionalised the ligands first and coordinated these to the metal centres in the last step. The clear disadvantage of this strategy is that substantial work can be put into developing a synthesis of a functionalised ligand only to then find that formation of the complex is energetically unfavourable, possibly due to steric clash or electrostatic repulsion between the ligands. This inefficiency could be overcome using a post assembly modification strategy. If functionalisation occurred on the ligand after the cylinder has already formed, unfavourable sterics or electrostatic effects may result in only one of the ligands being functionalised at each end of the cylinder. The desired functionality would still be provided, while the detrimental impact of steric clash on complex stability would be reduced.

Strain promoted alkyne-azide cycloaddition (SPAAC) offers a potential means to achieve post assembly modification. As with the thermally driven or Cu(I) catalysed versions of this reaction already discussed in Chapter 2, a cycloaddition occurs between an alkyne and an azide to form a 1,2,3-triazole. However, SPAAC reactions are catalyst-free and driven by the relief of the ring strain in a cyclooctyne molecule (Figure 3.1). Using SPAAC removes the need

to apply excessive heat to the reaction which would cause the cylinder to degrade in solution, or to use a Cu(I) catalyst. Avoiding the use of the catalyst is desirable as Cu(I) has been shown to form double stranded cylinders,[3] as well as cellular toxicity.[4] Another key attraction of SPAAC is that it is bioorthogonal. As alkynes and azides are not naturally present within living cells, no biological machinery should directly interfere with the reaction. A potential drawback is the reported side reactions of cyclooctynes with intracellular thiol groups, [5,6] but analogues have been developed which overcome this through speeding up the rate of the SPAAC reaction.[7] As such, these reactions can occur within cells and there are several reports of tagging fluorescent groups to intracellular targets using SPAAC.[7–10]

The work described in this chapter concerns the synthesis and DNA-binding of two azide functionalised metallosupramolecular cylinders: $Fe_2L^A{}_3Cl_4$ and $Fe_2L^B{}_3Cl_4$ (**34** and **35** respectively, Figure 3.2), which have potential to undergo post-assembly modification using SPAAC click chemistry. These cylinders have a different number of atoms connecting the azide groups to the pyridyl rings of the ligand's core, with $Fe_2L^A{}_3Cl_4$ having one atom between the azide and the pyridyl ring and $Fe_2L^B{}_3Cl_4$ incorporating three. Reliable synthetic routes to each cylinder will be discussed, and their binding properties to dsDNA and a DNA 3WJ will be compared to those of $Fe_2L_3Cl_4$. This comparison will determine whether the favourable DNA binding properties of $Fe_2L_3Cl_4$ are retained.

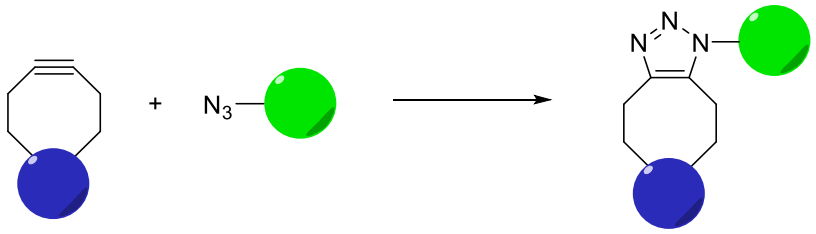

Figure 3.1 Illustration of the strain promoted alkyne-azide cycloaddition (SPAAC), which is driven by relief of the ring strain in the cyclooctyne starting material.

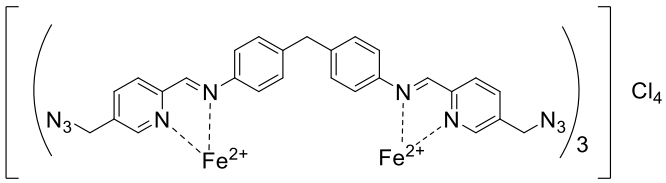

$Fe_2L^A{}_3Cl_4$ (34)

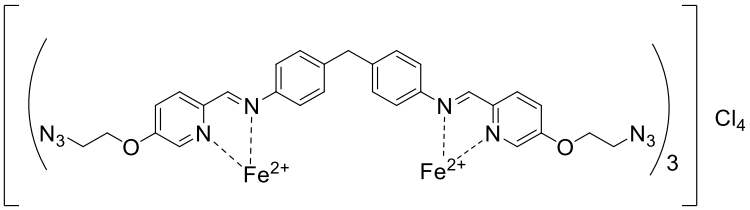

$Fe_2L^B{}_3Cl_4$ (35)

Figure 3.2 Structures of the two azide functionalised cylinders under investigation in this chapter.

3.2 Synthesis of $Fe_2L_3Cl_4$

Whenever any new substituents are introduced onto a cylinder structure, the properties of the novel cylinder need to be compared to those of the originally reported $M_2L_3X_4$ cylinder which was described in section 1.4. This comparison gives an indication as to whether the desirable DNA binding properties of the original cylinders have been conserved. To provide the material necessary for such a comparison, $Fe_2L_3Cl_4$ (**37**) was synthesised using a modified procedure to that reported in reference 11, shown in Scheme 3.1. In the first step, two equivalents of pyridine-2-carboxaldehyde were condensed with 4,4'-methylenedianiline to form the ligand. This reaction was performed in ethanol, as the ligand precipitates out of solution and was easily isolated by vacuum filtration. After extensive washing with ethanol, ligand L (**36**) was isolated with a yield of 89%. Formation of the triple stranded helicate was achieved by heating three equivalents of **36** with two equivalents of iron(II) chloride under reflux for two hours. In order to isolate $Fe_2L_3Cl_4$ in sufficient purity, a sequence of anion exchange steps were then performed. A saturated methanolic solution of ammonium hexafluorophosphate was added to the cooled solution, precipitating the cylinder as a PF_6 salt. This light purple solid was collected by vacuum filtration and washed thoroughly with methanol to remove any uncoordinated ligand. The complex was then resuspended in

methanol and mixed with DOWEX 1X8 chloride form for two hours at room temperature. This anion exchange resin introduces an excess of Cl^-, which replaces the PF_6^- as the counterion of the complex. As the chloride form of the cylinder is soluble in methanol, $Fe_2L_3Cl_4$ dissolves upon formation. The exchange resin was removed by vacuum filtration and washed thoroughly with methanol. The filtrate was concentrated under reduced pressure to yield $Fe_2L_3Cl_4$ (**37**) as a dark purple solid with a yield of 60%. Data collected from ^1H NMR spectroscopy (shown in Figure 3.3), MS, and UV-Vis spectroscopy (Figure 3.4) are consistent with those already reported.[12] The ^1H NMR spectrum shows the phenyl proton resonances as broad singlets due to rotation of the phenyl rings during the NMR timescale. The broad peak around 7.0 ppm on the ^1H NMR spectrum proved difficult to integrate, although visually it is comparable to the peak around 5.6 ppm. On the UV-Vis spectrum, the characteristic metal to ligand charge transfer band is present around 570 nm, which is responsible for giving the cylinder its prominent purple colour in solution.

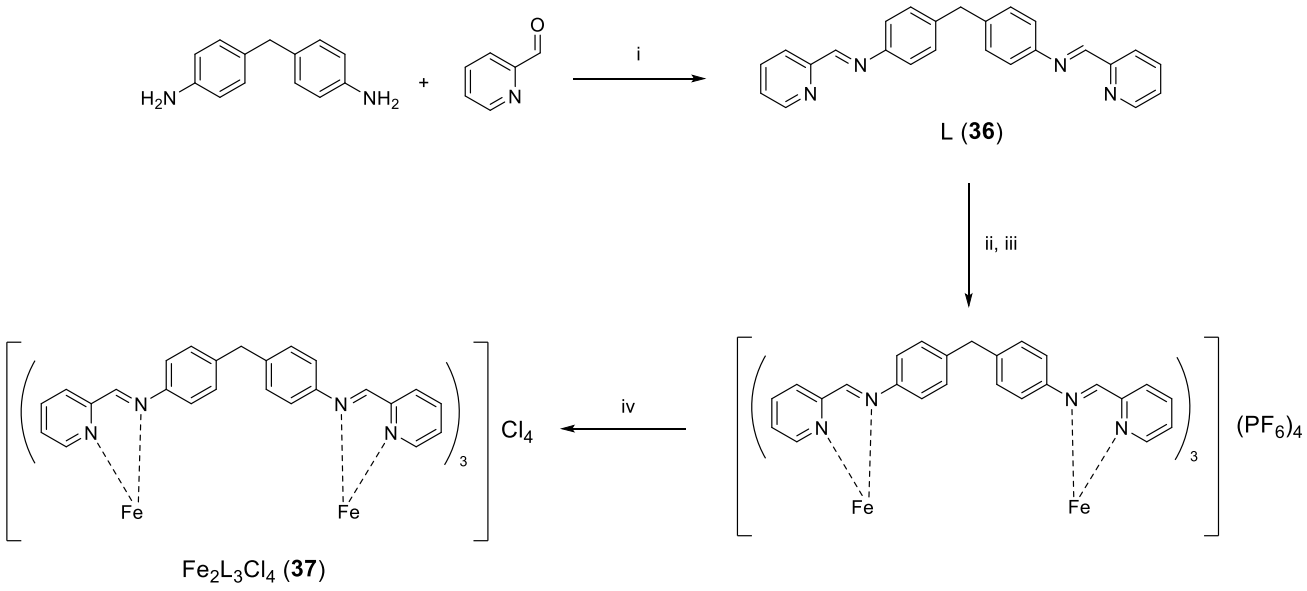

Scheme 3.1 Synthesis of $Fe_2L_3Cl_4$, adapted from the procedure in reference 11. (i) EtOH, RT, 19 h; (ii) $FeCl_2{\cdot}4H_2O$, MeOH, reflux, 2 h; (iii) NH_4PF_6; (iv) DOWEX 1x8 Cl, MeOH, RT, 2 h.

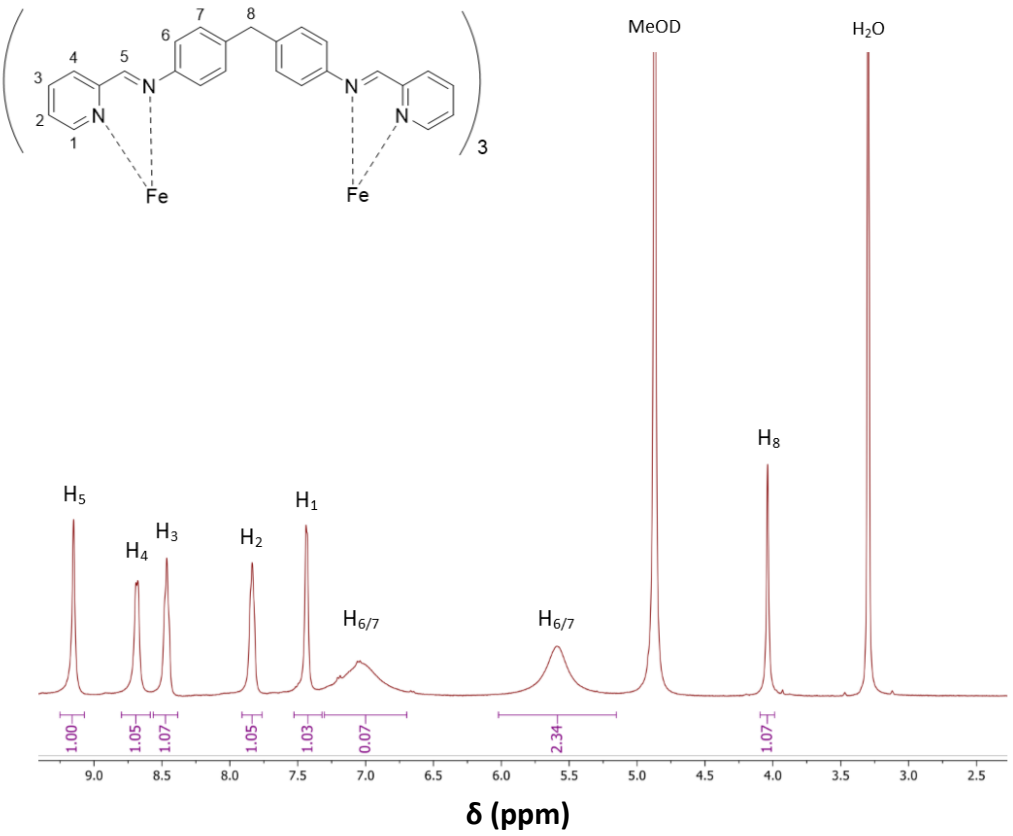

Figure 3.3 1H NMR spectrum of $Fe_2L_3Cl_4$. The phenyl peaks appear broad due to rotation of the phenyl rings during the NMR timescale.

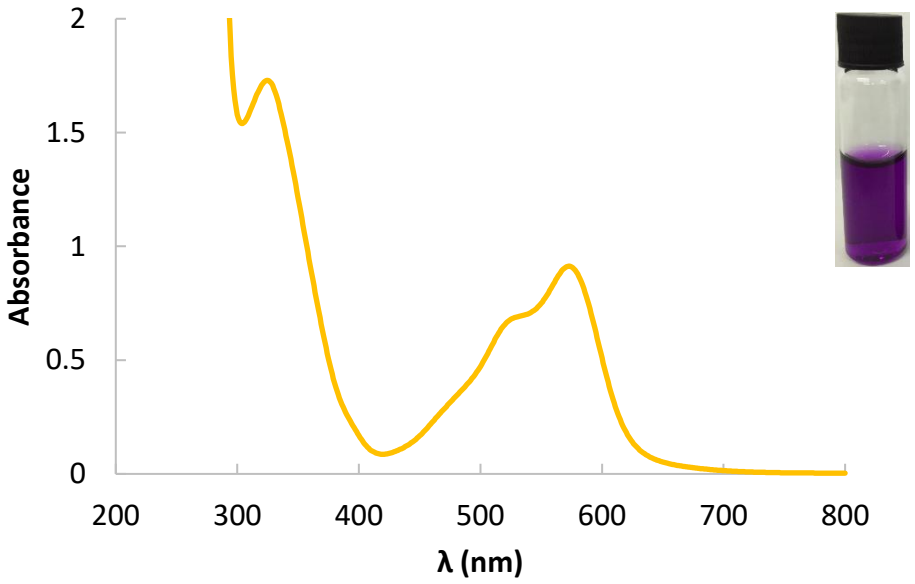

Figure 3.4 UV-Vis spectrum of a solution of $Fe_2L_3Cl_4$ (60 µM in H_2O), with a prominent MLCT band around 570 nm. *Insert*: the solution in a sample vial.

3.3 Synthesis of azide functionalised cylinders $Fe_2L^A{}_3Cl_4$ and $Fe_2L^B{}_3Cl_4$

The synthetic routes used to produce the two azide functionalised cylinders were influenced by work previously performed in section 2.3, which aimed to use CuAAC click chemistry to form a tripodal capping moiety. Figure 3.5 highlights the retrosynthetic approach used for the ligand design. As with the work described in Chapter 2, the 5-position of the pyridine ring was chosen so as to minimise any detrimental influence the substituent may have when binding to DNA 3WJs, which has been attributed to the phenyl rings at the core of the cylinder's structure.[13]

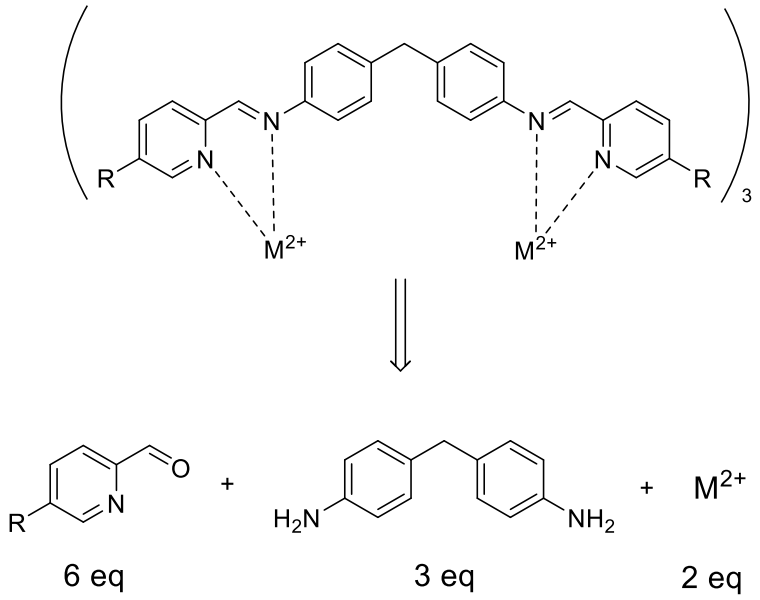

Figure 3.5 Retrosynthetic approach to a metallohelicate cylinder with functionalisation in the 5-position of the constituent pyridine rings.

Schemes 3.2 and 3.3 highlight the synthetic route used to generate the key pyridyl intermediates (**42** and **43**) required to synthesise the azide functionalised cylinder ligands. Scheme 3.2 uses 5-hydroxymethyl pyridine **24** as a starting material, the synthesis of which has already been described in Chapter 2. In the first step, **24** is treated with *tert*-butyldimethylsilyl chloride (TBDMSCl) to protect the hydroxyl group from deprotonation by *n*-BuLi in step ii. Triethylamine is included to neutralise the HCl generated as the reaction proceeds. This protection step proceeded quickly (1.5 h) and in high yield (91%). The following two steps are performed in succession in the same flask. Silyl ether **39** is first treated with *n*-BuLi to form a pyridyl-lithium intermediate through lithium-halogen exchange, which

is then reacted with DMF and hydrolysed to form the aldehyde in the 2-position of the pyridine ring.[14] This reaction can be considered as a form of the Bouveault aldehyde synthesis, using an organolithium intermediate rather than the Grignard reagents that Bouveault is associated with.[15] This aldehyde synthesis proceeded with a combined yield of 40%. With the aldehyde group now introduced in the 2-position, the silyl protecting group was removed by stirring **39** in a solution of *tert*-butylammonium fluoride (TBAF) with a yield of 90%. The hydroxyl group of **40** was then converted to mesylate **41** using methanesulfonic anhydride, with a yield of 66%. Finally, the mesylate was converted to the azide by mixing with sodium azide. 18-crown-6 was included as a phase transfer reagent, which allowed THF

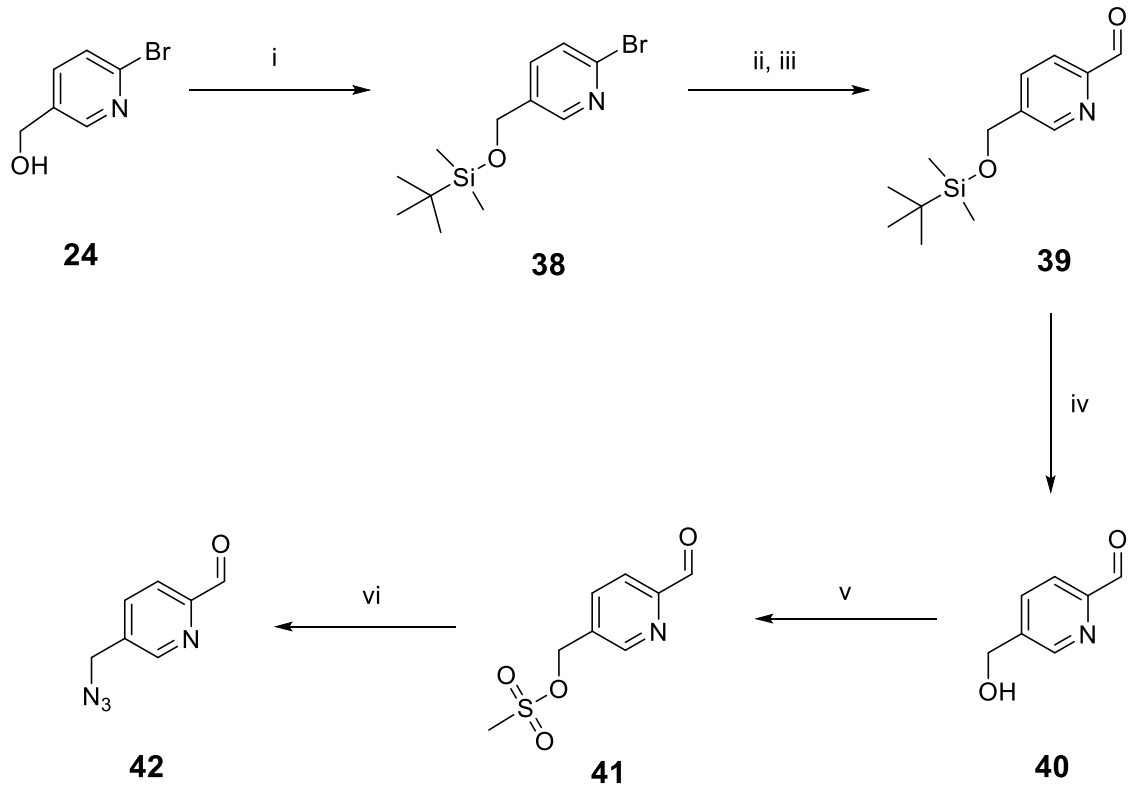

24 38 39 40 41 42

Scheme 3.2 Synthesis of 5-azidomethyl-2-pyridinecarboxaldehyde (**42**). (i) TBDMSCl, Et_3N, DMF, Ar, RT, 1.5 h; (ii) *n*-BuLi, THF, Ar, -78 °C, 1 h; (iii) DMF, -78 °C, 2 h; (iv) TBAF, THF, 0 °C – RT, 22 h; (v) $(MeSO_2)_2O$, Et_3N, DCM, 0 °C – RT, 6 h; (vi) NaN_3, 18-crown-6, THF, RT, 18 h.

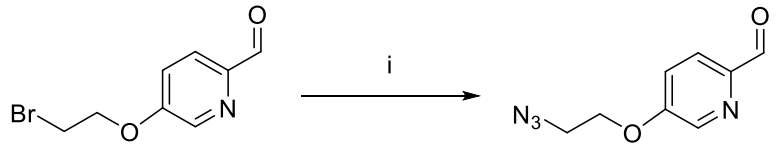

32 **43**

Scheme 3.3 Synthesis of 5-azidoethoxy-2-pyridinecarboxaldehyde (**43**). (i) NaN_3, 18-crown-6, $MeCN/H_2O$, 60 ^oC, 2 h.

to be used as the solvent rather than DMF (as was used in similar conversion in section 2.3). Once the reaction had reached completion, the THF was removed under reduced pressure before the reaction residue was partitioned between ethyl acetate and aqueous sodium bicarbonate. With no residual DMF, less product was lost in the aqueous layer and **42** was isolated as a yellow oil with a yield of 84%. This yield is higher than the 61% achieved with the preparation of analogous compound **26** in DMF (section 2.3). Subsequent ^1H NMR experiments suggested that **42** was prone to decomposition at room temperature and when stored at -18 ^oC. As such, the material obtained was quickly used to generate L^A (**44**, Scheme 3.4).

Synthesis of azide functionalised pyridine **43** starts with **32**, the synthesis of which has already been described in section 2.5**.** **32** was converted to the corresponding azide by mixing with sodium azide, again using 18-crown-6 to avoid the use of DMF. **43** was isolated with a yield of 59%.

With the key azido-pyridyl intermediates synthesised, the azide functionalised iron helicate cylinders were produced as shown in Scheme 3.4. 4,4'-methylenedianiline is mixed with an excess of either **42** or **43** in ethanol to generate ligands **44** and **45** respectively. As with the synthesis of $Fe_2L_3Cl_4$, the ligands precipitated out of solution upon formation and were isolated by vacuum filtration. **44** was isolated with a yield of 64% and **45** was isolated with a yield of 70%. These ligands were then complexed to iron by heating under reflux in methanol with a ligand:metal molar ratio of 3:2. After heating for two hours, the methanol was removed under reduced pressure. The resultant purple films were then redissolved in the minimum quantity of methanol before being precipitated by dropwise addition to a cold (-18 ^oC) solution of diethyl ether. This isolation method is preferred at small scales, as less material

is lost than with the anion exchange method used during the synthesis of $Fe_2L_3Cl_4$. $Fe_2L^A{}_3Cl_4$ (**34**) and $Fe_2L^B{}_3Cl_4$ (**35**) were isolated in yields of 80% and 79% respectively.

The assigned ^1H NMR spectra of $Fe_2L^A{}_3Cl_4$ and $Fe_2L^B{}_3Cl_4$ are shown in Figures 3.6 and 3.7. The spectrum of $Fe_2L^A{}_3Cl_4$ (Fig 3.6) is similar to that of $Fe_2L_3Cl_4$ (Fig. 3.3) with one less pyridyl peak and one more CH_2 peak, as expected. An extra CH_2 is visible between 3.5 and 4.5 ppm in Figure 3.7, and one of the pyridyl resonances (H_5) has overlapped with one of the broad singlets corresponding to the phenyl proton resonances around 7 ppm. Both cylinders were also analysed by ESI-MS. For $Fe_2L^A{}_3Cl_4$, peaks corresponding to the expected masses of $[cylinder]^{4+}$ and $[cylinder+Cl]^{3+}$ were found. For $Fe_2L^B{}_3Cl_4$, peaks corresponding to $[cylinder+Cl]^{3+}$ and $[cylinder-ligand+2Cl]^{2+}$ were found. The UV-Vis spectrums of both novel cylinders were also measured, and these spectra have been compared to that of the $Fe_2L_3Cl_4$ in Figure 3.8. From this comparison, it can be observed that MLCTs similar to that of the original cylinder occur for both of the novel azide cylinders, with that of $Fe_2L^B{}_3Cl_4$ showing a slight blue shift. The presence of these bands confirm that the azide functionalised ligands have coordinated to the iron metal centres. The different relative intensities of these MLCT bands may be indicative of the different strengths of the coordination bonds between the ligands and the iron centres. Given the additional electron density introduced by the azide groups, it can be rationalised that the resultant repulsions between them may prevent the ligands of $Fe_2L^A{}_3Cl_4$ and $Fe_2L^B{}_3Cl_4$ from coordinating as closely to the metal centres of the ligands in $Fe_2L_3Cl_4$. The lower relative intensity of the MLCT of $Fe_2L^B{}_3Cl_4$ compared to that of $Fe_2L^A{}_3Cl_4$ may be due to the additional electron density of the oxygens in the structure of ligand L^B.

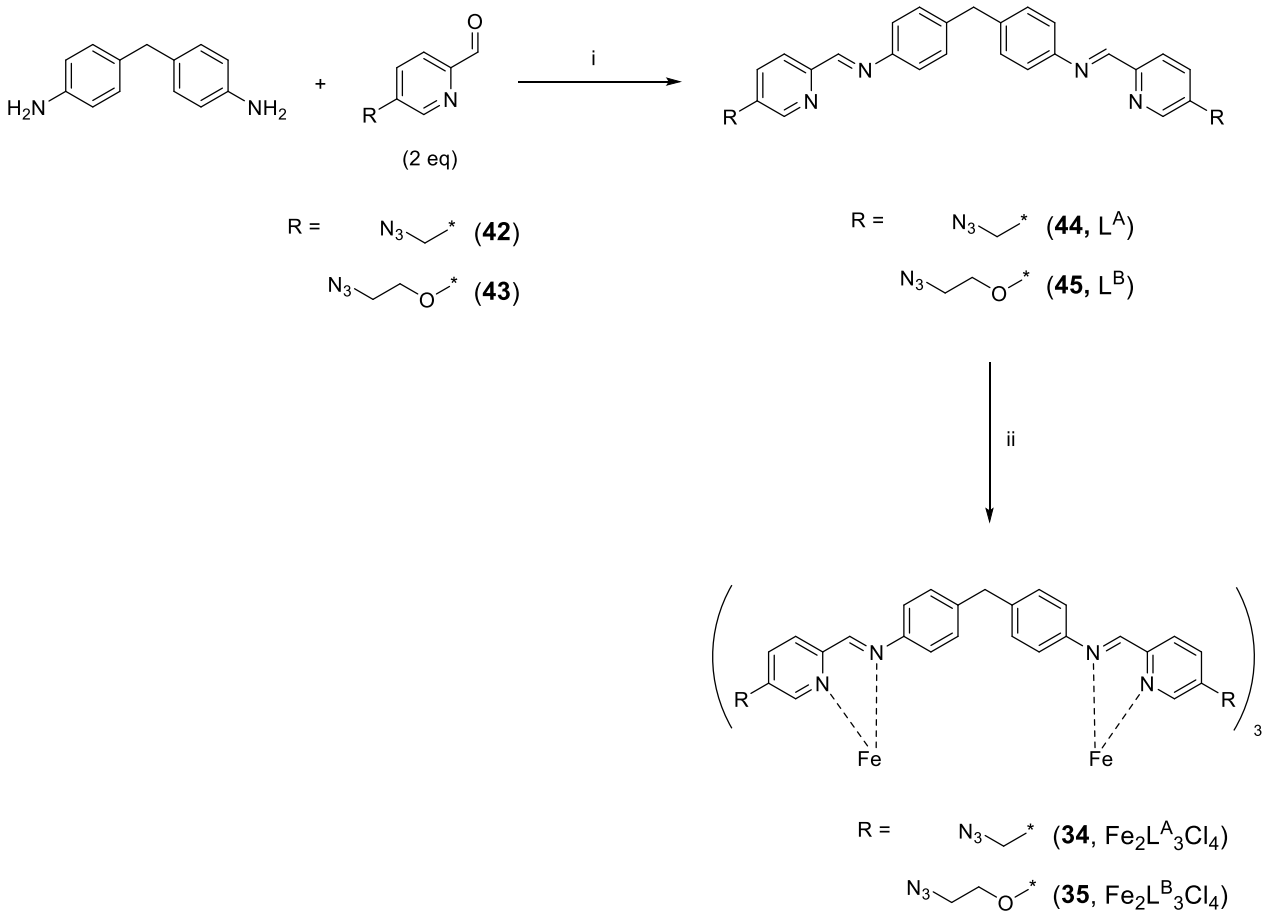

Scheme 3.4 Synthesis of azide functionalised iron cylinders **34** and **35**. (i) EtOH, RT, 21 h; (ii) $FeCl_2 \cdot 4H_2O$, MeOH, reflux, 2 h.

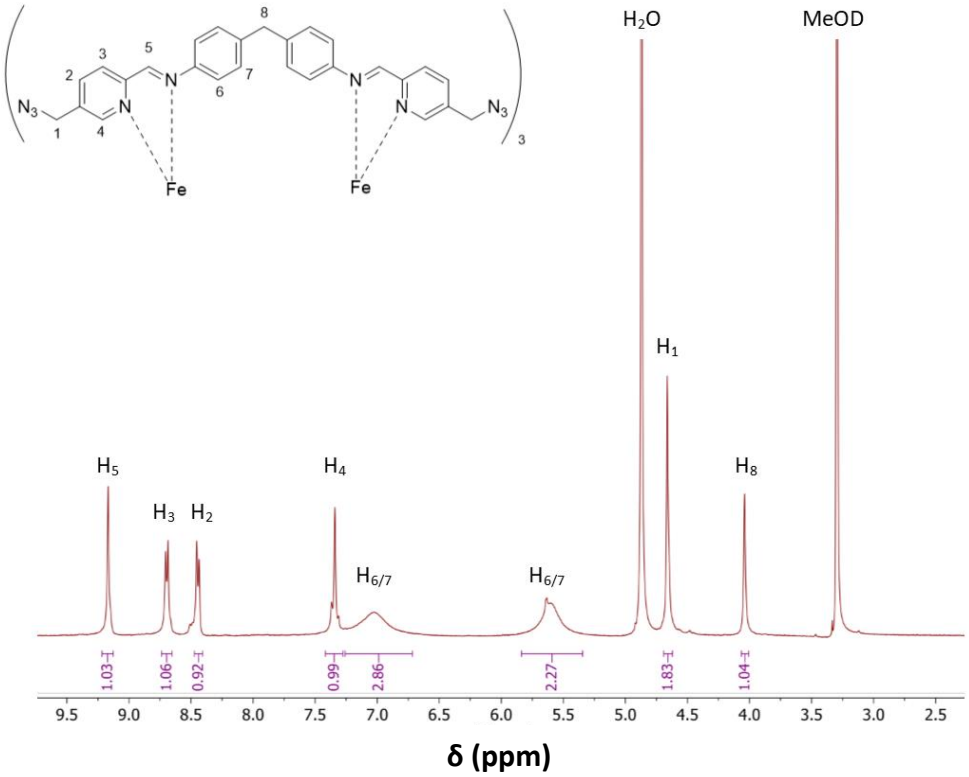

Figure 3.6 ^{1}H NMR spectrum of $Fe_2L^{A}{}_3Cl_4$ (**34**) with assigned proton shifts.

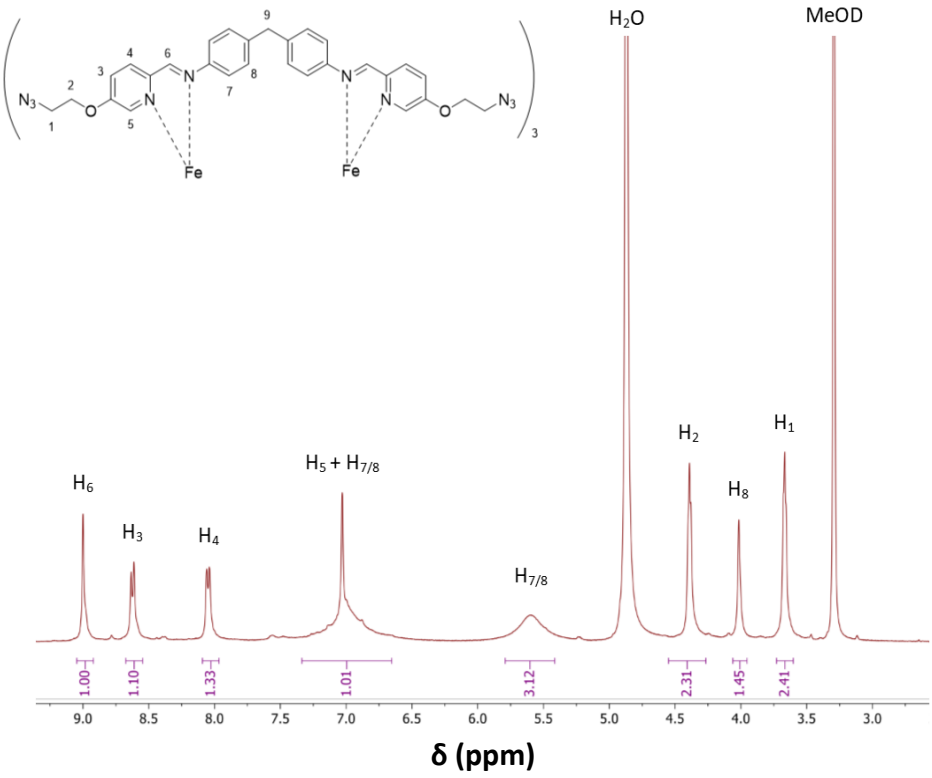

Figure 3.7 ^{1}H NMR spectrum of $Fe_2L^{B}{}_3Cl_4$ (**35**) with assigned proton shifts.

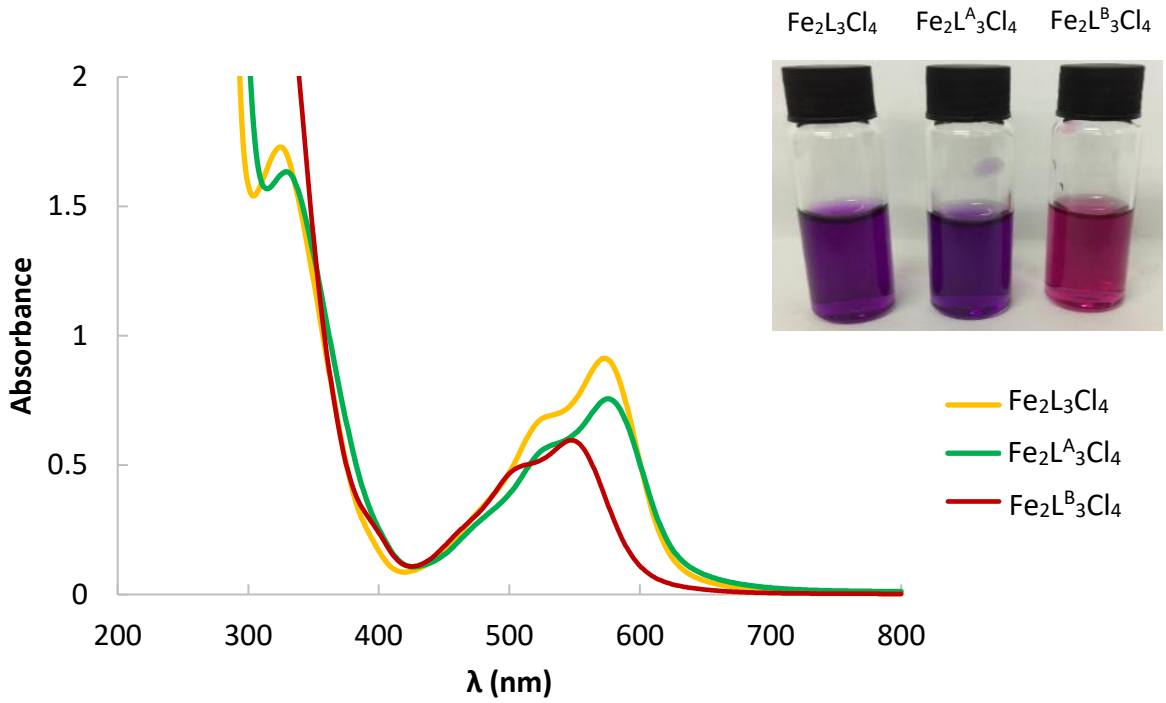

Figure 3.8 Overlay of UV-Vis spectra for aqueous solutions of $Fe_2L_3Cl_4$ (**37**), $Fe_2L^A{}_3Cl_4$ (**34**) and $Fe_2L^B{}_3Cl_4$ (**35**). *Insert:* aqueous solutions of the three cylinders in sample vials.

3.4 Investigations into the dsDNA binding properties of azide functionalised cylinders

With synthetic routes to two novel azide functionalised cylinders established, work was carried out to investigate their DNA binding properties. The aim with any functionalisation of the cylinder is to retain as much of the desirable DNA binding properties that were exhibited by the original cylinders as possible, so a series of experiments were performed where the binding behaviour of the novel azide functionalised cylinders were compared to those of $Fe_2L_3Cl_4$. Circular dichroism and linear dichroism experiments were performed to observe the binding properties of the cylinders to dsDNA, while polyacrylamide gel electrophoresis (PAGE) experiments were performed to observe the binding properties to DNA 3WJs (covered in section 3.5).

3.4.1 dsDNA binding investigations using circular dichroism spectroscopy

Circular dichroism (CD) spectroscopy is used to investigate the absolute configuration of chiral systems. It is widely used to investigate the optical properties of biomolecules such as DNA and proteins. Circular dichroism is a phenomenon where a chiral species absorbs left handed and right handed circularly polarised light to different extents. Light becomes circularly polarised when the oscillations of the vertical and horizontal component are out of phase by a quarter wave. This causes the electric field vector to rotate in a helical fashion around the direction of propagation, as shown in Figure 3.9. Similarly to helical DNA, the direction of twist for this rotation can be left handed or right handed. If a viewer were to directly face the source of the light and observe the light vector going around clockwise, it would be right handed. If it were moving anticlockwise, it would be left handed.[16] Circular dichroism spectroscopy passes both right handed and left handed circularly polarised light through a chiral analyte, measuring the absorbance of both and plotting the difference between them. Conventionally, CD = $A_L - A_R$, with A_L being the absorbance of left handed circularly polarised light, and A_R the absorbance of right handed circularly polarised light. The old measure of CD was ellipticity, which was a measure of how much linear polarised light was distorted to from elliptically polarised light when passing through a chiral substrate.[17] The measure of ellipticity is often still used in the presentation of CD data. The Chirascan software (Applied Photophysics) used in these experiments automatically converts Δabsorbance to ellipticity by multiplying it by a factor of 32.98 (ellipticity in degrees = 32.98 ΔAbs).

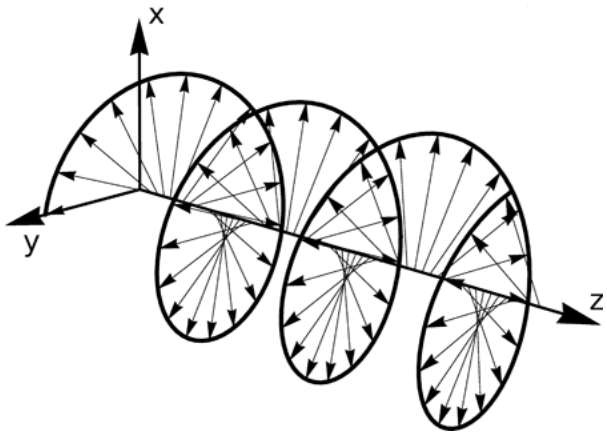

Figure 3.9 Graphical representation of circularly polarised light, where z is the direction of propagation. Taken with permission from reference 18.

The chiral nature of the component nucleotides confer chirality to the whole DNA structure, as discussed in Chapter 1. Different forms of DNA have a characteristic CD spectra,[19] and Figure 3.10 shows the characteristic spectrum for helical B-DNA. This spectrum shows a low magnitude negative signal around 210 nm, a low magnitude positive signal around 220 nm, a high magnitude negative signal around 246 nm, and a high magnitude positive signal around 268 nm. The sugar-phosphate backbone does not demonstrate any observable UV active electric transitions above 180nm, so these signals arise from the nucleobases. The signals shown do not correspond to individual nucleobase transitions, but rather are a superimposed result of all the nucleobase transitions, including secondary transitions initiated by neighbouring nucleobases.[17] The signal at 220 nm is associated with hydrogen bond interactions between bases, while the signal at 246 nm and 268 nm are associated with the helicity of the B-DNA and the stacking interactions between bases, respectively.[20] Any changes observed to this spectrum upon addition of an achiral binding agent indicate that the binder is altering the structure in some way. If induced CD (ICD) signals are observed at wavelengths where the binding agent absorbs, it shows that the binder is situated within a chiral environment and therefore has an interaction with the DNA structure. While cylinders exist as two enantiomers, M (left handed) and P (right handed), their synthesis produces a racemic mixture of the two. Unless these enantiomers are separated, the cylinder does not produce a CD signal as the CD spectrum for each is the inverse of the other, as illustrated in Figure 3.11.[21] Unless these enantiomers are separated, the cylinder is considered to be achiral.

CD titration experiments were performed where the concentration of cylinder in a dsDNA solution were increased in a stepwise manner. The CD spectrum between 200 and 700 nm was recorded after each addition. Titrations was performed with $Fe_2L_3Cl_4$, $Fe_2L^A{}_3Cl_4$, and $Fe_2L^B{}_3Cl_4$ so that the effect of each azide cylinder could be compared to that $Fe_2L_3Cl_4$. Commercially available calf-thymus DNA (ctDNA) was used as a natural source of dsDNA, and a 100 µM solution of ctDNA in 20 mM NaCl, 1 mM Na cacodylate (pH 6.8) buffer (solution A) served as the starting point for each titration experiment. Commercial ctDNA is naturally extracted, consisting of a mixture of different DNA strands with varying length. On average, these strands have 41.9 mol% A-T base pairs, and 58.1 mol% C-G base pairs.[22] Due to the inconsistency in length of the DNA strands, the concentration is expressed in terms of

individual DNA nucleobases present. The concentration of stock solutions were calculated by measuring the absorbance at 260 nm and using a molar extinction coefficient (ε) of 6600 M^{-1} cm^{-1}.

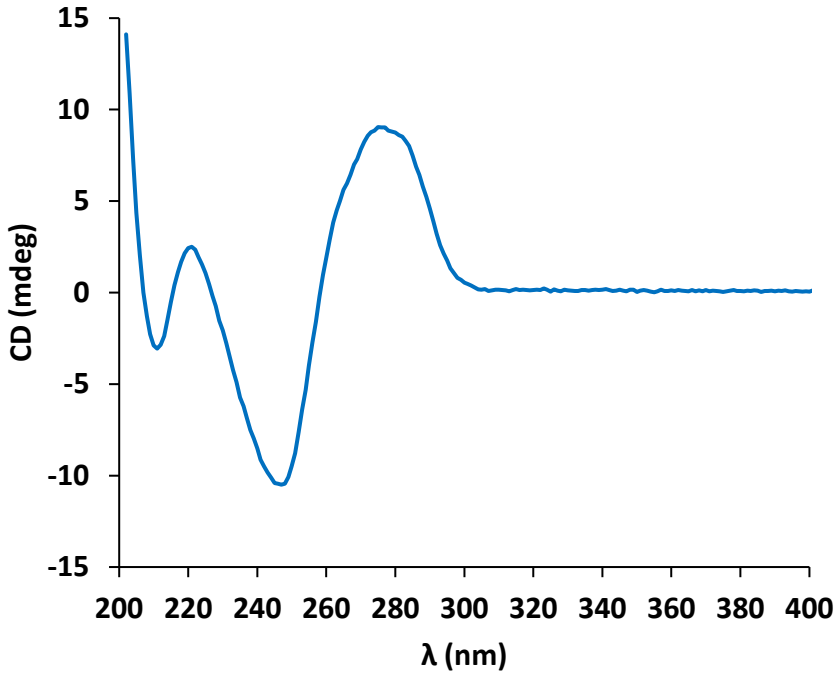

Figure 3.10 CD spectrum of 100 µM ctDNA between 200 and 400 nm, in 20 mM NaCl, 1 mM Na cacodylate buffer.

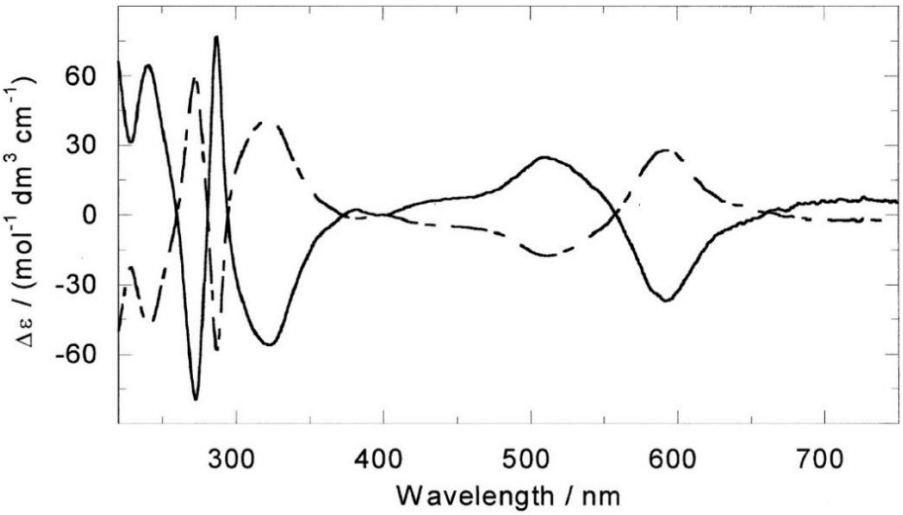

Figure 3.11 CD spectrum of the M enantiomer (solid line) and the P enantiomer (dotted line) of $Fe_2L_3Cl_4$, taken from reference 21. With a racemic mixture, the signals cancel each other out.

At each step of the titration, an aliquot of an aqueous solution of cylinder (solution B) was added to increase the ratio of [nucleobase]:[cylinder]. An equal volume of a solution containing 200 µM ctDNA, 40 mM NaCl, and 2 mM Na cacodylate (solution C) was also added to keep the concentration of ctDNA and buffer constant for each CD measurement.

Each titration consisted of seven stepwise additions of solutions B and C. The CD spectrum was recorded three times after each step, and an average trace taken to compensate for any instrument error. The steps gave [nucleobase]:[cylinder] values of 40:1, 20:1, 15:1, 10:1, 8:1, 6:1 and 4:1. At complex concentrations higher than this, precipitation of the DNA-cylinder adduct was observed in the cuvette which gave unreliable readings due to light scattering. The total volume of cylinder solution (x) required to achieve the desired cylinder concentration for the each step was calculated as follows:

$$C_1V_1 = C_2V_2$$

$$(C_{stock})x = (C_{desired})(start\ volume + 2x)$$

$$(C_{stock})x = (C_{desired})(start\ volume) + (C_{desired})(2x)$$

$$(C_{stock})x - (C_{desired})(2x) = (C_{desired})(start\ volume)$$

$$x\,(C_{stock} - 2C_{desired}) = (C_{desired})(start\ volume)$$

$$x = \frac{(C_{desired})(start\ volume)}{(C_{stock} - 2C_{desired})}$$

Where C_{stock} is the concentration of solution B, $C_{desired}$ is the desired cylinder concentration in the cuvette, and $start\ volume$ is the volume in the cuvette before addition of solutions B and C. For the first step, x gave the volume to be added. For subsequent steps, the total volume of solution B already added over the course of the previous steps was subtracted from x to give the volume required for that step. The table used to calculate the volumes of solutions B and C required is included in Appendix 1.

Figure 3.12a shows the overlay of the CD spectra recorded during the titration of increasing concentrations of $Fe_2L_3Cl_4$ to 100 µM ctDNA. ICD bands can be observed around 340 nm, 400 nm, 540 nm, and 600 nm. The more prominent ICD signals match the regions where we see absorbance transitions of the complex ligands (≈340 nm) and the MLCT of the complex (≈600 nm), as shown in Figure 3.4. The CD spectra of the M and P enantiomers also show bands in

these regions, as highlighted in Figure 3.11. The presence of these ICD bands in Figure 3.12a indicates that there is a binding interaction between $Fe_2L_3Cl_4$ and the ctDNA. This result is consistent with previous reports from the Hannon group.[23,24] Figure 3.12b shows the overlays of spectra recorded up to a [nucleobase]:[cylinder] ratio of 8:1. Trends of the peak shifts are highlighted with red arrows. The general signal shape between 200 nm and 400 nm is retained, and the peak around 268 nm undergoes relatively minor changes. As this peak is related to the stacking interactions of the base pairs,[20] these minor changes suggest that the B-DNA conformation is not dramatically altered upon cylinder binding at these concentrations. This observation is consistent with the hypothesis that the cylinder binds in the major groove of helical DNA. At concentrations above 8:1 [nucleobase]:[cylinder], there is an observable change in behaviour. At these higher concentrations, the B-DNA structure could be altered, or the cylinder could be binding in concentrations high enough to produce competing CD signals at these wavelengths. Figure 3.13 shows magnified sections of the overlay at the regions where ICD peaks are observed, highlighting the general increase in the magnitude of ICD peaks with increasing concentration of cylinder.

Similar CD titration experiments where performed using the two azide functionalised cylinders, $Fe_2L^A{}_3Cl_4$ and $Fe_2L^B{}_3Cl_4$. Figure 3.14 shows the spectra obtained during the titration of $Fe_2L^A{}_3Cl_4$ to ctDNA. The positions of the ICD peaks are similar to those observed during the titration of $Fe_2L_3Cl_4$ to ctDNA (Fig 3.12a) however the magnitude of the peaks are lower. As can be seen from Figure 3.14b, higher concentrations of this azide cylinder are tolerated before the characteristic shape of the B-DNA CD signal is lost (6:1 [nucleobase]:[cylinder] as opposed to 8:1 with $Fe_2L_3Cl_4$). This may indicate that $Fe_2L^A{}_3Cl_4$ is binding to ctDNA to a lesser extent than $Fe_2L_3Cl_4$. This can be rationalised by considering the additional electron density that has been introduced by incorporating methylene azide groups at the ends of the cylinder, which may have a repulsive effect with the negatively charged sugar phosphate backbone.

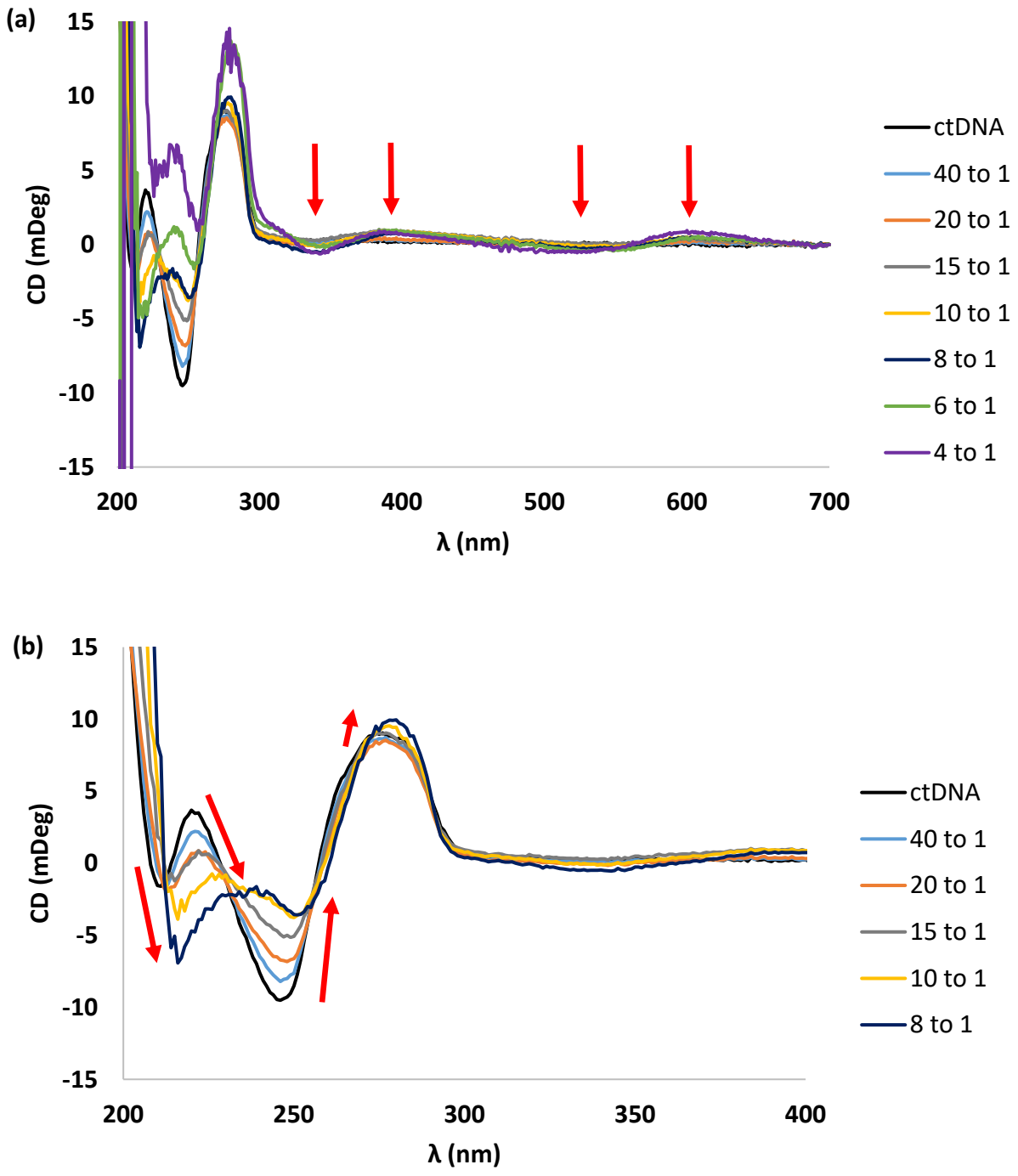

Figure 3.12 Overlay of CD spectra recorded during titration of increasing concentrations of $Fe_2L_3Cl_4$ to 100 µM ctDNA in 20 mM NaCl, 1 mM Na cacodylate (pH 6.8). (a) Full scan between 200 nm and 700 nm. Positions of ICD peaks are highlighted by red arrows. (b) Overlay showing the B-DNA conformation is retained up to a [nucleobase]:[cylinder] concentration of 8:1. The red arrows highlight the direction and magnitude of the shift of key signals.

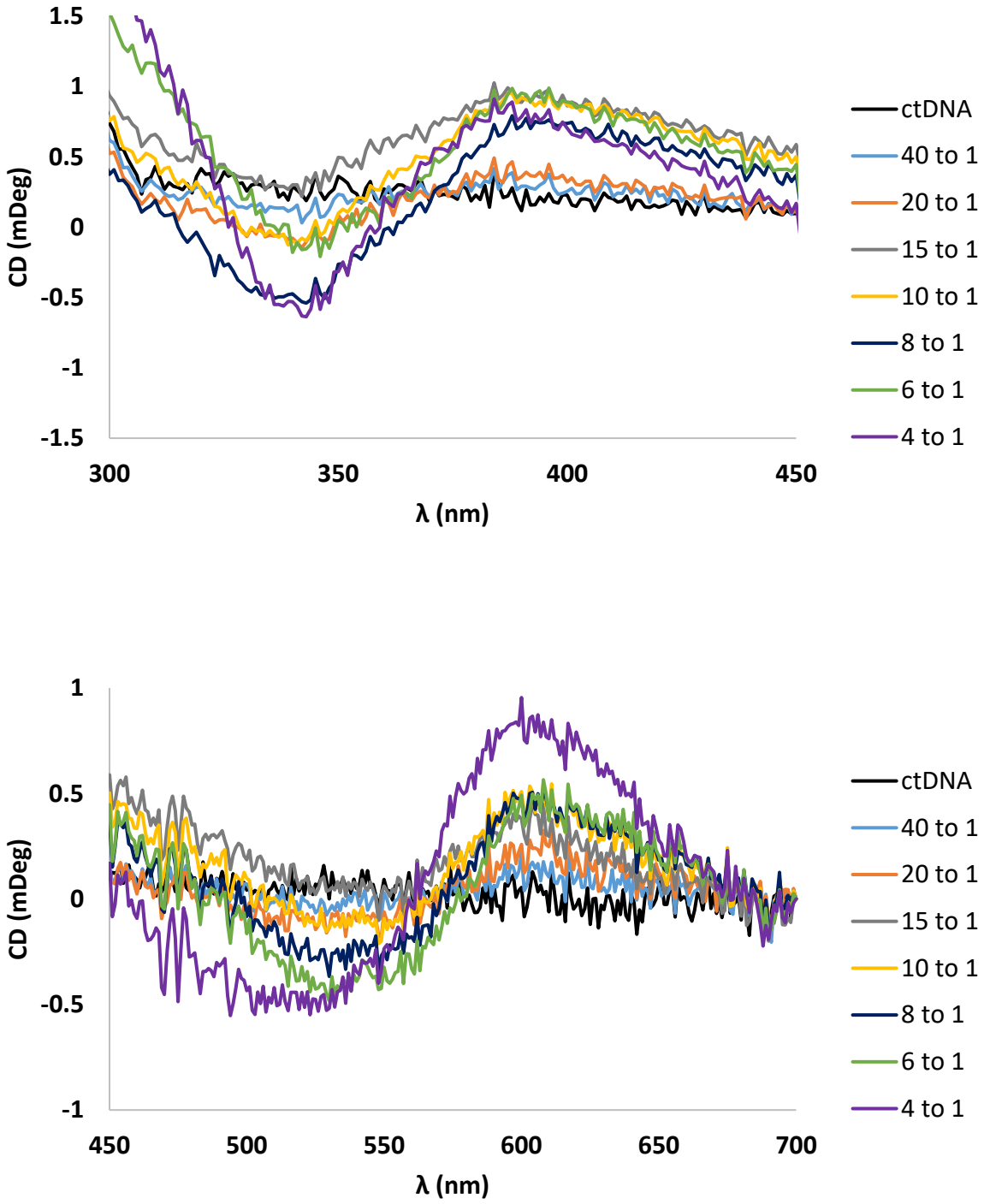

Figure 3.13 Magnified regions of the CD spectra overlays presented in Figure 3.12a, highlighting ICD signals. In general, the magnitude of these ICD signals increases with increasing concentration of $Fe_2L_3Cl_4$.

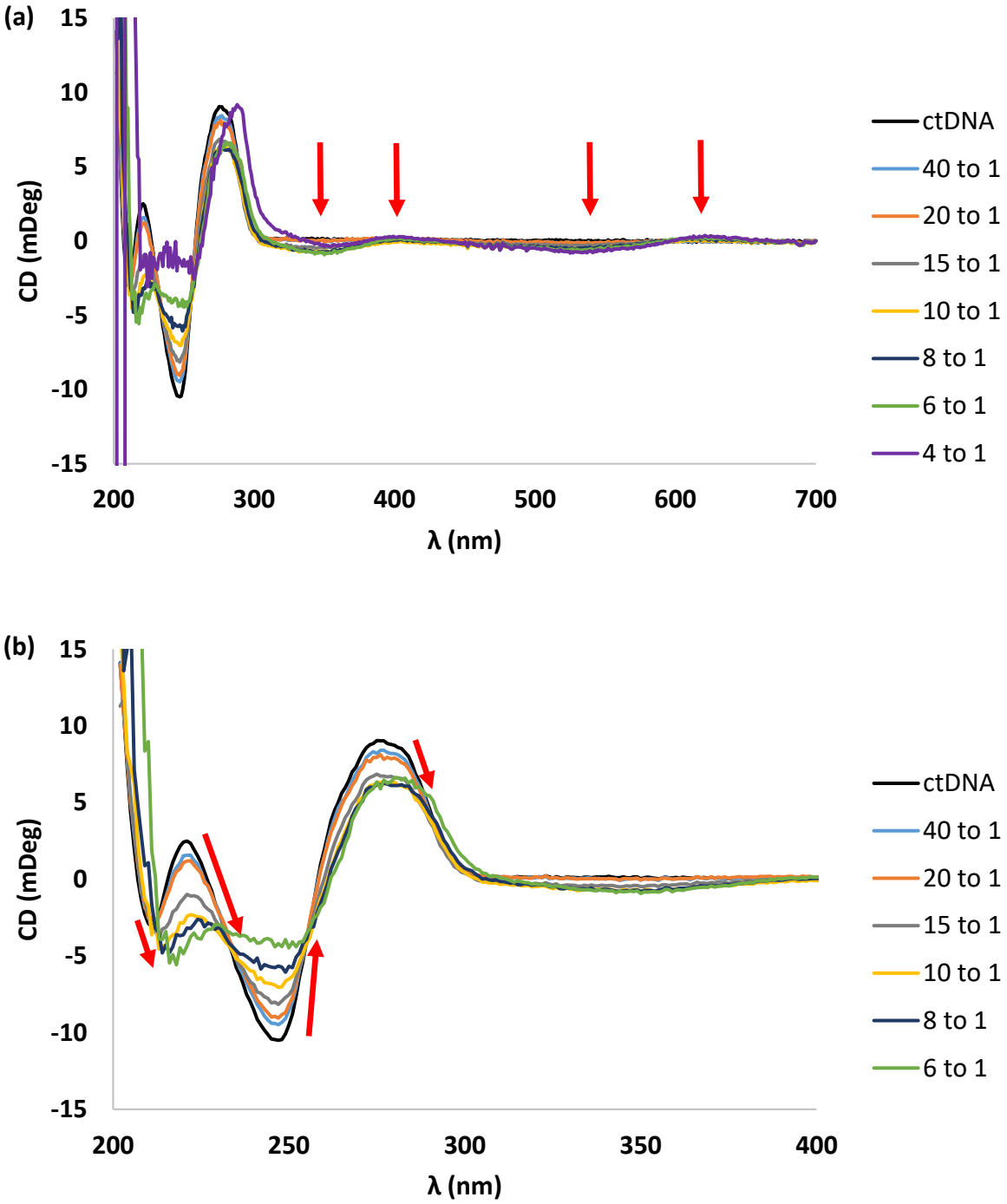

Figure 3.14 Overlay of CD spectra recorded during titration of increasing concentrations of $Fe_2L^A{}_3Cl_4$ to 100 µM ctDNA in 20 mM NaCl, 1 mM Na cacodylate (pH 6.8). (a) Full scan between 200 nm and 700 nm. Positions of ICD peaks are highlighted by red arrows. (b) Overlay showing the B-DNA conformation is retained up to a [nucleobase]:[cylinder] concentration of 6:1. The red arrows highlight the direction and magnitude of the shift of key signals.

Figure 3.15 shows the overlays of the CD spectra recorded with increasing concentrations of $Fe_2L^B{}_3Cl_4$. The most notable difference between these spectra and that obtained for $Fe_2L_3Cl_4$ is that the ICD peak around 315 nm is positive rather than negative, and there is a much larger increase in magnitude of this peak with increasing concentration of cylinder. Previous work in the Hannon group has suggested that the M helical isomer of $Fe_2L_3Cl_4$ binds in the major groove, while the P isomer situates randomly on top of the minor groove.[25] This change in the ICD signal may indicate that the binding mode has changed. Considering that a six atom substituent has been added to each end of the cylinder, it may be that the M isomer does not fit as well into the major groove. However, such a claim cannot be stated with any certainty without further investigation. Major groove binding was first concluded after observing interactions between $Fe_2L_3Cl_4$ and the DNA bases through NOE NMR spectroscopy.[23] Similar experiments could be performed with $Fe_2L^B{}_3Cl_4$ to gain more insight. As with $Fe_2L^A{}_3Cl_4$, the characteristic B-DNA signal shape is conserved at higher concentrations of $Fe_2L^B{}_3Cl_4$ (Fig 3.15b). This time, the shape is still apparent even at concentrations as high as 4:1. Again, retention of spectrum shape at these high concentrations could indicate that $Fe_2L^B{}_3Cl_4$ has a weaker binding interaction than $Fe_2L_3Cl_4$, likely a consequence of increasing the cylinder's size and introducing a higher degree of electron density at each end of the complex.

In each case, ICD peaks corresponding to regions where the cylinder ligands and MLCT band absorb have been observed upon adding cylinder to dsDNA. This suggests that incorporation of the azide functionalities has not dramatically decreased the ability of the azide cylinders to bind to dsDNA.

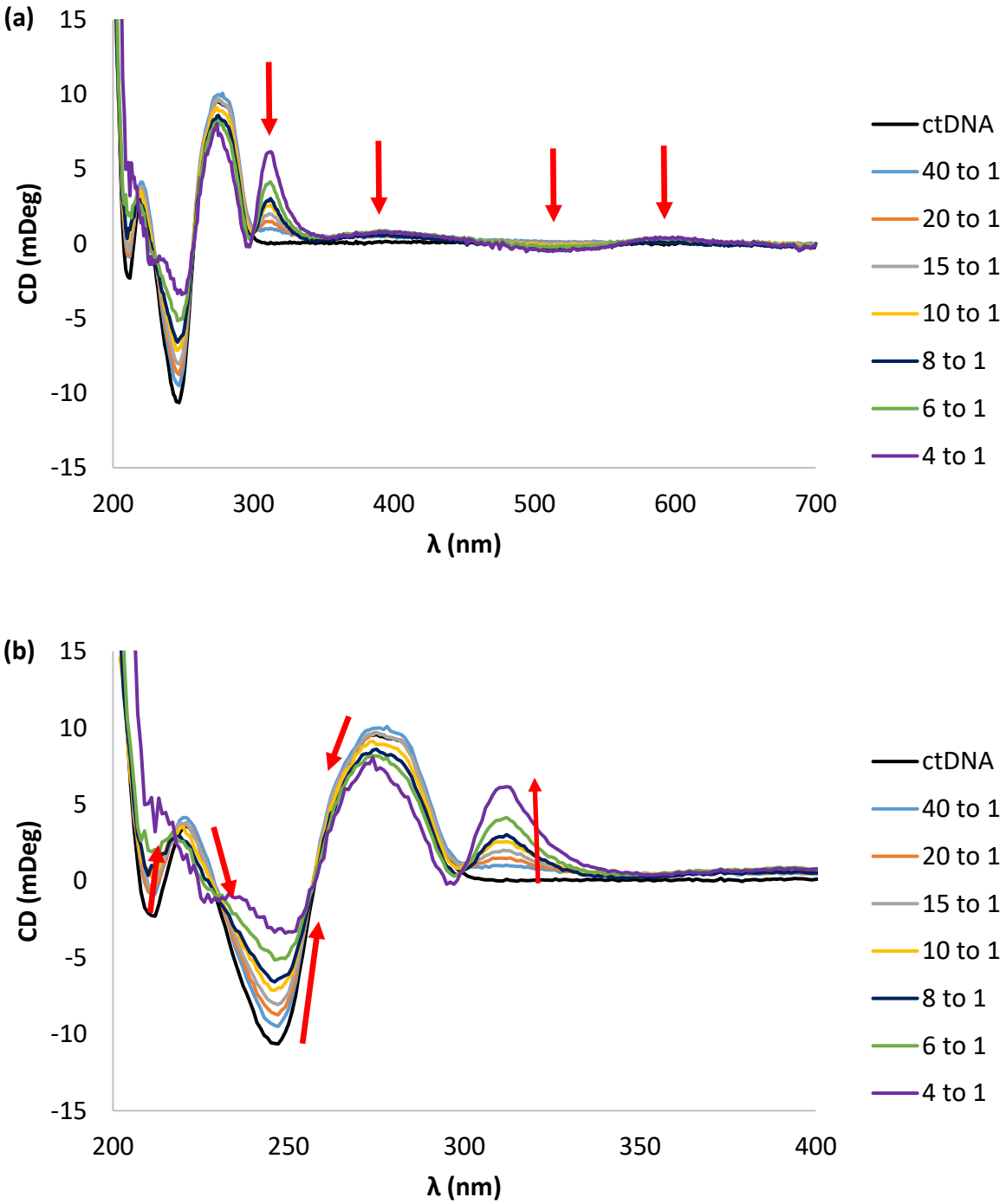

Figure 3.15 Overlay of CD spectra recorded during titration of increasing concentrations of $Fe_2L^B{}_3Cl_4$ to 100 µM ctDNA in 20 mM NaCl, 1 mM Na cacodylate (pH 6.8). (a) Full scan between 200 nm and 700 nm. Positions of ICD peaks are highlighted by red arrows. (b) Overlay showing the B-DNA conformation is retained up to a [nucleobase]:[cylinder] concentration of 4:1. The red arrows highlight the direction and magnitude of the shift of key signals.

3.4.2 dsDNA binding investigations using linear dichroism spectroscopy

Flow linear dichroism (LD) spectroscopy is a technique that can be used alongside CD spectroscopy to investigate the effect of a binding agent on the secondary structure of DNA. Flow linear dichroism is defined as the difference between the absorption of light polarised parallel and perpendicular to a major orientation axis: $LD = A_{\parallel} - A_{\perp}$. When studying helical DNA by flow LD, this axis is conventionally the helical axis around which the base pairs are orientated. Before any absorption measurements are performed, the dsDNA solution is subject to shear force which stretches out the helices with the helical axis running parallel to the direction of shear. This stretching of the DNA is achieved using a Couette cell (Figure 3.16) which consists of a cylindrical sample chamber with a quartz rod in the centre. The Couette cell is engineered such that there is a 0.5 mm ring-shaped gap between the rod surface and the walls of the sample chamber. A buffered solution of DNA is first placed into the sample chamber and the rod is then inserted, pushing the solution into this gap. Shear force is applied by spinning the sample chamber while the central rod remains stationary, stretching out the dsDNA along the helical axis. When DNA bases absorb light, the $\pi - \pi^*$ transitions result in polarisation across the plane of the base.[17] With B-DNA stretched out, the bases are orientated at angles that are close to being perpendicular to the helical axis, resulting in $A_{\perp}$ being higher in magnitude than $A_{\parallel}$. As such, a negative LD signal will be observed around wavelengths were the nucleobases absorb, with a λ_{max} at 260 nm. Figure 3.17 shows the characteristic LD spectrum for B-DNA. As with CD, measuring the LD spectra of ctDNA with increasing concentrations of a binding agent can offer some insight into the effect of the agent's binding on the secondary structure of the DNA.

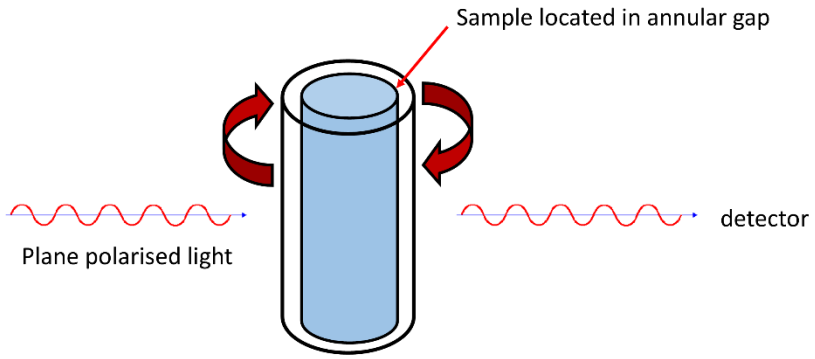

Figure 3.16 Diagram of a Couette cell, as used in LD spectroscopy.

LD spectroscopic titrations were performed in a similar manner to those performed using CD spectroscopy. The effect of increasing concentrations of both the azide functionalised cylinders were measured and compared to that of $Fe_2L_3Cl_4$. 100 µM ctDNA in 20 mM NaCl, 1 mM Na cacodylate (pH 6.8, 200 µL) served as the starting solution (solution A). The LD measurement of this between 200 and 700 nm, prior to any spinning, served as the baseline which was subtracted from all subsequent LD measurements. Solution A was spun at 40 revolutions per second for 3 min prior to the recording of the LD spectrum between 200 nm and 700 nm. Aliquots of 167 µM of the cylinder under investigation (solution B) were added such that the ratio of [nucleobase]:[cylinder] was increased from 40:1 to 6:1. For $Fe_2L_3Cl_4$, cylinder concentrations higher than 6:1 were not recorded, as precipitation of the DNA was observed in the solution after spinning. For the azide functionalised cylinders, precipitation was not observed until higher complex concentrations which allowed for more titration steps to be included. Each addition of solution B was accompanied by an equal volume of solution C (200 µM ctDNA, 40 mM NaCl, 2 mM Na cacodylate) to keep the concentration of DNA and buffer constant.

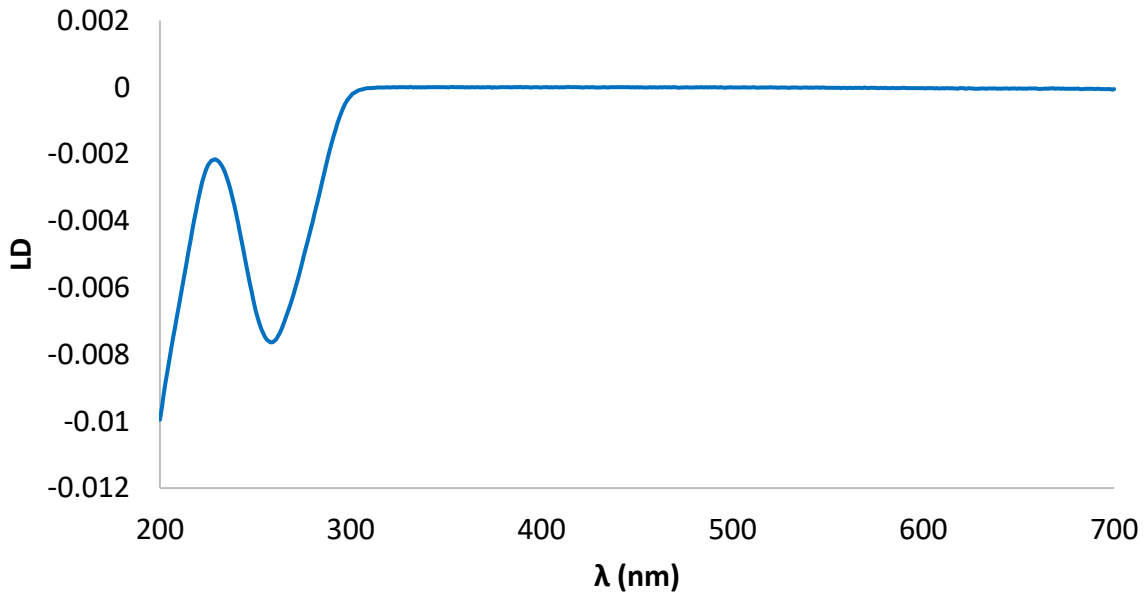

Figure 3.17 LD spectrum of 100 µM ctDNA in 20 mM NaCl, 1 mM Na cacodylate aqueous buffer.

Figure 3.18 shows the overlay of the LD spectra obtained during the titration of increasing concentrations of $Fe_2L_3Cl_4$ to ctDNA. The concentration ratios are listed, with the concentration of ctDNA expressed in terms of nucleobases present. The characteristic negative LD signal at 260 nm decreases in magnitude with increasing concentration of $Fe_2L_3Cl_4$. This decrease suggests that the DNA helices are shortening along the helical axis, which would result in less of a difference between $A_{\parallel}$ and $A_{\perp}$. An induced LD (ILD) band can also be observed around 370 nm, which increases in magnitude with increasing concentration of the complex. As already discussed in relation to a similar effect observed with the CD titration, this is the region where the cylinder ligands absorb. The presence of this ILD band indicates that the cylinder is binding in a specific manner rather than randomly along the length of the DNA. In the longer wavelength region (where we would expect to see the MLCT band) the spectrum appears to have a non-flat baseline, likely caused by light scattering. This non-flat baseline may be masking a weak ILD arising from the MLCT of the cylinder. This scattering could be due to some of DNA strands becoming coiled, forming sphere-like particles. DNA coiling at higher cylinder concentrations is consistent with previous work performed by the group, where $Fe_2L_3Cl_4$ was observed to have a supercoiling effect of helical DNA through atomic force microscopy.[23]

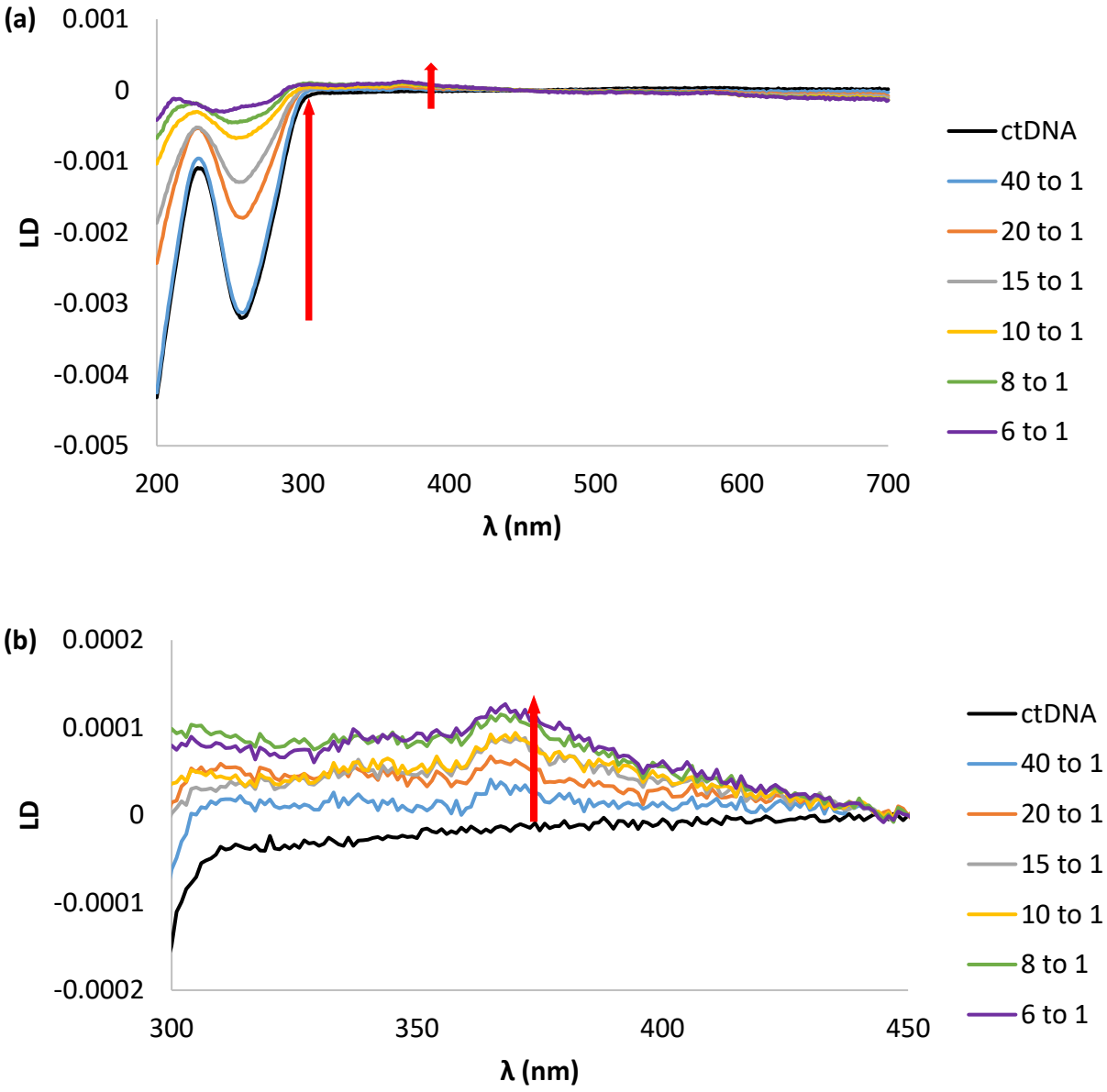

Figure 3.18 (a) Overlay of LD spectra obtained during the titration of increasing concentrations of $Fe_2L_3Cl_4$ to 100 µM ctDNA in 20 mM NaCl, 1 mM Na cacodylate. (b) Magnified view of the ILD band around 370 nm.

Figure 3.19 shows the overlay of the LD spectra measured during a similar titration of $Fe_2L^A{}_3Cl_4$. While the magnitude of the signal around 260 nm does decrease during the titration, there is less of an effect than that observed with $Fe_2L_3Cl_4$ which suggests that the DNA is shortening to a lesser extent. No notable ILD bands appear during the titration, which again suggests that $Fe_2L^A{}_3Cl_4$ has a weaker binding interaction than $Fe_2L_3Cl_4$. Higher concentrations of $Fe_2L^A{}_3Cl_4$ were tolerated. A [nucleobase]:[cylinder] ratio of 3:1 did not

result in visible precipitation, as happened with $Fe_2L_3Cl_4$. The spectrum obtained at this concentration is included in the overlay, and it can be seen that at this concentration the spectrum has a similar shape to that obtained with a [nucleobase]:[$Fe_2L_3Cl_4$] of 6:1.

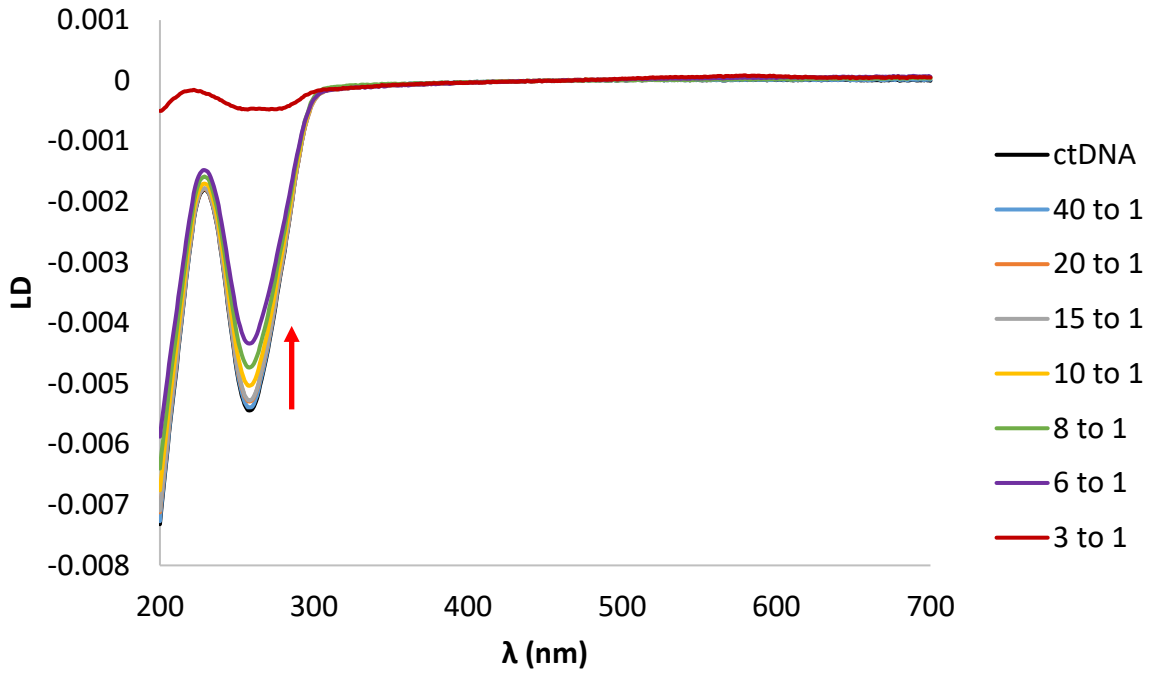

Figure 3.19 Overlay of LD spectra obtained during the titration of increasing concentrations of $Fe_2L^A{}_3Cl_4$ to 100 µM ctDNA in 20 mM NaCl, 1 mM Na cacodylate.

Figure 3.20 shows the LD spectra obtained during the titration of increasing concentrations of $Fe_2L^B{}_3Cl_4$ to ctDNA. As with $Fe_2L_3Cl_4$, the magnitude of the negative signal around 260 nm decreases with increasing cylinder concentration, indicating that the DNA helices are shortening. A very weak positive ILD signal can be seen around 540 nm (Fig 3.20b), in the region of the MLCT absorbance of $Fe_2L^B{}_3Cl_4$, indicating that the complex has bound to the DNA.

Qualitatively, when comparing the LD titration spectra of both $Fe_2L^A{}_3Cl_4$ and $Fe_2L^B{}_3Cl_4$ to that of $Fe_2L_3Cl_4$, it can be observed that the $Fe_2L^B{}_3Cl_4$ data more closely resembles that of $Fe_2L_3Cl_4$. This comparison is presented quantitatively in Figure 3.21, which plots the magnitude of the signal at 260 nm against concentration of complex (expressed as a percentage molar equivalent in relation to the concentration of nucleobases). From Fig 3.21, it can be seen that

the cylinders all behave similarly at low concentrations, as seen at 2.5 mol% cylinder (40:1 [nucleobase]:[cylinder]), but that the difference in their binding interactions becomes more apparent at higher concentrations. At 12.5 mol% (8:1 [nucleobase]:[cylinder], where the characteristic B-DNA shape is still maintained on the CD spectrum), it can be seen that $Fe_2L_3Cl_4$ has resulted in a 86% decrease in signal at 260 nm. In comparison, $Fe_2L^A{}_3Cl_4$ has reduced the signal by 13% and $Fe_2L^B{}_3Cl_4$ has reduced the signal by 38%. The stronger binding interaction of $Fe_2L^B{}_3Cl_4$ compared to $Fe_2L^A{}_3Cl_4$ can be rationalised by considering that the longer atom chain between the azide and the pyridyl ring allows the azide groups to be orientated further away from the major groove.

Investigations into the CD and LD binding properties of $Fe_2L^A{}_3Cl_4$ and $Fe_2L^B{}_3Cl_4$ suggest that both show dsDNA binding behaviour similar to that of $Fe_2L_3Cl_4$. Both cylinders show evidence of binding to dsDNA without causing dramatic changes in its secondary structure, until very high cylinder concentrations are reached. The LD experiments suggest that ctDNA is not shortened as much by either of the azide cylinders as it is by $Fe_2L_3Cl_4$, which may be due to weaker binding interactions. An explanation for weaker binding may be the presence of additional electron density in the azide groups, which can disfavour groove binding due to their vicinity to the negatively charged DNA backbone.

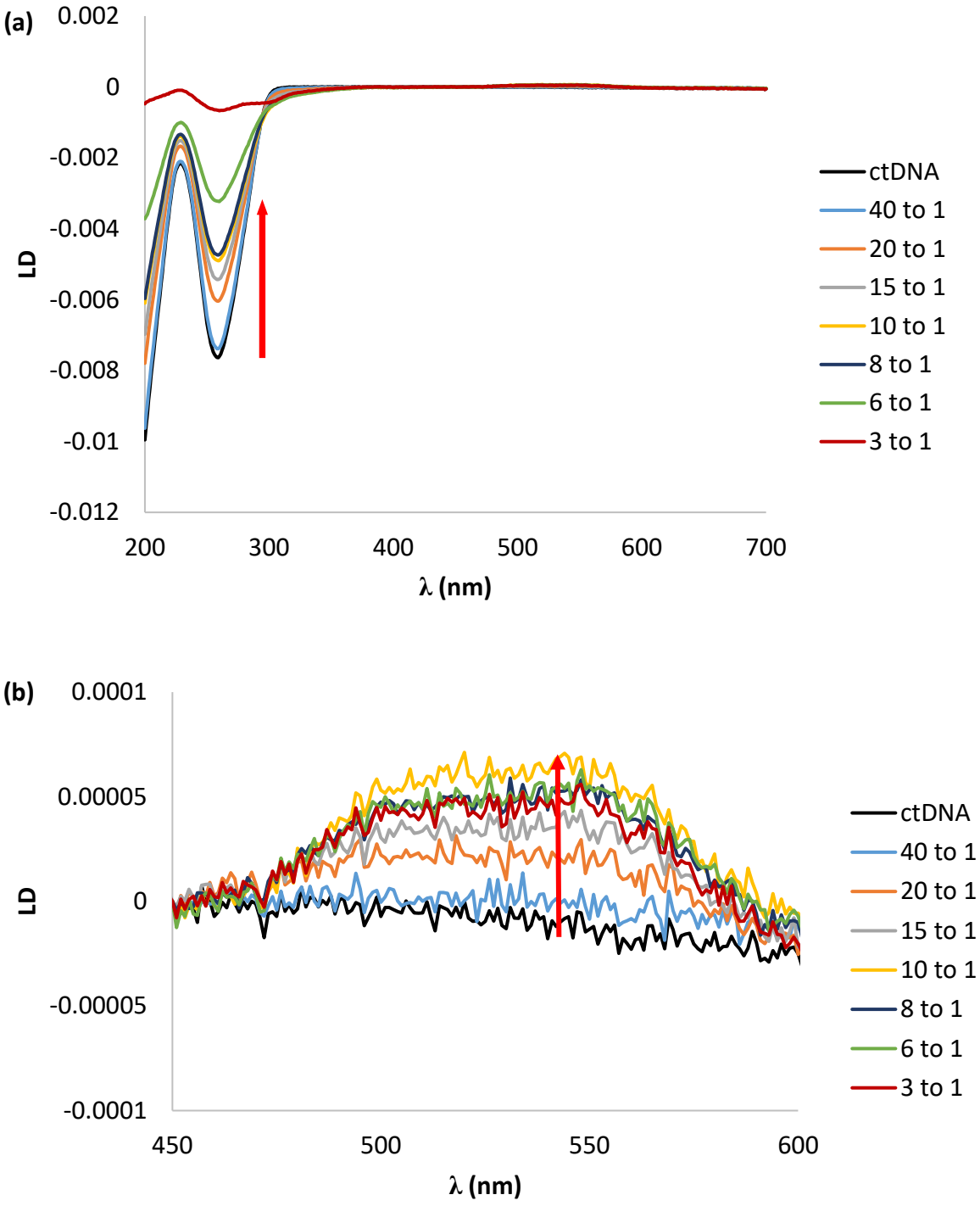

Figure 3.20 (a) Overlay of LD spectra obtained during the titration of increasing concentrations of $Fe_2L^B{}_3Cl_4$ to 100 µM ctDNA in 20 mM NaCl, 1 mM Na cacodylate. (b) magnified region showing a weak ILD band around 540 nm.

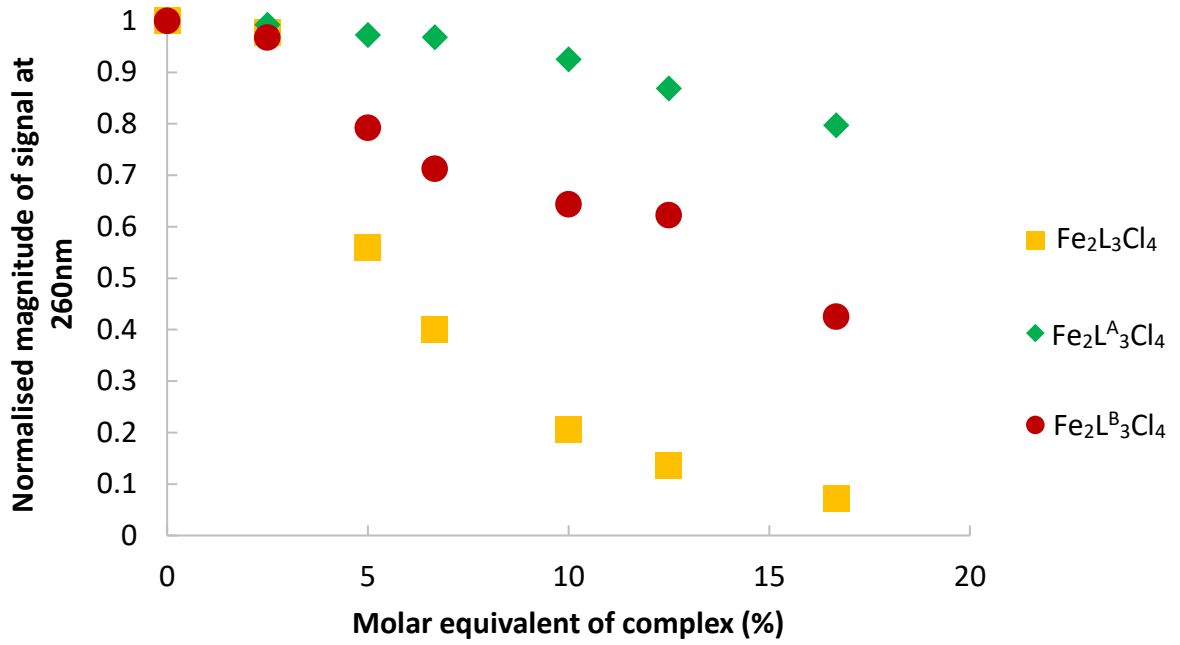

Figure 3.21 Plot of the magnitude of the LD signal observed at 260 nm (normalised) against the concentration of each of the complexes under investigation.

3.5 Investigations into the 3WJ binding properties of azide functionalised cylinders

3.5.1 3WJ binding experiments using polyacrylamide gel electrophoresis

Gel electrophoresis is a universal technique used in the analysis of biomolecules, including nucleic acids. Aqueous samples of biomolecules are loaded into one end of a porous gel, which can be made of a variety of polymers such as agarose or starch. A potential difference is then applied across the gel, and the biomolecules move through the gel pores towards the electrode of opposite charge. This potential difference separates the biomolecules based on their electrophoretic mobility, which is dependent on their overall size, shape and charge. Generally, lower molecular weight analytes move through the gel faster than those of higher molecular weights. Polyacrylamide gel electrophoresis (PAGE) uses polyacrylamide as the separation medium. PAGE is often used to separate small nucleic acids, as a sufficiently small pore size can be achieved which grants good resolution between small molecular weights.[26] PAGE is usually performed with vertical gels, with nucleic acid analytes loaded by pipette into wells at the top. The upper and lower electrode chambers are filled with buffer of the same

composition as that used to form the gel to ensure smooth conductivity between the two electrodes. A schematic representation of the equipment used is given in Figure 3.22.[27] When running the gel, the negatively charged nucleic acids are pulled towards the positively charged anode at the bottom of the gel, with smaller molecular weight nucleic acids travelling further down the gel than larger ones. Once the gel has been run for a certain time, the electric field is removed and the relative positions of the analytes (referred to as "bands") visualised. Visualisation is usually achieved using a commercial stain.[26]

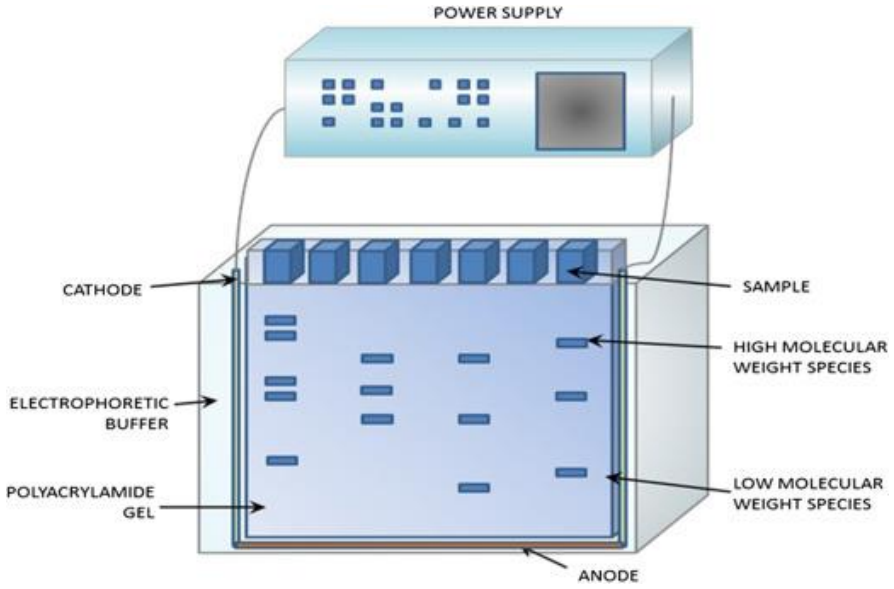

Figure 3.22 Schematic showing the separation of high and low molecular weight analytes using PAGE. Taken with permission from reference 27.

PAGE experiments have previously been used to investigate the 3WJ binding properties of $Fe_2L_3Cl_4$ as well as functionalised derivatives.[28,29] Similar experiments were performed to investigate the 3WJ binding properties of $Fe_2L^A{}_3Cl_4$ and $Fe_2L^B{}_3Cl_4$. The reasoning behind each stage of the experimental set up is discussed throughout this section. The general procedure for these experiments incubates the complex of interest with three synthetic oligonucleotides (S1, S2 and S3) which have a base sequence designed to form a 3WJ (Figure 3.23). These 3WJ strands were first investigated by Leontis and co-workers in 1995, who showed that this 3WJ is stable at 5 ^oC but not at room temperature.[30] As such, when loaded onto a gel run at room temperature only a single band corresponding to the single stranded oligonucleotides

(ssDNA) is observed. When $Fe_2L_3Cl_4$ is included in the incubation, it stabilises the 3WJ at room temperature and the resultant 3WJ-cylinder adduct migrates more slowly through the gel than the free ssDNA.[28] A comparison of the lane appearance of samples containing S1, S2 and S3 with and without $Fe_2L_3Cl_4$ is shown in Figure 3.24.

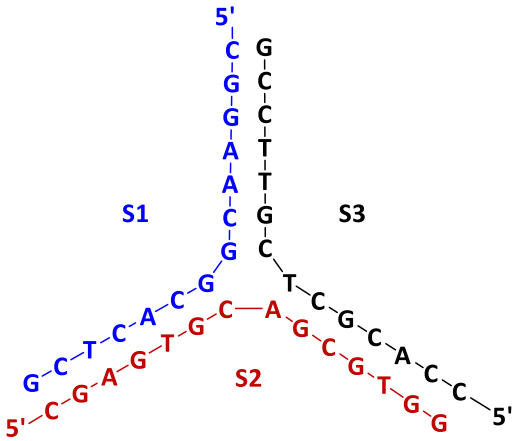

Figure 3.23 Illustration of the sequence of three oligonucleotides used in the PAGE experiments, and how base pairs come together to form a 3WJ.

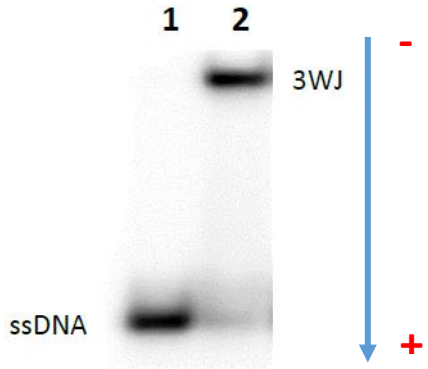

Figure 3.24 Representative PAGE run showing the 3WJ stabilising effect of $Fe_2L_3Cl_4$. Well 1: S1*, S2, S3. Well 2: S1*, S2, S3 and $Fe_2L_3Cl_4$. * indicates the radiolabelled strand.

3.5.2 Radiolabelling the oligonucleotide

Radiolabelling was used as the visualisation method in these experiments. Radiolabelling was achieved enzymatically prior to the PAGE experiments. One of the oligonucleotide strands (usually S1) was incubated with T4 polynucleotide kinase enzyme and commercially available γ-adenosine triphosphate (ATP), which has a terminal phosphate group with β-emitting ^{32}P. The enzyme phosphorylates the 5' end of the strand with the radioactive phosphate, as illustrated in Figure 3.25. After a 1 h incubation at room temperature, the enzyme was denatured and a commercially available purification kit (QIAGEN Nucleotide Removal Kit) was used to precipitate out the labelled strand, wash it several times, and then resuspend it in water to a 4 μM solution. Using a radiolabelled strand allows the positions of the 3WJ and ssDNA to be detected by exposing the gel to a phosphor screen, which is then imaged using a molecular imager to reveal the positions of the bands. The advantage of using radiolabelling to visualise the gel is that it does not interfere with the cylinder binding to the 3WJ. Many traditional visualisation methods rely on a DNA binding dye that may compete with the cylinder. If the cylinder is displaced, the 3WJ will be destabilised and the strands may begin to diffuse through the gel, giving poor resolution of the band. ^{32}P has a life-life of 14 days, and the initial activity of the γ-ATP allowed the same stock of radiolabelled strand to be used for multiple experiments, even after three half-lives.

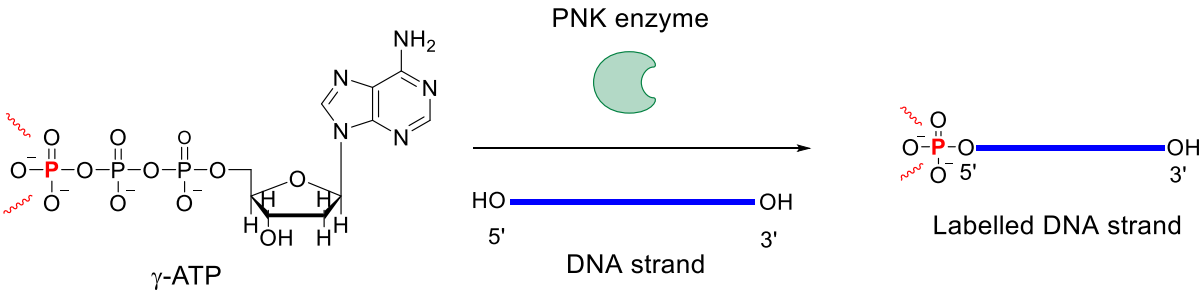

Figure 3.25 Illustration of the labelling experiment, where the 5' end of one of the DNA strands is phosphorylated with a radioactive phosphate by T4 polynucleotide kinase enzyme.

3.5.3 Preparation of the polyacrylamide gel

Polyacrylamide gels were prepared fresh on the day of each experiment. Commercially available stock of 30% acrylamide/biscrylamide mixture (with the ratio 37.5:1 acrylamide/bisacrylamide) was diluted with 2 x tris base-boric acid (TB) buffer to give a 15% acrylamide/bisacrylamide solution in 1 x TB buffer (89 mM tris(hydroxymethyl)-aminomethane; 89 mM boric acid, pH 8.3). In many electrophoresis protocols, TBE buffer is used which contains tris base, boric acid and EDTA. EDTA was intentionally absent from all the buffers used in these PAGE experiments, as it is known to coordinate to the metal ions of cylinders, displacing the cylinder ligands and effectively breaking the cylinder apart. Acrylamide is the monomer that forms the polymer chains and bisacryalmide is a crosslinker connecting these together to form the gel. To initiate polymerisation, small quantities of 10% w/v ammonium persulfate aqueous solution and tetramethylethylenediamine (TEMED) were added. The polymerisation follows a radical mechanism, with ammonium persulfate serving as a photoinitiator. The TEMED stabilises the sulfate radicals which accelerates the rate of polymerisation. The role of persulfate, acrylamide, and bisacrylamide in the polymerisation process is highlighted in Figure 3.26. As soon as the persulfate and TEMED were added, the solution was gently mixed and poured between two glass plates. A well comb was inserted into the solution between the glass plates at the top to form the wells. The gel was left to set between the glass plates for at least 1 h.

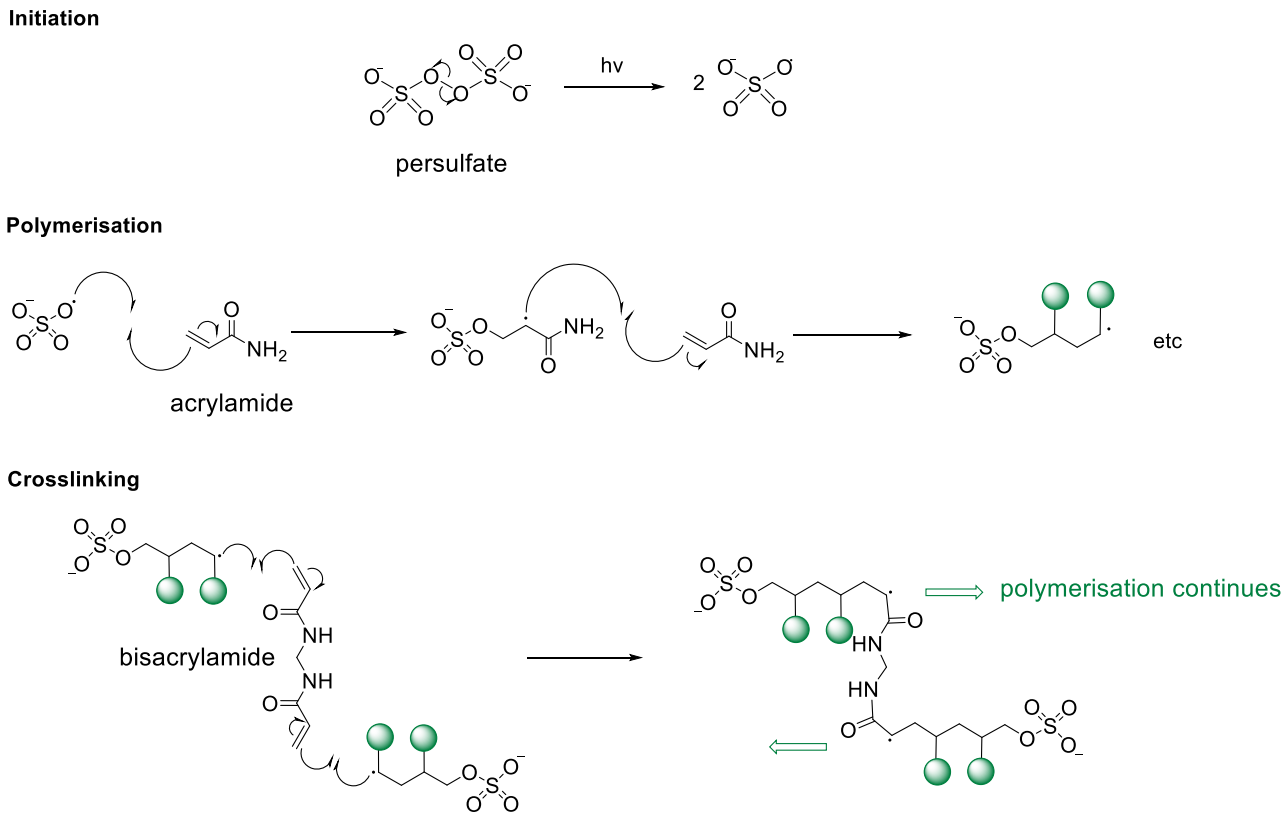

Figure 3.26 Illustration of the stages of the radical polymerisation process that forms the polyacrylamide gel used in PAGE. Persulfate is the photoinitiator, which reacts with acrylamide to start polymerisation. Bisacrylamide crosslinks the polyacrylamide chains, forming them into a gel.

3.5.4 Sample preparation and gel loading

For the PAGE experiments, 13 samples were prepared in 1.5 mL Eppendorf tubes. The contents of each sample are listed in Table 3.1. Additionally, 1 µL of 10 x TBN buffer (TB buffer with additional NaCl) was added to each. The final volume was made up to 10 µL by addition of nuclease free water to give a buffer concentration of 89 mM tris; 89 mM boric acid; 100 mM NaCl in each sample. The presence of sodium ions has been linked to 3WJ stability,[31] which is why they were included in the incubation buffer. The sample concentration of each oligonucleotide was 0.4 µM. 4 µM solutions of each cylinder ($Fe_2L_3Cl_4$, $Fe_2L^A{}_3Cl_4$, and $Fe_2L^B{}_3Cl_4$) were prepared and volumes of each were then added to four samples such that concentrations of 0.2, 0.4, 0.8, and 1.2 µM (0.5, 1, 2 and 4 equivalents of cylinder per 3WJ, respectively) were achieved. Samples with $Fe_2L_3Cl_4$ were used as the positive control. The

first sample contained no complex, so served as the negative control. The samples were left at room temperature for 1 h. 15 µL of 30% v/v glycerol in water was then added to each sample tube prior to gel loading, resulting in each sample settling at the bottom of the well after loading. Each sample was loaded into a separate well, and the gel was run at a constant voltage of 140 V for 2 h. Once run, the gel was removed from the tank and placed in an exposure cassette with a phosphor screen. Exposure times varied from 45 min to 2 h, depending on the radioactivity count of the gel as measured by Geiger counter. The screen was then imaged using a BioRad Personal Molecular Imager.

Table 3.1 Sample contents for PAGE investigation into 3WJ binding of cylinders.

Sample	Contents
1	S1, S2, S3 (all 0.4 µM)
2	S1, S2, S3 (all 0.4 µM); $Fe_2L_3Cl_4$ (0.2 µM)
3	S1, S2, S3 (all 0.4 µM); $Fe_2L_3Cl_4$ (0.4 µM)
4	S1, S2, S3 (all 0.4 µM); $Fe_2L_3Cl_4$ (0.8 µM)
5	S1, S2, S3 (all 0.4 µM); $Fe_2L_3Cl_4$ (1.2 µM)
6	S1, S2, S3 (all 0.4 µM); $Fe_2L^A{}_3Cl_4$ (0.2 µM)
7	S1, S2, S3 (all 0.4 µM); $Fe_2L^A{}_3Cl_4$ (0.4 µM)
8	S1, S2, S3 (all 0.4 µM); $Fe_2L^A{}_3Cl_4$ (0.8 µM)
9	S1, S2, S3 (all 0.4 µM); $Fe_2L^A{}_3Cl_4$ (1.2 µM)
10	S1, S2, S3 (all 0.4 µM); $Fe_2L^B{}_3Cl_4$ (0.2 µM)
11	S1, S2, S3 (all 0.4 µM); $Fe_2L^B{}_3Cl_4$ (0.4 µM)
12	S1, S2, S3 (all 0.4 µM); $Fe_2L^B{}_3Cl_4$ (0.8 µM)
13	S1, S2, S3 (all 0.4 µM); $Fe_2L^B{}_3Cl_4$ (1.2 µM)

3.5.5 Comparison of the 3WJ binding of $Fe_2L^A{}_3Cl_4$ and $Fe_2L^B{}_3Cl_4$ to $Fe_2L_3Cl_4$ by PAGE

Four gel experiments were run and the images obtained are included in Appendix 2. For one of the gels, only one well with $Fe_2L_3Cl_4$ (1 eq) was included as the positive control. Visually, the results were consistent. Figure 3.27 shows the gel image with the highest band resolution

(gel 3 in Appendix 2). It can be observed that both $Fe_2L^A{}_3Cl_4$ and $Fe_2L^B{}_3Cl_4$ show 3WJ binding properties. All gel images were analysed using Bio-Rad's Quantity One software. The boundaries of each band are judged by eye and defined by drawing boxes around each band. The software measures the intensity of each pixel within the defined box to give a total intensity expressed as counts. An approximation of the percentage of labelled strand that is in the 3WJ form is calculated by comparing the intensities of each lane's 3WJ and ssDNA bands. Table 3.2 presents the results of the analysis performed on the gel shown in Figure 3.27. The result for lane 5 and 13 seems out of trend, which can be attributed to the observed precipitation of some of the DNA in the well at the top of the lane. The same analysis was performed on the other gel images and an average %3WJ ± SD for each lane was calculated, based on the triplicate results for each cylinder that were most in agreement. The results of this analysis are shown in Figure 3.28. There is no observable difference between the %3WJ values of the cylinders at 4.0 equivalents. The results at 1.0 and 2.0 equivalents show an observable difference between $Fe_2L_3Cl_4$ and the two azide cylinders, however no difference is observed between $Fe_2L^A{}_3Cl_4$ and $Fe_2L^B{}_3Cl_4$. The result at 0.5 equivalents is puzzling, as the data from $Fe_2L_3Cl_4$ suggests that over 50% of the DNA is in the 3WJ form. Taken at face value, this result suggests that one cylinder can induce and stabilise multiple 3WJs. A more likely explanation is that the purification protocol used to isolate the radiolabelled strand is not 100% efficient. Some of the labelled strand could remain stuck to the filter during the final resuspension step. Any retention of DNA on the filter would give a lower concentration of the radiolabelled strand than calculated, meaning that the maximum possible concentration of 3WJs in the incubation mixture is less than desired. This suggestion is consistent with the observation that there is measurable radioactivity in the spin filter after the final DNA elution step. There is no significant difference (defined as $p > 0.05$) between the %3WJ for $Fe_2L_3Cl_4$ at 0.5 and 1.0 eq, which highlights a need for this experiment to be optimised. Measuring the concentration of all the 3WJ strands prior to incubation may help. Such a measurement may be possible with instrumentation such as a NanoDrop (Thermo Scientific), which is designed to measure the absorbance of microliter quantities of aqueous DNA solutions. However, an instrument dedicated to ^{32}P radioactive work would be required to comply with safety protocols. Despite these limitations, this experiment does qualitatively show that $Fe_2L^A{}_3Cl_4$ and $Fe_2L^B{}_3Cl_4$ can stabilise DNA 3WJs.

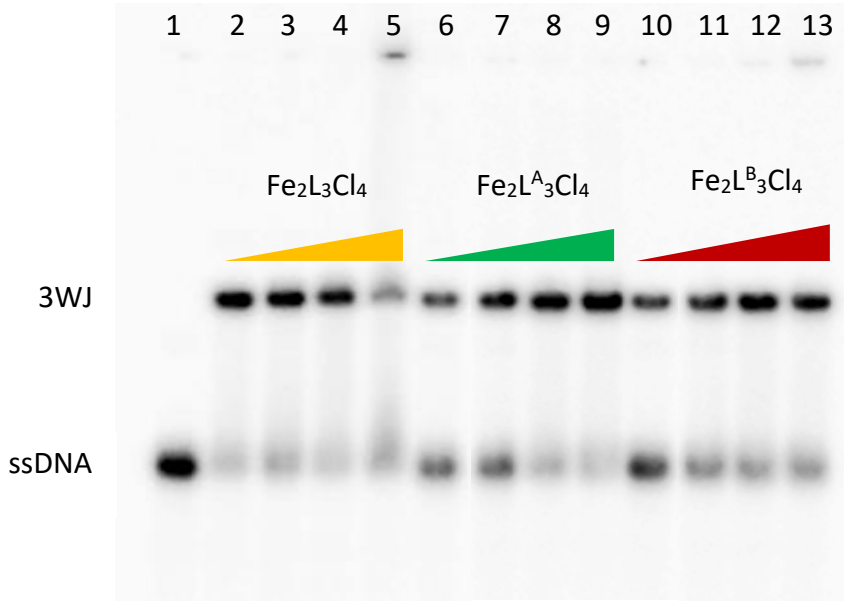

Figure 3.27 Radiogram of PAGE gel experiment investigating the 3WJ forming properties of $Fe_2L_3Cl_4$, $Fe_2L^A{}_3Cl_4$, and $Fe_2L^B{}_3Cl_4$. The yellow wedge indicates increasing concentration of $Fe_2L_3Cl_4$, with green and red wedges indicating increasing concentrations of $Fe_2L^A{}_3Cl_4$ and $Fe_2L^B{}_3Cl_4$, respectively.

Table 3.2 Intensity counts for each band observed in Figure 3.27, and % 3WJ for each well.

Well	Complex	3WJ band (counts)	ssDNA band (counts)	% 3WJ
1	-	-	27307	-
2	0.5 eq $Fe_2L_3Cl_4$	22484	4859	82
3	1 eq $Fe_2L_3Cl_4$	20282	6627	75
4	2 eq $Fe_2L_3Cl_4$	16461	3546	82
5	4 eq $Fe_2L_3Cl_4$	7106	4460	61
6	0.5 eq $Fe_2L^A{}_3Cl_4$	11519	11924	49
7	1 eq $Fe_2L^A{}_3Cl_4$	18482	13378	58
8	2 eq $Fe_2L^A{}_3Cl_4$	22879	6596	78
9	4 eq $Fe_2L^A{}_3Cl_4$	25732	5053	84
10	0.5 eq $Fe_2L^B{}_3Cl_4$	10707	14720	42
11	1 eq $Fe_2L^B{}_3Cl_4$	16665	10557	61
12	2 eq $Fe_2L^B{}_3Cl_4$	20936	8548	71
13	4 eq $Fe_2L^B{}_3Cl_4$	17489	7809	69

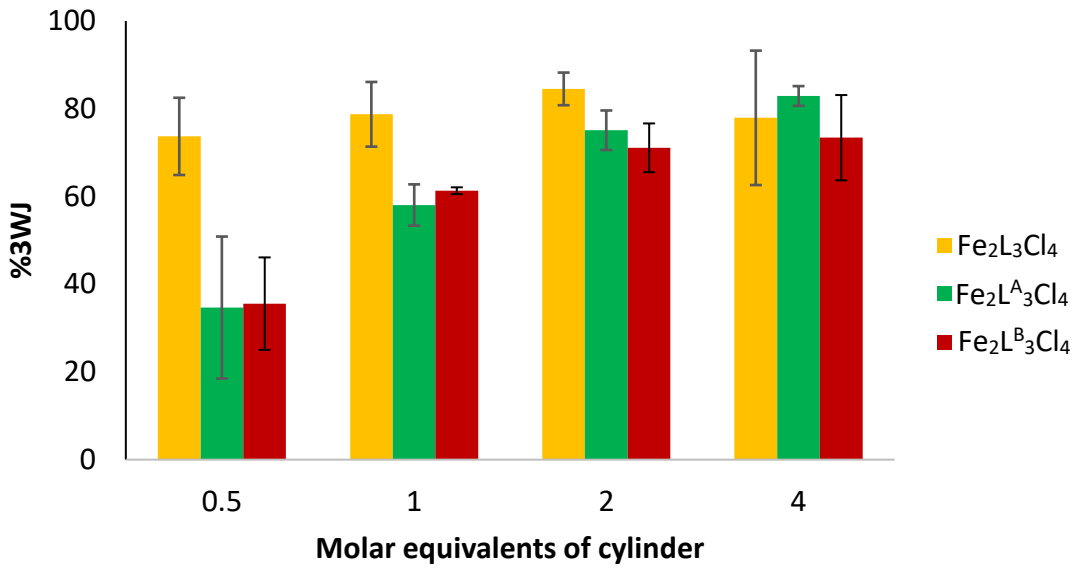

Figure 3.28 Plot of average %3WJ ± SD (measured from intensities of the bands observed by PAGE experiments) for each concentration of cylinder, expressed as molar equivalents per 3WJ in solution.

3.5.6 Using PAGE to observe reactivity of $Fe_2L^A{}_3Cl_4$ and $Fe_2L^B{}_3Cl_4$

The work described so far has yet to show whether the azides of $Fe_2L^A{}_3Cl_4$ and $Fe_2L^B{}_3Cl_4$ are able to react with strained cyclooctynes as part of a SPAAC reaction. Initial synthetic approaches involved mixing each azide functionalised ligand (**44** and **45**) with an excess of commercially available dibenzocyclooctyne-amine (DBCO-amine, Figure 3.29). ^{1}H NMR of the reaction mixtures, taken after four hours of stirring in methanol at room temperature, proved difficult to analyse due to overlapping, poorly resolved aromatic resonances. Due to this uncertainty, an alternative approach using PAGE was trialled. This experiment incubated an aqueous soluble analogue of DBCO-amine (DBCO-sulfo-N-hydroxysuccinimidyl ester, Figure 3.29) with each of the azide functionalised cylinders in the presence of S1*, S2, and S3 for 1 h at room temperature. The procedure followed was largely the same as the previous PAGE experiment, but also included cyclooctyne solution as a final additive. The rationale behind this experiment was that if the cyclooctyne clicked onto the azide cylinders, any 3WJ adducts formed would be slightly larger in size. The extra bulk would prevent the 3WJ strands from getting as close together as they would do otherwise. This increased size would result in the

3WJ band appearing further up the gel, as a result of a reduction in its electrophoretic mobility. Such an effect has already been reported when investigating the 3WJ binding of arginine functionalised cylinders.[29]

A concentration ratio of 2:1 cylinder:3WJ was used in each sample, as the resolutions of the 3WJ band at this ratio are well defined for each of the three cylinders in Figure 3.27. Three samples were set up per cylinder, with cyclooctyne concentrations of 0, 24, and 100 μM (0, 5, and 20 equivalents of cyclooctyne per azide group, respectively). The contents of each well are listed in Table 3.3 and the resultant radiogram is shown in Figure 3.30**.** Lanes 2-4 each show a 3WJ band at the same position, which shows that the cyclooctyne itself does not interfere with the binding of $Fe_2L_3Cl_4$ to the 3WJ. Lanes 11 and 12 serve as a control to show that the cyclooctyne has no stabilising effect on 3WJ formation. Lane 10 appears slightly higher than the band of lane 8, indicating that the cyclooctyne is having an effect at higher concentrations with $Fe_2L^B{}_3Cl_4$. Such an effect is not observed with $Fe_2L^A{}_3Cl_4$, which may be due to the unavailability of the azide groups as they are situated much closer to the DNA of the 3WJ due to the shorter chain length. This tantalising result warrants further investigation. In this experiment the DNA strands were added to the buffer first, followed by the cylinder and finally the cyclooctyne. Both the 3WJ formation and the SPAAC click reaction are expected to occur rapidly but it is not known which of these has the faster reaction rate. If the 3WJ forms around the cylinder more quickly then it may be difficult for the SPAAC reaction to proceed, especially with the shorter substituent chain length of $Fe_2L^A{}_3Cl_4$. It would be interesting to compare the results obtained if the cylinder and cyclooctyne are premixed before addition to the 3WJ oligonucleotides. Premixing the cylinder and cyclooctyne would allow the SPAAC reaction to occur first, which may result in less 3WJ being formed or a larger reduction in the observed mobility of the 3WJ band. The ultimate goal would be to perform the SPAAC reaction intracellularly, so a series of investigations looking at whether other DNA structures (for example, dsDNA, GQs, and ssDNA capable of forming multiple junction structures) interfere with the SPAAC reaction would be an interesting follow-up to this preliminary work.

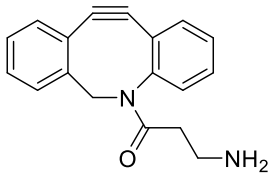

DBCO-amine

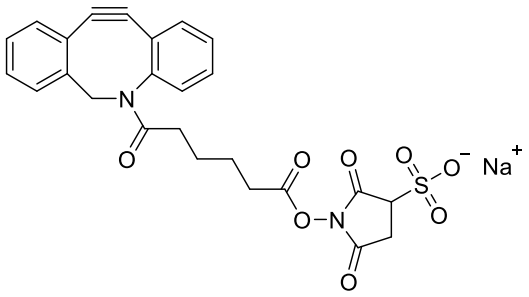

DBCO-sulfo-NHS ester

Figure 3.29 Structures of the dibenzylcyclootynes discussed in Section 3.5.6. The DBCO-sulfo-NHS ester is water soluble, making it compatible with DNA binding experiments.

Table 3.3 Sample contents of the PAGE gel run to investigate whether DBCO-sulfo-N-hydroxysuccinimidyl ester reacts with $Fe_2L^A{}_3Cl_4$ and $Fe_2L^B{}_3Cl_4$ in the presence of 3WJ oligonucleotides.

Sample	Contents
1	S1, S2, S3 (all 0.4 μM)
2	S1, S2, S3 (all 0.4 μM); $Fe_2L_3Cl_4$ (0.8 μM)
3	S1, S2, S3 (all 0.4 μM); $Fe_2L_3Cl_4$ (0.8 μM); cyclooctyne (24 μM)
4	S1, S2, S3 (all 0.4 μM); $Fe_2L_3Cl_4$ (0.8 μM); cyclooctyne (100 μM)
5	S1, S2, S3 (all 0.4 μM); $Fe_2L^A{}_3Cl_4$ (0.8 μM)
6	S1, S2, S3 (all 0.4 μM); $Fe_2L^A{}_3Cl_4$ (0.8 μM); cyclooctyne (24 μM)
7	S1, S2, S3 (all 0.4 μM); $Fe_2L^A{}_3Cl_4$ (0.8 μM); cyclooctyne (100 μM)
8	S1, S2, S3 (all 0.4 μM); $Fe_2L^B{}_3Cl_4$ (0.8 μM)
9	S1, S2, S3 (all 0.4 μM); $Fe_2L^B{}_3Cl_4$ (0.8 μM); cyclooctyne (24 μM)
10	S1, S2, S3 (all 0.4 μM); $Fe_2L^B{}_3Cl_4$ (0.8 μM); cyclooctyne (100 μM)
11	S1, S2, S3 (all 0.4 μM); cyclooctyne (24 μM)
12	S1, S2, S3 (all 0.4 μM); cyclooctyne (100 μM)

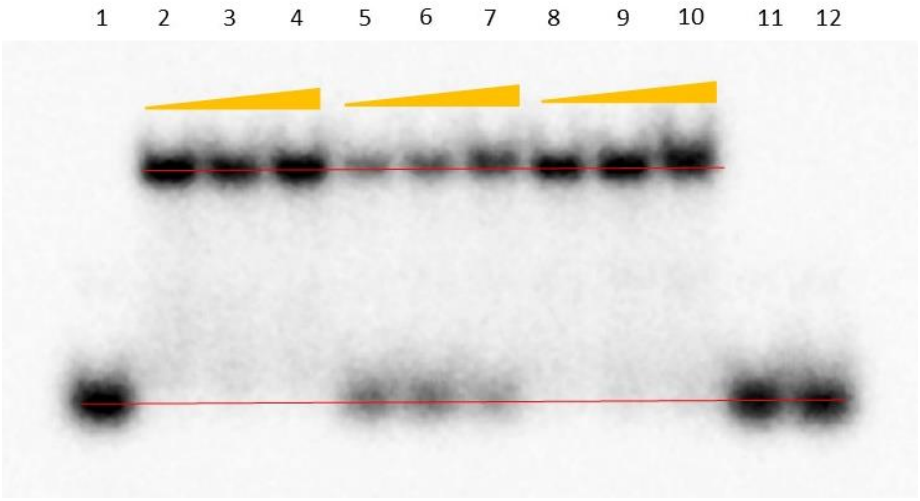

Figure 3.30 Radiogram of gel run to investigate the binding of DBCO-sulfo-N-hydroxysuccinimidyl ester with $Fe_2L^A{}_3Cl_4$ and $Fe_2L^B{}_3Cl_4$. The gold wedges represent increasing concentrations of the cyclooctyne.

3.6 Conclusions and further work

Two novel iron cylinders functionalised with azide groups, $Fe_2L^A{}_3Cl_4$ and $Fe_2L^B{}_3Cl_4$, have been synthesised and their DNA binding properties have been investigated. These two cylinders differ in the number of atoms that connect the azide group to the 5-positon of the pyridyl rings of the ligands, with $Fe_2L^A{}_3Cl_4$ having an azide group connected to the pyridyl ring by a single CH_2 and $Fe_2L^B{}_3Cl_4$ connecting the azide with OCH_2CH_2. Their binding to dsDNA was investigated by a combination of circular and linear dichroism spectroscopy. Both investigations involved titrating increasing concentrations of each cylinder to a constant concentration of ctDNA, while any resultant differences in the characteristic CD and LD spectra of ctDNA were observed. These differences were measured and directly compared to those observed when the same titrations were performed with the original iron cylinder, $Fe_2L_3Cl_4$. While similar changes to the spectra were observed during the titrations, both of the azide cylinders produced less of a change than $Fe_2L_3Cl_4$, with $Fe_2L^A{}_3Cl_4$ showing the least. These observations may be indicative of a weaker binding interaction, however this cannot be said with certainty without further experiments to probe changes in the dsDNA's behaviour, such as UV-melting and viscosity measurements. A series of PAGE experiments were performed where the cylinders were incubated with three short oligonucleotides of sequences that allow formation of a 3WJ. An approximation of the percentage of DNA that

formed 3WJs was measured for each of the cylinders, and no differences between the 3WJ stabilising abilities of the three cylinders could be observed with concentrations ratios of 1:1 3WJ:cylinder and higher. A difference was observed with 0.5 equivalents of cylinder, but the result with $Fe_2L_3Cl_4$ at this concentration indicates that there may be less of the labelled DNA strand present than calculated. If the concentration of labelled stock is less than calculated, then the overall concentration of available 3WJ in each sample is less than desired. Another PAGE experiment was performed where the cylinders were incubated with a strained cyclooctyne, in the hope that conjugation to the cylinder-3WJ adduct would result in an observed reduction in the electrophoretic mobility of the 3WJ band. A reduction was observed with $Fe_2L^B{}_3Cl_4$ at high cyclooctyne concentrations but not with $Fe_2L^A{}_3Cl_4$. This difference may be due to the different lengths of chain that connect the azide groups to the pyridyl rings of the cylinder ligands. The azide groups of $Fe_2L^A{}_3Cl_4$ may be unavailable to click to the cyclooctyne due to their close vicinity to the 3WJ, while the azide groups of $Fe_2L^B{}_3Cl_4$ may be situated far enough away to allow the click reaction to occur. The key conclusion from this work is that the desirable dsDNA and 3WJ binding exhibited by $Fe_2L_3Cl_4$ is not lost with the incorporation of azide functionalities at the ends of the cylinder. This finding warrants further investigation into their potential to take part in biorthogonal SPAAC reactions.

The work outlined in this chapter sets a foundation for substantial further work. The first step should be the scale up of the syntheses of both azide functionalised cylinders so that further characterisation can be performed, including x-ray crystallography which would require reproducible crystal growing conditions to be found. Crystallography could offer insight into how the azide groups are orientated for each cylinder, and whether the functionalised ligands result in a longer bond length between the ligands and the metal centre compared to $Fe_2L_3Cl_4$. Additional evidence that cyclooctyne compounds click to the azide functionalised cylinders is required. Ideally, evidence would be obtained by analysis of ^{1}H NMR spectroscopy of the clicked complex, along with observation of the $[M]^{4+}$ peak by mass spectrometry. There are two hurdles to obtaining this evidence. Firstly, the aromatic ring proton peaks of DBCO-amine analogues tend to overlap those of the cylinders on ^{1}H NMR spectra, which does not lend itself to confident structural determination. Secondly, the high cost of buying these reagents commercially is a barrier to reaction repetition, which may be required before optimised mass spectrometry methods can be found. A model cyclooctyne could be synthesised and used

instead, which would overcome both hurdles. Scheme 3.5 highlights a three-step route to a carboxylic acid functionalised cyclooctyne, used in a previously reported bioconjugation procedure.[32] This model cyclooctyne can be sufficiently purified by SiO_2 column chromatography, and the acid functionality offers the possibility of attaching other functionalities through amide coupling reactions prior to clicking it onto an azide cylinder.

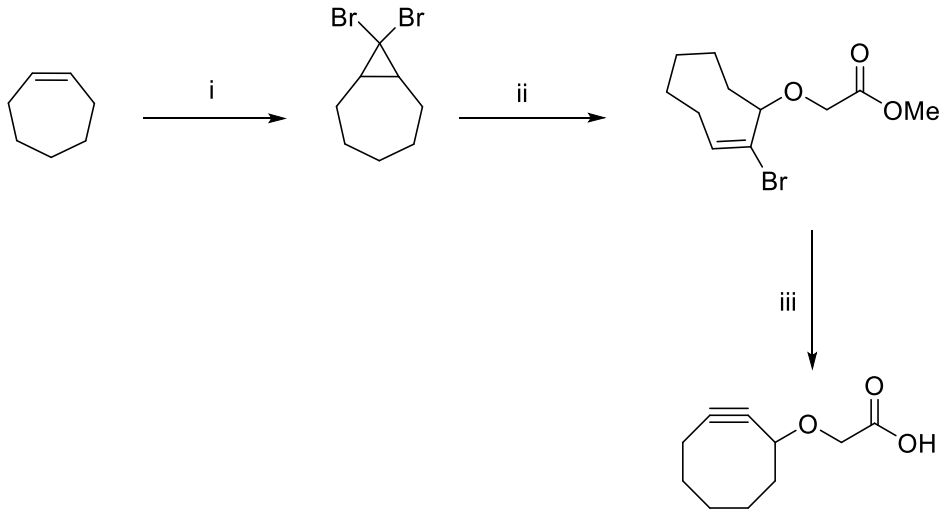

Scheme 3.5 Proposed synthesis of a model cyclooctyne, as used in reference 32. Reported conditions: (i) $CHBr_3$, KO^tBu, pentane, Ar, -10 ^oC, overnight; (ii) $AgClO_4$, methyl glycolate, toluene, RT, 1.5 h; (iii) NaOMe, DMSO, RT, overnight.

If this model cyclooctyne was mixed in methanol with either $Fe_2L^A{}_3Cl_4$ or $Fe_2L^B{}_3Cl_4$, then any unreacted cyclooctyne could be separated from the product by precipitating the resultant complexes out of solution. Precipitation could be achieved by exchanging the anion for PF_6^-, as was done during the synthesis of $Fe_2L_3Cl_4$. The precipitated PF_6 cylinder could then be washed thoroughly with methanol and analysed. The ^1H NMR spectrum would likely be complex in the CH_2 region due to the proton resonances of the cyclooctyne ring, however those of the CH_2 α to the carbonyl should be of higher shift than the others. This would allow determination of how many cyclooctynes, on average, had clicked to the cylinder through comparison of the integrations of this peak and that of the cylinder's imine protons.

Once sufficient evidence of cyclooctynes clicking onto azide cylinders has been obtained, there are two longer term goals to pursue. The first involves using a cyclooctyne-dye to add fluorescent moieties onto the azide cylinders. This would then allow the movement of the cylinder to be monitored in cellular models using a fluorescent microscope. It would be interesting to use this technique to investigate the cellular uptake of cells in real time, rather than relying on time consuming destructive techniques such as inductively-coupled-plasma mass spectrometry (ICP-MS), which has been used to measure metal content in cells by the group previously.[33] The second goal would be to design a system where the SPAAC reaction could occur *in situ* within cells. Again, cyclooctyne analogues attached to fluorescent moieties could be used. Such an experiment could pre-treat the cells with cyclooctyne-dye before incubating with azide cylinder. Hopefully, once the azide cylinder was taken up, it would react with the cyclooctyne-dye and fluorescence would be observed primarily at the nucleus due to the cylinder binding to nucleic DNA. Ideally this would be compared to a control where the cylinder is absent, which would show a different accumulation of fluorescence. This would indicate that the cyclooctyne-dye and the azide cylinder have reacted together intracellularly. Such an experiment relies on the cyclooctyne-dye demonstrating good cellular uptake, which may exclude DBCO analogues which have thus far only been used to image cell membranes.[34–36] However, there have been reports of other cyclooctyne analogues demonstrating good cellular uptake,[7,10,37] although some require long syntheses. Both goals offer up exciting possibilities to further probe the behaviour of cylinders within living systems.

3.7 References

1 J. Norman, PhD Thesis, University of Birmingham, 2012.

2 J. White, PhD Thesis, University of Birmingham, 2016.

3 L. J. Childs, J. Malina, B. E. Rolfsnes, M. Pascu, M. L. Prieto, M. L. Broome, P. M. Rodger, E. Sletten, V. Moreno, A. Rodger and M. J. Hannon, *Chem. Eur. J.*, 2006, **12**, 4919–4927.

4 D. C. Kennedy, C. S. McKay, M. C. B. Legault, D. C. Danielson, J. A. Blake, A. F. Pegoraro, A. Stolow, Z. Mester and J. P. Pezacki, *J. Am. Chem. Soc.*, 2011, **133**, 17993–18001.

5 P. V Chang, J. A. Prescher, E. M. Sletten, J. M. Baskin, I. A. Miller, N. J. Agard, A. Lo and C. R. Bertozzi, *Proc. Natl. Acad. Sci.*, 2010, **107**, 1821 LP – 1826.

6 R. van Geel, G. J. M. Pruijn, F. L. van Delft and W. C. Boelens, *Bioconjug. Chem.*, 2012, **23**, 392–398.

7 J.-J. Shie, Y.-C. Liu, J.-C. Hsiao, J.-M. Fang and C.-H. Wong, *Chem. Commun.*, 2017, **53**, 1490–1493.

8 K. E. Beatty, J. D. Fisk, B. P. Smart, Y. Y. Lu, J. Szychowski, M. J. Hangauer, J. M. Baskin, C. R. Bertozzi and D. A. Tirrell, *ChemBioChem*, 2010, **11**, 2092–2095.

9 K. E. Beatty, J. Szychowski, J. D. Fisk and D. A. Tirrell, *ChemBioChem*, 2011, **12**, 2137–2139.

10 S. H. Alamudi, D. Su, K. J. Lee, J. Y. Lee, J. L. Belmonte-Vázquez, H.-S. Park, E. Peña-Cabrera and Y.-T. Chang, *Chem. Sci.*, 2018, **9**, 2376–2383.

11 M. J. Hannon, C. L. Painting, A. Jackson, J. Hamblin and W. Errington, *Chem. Commun.*, 1997, 1807–1808.

12 A. C. Hotze, N. J. Hodges, R. E. Hayden, C. Sanchez-Cano, C. Paines, N. Male, M. K. Tse, C. M. Bunce, J. K. Chipman and M. J. Hannon, *Chem Biol*, 2008, **15**, 1258–1267.

13 A. Oleksi, A. G. Blanco, R. Boer, I. Usón, J. Aymamí, A. Rodger, M. J. Hannon and M. Coll, *Angew. Chemie Int. Ed.*, 2006, **45**, 1227–1231.

14 M. van den Heuvel, T. A. van den Berg, R. M. Kellogg, C. T. Choma and B. L. Feringa, *J. Org. Chem.*, 2004, **69**, 250–262.

15 J. J. Li, *Name Reactions: A Collection of Detailed Reaction Mechanisms*, Springer-Verlag, Berlin, Second., 2003.

16 R. P. Feynman, R. B. Leighton and M. L. Sands, *The Feynman Lectures on Physics, Volume 1*, Pearson, London, Definitive., 2006.

17 A. Rodger and B. Norden, *Circular Dichroism and Linear Dichroism*, Oxford University Press, Oxford, 1997.

18 I. Warnke and F. Furche, *Wiley Interdiscip. Rev. Comput. Mol. Sci.*, 2012, **2**, 150–166.

Figure 3.9 reproduced with permission. Copyright 2011 John Wiley & Sons, Ltd.

19 J. Kypr, I. Kejnovská, D. Renčiuk and M. Vorlíčková, *Nucleic Acids Res.*, 2009, **37**, 1713–1725.

20 A. Kellett, N. P. Farrell, V. McKee, Z. Molphy and C. Slator, *Chem. Soc. Rev.*, 2019, **48**, 971–988.

21 M. J. Hannon, I. Meistermann, C. J. Isaac, C. Blomme, J. R. Aldrich-Wright and A. Rodger, *Chem. Commun.*, 2001, 1078–1079.

Figure 3.11 reproduced with permission of Royal Society of Chemistry from Paper: a cheap yet effective chiral stationary phase for chromatographic resolution of metallo-supramolecular helicates, M. J. Hannon, I. Meistermann, C. J. Isaac, C. Blomme, J. R. Aldrich-Wright *Chemical Communications*, 2001; permission conveyed through Copyright Clearance Center, Inc.

22 T. Šmidlehner, I. Piantanida and G. Pescitelli, *Beilstein J. Org. Chem.*, 2018, **14**, 84–105.

23 M. Hannon, I. Meistermann, C. J. Isaac, A. Rodger, V. Moreno, M. J. Prieto, E. Sletten and E. Moldrheim, *Angew. Chemie - Int. Ed.*, 2001, **86**, 879–884.

24 L. Cardo and M. J. Hannon, *Inorganica Chim. Acta*, 2009, **362**, 784–792.

25 I. Meistermann, V. Moreno, M. J. Prieto, E. Moldrheim, E. Sletten, S. Khalid, P. M. Rodger, J. C. Peberdy, C. J. Isaac, A. Rodger and M. J. Hannon, *Proc. Natl. Acad. Sci.*, 2002, **99**, 5069–5074.

26 R. Westermeier, *Electrophoresis in Practice : A Guide to Methods and Applications of DNA and Protein Separations*, John Wiley & Sons, Incorporated, Weinheim, Germany, Fifth., 2016.

27 A. Drabik, A. Bodzoń-Kułakowska and J. Silberring, in *Proteomic Profiling and Analytical Chemistry*, eds. P. Ciborowski and J. B. T.-P. P. and A. C. (Second E. Silberring, Elsevier, Boston, Second Ed., 2016, pp. 115–143.

Figure 3.22 reprinted from *Proteomic Profiling and Analytical Chemistry*, **2nd edition**, A. Drabik, A. Bodzoń-Kułakowska, J. Silberring, Gel Electrophoresis, pages 115-143, Copyright (2016), with permission from Elsevier.

28 J. Malina, M. J. Hannon and V. Brabec, *Chem. Eur. J.*, 2007, **13**, 3871–3877.

29 L. Cardo, V. Sadovnikova, S. Phongtongpasuk, N. J. Hodges and M. J. Hannon, *Chem. Commun.*, 2011, **47**, 6575–6577.

30 J. L. Kadrmas, A. J. Ravin and N. B. Leontis, *Nucleic Acids Res.*, 1995, **23**, 2212–2222.

31 M. O. Fenley, G. S. Manning, N. L. Marky and W. K. Olson, *Biophys. Chem.*, 1998, **74**, 135–152.

32 A. Bernardin, A. Cazet, L. Guyon, P. Delannoy, F. Vinet, D. Bonnaffé and I. Texier, *Bioconjug. Chem.*, 2010, **21**, 583–588.

33 L. Cardo, I. Nawroth, P. J. Cail, J. A. McKeating and M. J. Hannon, *Sci. Rep.*, 2018, **8**, 13342.

34 S. T. Laughlin, J. M. Baskin, S. L. Amacher and C. R. Bertozzi, *Science (80-.).*, 2008, **320**, 664 LP – 667.

35 J. C. Jewett, E. M. Sletten and C. R. Bertozzi, *J. Am. Chem. Soc.*, 2010, **132**, 3688–3690.

36 L. Collenburg, T. Walter, A. Burgert, N. Müller, J. Seibel, L. Japtok, B. Kleuser, M. Sauer and S. Schneider-Schaulies, *J. Immunol.*, 2016, **196**, 3951 LP – 3962.

37 S. J. Siegl, J. Galeta, R. Dzijak, M. Dračínský and M. Vrabel, *Chempluschem*, 2019, **84**, 493–497.

Chapter 4:

Summary and outlook

Investigations into the DNA binding properties of metallosupramolecular helicate cylinders has been a key focus of research in the Hannon group for over two decades. These cylinders have the general formula $M_2L_3X_4$, where M is a metal, L is a diimine ligand, and X is a counterion. The work presented in this thesis has been focused on the development and investigation of synthetic analogues of $Fe_2L_3Cl_4$, which is the most studied of Hannon's cylinders due to the relative ease of its synthesis and its aqueous solubility. Prior work in the group has shown that $Fe_2L_3Cl_4$ exhibits an affinity for DNA three-way junctions (3WJs), which are transiently formed during cell replication. As cancer is associated with uncontrolled cell replication, $Fe_2L_3Cl_4$ therefore has potential for use as an anticancer agent. However, $Fe_2L_3Cl_4$ shows no selectivity between cancer cells over healthy cells, a common challenge across the field of small molecule anti-cancer agents. Prior efforts to introduce some sort of selectivity have included functionalising the cylinder ligands with receptor targeting moieties, and incorporating links to attach the cylinder to nanoparticle surfaces. Such strategies have faced hurdles relating to a loss of solubility and decreased cylinder stability. These issues largely arise from the fact that the ligands were functionalised prior to formation of the helicate complex. This synthetic approach adds three functionalities at each end of the cylinder, making the resultant cylinder less stable due to steric clash and unfavourable electrostatic effects. These additional functionalities also tended to be relatively lipophilic, which resulted in these cylinders having low aqueous solubility. The work presented in this thesis aims to address these challenges, marking notable progress in two areas of work that have been unexplored by the Hannon group until now. The first aimed to develop a "capped" cylinder, while the second involved the development of functionalised cylinders that could undergo post-assembly modifications.

Efforts to cap the cylinder structure, presented in Chapter 2, aimed to do so through use of a quaternary carbon based "tripod" moiety. The aim was to connect the three pyridyl rings at the end of the cylinder to the "arms" of the tripod, which themselves would attach to a functional head group. This strategy would effectively replace three sites of functionalisation

with just one, minimising any detrimental steric and electrostatic effects that might be introduced with the attachment of a desired functionality. It was hoped that connecting the ends of the cylinder would further improve the cylinder's stability by effectively holding the ligands in place. Following the establishment of a reliable synthetic route to a capped cylinder, the next aim would be to conjugate useful functionality at the head group. Examples of useful functionality in this context could include a fluorescent tag, allowing the cylinder to be tracked *in vivo*, or a moiety that would target receptors commonly over-expressed by cancer cells. The bulk of the work discussed in Chapter 2 was focussed on identifying a suitable linker to connect the tripod to the pyridyl rings of the cylinder ligands. This work proved synthetically challenging, as conjugation reactions were required at three sites on the same molecule. Amide coupling, copper catalysed alkyne-azide cycloadditions, and Mitsunobu methodologies were trialled but all faced problems with low yield and a lack of reproducibility. A trialdehyde capping moiety (**33**) was successfully synthesised and isolated with desired purity through a Williamson-type ether synthesis. Trial experiments to react **33** with iron(II) chloride and 4,4'-methylenedianiline were performed in the hope that a cylinder capped at both ends would self-assemble under these conditions, however an insoluble precipitate (likely an organometallic polymer) formed immediately. This work should be continued by trialling this last step in high dilution concentrations, which may favour the formation of the discrete complex rather than the polymeric species. The synthetic strategy could be adapted to cap the cylinder at only one end which, in combination with high dilution conditions, could reduce the amount of polymeric species that forms. Such an adaption could react trialdehyde **33** with three equivalents of azo "half-ligand", using one equivalent of metal as a template to bring the three arms of **33** together (as was described in section 2.7). While capping the cylinder remains a huge synthetic challenge, the possible benefits that a capped cylinder could bring justify further work. The work presented in Chapter 2 offers a solid foundation for continued efforts to tackle this challenge. If solved, a synthetic route to a capped cylinder brings the possibility of producing a vast range of cylinders that are novel, smart functionalised, and stable in solution.

The work presented in Chapter 3 aimed to produce functionalised cylinders that could undergo post-assembly modifications. Two novel cylinders functionalised with azides at each end of the cylinder were produced, which were intended to undergo strain promoted alkyne-

azide cycloaddition (SPAAC) click reactions with strained cyclooctynes. $Fe_2L^A{}_3Cl_4$ and $Fe_2L^B{}_3Cl_4$ vary in the number of atoms which connect the azide groups to the pyridyl rings at each end of the cylinder. Reproducible syntheses were identified and the novel cylinders were characterised by NMR, ESI-MS, and UV-Vis spectroscopy. The DNA binding behaviour of $Fe_2L^A{}_3Cl_4$ and $Fe_2L^B{}_3Cl_4$ was then investigated, to check whether the inclusion of the azide functionalities had affected the desirable DNA binding properties of the original $Fe_2L_3Cl_4$ cylinder. Circular dichroism and linear dichroism titrations were performed. These titrations involved adding an increasing amount of cylinder to a solution of double stranded DNA, and observing the resultant effect on the DNA's characteristic spectrum. The same experiments were conducted with $Fe_2L_3Cl_4$ and the results were compared. It was observed that both azide cylinders behaved in a similar manner to the original cylinder. A series of polyacrylamide gel electrophoresis (PAGE) experiments were then performed to investigate the binding behaviour of $Fe_2L^A{}_3Cl_4$ and $Fe_2L^B{}_3Cl_4$ to a DNA 3WJ. It was observed that the novel azide cylinders still retained the affinity for DNA 3WJs exhibited by $Fe_2L_3Cl_4$. An initial experiment was then performed to investigate whether the azide functionalised cylinders could undergo a SPAAC reaction in the presence of a DNA 3WJ. This PAGE experiment incubated each cylinder with the 3WJ and a varying concentration of cyclooctyne, prior to loading onto the gel. A slight decrease in the electrophoretic mobility of the 3WJ band was observed with $Fe_2L^B{}_3Cl_4$ and high concentrations of cyclooctyne, however this result was not conclusive. In order to move this work forward, more evidence that the novel azide cylinders undergo SPAAC reactions is needed. One of the main hurdles with obtaining more evidence is the high cost of commercially available strained cyclooctynes. Section 3.6 outlines a relatively short synthetic scheme which could be used to produce an alternative cyclooctyne. Once sufficient material had been produced, the SPAAC reaction could be carried out on a scale that is large enough to allow a counterion exchange to be performed. This counterion exchange would cause the resultant complex to precipitate out of the reaction solvent and, once isolated, the structure could be investigated using NMR and MS techniques. Hopefully, this analysis would show that the cylinder had conjugated to the cyclooctyne. If this was the case, this would be the first example of a Hannon cylinder being functionalised after assembly of the complex. The SPAAC reaction is considered biorthogonal, meaning that such reactions could take place in cellular environments. Coordinating useful functionalities such as fluorescent tags to the cylinder *in vivo* may offer an unprecedented insight into the behaviour of these cylinders once

inside a cell. These potential advancements justify further work being done to investigate these novel azide cylinders in more detail.

Chapter 5:

Experimental

5.1 General information

Solvents and commercially available reagents were purchased from Sigma-Aldrich, VWR, Fisher Scientific and Arcos Organics and were used without further purification. Deuterated NMR solvents were purchased from Goss Scientific or Sigma Aldrich. Deionised water was obtained using an Elga Option 3 water purifier.

NMR spectra were recorded using Brüker AVIII300 (300 MHz) and AVIII400 (400 MHz) spectrometers. Chemical shifts (δ) are quoted in parts per million (ppm), using residual protonated solvent as an internal standard. Peak assignments have been made based on chemical shift and coupling constants using ^{1}H COSY and ^{1}H-^{13}C HSQC experiments where necessary. Quaternary carbons and those not appearing on a dept 45 spectrum have been assigned as "C_q". Multiplet abbreviations used are: s (singlet), d (doublet), dd (doublet of doublets), t (triplet), q (quartet), and m (multiplet). Coupling constants (*J*) are quoted to the nearest 0.1 Hz. Electrospray ionisation (ESI) mass spectrometry was performed using a Waters Xevo G2-XS TOF mass spectrometer and electron ionisation (EI) mass spectrometry was performed using a Waters GCT TOF mass spectrometer, with *m/z* values reported in Daltons. Where isotopic distributions are present, the *m/z* value of the highest intensity peak has been quoted. MS analysis was performed by staff of the Analytical Facility in the School of Chemistry, University of Birmingham. UV-Vis measurements were made using a Varian Cary 5000 UV-Vis-NIR spectrophotometer using quartz cuvettes with a 1 cm path length. IR spectra were recorded on a Agilent 670 FT-IR spectrometer using 32 scans for each measurement.

Thin layer chromatography was performed using pre-coated aluminium sheets (Silica Gel 60 F_{254}). Spots were visualised under a 254 nm UV lamp, or by use of a TLC stain. Phosphomolybdic acid stain was made by dissolving 10 g phosphomolybdic acid in 100 mL ethanol. $KMnO_4$ stain was made by dissolving 1.5 g of $KMnO_4$, 10 g of K_2CO_3, and 1.25 mL of 10% w/v NaOH in 200 mL deionised H_2O. Ninhydrin stain was made by dissolving 1.5 g

ninhydrin in 100mL of n-butanol and then adding 3.0 mL of acetic acid. Retention factors (R_f) are quoted with the solvent system used. Flash column chromatography was performed using silica gel 60A (particle size 40 – 63 μm) purchased from Fisher Scientific, using the solvent systems stated.

Reverse phase high pressure liquid chromatography (HPLC) analysis was performed using a Shimadzu LC20 Prominence system. Preparative HPLC was performed using a Dionex UlitMate 3000 pump and variable wavelength detector. Columns used were purchased from Phenomenex, with a 250 x 4.6 mm column used for analytical scale (flow rate = 1mL/min) and a 250 x 21.2 mm column used for preparative scale (flow rate = 15 mL/min). HPLC gradient grade solvents were used, purchased from Fisher Scientific and degassed with helium prior to use. UV detection was monitored at 210 nm and 265 nm for analytical HPLC, and 265 nm for preparative HPLC.

Where experimental procedures have been adapted from published sources, these have been referenced in the relevant chapter.

5.2 Experimental procedures from Chapter 2

Procedures used to synthesise the compounds described in Chapter 2 are presented below, in the order that they appear in the text. Procedures for unsuccessful syntheses have also been included, but the target compounds have not been numbered to distinguish them from those that were successfully isolated. Procedures for compounds 1-3 were followed directly from previous work in the group (L. Cardo and M. Hannon, *Inorganica. Chim. Acta*, 2009, **362**, 784-792).

Methyl 6-formylnicotinate (1)

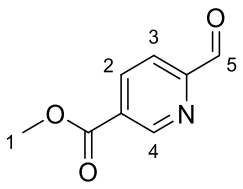

Methyl 6-methylnicotinate (3.0 g, 19.8 mmol) was dissolved in DMSO (5 mL). Iodine (5.04 g, 19.8 mmol) was dissolved in DMSO (5 mL) in a separate flask. The solutions were then mixed and added dropwise over 10 minutes to DMSO (30 mL) that had been heated to 130 °C. After addition, the resultant reaction mixture was slowly heated to 160 °C and stirred for 1 h. The reaction mixture was then cooled to room temperature, and neutralised by addition of 60 mL of sat. Na_2CO_3 (aq). The product was extracted into diethyl ether (75 mL), before deionised H_2O (100 mL) and brine (50 mL) were added to aid layer separation. The product was re-extracted from the aqueous layer using diethyl ether (5 x 50 mL). The organics were then combined, dried over $MgSO_4$, and concentrated under reduced pressure to yield an orange solid. This was purified by SiO_2 column chromatography using 20 – 30% EtOAc in hexane as eluent. The product containing fractions were combined and concentrated under reduced pressure to give 0.91 g (28%) of the title compound as a pale yellow solid.

TLC (25% EtOAc in hexane): R_f 0.36

^{1}H NMR (300 MHz, $CDCl_3$): δ 10.15 (1H, d, *J* = 0.9 Hz, H_5), 9.37 (1H, dd, *J* = 2.1, 0.9 Hz, H_4), 8.48 (1H, ddd, *J* = 8.1, 2.0, 0.9 Hz, H_2), 8.04 (1H, dd, *J* = 8.1, 0.9 Hz, H_3), 4.01 (3H, s, H_1).

^{13}C NMR (400 MHz, $CDCl_3$): δ 192.5 (C_7), 164.7 (C_q), 154.9 (C_q), 151.1 (C_4), 138.3 (C_2), 129.2 (C_q), 121.0 (C_3), 52.8 (C_1)

Mass spectrum (+ve ESI): *m/z* 166 $[M+H]^+$

Methyl 6-(dimethoxymethyl)nicotinate (2)

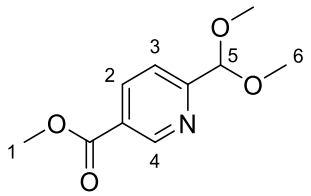

To a flask of **1** (0.88g, 5.33 mmol) was added trimethylorthoformate (21.0 mL, 191 mmol). The mixture was heated to 50 °C before addition of formic acid (2.8 mL) and 5 drops of 95% H_2SO_4 (aq). The reaction mixture was stirred for 10 mins at 50 °C. The reaction was allowed to cool to room temperature and stirred for 17 h. Deionised H_2O (30 mL) was added before

the product was extracted into diethyl ether (3 x 30 mL). The organics were combined, washed with brine (30 mL), dried over $MgSO_4$ and concentrated under reduced pressure to yield a yellow oil. Purification by SiO_2 column chromatography, using 20 – 25% EtOAc in hexane as eluent, yielded 0.85 g (77%) of the title compound as a pale yellow oil.

TLC (25% EtOAc in hexane): R_f 0.38

^{1}H NMR (300 MHz, $CDCl_3$): δ 9.18 (1H, dt, *J* = 2.0, 0.9 Hz, H_4), 8.35 – 8.28 (1H, m, H_2), 7.63 (d, *J* = 8.2 Hz, H_3), 5.41 (1H, s, H_5), 3.92 (3H, d, *J* = 0.8 Hz, H_1), 3.38 (6H, d, *J* = 0.8 Hz, H_6)

Mass spectrum (EI +ve): *m/z* 234.1 $[M+Na]^+$

6-(dimethoxymethyl)nicotinic acid (3)

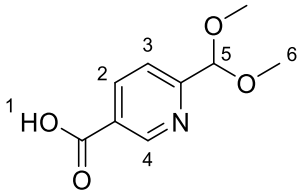

2 (0.85 g, 4 mmol) was dissolved in methanol (10 mL) and 10 mL of 1M NaOH (aq) was added. The reaction was stirred at room temperature for 17 h. The reaction mixture was then acidified by addition of 20 mL of 1M HCl (aq) and the product extracted into EtOAc (3 x 30 mL). The organics were combined, dried over $MgSO_4$, and concentrated under reduced pressure to give 0.49 g (62%) of the title compound as a cream solid.

^{1}H NMR (300 MHz, $CDCl_3$): δ 9.30 (1H, dd, *J* = 2.1, 0.9 Hz, H_2), 8.41 (1H, dd, *J* = 8.2, 2.2 Hz, H_4), 7.71 (1H, d, *J* = 8.6 Hz, H_5), 5.47 (1H, s, H_7), 3.44 (6H, s, H_8)

^{13}C NMR (400 MHz, $CDCl_3$) δ 168.9 (C_q), 161.3 (C_q), 150.3 (C_4), 138.9 (C_2), 126.0 (C_q), 121.4 (C_3), 102.9 (C_5), 53.8 (C_6).

Mass spectrum (ESI -ve): *m/z* 196.2 $[M-H]^-$

Dimethyl 4-(3-methoxy-3-oxopropyl)-4-nitroheptanedioate (4)

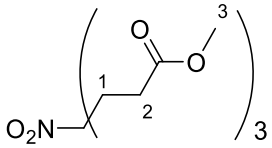

Benzyltrimethylammonium hydroxide (0.5 mL, 2.8 mmol) was added to a mixture of nitromethane (0.51 mL, 9.4 mmol) and DME (10 mL). This mixture was heated to 70 ^oC and methyl acrylate (2.8 mL, 31 mmol) added dropwise over 30 min. The mixture was stirred at 70 ^oC for 17 h. Additional methyl acrylate (0.17 mL, 1.9 mmol) and benzyltrimethylammonium hydroxide (0.1 mL, 0.56 mmol) were added to further promote formation of the triester. After stirring at room temperature for 8 h, the solvent was removed under reduced pressure to yield a brown oil. The residue was suspended in $CHCl_3$ (15 mL) and washed with 10 mL of 0.5 M HCl (aq), followed by brine (3 x 10 mL) before being dried over $MgSO_4$. Concentration under reduced pressure yielded a yellow oil, which was purified by SiO_2 column chromatography using 25% EtOAc in hexane as eluent. The product containing fractions were combined and concentrated under reduced pressure to give 1.01 g (32%) of the tile compound as a pale yellow oil.

TLC (25% EtOAc in Hexane): R_f 0.2. Phosphomolybdic acid stain used to visualise.

^1H NMR (300 MHz, $CDCl_3$) δ 3.68 (9H, s, H_3), 2.36 – 2.20 (12H, m, $H_{1/2}$)

^{13}C NMR (400 MHz, $CDCl_3$) δ 172.2 (C_q), 91.8 (C_q), 52.1 (C_3), 30.2 (C_2), 28.5 (C_1)

Mass spectrum (ESI +ve): *m/z* 342 $[M+Na]^+$, *m/z* 295.1 $[M-NO_2+Na]^+$, *m/z* 273 $[M-NO_2+H]^+$

4-(2-carboxyethyl)-4-nitroheptanedioic acid (5)

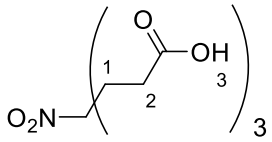

Dimethyl 4-(3-methoxy-3-oxopropyl)-4-nitroheptanedioate (**4**, 0.82 g, 2.46 mmol) was dissolved in methanol (10 mL) and 10 mL of 1M NaOH (aq) was added. The reaction mixture was left stirring at room temperature for 18 h. Once no more starting material was visible by TLC, the methanol was removed under vacuum and conc. H_2SO_4 (aq) was added until pH 2 was achieved. The resultant white precipitate was collected by vacuum filtration and washed with 20 mL of deionised H_2O chilled to 4 °C. After drying on high vacuum for 5 days, 0.6 g (88%) of the title compound was obtained as a white solid.

^{1}H NMR (300 MHz, DMSO-d_6) δ 12.29 (3H, s, H_3), 2.23 – 2.07 (12H, m, H_{1+2}).

^{13}C NMR (400 MHz, DMSO-d_6) δ 173.26 (C_q), 92.86 (C_q), 29.79 (C_2), 28.24 (C_1).

Mass spectrum (ESI -ve): *m/z* 276 $[M-H]^-$.

3-(2-aminoethyl)-3-nitropentane-1,5-diamine triamine trishydrochloride (6)

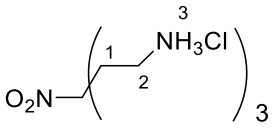

To 4-(2-carboxyethyl)-4-nitroheptanedioic acid (**5**, 2.83 g, 9.72 mmol) was added thionyl chloride (20 mL, 274 mmol) in a round bottomed flask. With vigorous stirring, the reaction was heated to 70 °C and stirred under reflux for 3 h. After cooling to room temperature, excess thionyl chloride was removed by vacuum distillation, leaving a brown viscous liquid

which solidified overnight under atmosphere. The flask was sealed and purged with N_2. The crude acyl chloride was then dissolved in anhydrous 1,4-dioxane (30 mL) before being transferred to a multi-necked flask which was put under Ar using a Schlenk line. Trimethylsilylazide (4.2 mL, 31.8 mmol) was added dropwise with stirring. The reaction mixture was then heated to 80 °C for 30 min, then cooled to 45 °C. Acetone (20 mL) followed by 8 mL of 32% conc. HCl (aq) was added and the reaction was stirred at 45 °C for 1 h. 12 mg of brown precipitate was isolated by vacuum filtration. The filtrate was poured into cold acetone (200 mL) but no further precipitate was observed. The solvent was removed in vacuo, leaving a brown solid which was partitioned between EtOAc (50 mL) and 2M NaOH (50 mL). The aqueous layer was re-extracted with EtOAc (2 x 50 mL) and the combined organic layers dried over $MgSO_4$. Concentration under vacuum did not yield any observable material. Analysis was performed on 12 mg (0.4%) of brown precipitate initially isolated.

^{1}H NMR (300 MHz, DMSO-d_6) δ 8.15 – 7.95 (br s, 9H, H_3), 2.88 – 2.70 (m, 6H, H_2), 2.32 – 2.16 (m, 6H, H_3)

Mass spectrum (ESI +ve): *m/z* 191.1$[M+H]^+$

2-methyl-5-nitropyridine (7)

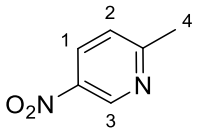

A mixture of sodium (2.53 g, 110 mmol) and diethyl malonate (11.7 mL, 110 mmol) in toluene (40 mL) was heated at 90 °C for 2 h. The temperature was increased to 120 °C and the mixture left stirring at this temperature for 10 min before being allowed to cool to room temperature. 2-chloro-5-nitro-pyridine (10 g, 63 mmol) in toluene (60 mL) was then added. The mixture was heated to 110 °C and stirred under reflux for 1.5 h. After cooling to room temperature, the volatiles were removed under vacuum and 200 mL of 6M HCl (aq) was added to the resultant red solid residue. This suspension was stirred vigorously under reflux (100 °C) for 4 h. After cooling to room temperature, the reaction mixture was left stirring overnight. Spatulas of solid Na_2CO_3 were added sequentially, with vigorous stirring, until a neutral pH

was achieved. The product was extracted into EtOAc (4 x 200 mL) and the combined organics were dried over $MgSO_4$. Concentrating under vacuum yielded a dark red solid, which was purified by silica column chromatography using 30% EtoAC in hexane as eluent. 3.51 g (40%) of the title compound were obtained as a light brown solid.

TLC (30% EtOAc in Hexane): R_f 0.34

^{1}H NMR (300 MHz, $CDCl_3$) δ 9.33 (1H, d, *J* = 2.8 Hz, H_3), 8.37 (1H, dd, *J* = 8.5, 2.7 Hz, H_1), 7.35 (1H, d, *J* = 8.6 Hz, H_2), 2.70 (3H, s, H_4)

^{13}C NMR (400 MHz, $CDCl_3$) δ 165.58 (C_q), 144.85 (C_3), 142.64 (C_q), 131.38 (C_1), 123.52 (C_2), 24.96 (C_4).

Mass spectrum (EI +ve): *m/z* 138 $[M]^+$, *m/z* 92 $[M\text{-}NO_2]^+$

5-nitropicolinaldehyde (8)

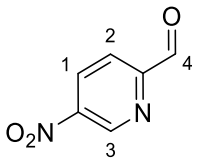

7 (1.5 g, 10.9 mmol) and SeO_2 (1.81 g, 16.4 mmol) were put under an Ar atmosphere in an oven dried, three necked flask equipped with a reflux condenser connected to a mineral oil bubbler. Anhydrous 1,4-dioxane (30 mL) was then added via syringe with stirring, and the reaction mixture slowly heated to 115 ^oC. The reaction was left stirring vigorously under reflux for 18 h. When the reaction appeared complete by TLC, the black selenium precipitate was removed by vacuum filtration. The filtrate was concentrated under vacuum to yield a red solid, which was purified by silica column chromatography using 2.5% MeOH in DCM as eluent. 0.87g (52%) of the title compound was obtained as a tan solid.

TLC (DCM): R_f 0.33

^{1}H NMR (300 MHz, $CDCl_3$) δ 10.18 (1H, d, *J* = 0.9 Hz, H_7), 9.59 (1H, dd, *J* = 2.5, 0.8 Hz, H_6), 8.67 (1H, ddd, *J* = 8.5, 2.4, 0.9 Hz, H_4), 8.16 (1H, dd, *J* = 8.5, 0.7 Hz, H_3)

^{13}C NMR (400 MHz, $CDCl_3$) δ 191.38 (C_4), 159.09 (C_q), 155.82 (C_q), 145.76 (C_3), 132.66 (C_1), 121.90 (C_2).

Mass spectrum (EI +ve): *m/z* 152 $[M]^+$, *m/z* 124 $[M\text{-}CO]^+$, *m/z* 78 $[M\text{-}NO_2\text{-}CO]^+$

2-(1,3-dioxolan-2-yl)-5-nitropyridine (9)

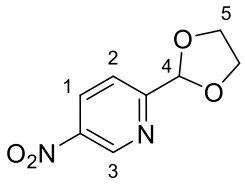

8 (0.8 g, 5.3 mmol) was dissolved in anhydrous toluene (20 mL). p-TsOH·H_2O (25 mg, 0.13 mmol) was added with stirring, followed by ethylene glycol (1.76 mL, 31.6 mmol). The reaction mixture was heated to 120 °C and stirred under reflux for 18 h. 20 mL of sat. $NaHCO_3$ (aq) was then added and the mixture stirred vigorously for 15 min before the layers were separated. The aqueous layer was further extracted with EtOAc (25 mL) and toluene (25 mL). The combined organics were washed with deionised H_2O (20 mL) and brine (20 mL) before being dried over $MgSO_4$. Concentration under vacuum yielded a yellow solid which was purified by silica column chromatography using 25-30% EtOAc in hexane as eluent. 0.86 g (83%) of the title compound was obtained as a white solid.

TLC (30% EtOAc in hexane): R_f 0.24

^{1}H NMR (300 MHz, $CDCl_3$) δ 9.43 (1H, dd, *J* = 2.6, 0.7 Hz, H_3), 8.53 (1H, dd, *J* = 8.6, 2.6 Hz, H_1), 7.76 (1H, dd, *J* = 8.6, 0.7 Hz, H_2), 5.94 (1H, s, H_4), 4.22 – 4.08 (4H, m, H_5).

^{13}C NMR (400 MHz, $CDCl_3$) δ 163.14 (C_q), 144.95 (C_3), 144.42 (C_q), 132.12 (C_1), 121.13 (C_2), 102.69 (C_4), 65.98 (C_5).

Mass spectrum (AP +ve): *m/z* 197 $[M+H]^+$

2-(1,3-dioxolan-2-yl)-5-aminopyridine (10)

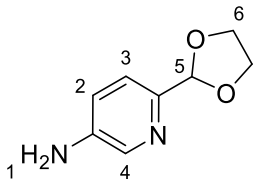

An oven-dried, three necked flask with **9** (0.1 g, 0.5 mmol) was placed under Ar, and 10% Pd/C (10 mg, 10 wt%) added. EtOH (10 mL) was then added, and a hydrogen atmosphere established using a balloon of H_2 (g). The reaction was left stirring under H_2 for 20 h and then the reaction mixture was filtered through Celite. The filtrate was concentrated under vacuum, yielding 94 mg (113%) of the title compound as a yellow oil. This material was used without any further purification.

^{1}H NMR (300 MHz, DMSO-d6) δ 7.84 (dd, *J* = 2.7, 0.7 Hz, 1H, H_4), 7.15 (dd, *J* = 8.4, 0.7 Hz, 1H, H_2), 6.92 (dd, *J* = 8.4, 2.7 Hz, 1H, H_3), 5.51 (s, 1H, H_5), 5.45 (b.s., 2H, D_2O exchangeable, H_5), 4.06 – 3.85 (m, 4H, H_6).

Mass spectrum (+ve EI): *m/z* 166 $[M]^+$, *m/z* 123 $[M\text{-}CH_2CH_2OH]$

Attempted synthesis of N1,N7-bis(6-(1,3-dioxolan-2-yl)pyridin-3-yl)-4-(3-((6-(1,3-dioxolan-2-yl)pyridin-3-yl)amino)-3-oxopropyl)-4-nitroheptanediamide

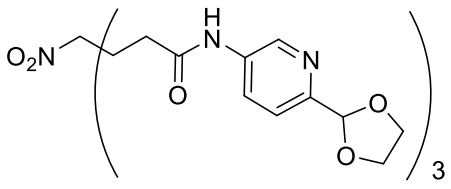

To a round bottomed flask containing **10** (56 mg, 0.34 mmol) was added **5** (25 mg, 0.09 mmol) and HBTU (140 mg, 0.36 mmol). The flask was equipped with a rubber septum and purged with N_2. Anhydrous DMF (3 mL) was then added via syringe, followed by DiPEA (0.13 mL, 0.72

mmol). The reaction was heated to 45 °C and stirred under N_2 for 74 hours. The solvent was then removed under vacuum. 20 mL of sat. $NaHCO_3$ (aq) was added, and extraction attempted with EtOAc (3 x 20 mL). The organics were combined, washed with brine (25 mL), dried over $MgSO_4$ and concentrated to yield a brown oil. TLC of the crude material (10% MeOH in DCM) showed only the starting material. The crude was passed through a SiO_2 column, eluting with 2 – 10% MeOH in DCM. Non-staring material was detected with R_f 0.53 (10% MeOH in DCM) eluting before the pyridyl starting material (R_f 0.36). This was collected and concentrated under vacuum to yield 2 mg of a yellow oil. ^1H NMR appeared complex and inconclusive.

Di-tert-butyl (4-(3-((tert-butoxycarbonyl)amino)propyl)-4-nitroheptane-1,7-diyl)dicarbamate (11)

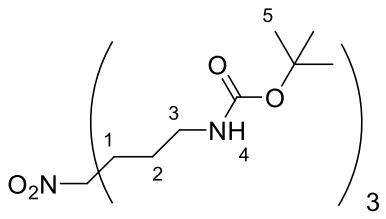

Tris-(2-cyanoethyl)-nitromethane (1.1 g, 5 mmol) was dissolved in anhydrous THF (5 mL) by heating to 50 °C with vigorous stirring. After cooling to room temperature, BH_3·THF (30 mL of 1M solution in THF, 30 mmol) was added dropwise over 20 min and the reaction heated under reflux (72 °C) for 17 h. Excess BH_3 was destroyed by suspending the resultant white precipitate in methanol (20 mL) and adding 4M HCl (aq) until pH 1 was achieved. The resultant mixture was heated at 74 °C for 20 min before neutralising with 10 mL of 6M NaOH (aq). Boc_2O (3.79 mL, 16.5 mmol) was added dropwise with MeOH (10 mL). Et_3N (2.78 mL, 20 mmol) was then added. The reaction mixture was heated to 82 °C and left stirring under reflux for 20 h. After cooling to room temperature, EtOAc (100 mL) and deionised H_2O (50 mL) were added, and the aqueous layer re-extracted with EtOAc (2 x 50 mL). The combined organics were washed with brine (40 mL), dried over $MgSO_4$, and concentrated under vacuum to yield

a pale yellow oil. This was purified by silica column chromatography, using 30 – 50% EtOAc in hexane as eluent, giving 0.67 g (25%) of the title compound as a colourless oil.

TLC (50% EtOAc in hexane): R_f 0.3

^{1}H NMR (300 MHz, $CDCl_3$) δ 4.63 (3H, s, H_4), 3.10 (6H, q, *J* = 6.6 Hz, H_3), 1.94 – 1.84 (6H, m, H_1), 1.43 (33H, m, $H_{2/5}$)

^{13}C NMR (400 MHz, $CDCl_3$): δ 156.0 (C_q), 93.8 (C_q), 79.5 (C_q), 40.2 (C_3), 32.6 (C_1), 28.4 (C_5), 24.3 (C_2)

Mass spectrum (ESI +ve): *m/z* 555 $[M+Na]^+$

4-(3-aminopropyl)-4-nitroheptane-1,7-diamine trishydrochloride (12)

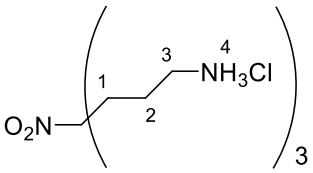

Di-tert-butyl (4-(3-((tert-butoxycarbonyl)amino)propyl)-4-nitroheptane-1,7-diyl)dicarbamate (**12**, 0.54 g, 1.01 mmol) was dissolved in anhydrous 1,4-dioxane (5 mL) and 4M HCl in anhydrous dioxane (5 mL, 20 mmol) was added via syringe. After 2 hours of vigorous stirring at room temperature, the dioxane was removed under vacuum. The resultant white solid was stirred in EtOAc for 30 min before the suspended solid was collected by vacuum filtration. After drying under high vacuum overnight, 0.32 g (92%) of the title compound was obtained as a white solid. This material was used without any further purification.

^{1}H NMR (400 MHz, MeOD-d_4) δ 3.00 (t, *J* = 7.5 Hz, 6H,H_3), 2.13 – 2.03 (m, 6H, H_1), 1.75 – 1.62 (m, 6H, H_2).

^{13}C NMR (400 MHz, MeOD-d_4) δ 192.1 (C_q), 39.0 (C_3), 31.8 (C_1), 21.6 (C_2).

Mass spectrum (ESI +ve): m/z 233.3 $[M+H]^+$, m/z 186.3 $[M-NO_2+H]^+$

N,N'-(4-(3-(6-(dimethoxymethyl)nicotinamido)propyl)-4-nitroheptane-1,7-diyl)bis(6-(dimethoxymethyl)nicotinamide) (13)

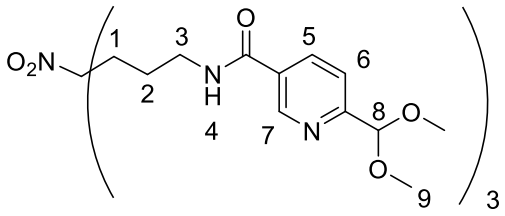

6-(dimethoxymethyl)nicotinic acid (**3**, 133 mg, 0.675 mmol) and CDI (163 mg, 1.01 mmol) were dispensed into a two necked flask equipped with stopcock adapter and rubber septum. An Ar atmosphere was established using a Schlenk line, and 2 mL of anhydrous DMF was added via syringe. This was stirred at room temperature for 3 h, during which time **12** (51 mg, 0.15 mmol) was stirred in Et_3N (0.13 mL 0.9 mmol) and anhydrous DMF (2 mL). The basic solution of **12** was then transferred to the acid/CDI mixture using a 1 mL pipette. An additional 1 mL of anhydrous DMF was used to rinse the amine solution flask, and this was then added to the reaction mixture. The reaction mixture was left stirring for 18 h at room temperature under Ar before the solvent was removed under vacuum. The residual yellow oil was redissolved in 7 mL of MeCN before purification by prep HPLC in 1 mL aliquots (0 – 65% MeCN in H_2O over 26 min, R_t = 19.9 min). MeCN was then removed under vacuum and the resultant aqueous solution freeze dried to yield 70 mg (61%) of the title compound as a white solid. The solid became a colourless oil upon exposure to atmosphere.

^{1}H NMR (400 MHz, $CDCl_3$) δ 9.00 (d, *J* = 2.2 Hz, 3H, H_7), 8.16 (dd, *J* = 8.2, 2.3 Hz, 3H, H_5), 7.61 (d, *J* = 8.2 Hz, 3H, H_6), 6.77 (s, 3H, H_4), 5.39 (s, 3H, H_8), 3.47 (q, *J* = 6.5 Hz, 6H, H_3), 3.39 (s, 18H, H_9), 2.03 – 1.95 (m, 6H, H_1), 1.57 (m, 6H, H_2).

^{13}C NMR (400 MHz, $CDCl_3$) δ 165.9 (C_q), 159.9 (C_q), 147.6 (C_7), 136.0 (C_5), 129.8 (C_q), 121.2 (C_6), 103.3 (C_8), 94.1 (C_q), 53.7 (C_9), 39.7 (C_3), 32.6 (C_1), 23.6 (C_2).

Mass spectrum (ESI +ve): *m/z* 792.4 $[M+Na]^+$

Attempted synthesis of N,N'-(4-(3-(6-formylnicotinamido)propyl)-4-nitroheptane-1,7-diyl)bis(6-formylnicotinamide)

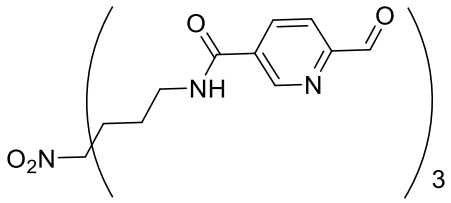

13 (40 mg, 0.06 mmol) was dissolved in 4 mL of anhydrous THF and cooled to 0 °C in an ice bath. 3 mL of 1M HCL (aq) was added dropwise over 10 minutes with vigorous stirring. The ice bath was then removed and the reaction mixture allowed to warm to room temperature. Reaction progress was monitored daily by analytical HPLC (0 – 100% MeCN + 0.05% TFA in H_2O + 0.05% TFA over 40 min). 200 µL aliquots of reaction mixture were neutralised with 1M NaOH (aq) prior to analysis. After several days, a complex mixture of peaks was observed. An additional 1 mL HCl (aq) was added after each monitoring to drive the reaction forward. After 6 days of stirring at room temperature, no clear product peak was observed. Extraction into 20 mL of EtOAc and *n*-butanol were unsuccessful, so the reaction was abandoned.

Methyl 6-(1,3-dioxolan-2-yl)nicotinate (14)

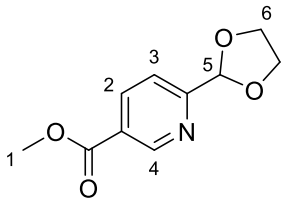

1 (2.48 g, 15 mmol) was dissolved in anhydrous toluene (60 mL). Ethylene glycol (2.72 mL, 48.75 mmol) was added with stirring, followed by *p*TsOH·H_2O (0.28 g, 1.5 mmol). The reaction flask was equipped with a reflux condenser attached to Dean-Stark apparatus. The temperature was slowly increased to 140 °C and the reaction mixture heated under reflux for

6 h, with collected water periodically drained from the side arm of the Dean Stark apparatus. The solvent was then removed under vacuum and the resultant crude solid purified by SiO_2 column chromatography using 60% EtOAc in hexane as eluent. Concentration of the product containing fractions yielded 2.73 g (87%) of the title compound as an off-white solid.

TLC (60% EtOAc in hexane): R_f 0.35.

^{1}H NMR (300 MHz, $CDCl_3$) δ 9.21 (dd, *J* = 2.1, 0.9 Hz, 1H, H_4), 8.34 (dd, *J* = 8.1, 2.1 Hz, 1H, H_2), 7.62 (dd, *J* = 8.2, 0.9 Hz, 1H, H_3), 5.90 (s, 1H, H_5), 4.21 – 4.04 (m, 4H, H_6), 3.95 (s, 3H, H_1).

^{13}C NMR (400 MHz, $CDCl_3$) δ 165.0 (C_q), 161.0 (C_q), 150.6 (C_4), 138.1 (C_2), 126.2 (C_q), 120.3 (C_3), 103.1 (C_5), 65.7 (C_6), 52.5 (C_1).

Mass spectrum (ESI +ve): *m/z* 166.1 $[M\text{-}C2H4O + H]^+$; *m/z* 210.1 $[M+H]^+$; *m/z* 232.1 $[M+Na]^+$

6-(1,3-dioxolan-2-yl)nicotinic acid (15)

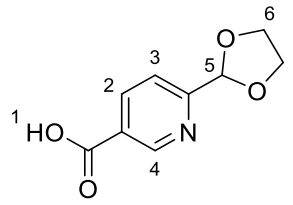

14 (1.46 g, 7 mmol) was dissolved in hot MeOH (15 mL). After dissolution, 10 mL of 1M NaOH (aq) was added with stirring. The reaction mixture was stirred for 29 h before the solvent was removed under vacuum. The residue was partitioned between 20 mL of 1M HCl (aq)and EtOAc (50 mL). Additional 1M HCl (aq) was added until pH 2 was achieved (approx. 50 mL, measured using indicator paper). The aqueous and organic layers were separated, and the aqueous layer re-extracted with EtOAc (3 x 75 mL). The organic layers were combined, washed with brine (100 mL) and dried over $MgSO_4$. Concentration under vacuum yielded 645 mg (44%) of the title compound as a white solid.

^{1}H NMR (300 MHz, DMSO-d_6) δ 13.51 (s, 1H, H_1), 9.05 (dd, *J* = 2.3, 1.0 Hz, 1H, H_4), 8.34 (dd, *J* = 8.1, 2.1 Hz, 1H, H_2), 7.67 (dd, *J* = 8.1, 0.9 Hz, 1H, H_3), 5.81 (s, 1H, H_5), 4.19 – 3.95 (m, 4H, H_6).

Mass spectrum (ESI +ve): *m/z* 196.1 $[M+H]^+$; *m/z* 218.0 $[M+Na]^+$; *m/z* 240 $[M+2Na-H]^+$.

4-(3-((6-(1,3-dioxolan-2-yl)nicotinoyl)oxy)propyl)-4-nitroheptane-1,7-diyl bis(6-(1,3-dioxolan-2-yl)nicotinate) (16)

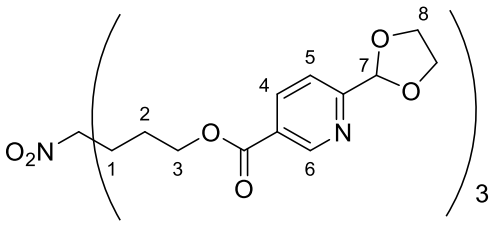

Nitromethanetrispropanol (73 mg, 0.31 mmol) was dissolved in anhydrous DCM (8 mL) and **15** (292 mg, 1.5 mmol) was added with stirring, followed by EDC·HCl (289 mg, 1.5 mmol) and DMAP (18 mg, 0.15 mmol). The reaction flask was equipped with a rubber septum, and the reaction left stirring under a N_2 balloon for 18 h. deionised H_2O (10 mL) and DCM (10 mL) were then added to the reaction mixture. After thorough mixing, the layers were separated and the aqueous layer re-extracted with DCM (2 x 25 mL). The combined organic layers were then dried over $MgSO_4$ before concentration under vacuum. The crude colourless oil was purified by SiO_2 column chromatography using 5% MeOH in DCM as eluent. The product containing fractions were combined and concentrated to yield 192 mg (81%) of the title compound as a colourless oil.

TLC (5% MeOH in DCM): R_f 0.55.

^{1}H NMR (400 MHz, $CDCl_3$) δ 9.17 (d, *J* = 1.9 Hz, 3H, H_6), 8.29 (dd, *J* = 8.1, 2.1 Hz, 3H, H_4), 7.61 (d, *J* = 8.1 Hz, 3H, H_5), 5.87 (s, 3H, H_7), 4.35 (t, *J* = 6.2 Hz, 6H, H_3), 4.18 – 4.03 (m, 12H, H_8), 2.16 – 2.05 (m, 6H, H_1), 1.78 – 1.67 (m, 6H, H_2).

^{13}C NMR (400 MHz) δ 164.8 (C_q), 161.3 (C_q), 150.5 (C_6), 138.0 (C_4), 125.9 (C_q), 120.4 (C_3), 103.1 (C_7), 93.1 (C_q), 65.7 (C_7), 64.4 (C_3), 32.0 (C_1), 23.2 (C_2).

Mass spectrum (ES+ve): *m/z* 767.3 $[M+H]^+$; *m/z* 789.3 $[M+Na]^+$

Attempted synthesis of 4-(3-((6-formylnicotinoyl)oxy)propyl)-4-nitroheptane-1,7-diyl bis(6-formylnicotinate)

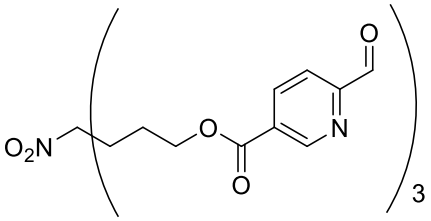

16 (190 mg, 0.25 mmol) was dissolved in acetone (38 mL) and deionised H_2O (4 mL) added. *p*TsOH·H_2O (400 mg, 2.1 mmol) was then added and the reaction mixture stirred thoroughly. A reflux condenser was equipped, and the reaction temperature gradually increased to 80 ^oC. The reaction mixture was stirred under reflux for 42 h. The reaction was monitored after 18 h, and again after 40 h. At these time points, 4 mL of the reaction mixture was concentrated under vacuum, and then the residue partitioned between deionised H_2O (15 mL) and DCM (15 mL). The layers were separated, and the DCM layer was washed with deionised H_2O (2 x 10 mL). The organic layer was then dried over $MgSO_4$, and concentrated under vacuum. The residue was then analysed by 1H NMR. After the second monitor, the solvent was removed from the remaining reaction mixture under vacuum. The residue was partitioned between deionised H_2O (20 mL) and DCM (30 mL). After separation, the DCM layer was washed with deionised H_2O (3 x 20 mL). After drying over $MgSO_4$, the DCM layer was concentrated under vacuum to yield 76 mg of a dark yellow oil (48% crude yield). Purification was attempted by SiO_2 column chromatography, using 5% MeOH in DCM as eluent. The product was not isolated to a desired purity and no further purification efforts were made.

5-((trimethylsilyl)ethynyl)picolinaldehyde (17)

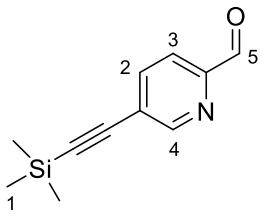

To a three-necked round bottom flask was dispensed 5-bormo-2-pyridinecarboxaldehyde (1.86 g, 10 mmol), bis(triphenylphosphine)palladium(II) dichloride (0.28 g, 0.4 mmol), copper(I) iodide (152 mg, 0.8 mmol), and triphenylphosphine (210 mg, 0.8 mmol). The flask was equipped with a reflux condenser and sealed before being placed under argon using a Schlenk line. Anhydrous THF (30 mL) was added, and Et_3N (40 mL) added by syringe to the stirring reaction mixture. Ethynyltrimethylsilane (1.95 mL, 14 mmol) was then added dropwise via syringe. The reaction mixture was then heated to 80 ^oC and stirred at this temperature for 4.5 h. The reaction was then removed from the heat and left stirring for a further 17 h at room temperature. The reaction mixture was filtered through Celite and the solvent removed from the filtrate under reduced pressure. The residue was partitioned between H_2O (100 mL) and EtOAc (100 mL), separated, and the organic layer washed with H_2O (2 x 100 mL). The organic layer was then dried over $MgSO_4$ and concentrated under reduced pressure to yield a dark brown oil. Purification by SiO_2 column chromatography was performed using DCM as eluent. The product containing fractions were combined and concentrated under reduced pressure to yield 1.21 g (60%) of the title compound as a dark brown solid.

TLC (DCM): R_f 0.25

^1H NMR (300 MHz, CDCl3) δ 10.06 (s, 1H, H_5), 8.81 (t, *J* = 1.4 Hz, 1H, H_4), 7.90 (d, *J* = 1.4 Hz, 2H, $H_{2,3}$), 0.28 (s, 9H, H_1).

^{13}C NMR (400 MHz, $CDCl_3$) δ 192.9 (C_5), 153.2 (C_4), 151.3 (C_q), 140.1 (C_2), 125.0 (C_q), 121.2 (C_3), 103.1 (C_q), 101.0 (C_q), 0.0 (C_1).

Mass spectrum (EI +ve): *m/z* 203.1 [M^+, 50%]; *m/z* 188.0 [M-CH_3^+, 100%].

5-ethynylpicolinaldehyde (18)

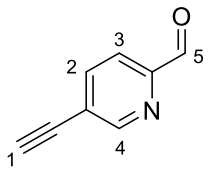

17 (1.0 g, 4.92 mmol) was dispensed into a two-necked round bottomed flask with K_2CO_3 (70 mg, 0.5 mmol). An argon atmosphere was established using a Schlenk line, and anhydrous MeOH (40 mL) added via syringe. The reaction was then stirred at room temperature for 2 h. The solvent was removed under reduced pressure and the residue partitioned between H_2O (50 mL) and EtOAc (50 mL). After separation, the organic layer was washed with sat. $NaHCO_3$ (aq) (50 mL) and brine (50 mL). The organic layer was then dried over $MgSO_4$ before concentration under reduced pressure. Purification was performed using SiO_2 column chromatography, using 10 - 15% EtOAc in hexane as eluent. The product containing fractions were combined and concentrated under reduced pressure to yield 347 mg (54%) of the title compound as a light brown solid.

TLC (20% EtOAC in hexane): R_f 0.29.

^{1}H NMR (400 MHz, $CDCl_3$) δ 10.05 (s, 1H, H_5), 8.83 (t, *J*= 1.4 Hz, 1H, H_4), 7.91 (t, *J* = 1.7 Hz, 2H, $H_{2,3}$), 3.43 (s, 1H, H_1).

^{13}C NMR (400 MHz, $CDCl_3$) δ 192.5 (C_5), 153.0 (C_4), 151.4 (C_q), 140.1 (C_2), 123.6 (C_q), 120.8 (C_3), 84.1 (C_q), 79.7 (C_1).

Mass spectrum (EI +ve): *m/z* 131.0 [M^+]; *m/z* 103.0 [M-CO]$^+$; *m/z* 77.0 [M-CO-C_2H]$^+$

4-(3-((methylsulfonyl)oxy)propyl)-4-nitroheptane-1,7-diyl dimethanesulfonate (19)

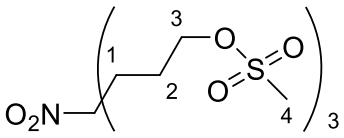

To a solution of nitromethanetrispropanol (1.18 g, 5 mmol) in THF (30 mL) was added Et_3N (3.14 mL, 22.5 mmol). The reaction mixture was then cooled to 0 ^oC and $MeSO_2Cl$ was added dropwise over 10 min. The reaction was allowed to gradually warm to room temperature and left stirring for 24 h. The solvent was removed under reduced pressure and the residue partitioned between H_2O (30 mL) and EtOAc (40 mL). The layers were separated, and the organic layer washed with 1M HCl (aq) (30 mL), sat. $NaHCO_3$ (aq) (30 mL) and brine (30 mL). The organic layer was then dried over $MgSO_4$ and the solvent removed under reduced pressure. Purification was performed by SiO_2 column chromatography, using 80- 100% EtOAc in hexane as eluent. The product containing fractions were combined and concentrated to yield 1.96 g (83%) of the title compound as a yellow oil.

TLC (80% EtOAc in hexane): R_f 0.14. Spots visualised with $KMnO_4$ stain.

^1H NMR (400 MHz, $CDCl_3$) δ 4.23 (t, *J* = 5.9 Hz, 6H, H_3), 3.02 (s, 9H, H_4), 2.12 – 2.03 (m, 6H, H_1), 1.74 – 1.64 (m, 6H, H_2).

^{13}C NMR (400 MHz, $CDCl_3$) δ 92.8 (C_q), 68.9 (C_3), 37.5 (C_4), 31.5 (C_1), 23.8 (C_3).

Mass spectrum (ESI +ve): m/z 492.1 $[M+Na]^+$; *m/z* 508 $[M+K]^+$

1,7-diazido-4-(3-azidopropyl)-4-nitroheptane (20)

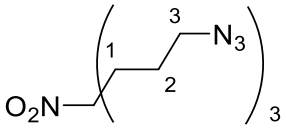

A two neck round bottomed flask containing **20** (1.96 g, 4.17 mmol) was purged with argon on a Schlenk line. Anhydrous DMF (30 mL) was then added and the solution cooled to 0 ^{o}C. With stirring, sodium azide (1.63 g, 25.02 mmol) was added in small portions against a counter flow of argon. The reaction was gradually allowed to cool to RT and left stirring for 17 h. The solvent was removed under reduced pressure and the residue partitioned between and H_2O (40 mL) and EtOAc (3 x50 mL). The combined organic layers were dried over $MgSO_4$ and concentrated under reduced pressure to yield a yellow oil. Purification was performed by SiO_2 column chromatography, using 10-25% EtOAc in hexane. The product containing fractions were combined and concentrated under reduced pressure to yield 706 mg (55%) of a pale yellow oil.

TLC (25% EtOAc in hexane): R_f 0.31 visualised with $KMnO_4$ stain.

^{1}H NMR (300 MHz, $CDCl_3$) δ 3.34 (t, *J* = 6.4 Hz, 6H, H_3), 2.04 – 1.92 (m, 6H, H_1), 1.55 – 1.41 (m, 6H, H_2).

IR (neat): 2922 (s, CH), 2852 (m, CH), 2090 (m, N_3), 1536 (s, NO_2), 1455 (m, CH), 1353 (m, NO_2), 1259 (m, CN) cm^{-1}.

Attempted synthesis of nitromethanetris(5-(1-propyl-1H-1,2,3-triazol-4-yl)picolinaldehyde)

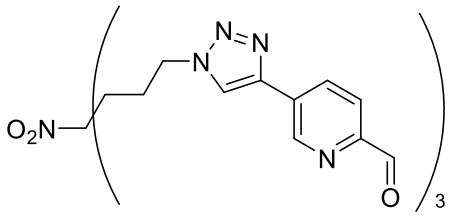

18 (46mg, 0.15 mmol) was suspended in 1:1 H_2O:*t*-BuOH (1 mL) and added to a solution of **20** (66 mg, 0.5 mmol) dissolved in *t*-BuOH (2 mL) at 40 °C. $CuSO_4 \cdot 5H_2O$ (7.5 mg, 0.03 mmol) was dissolved in H_2O (1.0 mL) and this was added to the heated reaction mixture, followed by a solution of sodium ascorbate in H_2O (1.0 mL). The reaction was stirred at 40 °C. Monitoring of the reaction's progress was performed by analytical HPLC (0 – 100% MeCN over 40 min) after 1.5 h, 3 h, and 4.5 h. Three new peaks were observed and collected for MS analysis. Due to the complexity of the mixture, no further efforts to isolate the product were made.

Benzyl (1,3-dihydroxy-2-(hydroxymethyl)propan-2-yl)carbamate (21)

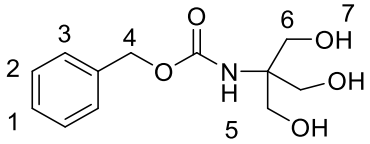

Tris(Hydroxymethyl)aminomethane (5.05 g, 41.7 mmol) was dissolved in EtOAc (40 mL). 20 mL of deionised H_2O was then added, followed by solid $NaHCO_3$ (5.25 g, 62.6 mmol). With vigorous stirring, CbzCl (7 mL, 50 mmol) was added dropwise at a rate of 1 drop per second. After 6 h of stirring at room temperature, the reaction mixture was allowed to settle and the white solid filtered under vacuum through a glass frit. The organic and aqueous layers were then separated, with product re-extracted from the aqueous layer using EtOAc (3 x 40 mL).

The combined organic layers were then washed with brine (40 mL) and dried over $MgSO_4$. The solvent was then removed under vacuum to yield a white solid, which was suspended in 400 mL of hot hexane. The solid was collected by vacuum filtration and left drying under vacuum in the fume hood overnight, yielding 7.68 g (72%) of the title compound as a white solid.

^{1}H NMR (400 MHz, $CDCl_3$) δ 7.42 – 7.29 (m, 5H, H_{1-3}), 5.81 (s, 1H, H_5), 5.08 (s, 2H, H_4), 3.99 (t, *J* = 6.4 Hz, 3H, H_7), 3.65 (d, *J* = 6.4 Hz, 6H, H_6).

^{13}C NMR (400 MHz, $CDCl_3$) δ 157.3 (C_q), 135.9 (C_q), 128.6; 128.4; 128.1 (C_{1-3}), 67.2 (C_6), 62.7 (C_7), 60.1 (C_q).

Mass spectrum (ESI +ve): *m/z* 278.1 $[M+Na]^+$

Attempted synthesis of benzyl (1,3-bis(prop-2-yn-1-yloxy)-2-((prop-2-yn-1-yloxy)methyl)propan-2-yl)carbamate

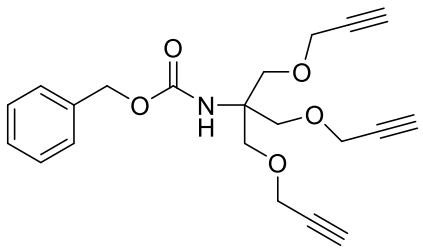

21 (577 mg, 2.26 mmol) was dispensed into a three necked round bottomed flask and an argon atmosphere established using a Schlenk line. Anhydrous DMF (10 mL) was added via syringe, and the resultant solution cooled to 0 °C. A solution of propargyl bromide (80 wt % in toluene, 1.51 mL, 13.6 mmol) was added dropwise to the stirring solution via syringe. After stirring for 10 minutes, KOH (763 mg, 13.6 mmol) was added in small portions over 15 min, against a counter flow of argon. The reaction was then heated to 35 °C and monitored by analytical HPLC (0 – 100% MeCN over 40 min) at T = 10 min, 2 h, 20 h, and 23 h. When no further change was observed, the reaction was diluted with EtOAc (200 mL). The combined organics were washed with brine (200 mL) before being dried over Na_2SO_4. Isolation of a product spot with TLC R_f 0.65 (30% EtOAC in hexane) was achieved by SiO_2 column chromatography, using 20 – 30% EtOAc in hexane as eluent. Concentration of the product

containing fractions yielded 254 mg of a yellow oil, ^{1}H NMR showed that the isolated product showed no aromatic hydrogens and so the reaction was abandoned.

4-nitro-1,7-bis(prop-2-yn-1-yloxy)-4-(3-(prop-2-yn-1-yloxy)propyl)heptane (22)

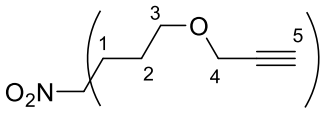

Nitromethanetrispropanol (59 mg, 0.25 mmol) was dissolved in anhydrous DMF (3 mL) under an argon atmosphere. The reaction solution was cooled to 0 °C and propargyl bromide (80 wt % in toluene, 0.28 mL, 2.5 mmol) was added dropwise via syringe. KOH (140mg, 2.5 mmol) was then added portionwise over 15 min against a counter flow of argon. The reaction was allowed to gradually warm to room temperature and stirred for 17 h. EtOAc (20 mL) was then added, and the organics washed with H_2O (4 x 20 mL). The organic layer was then dried over $MgSO_4$ and concentrated under reduced pressure to yield a brown oil. This was purified using SiO_2 column chromatography using 30% EtOAc ad eluent. The product containing fractions were combined and concentrated under reduced pressure to yield 44 mg (50%) of the title compound as a yellow oil.

TLC (40% EtOAC in hexane): R_f 0.4.

^{1}H NMR (400 MHz, $CDCl_3$) δ 4.11 (d, *J* = 2.4 Hz, 6H, H_4), 3.49 (t, *J* = 6.1 Hz, 6H, H_3), 2.42 (t, *J* = 2.4 Hz, 3H, H_5), 2.03 – 1.96 (m, 6H, H_1), 1.55 – 1.45 (m, 6H, H_2).

^{13}C NMR (400 MHz, $CDCl_3$) δ 94.1 (C_q), 79.7 (C_q), 74.5 (C_5), 69.3 (C_3), 58.1 (C_4), 32.3 (C_1), 23.9 (C_2).

Mass spectrum (ESI +ve): *m/z* 372.18 $[M+Na]^+$, m/z 325.18 $[M-C_2H+H]^+$

6-bromonicotinaldehyde (23)

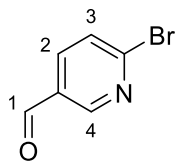

2,5-dibromopyridine (7.11 g, 30 mmol) was dispensed into a multi-necked flask and an argon atmosphere was established with a Schlenk line. Anhydrous Et_2O (80 mL) was added to the flask via syringe. After dissolution of the starting material, the solution was cooled to -78 °C in an acetone/dry ice bath. *n*-BuLi (1.6 M in hexane, 18.75 mL, 30 mmol) was then added dropwise over 15 min through the dropping funnel. The reaction mixture was mixed thoroughly during addition, and was left stirring at -78 °C for 1 h. Anhydrous DMF (2.55 mL, 33 mmol) was then added via syringe and the reaction mixture stirred at -78 °C for a further 1 h. The reaction vessel was then transferred to an ice bath and allowed to warm to 0 °C. The vessel was opened and 1M HCl (50 mL) was then added slowly with vigorous stirring. Deionised H_2O (50 mL) and Et_2O (50 mL) were then added to the reaction mixture, mixed thoroughly and the aqueous and organic layers separated. The aqueous layer was then re-extracted with Et_2O (2 x 100 mL). The combined organic layers were washed with brine (100 mL), dried over $MgSO_4$ and concentrated under vacuum. The crude material was purified by SiO_2 column chromatography, using 10 – 25% EtOAc in hexane as eluent. The product containing fractions were combined and concentrated under vacuum to yield 3.5 g (63%) of the title compound as a cream solid.

TLC (10% EtOAc in hexane): R_f 0.2.

^{1}H NMR (300 MHz, $CDCl_3$) δ 10.09 (d, *J* = 0.6 Hz, 1H, H_1), 8.83 (dd, *J* = 2.5, 0.8 Hz, 1H, H_4), 8.02 (dd, *J* = 8.2, 2.4 Hz, 1H, H_2), 7.68 (dt, *J* = 8.2, 0.8 Hz, 1H, H_3).

^{13}C NMR (400 MHz, $CDCl_3$) δ 189.4 (C_1), 152.5 (C_4), 150.7 (C_q), 138.4 (C_2), 130.6 (C_q), 129.0 (C_3).

Mass Spectrum (EI +ve): *m/z* 185.0 $[M]^+$; *m/z* 156 $[M\text{-}CHO]^+$; *m/z* 76 $[M\text{-}CHO\text{-}Br]^+$

(6-bromopyridin-3-yl)methanol (24)

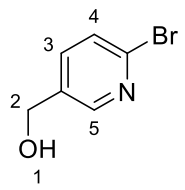

23 (3.4 g, 18.3 mmol) was dissolved in anhydrous MeOH (40 mL) and the solution cooled to 0 ^{o}C in an ice bath. $NaBH_4$ (0.9 g, 23.8 mmol) was then added slowly with vigorous stirring. The ice bath was then removed and the reaction allowed to warm to room temperature. After 1 h, 50 mL of sat NH_4Cl (aq) was slowly added to the reaction mixture. MeOH was removed under vacuum, and the product extracted from resultant aqueous solution with EtOAc (3 x 100 mL). The organic layers were combined, washed with 100 mL of sat. $NaHCO_3$ (aq), washed with brine (70 mL) and dried over $MgSO_4$. Concentration under vacuum yielded a yellow oil which was purified by SiO_2 column chromatography, using 60% EtOAc in hexane as eluent. The product containing fractions were concentrated to yield 2.96 g (86%) of the title compound as a white solid.

TLC (75% EtOAc in hexane): R_f 0.46.

^{1}H NMR (400 MHz, DMSO-d_6) δ 8.33 (d, *J* = 2.3 Hz, 1H, H_5), 7.69 (dd, *J* = 8.2, 2.3 Hz, 1H, H_3), 7.61 (d, *J* = 8.1 Hz, 1H, H_4), 5.44 (t, *J* = 5.5 Hz, 1H, H_1), 4.51 (d, *J* = 5.5 Hz, 2H, H_2).

^{13}C NMR (400 MHz, CDMSO-d_6) δ 148.77 (C_5), 139.60 (C_q), 138.06 (C_3), 137.73 (C_q), 127.66 (C_4), 59.89 (C_2).

Mass spectrum (EI +ve): *m/z* 187.0 $[M]^+$; *m/z* 158.0 $[M\text{-}CH_2OH]^+$

(6-bromopyridin-3-yl)methyl methanesulfonate (25)

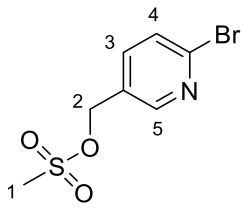

24 (1.5 g, 8 mmol) was dissolved in anhydrous DCM (15 mL) and Et_3N (3.3 mL, 24 mmol) was added. The mixture was cooled to 0 ^oC and methane sulfonic anhydride (2.09g, 12 mmol) was added. The reaction was gradually warmed to room temperature and stirred for 1 h. 40 mL of sat. $NaHCO_3$ (aq) was added to the reaction, and the product extracted into DCM (3 x 40 mL). The combined organics were dried over $MgSO_4$ and concentrated under reduced pressure to yield a brown solid, which was purified by SiO_2 column chromatography using 40-50% EtOAc as eluent. The product containing fractions were combined and concentrated under reduced pressure to yield 838 mg (39%) of the title compound as a white solid.

TLC (50% EtOAc in hexane): R_f 0.26

^1H NMR (400 MHz, $CDCl_3$) δ 8.40 (d, *J* = 2.3 Hz, 1H, H_5), 7.63 (dd, *J* = 8.3, 2.3 Hz, 1H, H_3), 7.53 (dd, *J* = 8.3, 0.7 Hz, 1H, H_4), 5.20 (s, 2H, H_2), 3.02 (s, 3H, H_1).

^{13}C NMR (400 MHz, $CDCl_3$) δ 150.1 (C_5), 143.2 (C_q), 138.8 (C_3), 128.8 (C_q), 128.4 (C_4), 67.2 (C_2), 38.3 (C_1).

Mass spectrum (ESI +ve): *m/z* 265.90 $[M+H]^+$; *m/z* 287.88 $[M+H]^+$

5-(azidomethyl)-2-bromopyridine (26)

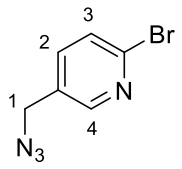

25 (400 mg, 1.5 mmol) was dissolved in anhydrous DMF (5 mL) under argon. The reaction was cooled to 0 °C and sodium azide (195 mg, 3 mmol) was added portionwise against a counter flow of argon. The reaction was left stirring at 0 °C for an additional 15 min before being allowed to gradually warm to room temperature. After 17.5 h of stirring, H_2O (10 mL) was slowly added to the reaction mixture. 5 mL of sat. $NaHCO_3$ (aq) was added and the product was extracted into EtOAc (3 x 25 mL). The combined organics were dried over $MgSO_4$ and concentrated under reduced pressure to yield a colourless oil. Purification was performed by SiO_2 column chromatography using 30% Et_2O in hexane as eluent. The product containing fractions were combined and concentrated under reduced pressure to yield 194 mg (61%) of the title compound as a colourless oil.

TLC (25% Et_2O in hexane): R_f 0.18.

^{1}H NMR (400 MHz, $CDCl_3$) δ 8.34 (dd, *J* = 2.0, 1.2 Hz, 1H, H_4), 7.54 – 7.51 (m, 2H, H_{2+3}), 4.37 (s, 2H, H_1).

^{13}C NMR (400 MHz, $CDCl_3$) δ 149.28 (C_4), 141.82 (C_q), 137.96 (C_2), 130.38 (C_q), 128.06 (C_3), 51.10 (C_1).

Mass spectrum (EI +ve): *m/z* 214.0 (Br isotope pattern, $[M]^+$); 185.9 (Br isotope pattern, $[M-N_2]^+$); 171.9 (Br isotope pattern, $[M-N_3]^+$; 157.9 (Br isotope pattern, $[M-CH_2N_3]^+$).

5,5'-(((((4-(3-((1-((6-bromopyridin-3-yl)methyl)-1H-1,2,3-triazol-4-yl)methoxy)propyl)-4-nitroheptane-1,7-diyl)bis(oxy))bis(methylene))bis(1H-1,2,3-triazole-4,1-diyl))bis(methylene))bis(2-bromopyridine) (27)

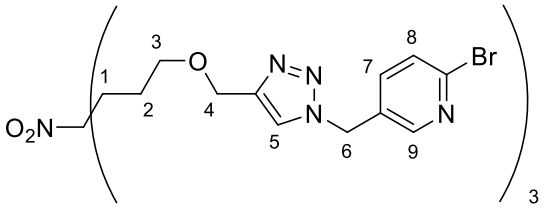

22 (18 mg, 0.05 mmol) and **26** (64 mg, 0.3 mmol) were dissolved in anhydrous THF (2 mL). $CuSO_4 \cdot 5H_2O$ (0.045 mmol) was dissolved in H_2O (1 mL) and added dropwise to the stirring reaction mixture. This was followed by a solution of sodium L-ascorbate (9 mg, 0.045 mmol) dissolved in 1 mL H_2O. The stirring solution was heated to 60 °C. After stirring for 17 h, further sodium L-ascorbate (9 mg, 0.045 mmol) was added to the stirring reaction mixture. The reaction was left stirring for a further 18 h at 60 °C before being allowed to cool to room temperature. The reaction mixture was diluted with EtOAc (10 mL) and sat. $NaHCO_3$ (aq) (10 mL) before separation of the aqueous and organic layers. The organic layer was washed with H_2O (10 mL) before being dried over $MgSO_4$. The organics were concentrated under reduced pressure to yield a dark yellow oil, which was purified using SiO_2 column chromatography using 5% MeOH in DCM as eluent. The product containing fractions were combined and concentrated under reduced pressure to yield 29 mg (59%) of the title compound as a pale yellow oil.

TLC (5% MeOH in DCM): R_f 0.14.

^{1}H NMR (400 MHz, $CDCl_3$) δ 8.35 (t, *J* = 1.8 Hz, 3H, H_9), 7.56 (s, 3H, H_5), 7.51 – 7.45 (m, 6H, H_{7+8}), 5.52 (s, 6H, H_4), 4.54 (s, 6H, H_6), 3.45 (t, *J* = 6.1 Hz, 6H,H_3), 1.96 – 1.86 (m, 6H, H_1), 1.43 (dq, *J* = 11.0, 5.7 Hz, 6H, H_2).

^{13}C NMR (400 MHz, $CDCl_3$) δ 148.5 (C_9), 145.0 (C_q), 137.6 ($C_{7/8}$), 137.3 ($C_{7/8}$), 128.9 (C_q), 121.5 (C_5), 93.0 (C_q), 68.9 (C_3), 63.2 (C_6), 49.7 (C_4), 31.1 (C_1), 22.9 (C_2).

Mass spectrum (ESI +ve): *m/z* 990.09 (triple Br isotope pattern, $[M+H]^+$); 495.56 (triple Br isotope pattern, $[M+2H]^{2+}$)

Attempted formylation of Compound 27

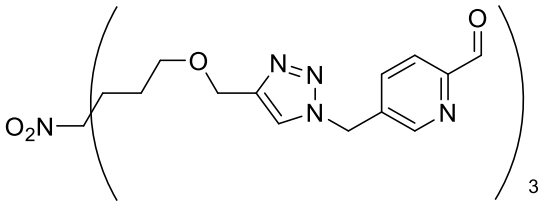

27 (20 mg, 0.02 mmol) was dissolved in anhydrous THF (0.5 mL) under an Ar atmosphere. The mixture was cooled to -78 °C and *n*-BuLi (2.5 M in hexane, 67 µL, 0.17 mmol) was added dropwise via syringe. The reaction mixture was left stirring for 2 h before anhydrous DMF (0.5 mL) was added. After a further 1 h of stirring at -78 °C, sat. NH_4Cl (aq) (2 mL) was added to quench the reaction and extraction with EtOAc (3 x 5 mL) was performed. The combined organics were dried over $MgSO_4$, and concentrated under reduced pressure to yield a brown-orange oil. TLC and 1H NMR of the crude material showed a complex mixture, and no purification was attempted.

5-hydroxy-2-methylpyridine 1-oxide (28)

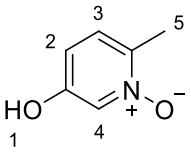

3-hydroxy-6-methylpyridine (16.37 g, 150 mmol) was suspended in acetic acid (200 mL) and H_2O_2 (30 wt% aq., 34 mL, 300 mmol) was added dropwise with stirring over 30 min. The reaction mixture was then heated under reflux (120 °C) for 3.5 h before being allowed to cool to room temperature, at which it was stirred for a further 17 h. The solvent volume was then reduced to approx. 50 mL under reduced pressure and poured into cold acetone (-20 °C, 250 mL). The resultant solution was then cooled in an ice bath for 3 h, and the resultant pale yellow crystals collected by vacuum filtration. The collected precipitate was washed with cold acetone (-20 °C, 4 x 30 mL) before being dried under high vacuum for 1 h. The filtrate was concentrated under reduced pressure to approx. 50 mL and the precipitation procedure

repeated. The collected precipitates were combined and dried under high vacuum to yield 13.84 g (74%) of the title compound as a pale yellow solid.

^{1}H NMR (400 MHz, DMSO-d_6) δ 10.26 (br s, 1H, H_1), 7.81 (d, J = 2.3 Hz, 1H, H_4), 7.24 (d, J = 8.6 Hz, 1H, H_3), 6.77 (dd, J = 8.6, 2.3 Hz, 1H, H_2), 2.22 (s, 3H, H_5).

^{13}C NMR (400 MHz, DMSO-d_6) δ 154.08 (C_q), 139.10 (C_q), 127.44 (C_4), 126.20 (C_3), 113.90 (C_2), 16.34 (C_5).

Mass spectrum (ESI +ve): *m/z* 126.05 $[M+H]^+$, 148.04 $[M+Na]^+$.

6-(acetoxymethyl)pyridin-3-yl acetate (29)

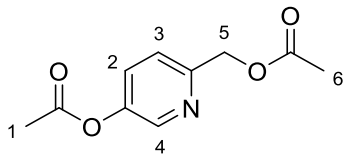

Acetic anhydride (40 mL) was heated to 110 °C and **28** (4 g, 32 mmol) was added portionwise with stirring over 10 min. The reaction mixture was then heated under reflux (130 °C) for 2 h. The reaction mixture was allowed to cool to room temperature and ethanol (20 mL) was added. After stirring thoroughly for 2 min, the mixture was concentrated under reduced pressure to yield a dark brown oil. This was dissolved in $CHCl_3$ (100 mL) before sat. $NaHCO_3$ (aq) (30 mL) was slowly added with gentle stirring to neutralise the mixture. The organic and aqueous layers were then separated and the organics dried over $MgSO_4$. Concentration under reduced pressure yielded 6.59 g (98%) of the title compound as a dark brown oil.

TLC (EtOAc): R_f 0.52

^{1}H NMR (400 MHz, $CDCl_3$) δ 8.34 (d, J = 2.6 Hz, 1H, H_4), 7.45 (dd, J = 8.5, 2.7 Hz, 1H, H_2), 7.35 (d, J = 8.5 Hz, 1H, H_3), 5.16 (s, 2H, H_5), 2.28 (s, 3H, H_1), 2.10 (s, 3H, H_6).

^{13}C NMR (400 MHz, $CDCl_3$) δ 170.65 (C_q), 168.90 (C_q), 152.91 (C_q), 146.68 (C_q), 142.92 (C_4), 130.01 (C_2), 122.50 (C_3), 66.24 (C_5), 20.95 (C_1), 20.87 (C_6).

Mass spectrum (EI +ve): *m/z* 209.08 $[M]^+$ (10%); 166.05 $[M\text{-}COCH_3]^+$ (50%); 124.03 $[M\text{-}COCH_3\text{-}COCH_3\text{+}H]^+$ (100%).

6-(hydroxymethyl)pyridin-3-ol (30)

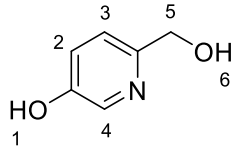

29 (6.31 g, 50.4 mmol) was suspended in conc. HCl (aq) (32% aq., 50 mL) and heated under reflux (110 °C) for 1 h. The mixture was allowed to cool to room temperature, and the volume reduced by half under reduced pressure. The resultant mixture was neutralised by slow addition of sat. Na_2CO_3 (aq) (100 mL). $CHCl_3$ (100 mL) was then added with stirring. The aqueous and organic layers were separated and the aqueous layer was concentrated under reduced pressure to yield a wet red residue. The residue was triturated with boiling MeCN (3 x 200 mL) and filtered under vacuum. The combined filtrates were concentrated under reduced pressure to yield a brown, oily solid which was triturated again with hot iPrOH (200 mL) before filtration (gravity). The filtrate was concentrated under reduced pressure to yield a yellow oil. This was further purified by SiO_2 column chromatography using 5 – 8% MeOH in DCM as eluent. The product containing fractions were concentrated under reduced pressure to yield 2.1 g (33%) of the title compound as a beige solid.

TLC (10% MeOH in DCM): R_f 0.16

^{1}H NMR (400 MHz, DMSO-d_6) δ 9.73 (s, 1H, H_1), 8.01 (d, *J* = 2.7 Hz, 1H, H_4), 7.25 (d, *J* = 8.5 Hz, 1H, H_3), 7.14 (dd, *J* = 8.5, 2.7 Hz, 1H, H_2), 5.22 (t, *J* = 5.8 Hz, 1H, H_6), 4.43 (d, *J* = 5.8 Hz, 2H, H_5).

^{13}C NMR (400 MHz, DMSO-d_6) δ 152.7 (C_q), 152.6 (C_q), 136.8 (C_4), 123.0 (C_2), 121.5 (C_3), 64.4 (C_5).

Mass spectrum (EI +ve): *m/z* 125.07 $[M]^+$; *m/z* 94.04 $[M\text{-}CH_2OH]^+$

5-hydroxypicolinaldehyde (31)

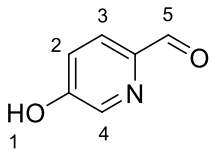

30 (400 mg, 3.2 mmol) and activated MnO_2 (1 g, 2.5 x mass of starting material) were dispensed into a multi-necked round bottomed flask equipped with a reflux condenser. The sealed flask was placed under an argon atmosphere and anhydrous iPrOH (10 mL) was added via syringe. The mixture was stirred under reflux (110 ^{o}C) for 2.5 h. The reaction mixture was then allowed to cool and centrifuged (6000 rpm, 15 min). The clear supernatant was separated from the black solids. The solids were resuspended in anhydrous iPrOH (15 mL) and the separation procedure repeated twice more. The combined supernatants were filtered through Celite and concentrated under reduced pressure to yield a dark brown solid. This was purified by SiO_2 column chromatography using 5% MeOH in DCM as eluent. The product containing fractions were combined and concentrated under reduced pressure to yield 140 mg (36%) of the title compound as a light brown solid.

TLC (5% MeOH in DCM): R_f 0.13.

^{1}H NMR (400 MHz, DMSO-d_6) δ 11.13 (s, 1H, H_1), 9.82 (d, *J* = 0.9 Hz, 1H, H_5), 8.31 (d, *J* = 2.7 Hz, 1H, H_4), 7.84 (d, *J* = 8.5 Hz, 1H, H_3), 7.32 (ddd, *J* = 8.5, 2.7, 0.9 Hz, 1H, H_2).

^{13}C NMR (400 MHz, DMSO-d_6) δ 192.3 (C_q), 158.4 (C_5), 145.2 (C_q), 139.3 (C_4), 124.2 (C_3), 122.9 (C_2).

Mass spectrum (EI +ve): *m/z* 123.03 $[M]^+$; *m/z* 95.03 $[M\text{-}CO]^+$

Attempted synthesis of 5,5'-((4-(3-((6-formylpyridin-3-yl)oxy)propyl)-4-nitroheptane-1,7-diyl)bis(oxy))dipicolinaldehyde using Mitsunobu chemistry

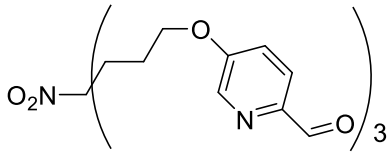

Triphenylphosphine (472 mg, 1.8 mmol) was dispensed into a multi-necked round bottomed flask and placed under N_2. Anhydrous THF (5 mL) was then added via syringe. The solution was cooled to 0 °C before diethyl azodicarboxylate (0.3 mL, 1.8 mmol) was added. This solution was mixed for 15 min at 0 °C before a solution of nitromethanetrispropanol (71 mg, 0.3 mmol) in anhydrous THF (1 mL) was added. After stirring for 30 min, a solution of **31** (222 mg, 1.8 mmol) in anhydrous THF (1 mL) was added via syringe. The reaction mixture was allowed to warm to room temperature and stirred for 40 h. The reaction mixture was analysed by analytical HPLC. Chromatograms obtained through monitoring at 210 nm, 265 nm, 300 nm, and 400 nm. Two new peaks were observed at 300 nm but neither of these could be identified as the desired product.

5-(2-bromoethoxy)picolinaldehyde (32)

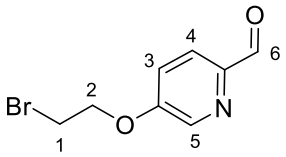

31 (123 mg, 1 mmol) and anhydrous K_2CO_3 were dispensed into a multi-necked round bottomed flask and an Ar atmosphere established. Anhydrous DMF (4 mL) was added via syringe and the mixture stirred vigorously. 1,2-dibromoethane (87 µL, 1 mmol) was added, and the reaction heated at 100 °C for 1 h. After cooling to room temperature, the reaction was diluted with H_2O (10 mL) and sat. $NaHCO_3$ (aq) (3 mL). EtOAc (20 mL) was added and the organic and aqueous layers separated. The organic layer was further washed with H_2O (3 x 10 mL) before being dried over $MgSO_4$. Concentration under reduced pressure yielded a dark

green oil which was purified by SiO_2 column chromatography using 50% EtOAc in hexane as eluent. The product containing fractions were combined and concentrated under reduced pressure to yield 120 mg (52%) of the title compound as a colourless oil.

TLC (50% EtOAc in hexane): R_f 0.32

^{1}H NMR (400 MHz, CDCl3) δ 9.99 (d, *J* = 0.8 Hz, 1H, H_6), 8.45 (dd, *J* = 2.9, 0.8 Hz, 1H, H_5), 7.97 (dd, *J* = 8.7, 0.8 Hz, 1H, H_4), 7.32 (ddd, *J* = 8.7, 2.9, 0.8 Hz, 1H, H_3), 4.43 (t, *J* = 6.0 Hz, 2H, H_2), 3.69 (t, *J* = 6.0 Hz, 2H, H_1).

^{13}C NMR (400 MHz, CDCl3) δ 192.4 (C_6), 158.0 (C_q), 147.4 (C_q), 139.2 (C_5), 123.8 (C_4), 121.3 (C_3), 68.8 (C_2), 28.5 (C_1).

Mass spectrum (EI +ve): *m/z* 229.0 (Br isotope pattern, $[M]^+$); 201.0 (Br isotope pattern, $[M\text{-}CO]^+$); 150.0 $[M\text{-}Br]^+$; 108.9 (Br isotope pattern, $[BrCH_2CH_2]^+$).

5,5'-((4-(3-((6-formylpyridin-3-yl)oxy)propyl)-4-nitroheptane-1,7-diyl)bis(oxy))dipicolinaldehyde (33)

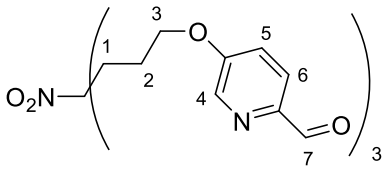

31 (616 mg, 5 mmol) and anhydrous K_2CO_3 (864 mg, 6.25 mmol) were dispensed into a multi-necked round bottomed flask and placed under Ar. Anhydrous DMF (8 mL) was added via syringe and the resultant mixture heated to 100 °C and mixed thoroughly for 1 h. A solution of **19** (587 mg, 1.25 mmol) in anhydrous DMF (2 mL) was then added via syringe before heating at 100 °C for a further 1 h. The reaction was allowed to cool at room temperature before the solvent was removed under reduced pressure. The resultant residue was partitioned between H_2O (20 mL) and EtOAc (60 mL). The layers were separated, and sat. $NaHCO_3$ (5 mL) was added to the aqueous layer. EtOAc was then used for further extraction (2 x 60 mL). The combined organics were dried over $MgSO_4$ and concentrated under reduced pressure to yield a brown oil. This was purified by SiO_2 column chromatography using 80 –

90% EtOAc in hexane as eluent. The product containing fractions were combined and concentrated under reduced pressure to yield 564 mg (82%) of the title compound as a pale brown solid.

TLC (80% EtOAc in hexane): R_f 0.1

^{1}H NMR (400 MHz, $CDCl_3$) δ 9.98 (d, *J* = 0.8 Hz, 3H, H_7), 8.41 (d, *J* = 2.8 Hz, 3H, H_4), 7.96 (d, *J* = 8.7 Hz, 3H, H_6), 7.28 (ddd, *J* = 8.7, 2.8, 0.8 Hz, 3H, H_5), 4.15 (t, *J* = 5.8 Hz, 6H, H_3), 2.30 – 2.21 (m, 6H, H_1), 1.93 – 1.82 (m, 6H, H_2).

^{13}C NMR (400 MHz, CDCl3) δ 192.1 (C_7), 158.1 (C_q), 146.8 (C_q), 138.7 (C_4), 123.5 (C_6), 120.7 (C_5), 93.4 (C_q), 68.0 (C_3), 32.3 (C_1), 23.8 (C_2).

Mass spectrum (ESI +ve): *m/z* 551.2 $[M+H]^+$; 573.2 $[M+Na]^+$; 605.2 $[M+CH_3OH+Na]^+$

Attempted synthesis of a dicapped Fe cylinder

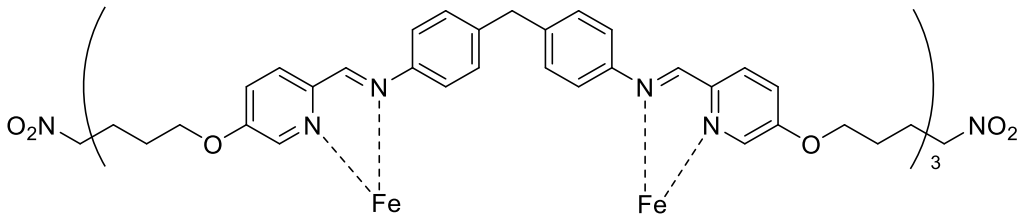

38 (67 mg, 0.12 mmol) was dissolved in MeOH (10 mL) and $FeCl_2{\cdot}4H_2O$ (24 mg, 0.12 mmol) was added. The reaction was heated to reflux (80 °C) and after stirring for 5 min, 4,4'-methylenedianiline (36 mg, 0.18 mmol) was added. A purple precipitate was observed, which did not dissolve with continued heating. After 2 hours of heating under reflux, the reaction was allowed to cool to room temperature and the purple precipitate collected by vacuum filtration. Attempts to dissolve this precipitate in other solvents (EtOH, MeCN, H_2O, DMSO, DMF) proved unsuccessful at room temperature and with heating. As such, no analysis was performed on the precipitate.

5.3 Experimental procedures from Chapter 3

5.3.1 Synthetic procedures

The procedures used to synthesise the compounds described in Chapter 3 are presented below, in the order that they appear in the reaction schemes contained within the chapter. Compounds have been numbered in the order that they appear in the text.

(1E,1'E)-N,N'-(methylenebis(4,1-phenylene))bis(1-(pyridin-2-yl)methanimine) (L, 36)

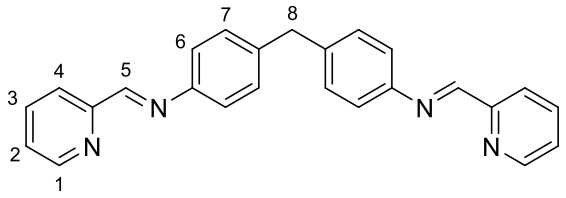

Pellets of 4,4'-methylenedianiline (1.98 g, 10 mmol) were added to EtOH (40 mL) and gentle heating (40 °C) was applied until full dissolution was achieved. 2-pyridinecarboxaldehyde (1.9 mL, 20 mmol) was added dropwise with stirring. A pale yellow precipitate formed rapidly. Additional EtOH (40 mL) was added to help suspend the precipitate and the reaction mixture was stirred for 19 h at room temperature. The precipitate was collected by vacuum filtration and the solid was washed with cold (4 °C) EtOH (5 x 10 mL). The product was collected and dried in a vacuum desiccator for 2 h, giving 3.34 g (89%) of the title compound as a pale yellow solid.

^{1}H NMR (300 MHz, MeCN-d_3) δ 8.69 (ddd, *J* = 4.9, 1.7, 1.0 Hz, 2H, H_1), 8.59 (d, *J* = 0.7 Hz, 2H, H_5), 8.16 (m, 2H, H_4), 7.92 – 7.84 (m, 2H, H_3), 7.44 (ddd, *J* = 7.8, 4.9, 1.3 Hz, 2H, H_2), 7.36 – 7.24 (m, 8H, H_{7+8}), 4.04 (s, 2H, H_8).

^{13}C NMR (400 MHz, CDCl3) δ 160.21 (C_5), 154.81 (C_q), 149.85 (C_1), 149.17 (C_q), 139.91 (C_q), 136.82 (C_3), 129.93 ($C_{6/7}$), 125.21 (C_2), 122.02 (C_4), 121.53 ($C_{6/7}$), 41.21 (C_8).

Mass spectrum (ESI +ve): *m/z* 377.2 $[M+H]^+$; 399.2 $[M+Na]^+$

$Fe_2L_3Cl_4$ (37)

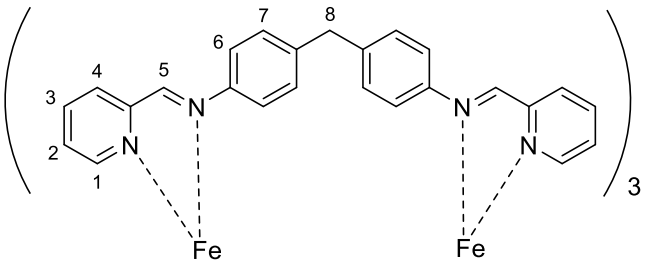

36 (2.0 g, 5.32 mmol) was suspended in MeOH (50 mL) and heated to 50 °C until full dissolution was achieved. $FeCl_2 \cdot 4H_2O$ (0.71 g, 3.55 mmol) was added, and the resultant purple solution heated under reflux (70 °C) for 1.5 h. The mixture was allowed to cool to room temperature and NH_4PF_6 (1.16 g, 7.1 mmol) was added. The resultant suspension was stirred at room temperature for 15 mins before the precipitate was collected by vacuum filtration. The solid was washed with MeOH (5 x 20 mL) and dried under suction in the fume cupboard for 2 h. The solid was then suspended in MeOH (40 mL) and excess DOWEX 1x8 Cl form (approx. 50 g) was added. The suspension was stirred vigorously at room temperature for 2 h. The DOWEX beads were separated from the solution by vacuum filtration and washed with MeOH (5 x 40 mL). The combined methanol filtrates were concentrated under reduced pressure to a volume of approx. 5 mL before being poured into cold (4 °C) Et_2O (150 mL). The resultant purple precipitate was collected by vacuum filtration and dried under high vacuum for 19 h, yielding 1.47 g (60%) of the title complex as a purple solid.

^{1}H NMR (400 MHz, MeOD-d4) δ 9.15 (s, 2H, H_5), 8.68 (d, *J* = 6.7 Hz, 2H, H_4), 8.46 (t, *J* = 6.7 Hz, 2H, H_3), 7.83 (t, *J* = 6.7 Hz, 2H, H_2), 7.43 (d, *J* = 4.9 Hz, 2H, H_1), 7.12 (br s, 4H, $H_{6/7}$), 5.59 (br. s, 4H, $H_{6/7}$), 4.04 (s, 2H, H_8).

Mass spectrum (ESI +ve): m/z 310.09 $[Fe_2L_3]^{4+}$; 428.46 $[Fe_2L_3+HCOO]^{3+}$; 477.10 $[Fe_2L_2+2(HCOO)]^{2+}$.

UV-Vis (H_2O) λ_{max} (ε_{max}/dm^3 mol^{-1} cm^{-1}): 325 (28,800); 528 (shoulder); 573 (15,200).

2-bromo-5-(((tert-butyldimethylsilyl)oxy)methyl)pyridine (38)

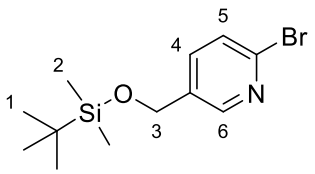

24 (3.14 g, 16.7 mmol) was dispensed into a two-necked flask equipped with an addition funnel and an Ar atmosphere was established. Anhydrous DMF (10 mL) was added via syringe, followed by Et_3N (3.5 mL, 25.05 mmol). A separate flask containing tert-butyldimethylsilylchloride (3.78 g, 25.1 mmol) was purged with nitrogen and anhydrous DMF (5 mL) was added. This solution was then transferred via syringe to the addition funnel, and added to the reaction mixture dropwise. The reaction mixture was stirred at room temperature for 1.5 h before Et_2O (150 mL) was added. The solvent was removed under reduced pressure and the residue partitioned between Et_2O (200 mL) and distilled H_2O (100 mL). After separation, further product was extracted from the aqueous layer with Et_2O (2 x 100 mL). The combined organic layers were washed with brine (100 mL), dried over $MgSO_4$ and concentrated under reduced pressure. The resultant crude solid was purified by SiO_2 column chromatography, using 3 – 5% EtOAc in hexane as eluent. The product containing fractions were combined and concentrated under reduced pressure to yield 4.57 g (91%) of the title compound as a colourless oil.

TLC (10% EtOAc in hexane): R_f 0.48.

^{1}H NMR (300 MHz, $CDCl_3$) δ 8.35 – 8.26 (m, 1H, H_6), 7.52 (ddt, *J* = 8.1, 2.5, 0.8 Hz, 1H, H_4), 7.43 (dd, *J* = 8.1, 0.8 Hz, 1H, H_5), 4.70 (d, *J* = 0.8 Hz, 2H, H_3), 0.92 (s, 9H, H_1), 0.09 (s, 6H, H_2).

^{13}C NMR (400 MHz, $CDCl_3$) δ 148.1 (C_6), 140.5 (C_q), 136.6 (C_4), 136.1 (C_q), 127.7 (C_5), 62.0 (C_3), 25.8 (C_1), 18.3 (C_q), -5.3 (C_2).

Mass spectrum (ES +ve): *m/z* 304.1 (Br isotope pattern, $[M+H]^+$).

5-(((tert-butyldimethylsilyl)oxy)methyl)picolinaldehyde (39)

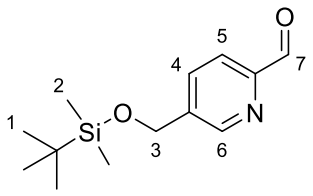

38 (4.42 g, 14.6 mmol) was dispensed into a two-necked flask and an Ar atmosphere was established. Anhydrous THF (25 mL) was added to the flask via syringe. After dissolution of the starting material, the solution was cooled to -78 °C in an acetone/dry ice bath. *n*-BuLi (1.6 M in hexane, 7 mL, 17.5 mmol) was then added dropwise over 15 min through the dropping funnel. The reaction mixture was mixed thoroughly during addition, and was left stirring at -78 °C for 1 h. Anhydrous DMF (1.35 mL, 17.5 mmol) was then added via syringe and the reaction mixture stirred at -78 °C for a further 1 h. Additional DMF (0.56 mL, 7.23 mmol) was added and the mixture left stirring for a further 1 h. The reaction vessel was then allowed to warm to room temperature. 40 mL of sat. NH_4Cl was added, and the organic THF removed under reduced pressure. The product was then extracted into EtOAc (3 x 50 mL). The combined organic layers were washed with brine (70 mL), dried over $MgSO_4$ and concentrated under reduced pressure. The crude red oil was purified by SiO_2 column chromatography, using 5 – 12% EtOAc in hexane as eluent. The product containing fractions were combined and concentrated under reduced pressure to yield 1.45 g (40%) of the title compound as a yellow oil. The purified product was stored under Ar to minimise atmospheric oxidation.

TLC (10% EtOAc in hexane): R_f 0.2

^{1}H NMR (300 MHz, $CDCl_3$) δ 10.05 (s, 1H, H_7), 8.71 (dd, *J* = 2.1, 0.9 Hz, 1H, H_6), 7.93 (d, *J* = 8.0 Hz, 1H, H_5), 7.82 (ddd, *J* = 8.0, 2.1, 0.9 Hz, 1H, H_4), 4.83 (s, 2H, H_3), 0.93 (s, 9H, H_1), 0.11 (s, 6H, H_2).

^{13}C NMR (400 MHz. $CDCl_3$) δ 193.1 (C_7), 171.1 (C_q), 151.9 (C_q), 148.1 (C_6), 141.7 (C_5), 121.4 (C_4), 62.5 (C_3), 25.8 (C_1)18.3 (C_q), -5.4 (C_2).

Mass Spectrum (EI +ve): *m/z* 251.3 $[M]^+$; *m/z* 236.2 $[M\text{-}CH_3]^+$; *m/z* 194.1 $[M\text{-}t\text{Bu}]^+$

5-(hydroxymethyl)picolinaldehyde (40)

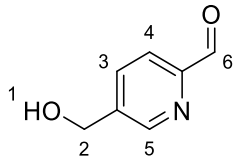

39 (1.44 g, 5.73 mmol) was dissolved in anhydrous THF (5 mL) and cooled to 0 ^{o}C in an ice bath. TBAF (1M in THF, 6.88 mL, 6.88 mmol) was added dropwise over 1 h from an addition funnel with stirring. The reaction mixture was allowed to warm to room temperature and stirred for 21 h. Several drops of distilled H_2O were then added, and the solvent removed under vacuum to yield an orange oil. This was purified by SiO_2 column chromatography, using 75 – 100% EtOAc in hexane as eluent. Concentration of the product containing fractions yielded 652 mg (90%) of the title compound as a yellow oil.

TLC (75% EtOAc in hexane): R_f 0.24

^{1}H NMR (300 MHz, DMSO-d6) δ 9.98 (d, *J* = 0.9 Hz, 1H, H_6), 8.75 (dd, *J* = 2.0, 0.9 Hz, 1H, H_5), 7.99 – 7.88 (m, 2H, H_{3+4}), 5.55 (t, *J* = 5.5 Hz, 1H, D_2O exchangeable, H_1), 4.66 (d, *J* = 5.5 Hz, 2H, H_2).

^{13}C NMR (400 MHz, DMSO-d6) δ 193.9 (C_6), 151.6 (C_q), 149.0 (C_5), 143.3 (C_q), 135.9 (C_3), 122.2 (C_4), 60.7 (C_2).

Mass spectrum (EI +ve): *m/z* 137.1 $[M]^+$; *m/z* 109.1 $[M\text{-}CO]^+$; *m/z* 92.1 $[M\text{-}CO\text{-}OH]^+$

(6-formylpyridin-3-yl)methyl methanesulfonate (41)

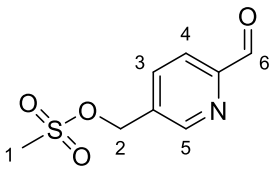

40 (590 mg, 4.3 mmol) was dissolved in anhydrous DCM (5 mL) and cooled to 0 °C. Et_3N (0.9 mL, 6.45 mmol) was added via syringe. Methanesulfonic anhydride (906 mg, 5.2 mmol) was then added portionwise over 5 min while the mixture was stirred. The reaction was stirred at 0 °C for 15 min before being allowed to gradually warm to room temperature. After stirring at room temperature for 5.5 h, the solvent was removed under reduced pressure and the residue partitioned between sat. $NaHCO_3$ (aq) (20 mL) and EtOAc (3 x 30 mL). The combined organic layers were dried over $MgSO_4$ and concentrated under reduced pressure to yield a yellow-brown solid. This was purified by SiO_2 column chromatography using 50 – 80% EtOAc in hexane as eluent. The product containing fractions were combined and concentrated under reduced pressure to yield 607 mg (66%) of the title compound as a white solid.

TLC (75% EtOAc in hexane): R_f 0.2

^{1}H NMR (300 MHz, $CDCl_3$) δ 10.09 (d, *J* = 0.8 Hz, 1H, H_6), 8.82 (dd, *J* = 2.1, 0.8 Hz, 1H, H_5), 8.05 – 7.91 (m, 2H, H_{3+4}), 5.34 (s, 2H, H_2), 3.08 (s, 3H, H_1).

Mass spectrum (ESI +ve): *m/z* 216.03 $[M+H]^+$

5-(azidomethyl)picolinaldehyde (42)

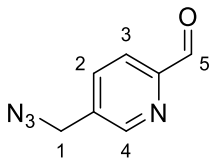

41 (320 mg, 1.49 mmol) was dissolved in anhydrous THF (10 mL) and 18-crown-6 (4 mg, 1 mol%) was added. Sodium azide (194 mg, 2.98 mmol) was added portionwise to the stirring reaction mixture. The reaction was left stirring at room temperature for 18 h before the solvent was removed under reduced pressure. H_2O (10 mL) and sat. $NaHCO_3$ (aq) (5mL) were added to the residue, and the product was extracted into EtOAc (3 x 25 mL). The combined organic layers were dried over $MgSO_4$ and concentrated under reduced pressure to yield a yellow oil. This was purified by SiO_2 column chromatography using 50% EtOAc in hexane as eluent. The product containing fractions were combined and concentrated under reduced pressure to yield 203 mg (84%) of the title compound as a yellow oil, which was carried through to the next step due to observed instability.

TLC (75% EtOAc in hexane): R_f 0.43.

^{1}H NMR (300 MHz, CDCl3) δ 10.09 (d, *J* = 0.9 Hz, 1H, H_5), 8.74 (dd, *J* = 2.1, 0.8 Hz, 1H, H_4), 8.00 (dd, *J* = 7.9, 0.8 Hz, 1H, H_3), 7.89 – 7.82 (m, 1H, H_2), 4.53 (s, 2H, H_1).

5-(2-azidoethoxy)picolinaldehyde (43)

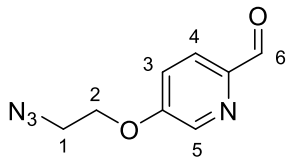

32 (195 mg, 0.85 mmol) was dissolved in MeCN (5 mL) and sodium azide (111 mg, 1.7 mmol) was added portionwise with stirring. 18-crown-6 (22 mg, 10 mol %) was added, and H_2O (1 mL) was added dropwise to the stirring reaction mixture to dissolve the suspended sodium azide. The reaction was heated to 60 ^oC and left stirring for 20 h. A further equivalent of sodium azide (0.85 mmol, 55 mg) was then added to drive the reaction forward and the mixture stirred at 60 ^oC for a further 6 h. The reaction was allowed to cool to room temperature before sat. $NaHCO_3$ (aq) (10 mL) was added. The product was extracted into EtOAc (3 x 30 mL) before the organics were dried over $MgSO_4$ and concentrated under reduced pressure. This gave a yellow oil which was purified by SiO_2 column chromatography using Et_2O as eluent. The product containing fractions were combined and concentrated under reduced pressure to yield 97 mg (59%) of the title compound as a yellow oil. Upon storing in the fridge, the compound solidified to a grey solid.

^1H NMR (400 MHz, $CDCl_3$) δ 9.99 (d, *J* = 0.9 Hz, 1H, H_6), 8.46 (d, *J* = 2.7 Hz, 1H, H_5), 7.97 (d, *J* = 8.6 Hz, 1H, H_4), 7.33 (ddd, *J* = 8.6, 2.7, 0.9 Hz, 1H, H_3), 4.28 (t, 2H, H_2), 3.69 (t, 2H, H_1).

^{13}C NMR (400 MHz, $CDCl_3$) δ 192.12 (C_6), 157.78 (C_q), 146.99 (C_q), 138.67 (C_5), 123.45 (C_4), 121.01 (C_3), 67.79 (C_2), 50.03 (C_1).

Mass spectrum (EI +ve): *m/z* 192.1 $[M]^+$ (5%); 164.1 $[M\text{-}CO]^+$ (100 %); 136.1 $[M\text{-}CO\text{-}N_2]^+$ (50%).

(1E,1'E)-N,N'-(methylenebis(4,1-phenylene))bis(1-(5-(azidomethyl)pyridin-2-yl)methanimine) (L^A, 44)

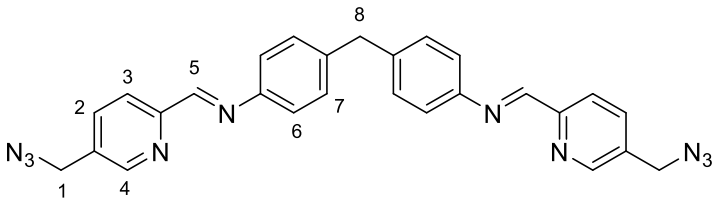

4,4'-methylenedianiline (155 mg, 0.78 mmol) was suspended in EtOH (5 mL) and sonicated until dissolution was achieved. **42** (279 mg, 1.72 mmol) was dissolved in EtOH (3 mL) and the resultant solution added dropwise to the stirring 4,4'-methylenedianiline solution via pipette. The reaction was left stirring at room temperature for 21 h before the precipitate was collected by vacuum filtration. The collected solid was washed with cold (4 °C) EtOH (5 x 1 mL) before being dried under high vacuum for 19 h. This yielded 243 mg (64%) of the title compound as a cream solid.

^{1}H NMR (400 MHz, $CDCl_3$) δ 8.65 (d, *J* = 2.3 Hz, 1H, H_4), 8.63 (s, 1H, H_5), 8.23 (dd, *J* = 8.2, 0.8 Hz, 1H, H_3), 7.79 (dd, *J* = 8.2, 2.3 Hz, 1H, H_2), 7.27 (br. s, 4H, H_{6+7}), 4.47 (s, 2H, H_1), 4.05 (s, 1H, H_8).

^{13}C NMR (400 MHz, $CDCl_3$) δ 159.50 (C_4), 154.87 (C_q), 149.26 (C_5), 149.00 (C_q), 140.08 (C_q), 136.51 (C_2), 132.78 (C_q), 129.96 (C_6), 121.98 (C_3), 121.58 (C_7), 52.10 (C_1), 41.22 (C_8).

Mass spectrum (ESI +ve): *m/z* 487.2 $[M+H]^+$

$Fe_2L^A_3Cl_4$ (34)

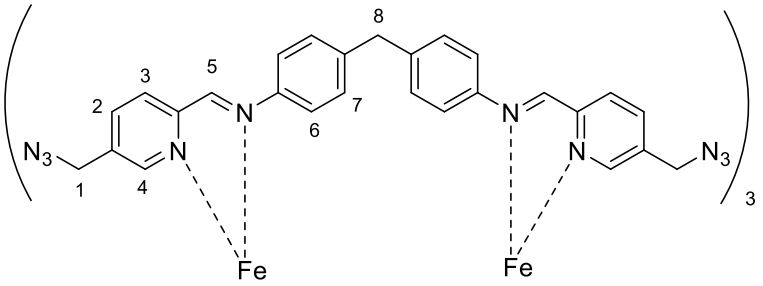

44 (48 mg, 0.098 mmol) and $FeCl_2 \cdot 4H_2O$ (13 mg, 0.065 mmol) were suspended in MeOH (4 mL) and stirred vigorously under reflux (85 °C) for 2 h. The resultant purple mixture was concentred under reduced pressure to an approximate volume of 1 mL. This was slowly poured into cold (-18 °C) Et_2O (25 mL) and the resultant precipitate collected by vacuum filtration. The resultant purple solid was washed with cold Et_2O (5 x 2 mL) before being dried under high vacuum for 1.5 h. This gave 45 mg (80%) of the title complex as a purple solid.

^{1}H NMR (400 MHz, MeOD-d_4) δ 9.17 (s, 2H, H_5), 8.70 (d, *J* = 7.8 Hz, 2H, H_3), 8.44 (d, *J* = 7.8 Hz, 2H, H_2), 7.35 (d, *J* = 10.9 Hz, 2H, H_4), 7.03 (br. s, 4H, $H_{6/7}$), 5.62 (br. s, 4H, $H_{6/7}$), 4.66 (s, 4H, H_1), 4.04 (s, 2H, H_8).

Mass spectrum (ESI +ve): *m/z* 392.87 $[Fe_2L^A_3]^{4+}$; 535.82 $[Fe_2L^A_3+Cl]^{3+}$

UV-Vis (H_2O) λ_{max} (ε_{max}/dm^3 mol^{-1} cm^{-1}): 325 (27,200); 528 (shoulder); 573 (12,600).

(1E,1'E)-N,N'-(methylenebis(4,1-phenylene))bis(1-(5-(2-azidoethoxy)pyridin-2-yl)methanimine) (L^B, 45)

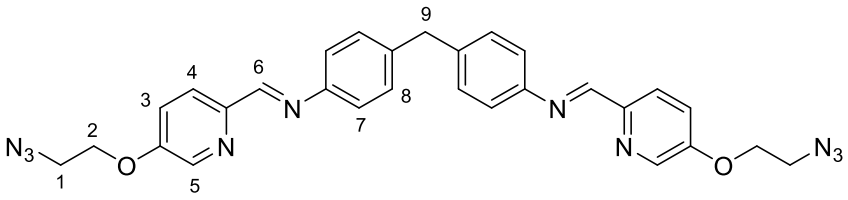

4,4'-methylenedianiline (42 mg, 0.21 mmol) was added to a solution of **43** (88 mg, 0.46 mmol) in EtOH (4 mL) and stirred for 17 h. The resultant precipitate was collected by vacuum filtration and washed with cold (4 ^{o}C) EtOH (5 x 2 mL). The washed solid was then dried under high vacuum for 1.5 h, yielding 80 mg (70%) of the title compound as an off white solid.

^{1}H NMR (400 MHz, $CDCl_3$) δ 8.62 (s, 1H, H_6), 8.46 (d, *J* = 2.8 Hz, 1H, H_5), 8.22 (d, *J* = 8.7 Hz, 1H, H_4), 7.38 (dd, *J* = 8.7, 2.9 Hz, 1H, H_3), 7.31 (d, *J* = 8.6 Hz, 4H, H_{7+8}), 4.34 – 4.31 (t, *J* = 4.9 Hz, 2H, H_2), 4.09 (s, 1H, H_9), 3.73 (t, *J* = 4.9 Hz, 2H, H_1).

^{13}C NMR (400 MHz, $CDCl_3$) δ 159.38 (C_6), 155.79 (C_q), 149.35 (C_q), 148.42 (C_q), 139.61 (C_q), 137.63 (C_5), 129.89 (C_7), 122.96 (C_4), 121.78 (C_3), 121.46 (C_8), 67.63 (C_2), 50.18 (C_1), 41.18 (C_9).

Mass spectrum (ESI +ve): *m/z* 547.23 $[M+H]^+$

$Fe_2L^B{}_3Cl_4$ (35)

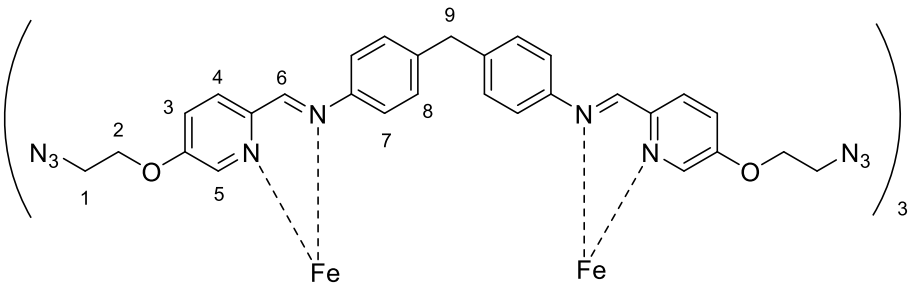

A mixture of **45** (80 mg, 0.15 mmol) and $FeCl_2{\cdot}4H_2O$ (20 mg, 0.1 mmol) in MeOH (5 mL) was heated under reflux (85 °C) for 2.5 h. The mixture was allowed to cool to room temperature before being slowly pured into cold (-18 °C) Et_2O. The resultant purple precipitate was collected by vacuum filtration and washed with cold Et_2O (3 x 5 mL). Drying on high vacuum for 18 h yielded 75 mg (79%) of the title compound as a pale purple solid.

^{1}H NMR (400 MHz, MeOD-d_4) δ 9.00 (s, 2H, H_6), 8.62 (d, *J* = 8.8 Hz, 2H, H_3), 8.04 (dt, *J* = 14.6, 7.2 Hz, 2H, H_4), 7.03 (d, *J* = 2.4 Hz, 2H, H_5), 5.60 (s, 3H, $H_{7/8}$), 4.39 (t, *J* = 4.6 Hz, 4H, H_2), 4.01 (s, 2H, H_8), 3.67 (t, *J* = 4.6 Hz, 4H, H_1).

Mass spectrum (ESI +ve): *m/z* 595.5 $[Fe_2L^B{}_3+Cl]^{3+}$; 637.72 $[Fe_2L^B{}_2+2Cl]^{2+}$

UV-Vis (H_2O) λ_{max} (ε_{max}/dm^3 mol^{-1} cm^{-1}): 511 (shoulder); 548 (9,900).

5.3.2 dsDNA binding studies

Solutions used in DNA binding studies were made using DNAse and RNAse free water, purchased from Fisher Scientific.

A 1 mM stock solution of calf thymus DNA (ctDNA) was prepared by suspending 10 mg of lyophilised fibrous type I ctDNA (Merck Sigma Aldrich) in 5 mL of water. This was left to solubilise fully for 20 h at 4 °C. Concentration of the solution was calculated based on the number of nucleobases present by measurement of the absorbance at 260 nm (ε = 6600 mol^{-}

^{1} L cm^{-1}). The solution was diluted with water to achieve a 1 mM concentration and separated into 1 mL aliquots which were stored frozen until needed.

A stock of 5 x DNA binding buffer was prepared by dissolving NaCl (584 mg) and sodium cacodylate trihydrate (107 mg) in 50 mL H_2O. Further H_2O was added to a final volume of 100 mL, giving a concentration of 100 mM NaCl; 5 mM sodium cacodylate.

5.3.2.1 Circular dichroism titrations

CD measurements were recorded using an Applied Photophysics Chirascan Plus spectrometer, using a 3 mL quartz cuvette with a 1 cm path length. Titrations were performed using three solutions with the following compositions:

Solution A: 100 µM ctDNA, 20 mM NaCl, 1 mM sodium cacodylate;

Solution B: 167 µM complex;

Solution C: 200 µM ctDNA, 40 mM NaCl, 2 mM sodium cacodylate.

With 1600 µL of solution A in the cuvette, aliquots of solution B were added such that the ratio of [complex] to [ctDNA] was varied from 60:1 increasing to 8:1. An equal volume of solution C was added with every aliquot of solution B to keep the concentration of ctDNA and buffer constant. After gently mixing the solution with a pipette, three measurements from 200 nm to 700 nm (1 nm step size, 0.5 s per step) were performed and the resultant spectra averaged. A background measurement with 1 x buffer in the cell was measured and this was subtracted from each averaged spectrum obtained.

5.3.2.2 Linear dichroism titrations

LD measurements were performed using an Applied Photophysics Chirascan Plus spectrometer equipped with the manufacturer's LD attachment, using a Couette cell with a 250 µL capacity. Solutions A, B, and C were used as with the CD titrations. 200 µL of solution A served as the starting point of the titration.

Prior to the ctDNA only measurement, the Couette cell was spun at 40 revolutions per second for 5 mins to linearise the DNA. Equal aliquots of solutions B and C were added to the Couette

cell to increase the concentration of complex while keeping the concentration of ctDNA and buffer constant. Prior to measurement, the Couette cell was spun at 40 revs s^{-1} for 3 min to ensure thorough mixing. Three LD measurements were taken between 200 nm and 700 nm (1 nm step size, 0.5 s per step) for each complex concentration and the resultant spectra averaged. A background measurement was recorded with 100 µM ctDNA in 1 x buffer in the cell, prior to any spinning. This was subtracted from each averaged spectrum obtained.

5.3.3 PAGE procedures

Oligonucleotides used (S1, S2, S3) were purchased from Merck Sigma-Aldrich and provided as lyophilised solids purified by HPLC. Sequences were as follows:

S1: 5'-CGGAACGGCACTCG

S2: 5'-CGAGTGCAGCGTGG

S3: 5'-CCACGCTCGTTCCG.

200 µM stock solutions of each were prepared using DNase and RNase free distilled water purchased from Fisher Scientific, which was used for all subsequent biological incubations.

"1 x TB" and "1 x TBN" aqueous buffers have the compositions listed below. "2 x" and "10 x" refer to multiplications of these concentrations.

TB: 89 mM tris(hydroxymethyl)aminomethane; 89 mM boric acid, pH 8.3.

TBN: 89 mM tris(hydroxymethyl)aminomethane; 89 mM boric acid; 100 mM sodium chloride. pH 8.3.

5.3.3.1 Radiolabelling of oligonucleotides

Oligonucleotide S1, S2 or S3 (1.2 µL of 200 µM stock) was diluted with water (13.8 µL) in a 1.5 mL Eppendorf tube. Bacteriophage T4 polynucleotide kinase (2 µL) and 10 x T4 polynucleotide kinase buffer A (2 µL), both purchased from Thermo Scientific, were then added. The resultant solution was gently mixed and ATP [γ-^{32}P] - 3000 Ci/mmol (1 µL, Perkin Elmer) was added. After gentle mixing, the mixture was incubated at 37 ^{o}C for 1 h. The enzyme was denatured by heating at 80 ^{o}C for 3 min. Purification was performed using a QIAquick

nucleotide removal kit (purchased from QIAGEN). 200 µL of PNI buffer was added to the incubation mixture, and this was transferred onto a QIAquick spin column with a 2 mL collection tube. After centrifugation (6000 rpm, 1 min), the column was transferred to a new collection tube and 500 µL of PE buffer was added. This was again centrifuged (6000 rpm, 1 min) and followed by a repeat of this wash step. The column was again transferred to a new collection tube and centrifuged (13000 rpm, 1 min) to fully remove any residual buffer from the precipitated oligonucleotide. The oligonucleotide was resuspended by adding 60 µL of H_2O to the column. This was left for 8 min before the column was transferred into an Eppendorf tube. Centrifugation (13000 rpm, 2 min) gave the labelled oligonucleotide with a concentration of 4 µM.

5.3.3.2 Preparation of PAGE gel

A 15% polyacrylamide gel solution was prepared by mixing 30% ProtoGel 37.5:1 Acrylamide to Bisacrylamide solution (25 mL, National Diagnostics) with 10 x TB buffer (5 mL) and H_2O (20 mL). 10% (w/v) ammonium persulfate aq. (400 µL) and TEMED (40 µL) was then added. The solution was gently inverted several times to mix and then poured between two glass electrophoresis plates. A 20-well comb was fitted and the gel left to polymerise for 1 h to give a gel with dimensions 17 cm (width) x 15cm (height). The comb was removed and the wells rinsed with TB buffer. The gel was mounted into an electrophoresis tank (Biometra V15.17, Analytik Jena) and pre-warmed at 300 V, 400 A for 5 min.

5.3.3.3 3WJ PAGE experiment

Samples were prepared with stoichiometric quantities of oligonucleotides S1, S2, and S3 (with one radiolabelled with ^{32}P) and the complex under investigation in TBN buffer. The final volume for each sample was 10 µL, with a 0.4 µM concentration of each oligonucleotide. The quantity of complex added was varied to give a complex concentration of 0.2, 0.4, 0.8 or 1.6 µM. The samples were incubated for 1 h at room temperature (18 – 20 ^{o}C). 5 µL of 30% (v/v) aqueous glycerol was added to each sample and gently mixed. Samples were loaded onto a prewarmed 15% polyacrylamide gel which was run for 2 h at a constant voltage of 140 V using a Biometra V15.17 (Analytik Jena) gel tank connected to a Bio-Rad Powerpac power supply. The gel was removed from the tank and exposed to a phosphor imaging plate for 1 – 16 h

depending on the measured radioactivity. The phosphor screen was scanned to form an autoradiograph using a Bio-Rad Personal Molecular Imager FX. Images were analysed using Bio-Rad Quantity One software.

Appendix 1:

Titration table for circular dichroism spectroscopy investigation

The following table was constructed to calculate the volume of solutions B and C required to achieve each step of the circular dichroism titration experiments discussed in Chapter 3. A similar table was used during the linear dichroism titrations. The formula derived on page 118 was used to calculate the values in the "total volume B added (µL)" column.

Titration	[DNA]:[cylinder]	[DNA] (µM)	[cylinder] (µM)	total vol B added (µL)	vol B to add (µL)	vol C to add (µL)	Total vol
1	60.00	100	1.67	16.3	16.3	16.3	1632.6
2	40.00	100	2.50	24.7	8.4	8.4	1649.4
3	30.00	100	3.33	33.3	8.6	8.6	1666.5
4	20.00	100	5.00	51.0	17.7	17.7	1701.9
5	15.00	100	6.67	69.4	18.5	18.5	1738.8
6	10.00	100	10.00	108.8	39.4	39.4	1817.7
7	8.00	100	12.50	140.8	32.0	32.0	1881.7
8	6.00	100	16.67	199.5	58.7	58.7	1999.0
9	4.00	100	25.00	341.9	142.4	142.4	2283.8

[DNA] in A (µM):	100
[cylinder] in B (µM):	167
[DNA] in C (µM):	200
starting volume in cuvette (µL):	1600

Appendix 2:

Images obtained from PAGE experiments

Gel 1:

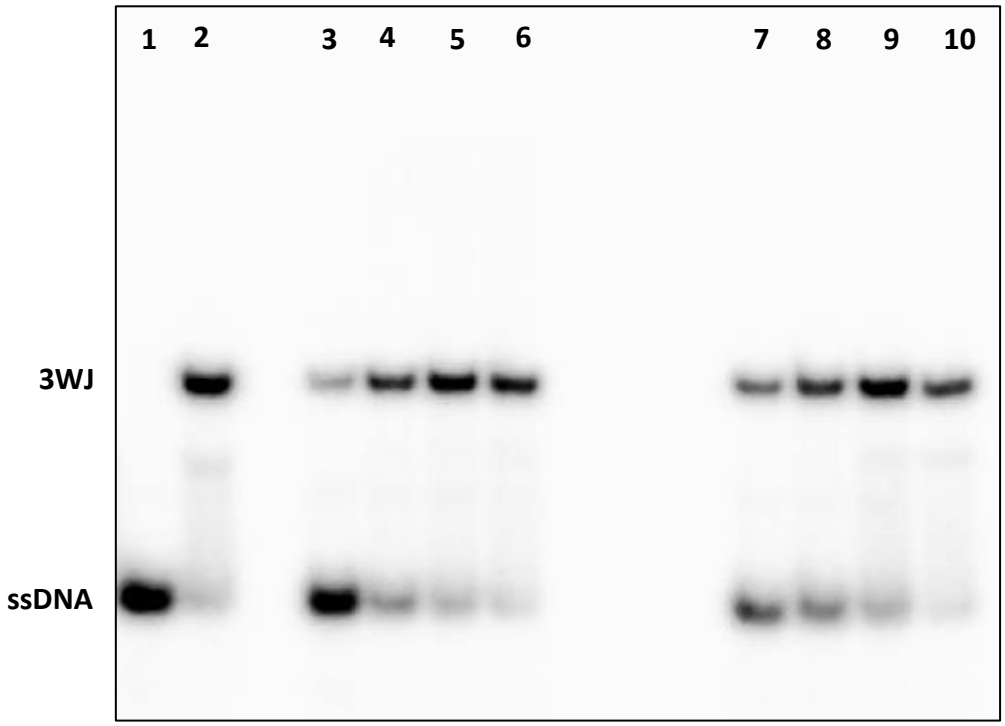

Well	Complex
1	-
2	1 eq $Fe_2L_3Cl_4$
3	0.5 eq $Fe_2L^A{}_3Cl_4$
4	1 eq $Fe_2L^A{}_3Cl_4$
5	2 eq $Fe_2L^A{}_3Cl_4$
6	4 eq $Fe_2L^A{}_3Cl_4$
7	0.5 eq $Fe_2L^B{}_3Cl_4$
8	1 eq $Fe_2L^B{}_3Cl_4$
9	2 eq $Fe_2L^B{}_3Cl_4$
10	4 eq $Fe_2L^B{}_3Cl_4$

Gel 2:

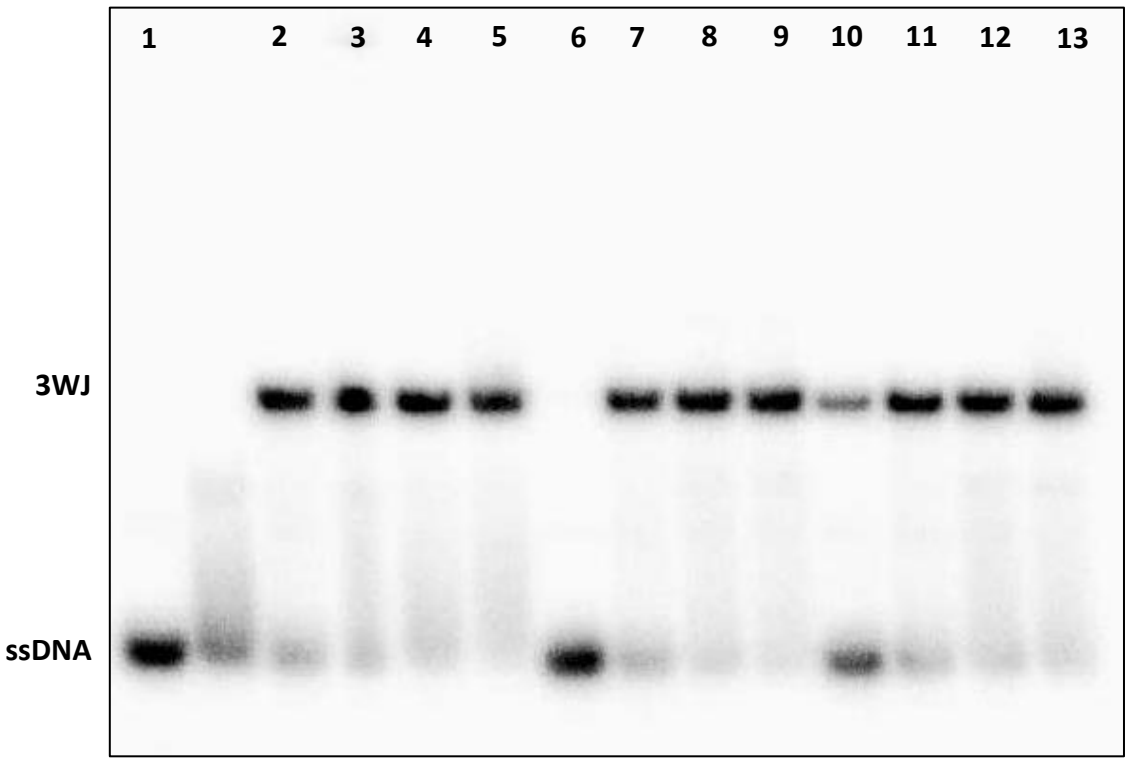

Well	Complex
1	-
2	0.5 eq $Fe_2L_3Cl_4$
3	1 eq $Fe_2L_3Cl_4$
4	2 eq $Fe_2L_3Cl_4$
5	4 eq $Fe_2L_3Cl_4$
6	0.5 eq $Fe_2L^A{}_3Cl_4$
7	1 eq $Fe_2L^A{}_3Cl_4$
8	2 eq $Fe_2L^A{}_3Cl_4$
9	4 eq $Fe_2L^A{}_3Cl_4$
10	0.5 eq $Fe_2L^B{}_3Cl_4$
11	1 eq $Fe_2L^B{}_3Cl_4$
12	2 eq $Fe_2L^B{}_3Cl_4$
13	4 eq $Fe_2L^B{}_3Cl_4$

Gel 3:

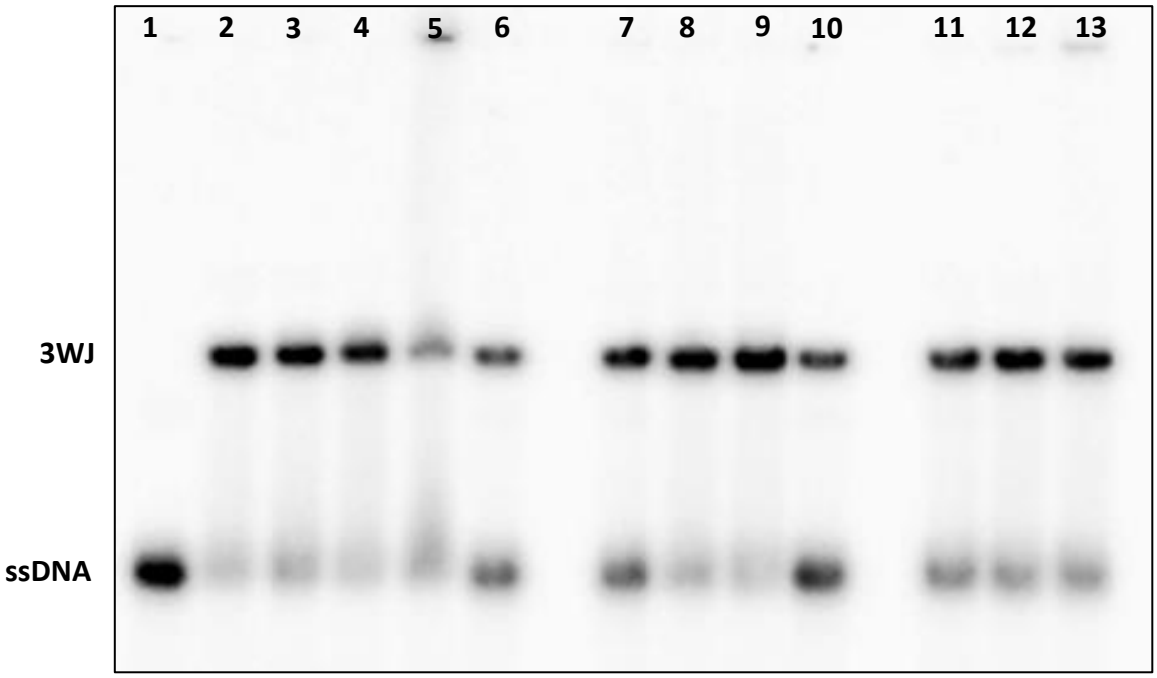

Well	Complex
1	-
2	0.5 eq $Fe_2L_3Cl_4$
3	1 eq $Fe_2L_3Cl_4$
4	2 eq $Fe_2L_3Cl_4$
5	4 eq $Fe_2L_3Cl_4$
6	0.5 eq $Fe_2L^A{}_3Cl_4$
7	1 eq $Fe_2L^A{}_3Cl_4$
8	2 eq $Fe_2L^A{}_3Cl_4$
9	4 eq $Fe_2L^A{}_3Cl_4$
10	0.5 eq $Fe_2L^B{}_3Cl_4$
11	1 eq $Fe_2L^B{}_3Cl_4$
12	2 eq $Fe_2L^B{}_3Cl_4$
13	4 eq $Fe_2L^B{}_3Cl_4$

This gel is presented as Figure 3.27 in the text, with the blank lanes removed.

Gel 4:

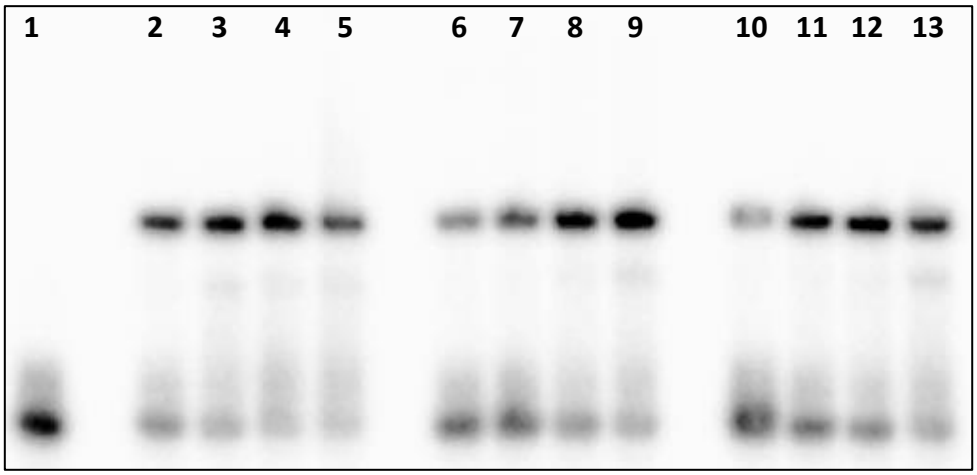

Well	Complex
1	-
2	0.5 eq $Fe_2L_3Cl_4$
3	1 eq $Fe_2L_3Cl_4$
4	2 eq $Fe_2L_3Cl_4$
5	4 eq $Fe_2L_3Cl_4$
6	0.5 eq $Fe_2L^A{}_3Cl_4$
7	1 eq $Fe_2L^A{}_3Cl_4$
8	2 eq $Fe_2L^A{}_3Cl_4$
9	4 eq $Fe_2L^A{}_3Cl_4$
10	0.5 eq $Fe_2L^B{}_3Cl_4$
11	1 eq $Fe_2L^B{}_3Cl_4$
12	2 eq $Fe_2L^B{}_3Cl_4$
13	4 eq $Fe_2L^B{}_3Cl_4$